To the Graduate Council:

I am submitting herewith a dissertation written by Brian Wayne Walther entitled "Electron Spin Resonance Characterization of Novel Radicals Produced by High Energy Radiation." I have examined the final copy of this dissertation for form and content and recommend that it be accepted in partial fulfillment of the requirements for the degree of Doctor of Philosophy, with a major in Chemistry.

T. Francon Williams
T. F. Williams, Major Professor

We have read this dissertation
and recommend its acceptance:

John E. Bloor

James Q. Chambers

Linda R. Painter

Accepted for the Council:

Vice Provost and
Dean of the Graduate School

ELECTRON SPIN RESONANCE CHARACTERIZATION OF NOVEL RADICALS PRODUCED BY HIGH ENERGY RADIATION

A Dissertation

Presented for the

Doctor of Philosophy

Degree

The University of Tennessee, Knoxville

Brian Wayne Walther

December 1984

ACKNOWLEDGEMENTS

The guidance and advice given by Dr. T. F. Williams, my major professor, is sincerely appreciated. In particular, his ability to solve complex analysis problems and his example of untiring dedication have served as both a challenge and an encouragement to the author which will be long remembered.

The members of my doctoral committee are thanked for their time spent with this dissertation.

Sincere gratitude is extended to Dr. R. L. Hudson for his patient tutoring of the basic aspects of ESR. Thanks are also extended to Dr. J. T. Wang, whose practical laboratory experience helped the author avoid many experimental problems.

Gifts of various compounds (a complete list given elsewhere) from Drs. D. Griller, J. T. Wang, J. K. Kochi, D. M. Lemal, and C. O. Christe are gratefully acknowledged.

It is a pleasure to thank several of my co-workers, not acknowledged earlier, L. D. Snow, D. N. Payne, X.-Z. Qin, and J. Aikens, for many thought provoking and stimulating discussions. Thanks are also extended to Dr. C. M. L. Kerr for installing and maintaining several computer programs on The University of Tennessee computer systems.

I would like to thank the Department of Chemistry for a graduate teaching assistantship and the Division of Chemical Sciences, Office of Basic Energy Sciences, U. S. Department of Energy for

financial support. The Department of Chemistry is also thanked for allowing me the opportunity of assuming the lecturing responsibilities for a General Chemistry course for two quarters. The Atlantic Richfield Company is gratefully acknowledged for their award of a fellowship for 1982-1984.

Thanks are also extended to Mrs. Georgia Bunn for typing this work.

Finally, the encouragement provided by my wife and family members is sincerely appreciated.

ABSTRACT

Using the technique of electron spin resonance, the structure and bonding of several radicals formed by γ-irradiation have been examined. The general types of radicals examined were either fluorine containing radical anions, organometallic radical cations, or carbon-centered neutral radicals.

By combining the technique of partial orientation with ^{13}C enrichment, both the ^{13}C and ^{19}F axially symmetric hyperfine tensors have been determined for $^{13}CF_3Br^-$ and $^{13}C_2F_4^-$. This has provided further insight into the structure of these radical anions. While neutral octafluorocyclooctatetraene (OFCOT) is known to be tub-shaped, the radical anion of OFCOT was found to be planar. In the radical anion of perfluoromethylcyclohexane, the unpaired electron was found to be primarily localized along the axial C-F bond which is adjacent to the CF_3 group. This represents the first example of a radical anion where the σ^* orbital is along a single C-F bond. The detection of ^{33}S satellite lines in natural abundances allowed the positive identification of two new members of the 35 and 41 electron family, SF_4^- and SF_4O^-, respectively. The characterization of the SF_4^- is of particular interest, since its detection is only the second example of a 35-electron radical.

The radical cations of the entire family of tetramethyl Group IVB metals (Si, Ge, Sn and Pb) were examined. While the radical cations of $(CH_3)_4Si$ and $(CH_3)_4Ge$ adopt a C_{2v} structure, the radical

cations of $(CH_3)_4Sn$ and $(CH_3)_4Pb$ were found to adopt a C_{3v} trigonal-pyramidal structure. An extensive study of some isotopically enriched tetramethyltin derivatives ($(CD_3)_4Sn$, $(^{13}CH_3)Sn$, and $(^{13}CD_3)_4Sn$) and some Q-band investigations helped confirm this analysis. The radical cations of a series of alkyltrimethyltin derivatives were examined. The magnitude and the temperature dependence of the hyperfine coupling constants were, in each case, consistent with a simple model based upon the results found for the tertbutyltrimethyltin radical cations. The σ orbital description given for the hexamethyl homonuclear di-metallic species (Me_3MMMe_3; M=Si, Ge and Sn), was found appropriate to explain the ESR results for two heterobimetallic analogues ($Me_3SiGeMe_3^+$) and ($Me_3SiSnMe_3^+$).

The family of $Me_3MCH_2\cdot$ neutral radicals where M=Si, Ge, Sn, and Pb, were examined. These results indicated the relative un-importance of $d(\pi)$ - $p(\pi)$ bonding in α-metal π radicals. The ^{13}C satellite lines which were detected in natural abundance for $CF_3CCl_2\cdot$ strongly support the argument that π-conjugative destabilization of the α-substituent is more significant than increasing the electro-negativity in inducing pyramidality of the alkyl radical.

TABLE OF CONTENTS

LIST OF TABLES

LIST OF FIGURES

FIGURE PAGE

FIGURE PAGE

FIGURE PAGE

FIGURE PAGE

FIGURE PAGE

FIGURE PAGE

CHAPTER I

INTRODUCTION

A. Electron Spin Resonance

Electron spin resonance (ESR) is a branch of spectroscopy which yields fundamental information about the distribution of unpaired electrons in atoms or molecules.[1] When an unpaired electron is localized in systems which possess magnetic nuclei, an interaction between the unpaired electron and the magnetic nuclei, termed hyperfine interaction, can be directly detected in an ESR experiment and, by first principles, related to the spin distribution.[2] Since the structure of molecules is frequently determined by the nature of the highest occupied orbital, ESR affords a direct technique to probe the electronic structure of paramagnetic molecular systems.[3-5]

Structural information concerning individual paramagnetic molecules or complexes, for which the largest class with one unpaired electron ($S = 1/2$) is generally called radicals, is important not only for a fundamental understanding of molecular bonding, but also for characterization of reaction intermediates. Since many proposed reaction mechanisms involve radicals, ESR is ideally suited to explore the nature of these species. Also, ESR results afford a stringent test of theoretical calculations on open-shell molecules.

B. Radical Generation and Stabilization

Since most radicals are extremely reactive, the reactive paramagnetic species itself is not what is initially purchased or prepared, but rather a diamagnetic molecule, termed the precursor, which by some mechanism can be changed into the described radical in a high-enough concentration to allow its detection. It should be noted that the ESR method, as the name implies, is specific for the detection of species which have non-zero electron spin. Therefore, diamagnetic molecules cannot be detected by this method, irrespective of their concentration. On the other hand, radical concentrations as low as 10^{-9} M can be detected under favorable conditions.[6] Often in ESR detection of radical ions, the precursor is simply the diamagnetic form of the desired paramagnetic molecule. For example, the bromotrifluoromethane radical anion can be formed by electron attachment to the diamagnetic bromotrifluoromethane molecule;[7] likewise, the radical cation of tetramethylsilane can be generated by oxidation of the parent diamagnetic molecule.[8] Also, radicals can be produced by either dissociation of or addition to a precursor molecule. For example, the $Me_3SiCH_2^{\cdot}$ free radical can be derived by the loss of a hydrogen atom from the precursor, tetramethylsilane,[9,10] while the vinyl radical ($C_2H_3^{\cdot}$) is obtained by hydrogen atom addition to acetylene.[11]

Historically, three different main approaches have been utilized to detect reactive radicals, namely matrix isolation, <u>in situ</u> steady state radical generation, and spin trapping.

Spin trapping is not in the strictest sense a radical-stabilizing technique since in this technique the radical is stabilized only by chemical addition to the double bond of a diamagnetic molecule, termed a spin trap, as exemplified below.[12-14]

$$\underset{\text{(paramagnetic, reactive)}}{R\cdot} + \underset{\text{(diamagnetic)}}{(CH_3)_3C\text{-}N{=}O} \xrightarrow{\text{fast}} \underset{\text{(paramagnetic, stable)}}{(CH_3)_3C\text{-}\overset{R}{\overset{|}{N}}\text{-}O\cdot}$$

Within the scope of the matrix isolation technique, the radical precursor is generally isolated in an inert matrix and then transformed into the desired radical while still isolated.[15,16] By virtue of the fact that the precursor molecules are rigidly fixed in position at low temperature, the method of radical generation is limited to some kind of radiation-induced process resulting from penetration of the matrix by high energy γ or X-rays or lower energy photons through the matrix. Once formed the radicals can have very long lifetimes owing to the fact that the natural decay mechanisms of the radical are blocked by the surrounding inert matrix. Consequently, sufficient radical concentrations can often be built up by simply increasing the radiation time. Inherent in the matrix-isolation technique is that translational and diffusional motion in the sample is completely quenched. There are two noteworthy variations of the above solid-state technique. First, if the desired radical has very little tendency to react with the diamagnetic form of itself[17] or, conversely, if that reaction is desired,[18] then the precursor need not be matrix isolated, and a pure solid sample can

be used. Also, if the radical can be formed in the gas phase, then certain small radicals under favorable conditions can be co-deposited with an inert matrix.[19]

In the in situ steady-state radical generation technique, on the other hand, fresh precursor is continuously being transformed into the desired radical which itself is continuously reacting into something else.[20] Under these conditions, the rate of radical formation balances the rate of radical disappearance. Since the steady-state technique implies the liquid phase, which allows for translational molecular motion, a greater variety of radical generation techniques are available,[21] such as chemical,[22] electrochemical,[23] thermal,[24] or photolytic.[25] However, the rate of radical generation must be very large to build up a detectable steady-state concentration.

In summary, then, sufficient radical concentrations for detection may be obtained in either of two ways. First, by utilizing matrix isolation techniques, which, although limited to the solid state, has the advantage that the radicals once generated are stable and can be studied at leisure. Second, by employing in situ steady-state techniques which, although requiring high rates of radical generation to ensure a sufficient steady-state concentration, has the decided advantage of allowing the use of the liquid phase. In some instances, radicals can be generated and probed using either technique. For example, the methyl radical can be observed by γ-irradiation of matrix-isolated iodomethane in argon at 4 K[26,27] or by

continuous irradiation of liquid methane.[20] There are other instances, however, when it seems unlikely that radicals observed by one technique will be observed by the other. For example, the matrix-isolated dimethylether radical cation was observed in γ-irradiated fluorotrichloromethane at 90 K,[28] but given that the dimethylether radical cation is known in the gas phase to abstract a hydrogen atom from a neutral dimethylether molecule on nearly every collision[29] it seems unlikely that the radical cation can be detected in the liquid phase.

Since the technique of matrix isolation was utilized exclusively in this research, greater attention will now be focused on the method of radical generation by this technique, and particularly the effects of γ-irradiation on solid samples.

Gamma rays are produced when ^{60}Co undergoes a beta decay followed by two nuclear transitions giving off two γ rays.[30]

$$^{60}Co \rightarrow {}^{60}Ni + \beta + \gamma\ (1.173\ MeV) + \gamma\ (1.332\ MeV) \qquad (1)$$

The half life of ^{60}Co is 5.27 years.[31] For γ-rays of this average energy (1.25 MeV), the most significant mechanism of energy transfer from the γ-ray to the medium is not due to the photoelectric effect[32] which involves a direct collision of a γ-ray with an electron followed by complete transfer of energy from the photon to the electron (Equation 2), but rather from the Compton[33,34] effect

which brings about the ejection of a recoil electron (e^{*-}) with an average energy of about 600 keV by scattering of the γ-ray path (Equation 3). However, in this latter case, the γ-ray continues through the medium, generating more Compton recoil electrons.

$$\overset{\gamma}{\sim\!\!\!\rightarrow} M \rightarrow M^{+\cdot} + e^{*-} \qquad (2)$$

$$\overset{\gamma}{\sim\!\!\!\rightarrow} M \rightarrow M^{+\cdot} + e^{*-} + \overset{\gamma}{\sim\!\!\!\rightarrow} \qquad (3)$$

In either case, these fast electrons traverse the medium ionizing non-specifically the molecules along their tracks thereby generating secondary electrons with energies ranging from 10 keV to about 20 eV with the average being around 100 eV (Equation 4).

$$e^{*} \text{ (~600 keV)} + M \rightarrow M^{+} + e^{*-} \text{ (~600 keV)} + e^{-} \text{ (100-20 eV)} \qquad (4)$$

Although the Compton recoil fast electrons have energies on the order of 600 keV, their track length is limited since each ionization with its secondary electron production costs energy, and eventually their energy falls to about kT. Likewise, but on a shorter scale, the multitude of secondary electrons generated from each fast electron will moderate their energy by further ionizations or excitations in a cluster close to the site of their original production until their energy also falls to about kT. Of course, the greater the initial energy that the secondary electron possesses, the further it will traverse through the medium. The short tracks of these secondary electrons are called spurs.

It should be noted that, although a cation is produced by the initial encounter of the about 1 MeV γ ray, the chemistry of this initial cation is insignificant when compared with the hundred thousand (10^5) or so cations produced by the fast and secondary electrons. Likewise, while the fast Compton recoil electron plays a significant role in the energy deposition, the eventual fate of this particular electron after thermalization is chemically insignificant when compared to the vast number produced by the corresponding thermalization of secondary electrons.

Having reached this state of thermal energy, the electrons will generally experience one of several fates,[35] such as recombination with its geminate cation (Equation (5)), solvation or trapping by liquids or solids, respectively, whereby the electron is not localized on a specific molecule (Equation (7)), and finally, formation of radical anions resulting from electron capture by a suitable molecule possessing a low-lying vacant orbital (Equation (7)). These initial processes are summarized below.

$$e^- (\sim kT) + M^{+\cdot} \rightarrow M^* \rightarrow \text{free radicals} \qquad (5)$$

$$e^- (\sim kT) + M \rightarrow M^{-\cdot} \qquad (6)$$

$$e^- + MTHF \rightarrow e^- (\text{trapped}) \qquad (7)$$

As shown by Equations 4-7, the three types of species that exist after a sample has been exposed to high energy radiation are: (a) positively-charged radicals, (b) negatively-charged radicals (assuming a suitable electron acceptor is available), and (c) neutral species, including free radicals, formed by annihilation reaction of a free electron with a positively charged species. Of course, all these species may be formed in an energetically excited state and can therefore dissociate to give additional products, both diamagnetic and paramagnetic. The stability of these reactive intermediates is not only linked to the inherent stability of the energetic molecule itself but is also very dependent upon its reactivity with the surrounding molecules.

In the course of this work, the following four different sample preparations were used: (a) pure tetramethylsilane (TMS) and 2-methyltetrahydrofuran (MTHF), (b) a perhalocarbon solute isolated in a hydrocarbon or hydrocarbon-like matrix, (c) an organometallic solute isolated in a perhalocarbon matrix, and (d) pure $Cs^+SF_5^-$ and $Cs^+SF_5O^-$ salts. In the following discussions the anticipated radiation chemical events will be considered for the first three of these cases.

Since MTHF has little tendency to stabilize electrons into a single molecule's molecular orbital, the thermalized electrons are

simply trapped into "holes" or vacancies in the matrix (Equation (7), page 7). Concurrently, the positively charged MTHF radical cations ($R\text{-}H^+$) can undergo proton transfer or abstract hydrogen atoms with the net result being the generation of a free radical and a protonated molecule (Equation (8), page 9). The product of an annihilation reaction will often undergo dissociation to form two neutral radicals (Equation (9)). Since TMS also has little tendency to trap electrons, the secondary electrons will either recombine with the geminite cations or become associated with something else.

$$RH^{+}\cdot + RH \rightarrow RH_2^{+} + R\cdot \qquad (8)$$

$$R^{+}\cdot + e^{-} \rightarrow [R^*] \rightarrow \text{free radical products} \qquad (9)$$

If molecules which have a high tendency to attach electrons and form negative ions, such as halocarbons, some aromatic hydrocarbons, and many metal-centered molecules, are incorporated into a saturated hydrocarbon or hydrocarbon-like matrix then the secondary electron will, after releasing their energy, preferentially be captured by these molecules. These molecules are often termed electron scavengers.[36,37] However, both the positively-charged species and the excited neutral molecules which are statistically produced in the saturated hydrocarbon, will undergo the same reactions as

previously mentioned. After electron capture, some electron scavengers (especially halogen substituted hydrocarbons) will immediately undergo dissociation to form a free radical and a negative halide ion (X^-) (Equation 10). This process is called

$$R\text{-}X + e^- \rightarrow R^{\cdot} + X^- \quad (X = Cl, Br, I) \qquad (10)$$

dissociative electron capture.[38] Implicit in the above discussion is that the system is maintained at a sufficiently low temperature to prevent the molecules or ions bearing opposite charges from diffusing to each other and neutralizing themselves. Generally, this rigidity requirement is satisfied by most hydrocarbon matrices at 77 K.

If, instead of a saturated hydrocarbon matrix, a perhalocarbon matrix, such as $CFCl_3$ is employed, then the low-energy electrons released by the passage of the fast electrons will ultimately be captured by the electron scavenger molecules which constitute the matrix. Since the positive ions are initially generated by the non-specific action of the fast electrons, in general the largest number of positive ions will initially be formed from the molecular species present in greatest concentration, which in this case is also the perhalogenated matrix. Under favorable conditions, however, the positive hole can be efficiently transferred through the matrix to a hydrocarbon or other suitable solute molecule (S)[39,40] (Equation (11), page 11). Empirically, the conditions necessary for efficient charge transfer would include the necessity of the matrix having a higher ionization potential than the solute. However, for the

solute radical cation to survive, the captured electron would need to be held tightly enough to prohibit annihilation reactions, and the solute cation should be isolated in the matrix so that the typical decay paths for organometallic radical cations can be blocked.[41] It should be noted that in some cases the cations and the matrix will form a cationic σ* complex.[42-45] Since in principle both radical cations and anions are being stabilized, some practical requirements must be satisfied in order for this technique to be useful spectroscopically.

$$CFCl_3^{+\cdot}\ CFCl_3\ S \rightarrow CFCl_3\ CFCl_3^{+\cdot}\ S \rightarrow CFCl_3\ CFCl_3\ S^{+\cdot} \qquad (11)$$

In summary, then, if one wishes to generate halocarbon or other radical anions by electron capture, a hydrocarbon or hydrocarbon-like (e.g., TMS) matrix is used; but if organic or organometallic radical cations are desired, then a halocarbon is used as a matrix. However, because of the need for ESR and/or optical characterization of the species, the experimental design is rarely this trivial, nor is it advisable to use only one matrix since each matrix has its own particularly useful properties. With experience and judicious design, the desired radical ion can often be generated and stabilized in a system that allows this potentially reactive species to be satisfactorily detected by ESR and/or optical spectroscopy.

C. Basic Concepts of ESR Analysis

Since none of the work in this dissertation explores new theoretical approaches to ESR and since the fundamentals of ESR theory are already well established,[46-49] the following discussion concerning the essentials of ESR theory is only intended to provide the necessary background for the interpretation of ESR spectra.

When an unpaired electron is subjected to an external magnetic field, the magnetic moment of the electron, by the Zeeman effect, will orient itself either parallel or anti-parallel to the magnetic field. Since the energy of an electron which has its magnetic moment parallel ($m_s = -1/2$) to the field is less than that of one which is anti-parallel ($m_s = +1/2$), a statistical distribution between the two spin states exists and follows the simple Boltzman distribution where

$$\frac{N_{m_s = +1/2}}{N_{m_s = -1/2}} = \exp(-\Delta E/kT) \approx 1 - \frac{\Delta E}{kT} \qquad (12)$$

since $kT >> \Delta E$ in a typical ESR experiment at X-band [50] and $T > 1$ K. Here $N_{m_s} = \pm 1/2$ is the population of the respective state and ΔE is the energy difference between the states. The magnitude of ΔE is obtained by the solution of the spin Hamiltonian,

$$\overline{H} = g\beta H\overline{S} \ , \qquad (13)$$

which yields

$$\Delta E = g\beta H \qquad (14)$$

where β is a constant, g is a dimensionless number ($g \approx 2$) and H

is the applied external magnetic field. By combining Equation 14 and Planck's law of electromagnetic radiation, $\Delta E = h\nu$, the resonance equation for an electron spin only system is simply

$$h\nu = g\beta H \ . \qquad (15)$$

Since a standard X-band ESR spectrometer operates at a constant frequency (between 9.0-9.5 x 10^9 Hertz), resonance, that is, transition from the $m_s = -1/2$ to the $m_s = +1/2$ state, is only achieved when the varying magnetic field allows Equation 15 to be satisfied.

Of much more interest than the single resonance which is described by Equation (15) are those cases in which additional resonances correspond to a hyperfine pattern. These arise from a nuclear hyperfine interaction between the unpaired electron and the magnetic moments of the nuclei. To include hyperfine interactions into the spin Hamiltonian, a hyperfine interaction term is added to Equation (13) to obtain

$$\overline{H} = g\beta H\overline{S} + hA\overline{I} \cdot \overline{S} \qquad (16)$$

where A, called the hyperfine coupling constant, represents the magnitude of the interaction between the unpaired electron and the nuclear magnetic moment. For completeness, a nuclear Zeeman term $-g_N\beta_N H\overline{I}$, should have been added to Equation (16), but it has been omitted since this term does not affect the transition energies except in special cases of higher-order effects--none of which were observed in this work. When the electronic Zeeman term is much larger than the hyperfine interaction term, as is generally the

situation, and when the field is designated as the Z axis, then Equation (16) reduces to

$$\overline{H} = g\beta H\overline{S}_z + hA\overline{S}_z\overline{I}_z \quad . \tag{17}$$

The use of Equation (17) will be illustrated by the hydrogen atom. In this case, the one unpaired electron (S = 1/2) has two possible M_S values, M_S = +1/2 and M_S = -1/2, and the hydrogen nucleus with a nuclear spin I = 1/2 has two possible M_I values, M_I = +1/2 and M_I = -1/2. Since the values of M_S and M_I are independent of each other, there are four possible (M_S, M_I) combinations, namely (+1/2, +1/2), (+1/2, -1/2), (-1/2, +1/2), and (-1/2, -1/2). To first-order, the four energy levels may be written as +1/2 gβH + 1/4 hA, + 1/2 gβH - 1/4 hA, - 1/2 gβH - 1/4 hA, and -1/2 gβH + 1/4 hA.

When the magnetic field is on the order of 3200 G, the high-field approximation may generally be made and the different states may be placed on an energy scale (Figure 1a, page 15). Since the allowed transitions in ESR are given by the selection rules $\Delta M_S = \pm 1$ and $\Delta M_I = 0$, there will be in this case only two absorption transitions, namely from (-1/2, +1/2) → (+1/2, +1/2) and (-1/2, -1/2) → (+1/2, -1/2) with energies of transition of gβH + 1/2 hA and gβH - 1/2 hA respectively. As previously mentioned, in a typical ESR experiment the frequency is held constant and the magnetic field is swept to bring the energy levels into resonance. To reflect this fact, Figure 1a may be redrawn as a function of H (Figure 1b, page 15).

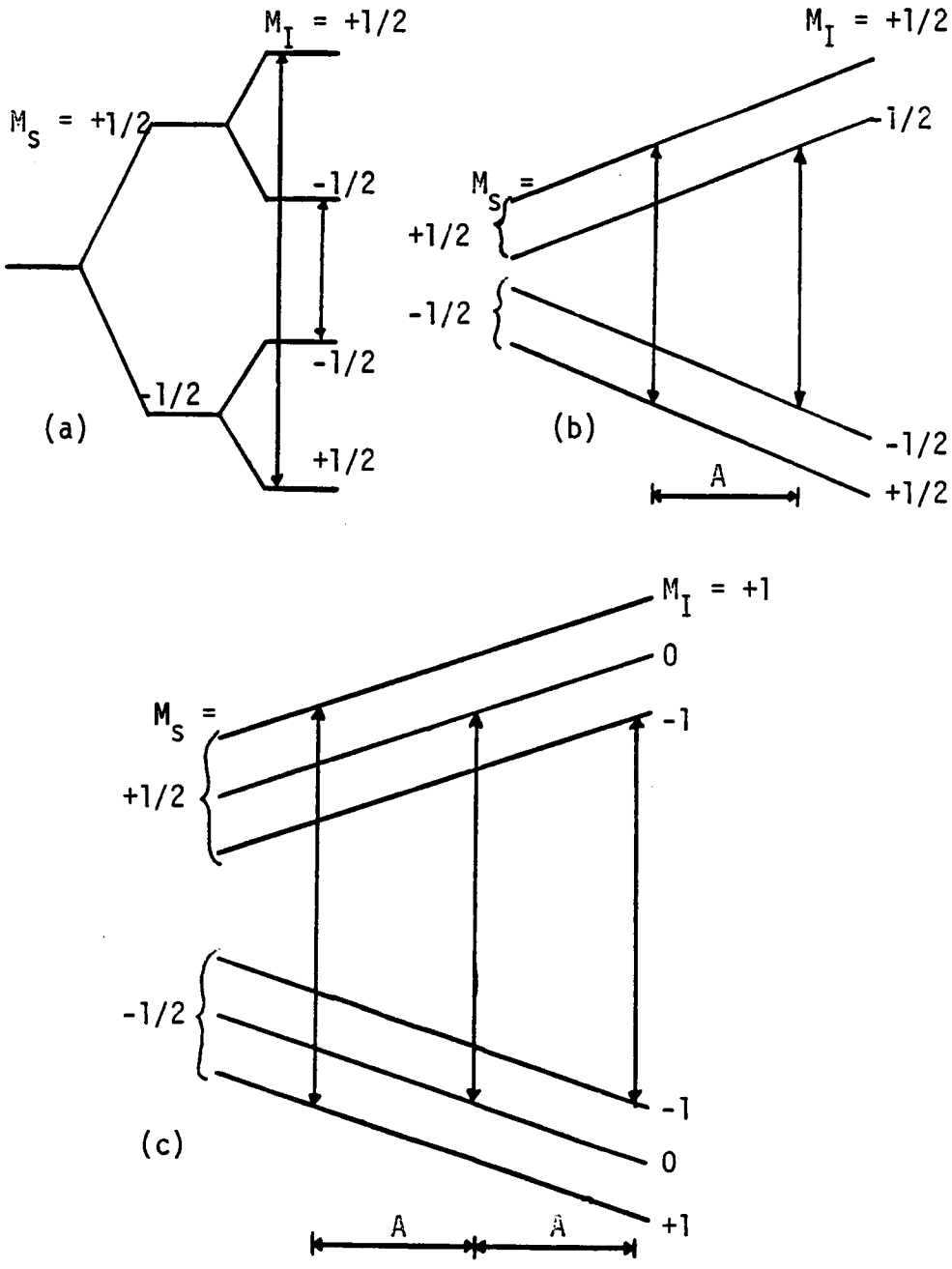

Figure 1. Energy levels and allowed transitions for the hydrogen atom (a) at constant field and (b) at constant frequency and for two equivalent hydrogen atoms (c) at constant frequency.

If a $RCH_2\cdot$ type radical is considered, then instead of just four (M_S, M_I) combinations there are six possible combinations, namely ($\pm 1/2$, +1), ($\pm 1/2$, 0), and ($\pm 1/2$, -1). In this case, to first order the energy levels are given by $\pm 1/2\ g\beta H \pm 1/2\ hA$, $\pm 1/2\ g\beta H$, and $\pm\ 1/2\ g\beta H \mp 1/2\ hA$. Using the ESR selection rules, it is found that there are three allowed transitions (Figure 1c, page 15, diagrammatically shows these three transitions). Once again, the spacing between the resonances is A to first-order.

For the general case, in order to analyze an ESR spectrum and thereby be able to extract the g and hyperfine parameters described by Equation (17), a three-step procedure is generally followed. First, the resonances of the observed ESR spectrum must be correlated into a pattern. Then, once the pattern is established, the spacings called the hyperfine coupling constants, between the resonances need to be determined. Finally, the g-factor can be calculated by determining the magnetic field position corresponding to the center of the symmetry pattern by using Equation (15) and the experimental frequency. The significance of each of these three pieces of information will be considered in the following discussion.

The hyperfine pattern provides information about the number and the spin of the magnetic nuclei which interact with the unpaired electron. Assuming for the sake of simplicity a first-order isotropic pattern, the number of resonances and their relative intensities are governed by very definite and predictable rules. For example, it can be shown that for a single nucleus of spin I,

(2I + 1) resonances are observed. In these cases, each of the different states can be labeled with an m_I value where m_I = I, I-1, . . . , -I and each m_I resonance is of equal intensity. For n equivalent nuclei (2nI + 1) resonances result. Each of these resonances are labeled with an M_I value, where M_I = I, I-1, . . . , -I where the total I is the sum of the nuclear spins, I, in the symmetry group. In these cases, the observed intensity of the individual M_I resonances is directly proportional to the degeneracy of the energy levels giving rise to the M_I transition. The degeneracy of a particular energy level can be straightforwardly determined by counting the number of combinations of m_I that sum to the M_I value. Thus, for the case where there are two equivalent nuclei with I = 1/2, the M_I states are labeled as +1, 0, and -1, and the relative intensities of the M_I states are a 1:2:1 triplet. If there are two groups of equivalent nuclei, n and m with nuclear spins of I and I', then the number of possible resonances is (2nI + 1) (2mI' + 1) where the resonances must, in these cases, be described with two M_I values. For example, for three nuclei with I = 1/2 coupling strongly and two nuclei with I = 3/2 coupling also, the expected pattern would be a widely separated 1:3:3:1 quartet pattern split by a 1:2:3:4:3:2:1 septet pattern; an observed example of this is shown in Chapter V, page 282.

The hyperfine coupling constant, A, can be utilized to calculate the spin density distribution of the unpaired electron. Assuming an isotropic first-order pattern, the observed hyperfine

coupling constant, A, can be directly related to the spin density by

$$\rho_s = \frac{A}{A_o} \tag{18}$$

where A_o is a constant. It[2] has been shown that for systems with one electron the isotropic interaction between the electron and the nucleus is given by

$$A_o = \left(\frac{8\pi}{3}\right) g\beta\, g_N\, \beta_N(\psi_o)^2 \text{ (for } r=0) \tag{19}$$

The wave functions used in Equation (19) are generally self-consistent-field (SCF) wave functions. A_o values[51] used in this work are collected and presented on page 25.

It should be noted that a mechanism exists whereby isotropic coupling may be observed in radicals which have nearly 100% p character for the orbital of the unpaired electron.[52,53] This mechanism is called spin-polarization and can be used to explain the observed couplings to the ring hydrogen nuclei of aromatic radicals.

In contrast to the direct nature in which fundamental information is gained from the hyperfine splitting pattern and the coupling constants, the conditions directly influencing the g-factor are often hard to quantify, but the qualitative aspects are understood.[54,55] Therefore, the g-factor is often utilized as an empirical parameter very useful for correlating electronically similar radicals. An excellent example of this is provided in the octafluorocyclooctatetraene radical anion study (page 109).

Although isotropic interactions have been assumed up to this point, when a radical is not reorienting rapidly on the ESR time-scale, an anisotropic hyperfine pattern will usually replace the isotropic pattern thus far assumed. This breakdown of the simple isotropic pattern, although complicating the ESR spectrum, is not necessarily undesirable, since it often leads to a more precise understanding of the spin distribution in the radical.

Anisotropy may arise either in the g tensor from coupling of the spin angular momentum with the orbital angular momentum or in the hyperfine tensor from a dipole-dipole interaction between the unpaired electron and the magnetic nuclei.[56,57] In either case, the characteristic feature of anisotropy is that for a given radical the resonances become angularly dependent; that is, the scalar quantities g and A are no longer appropriate and must be replaced with a tensor. Anisotropy in g will be considered first, followed by a discussion concerning hyperfine anisotropy.

Both the spin angular momentum and the orbital angular momentum may be thought of as vector quantities and may be labeled $\overline{M}_S$ and $\overline{M}_L$, respectively. Whereas $\overline{M}_S$ is always oriented with the field, $\overline{M}_L$, which is associated with the electrons moving in molecular orbitals, is tied to that molecular framework. In general, since the magnitude of $\overline{M}_S$ is much greater than $\overline{M}_L$, the directional character of the net moment which is simply $\overline{M}_S \cdot \overline{M}_L$, is primarily determined by $\overline{M}_S$ and the perturbation by $\overline{M}_L$ may be incorporated into

the g value. Thus the spin term of Equation (17), $g\beta H\bar{S}_z$, may be rewritten as

$$\beta S \cdot g \cdot H \tag{20}$$

or

$$\beta[S_x S_y S_z] \begin{bmatrix} g_{xx} & g_{xy} & g_{xz} \\ g_{yx} & g_{yy} & g_{yz} \\ g_{zx} & g_{yz} & g_{zz} \end{bmatrix} \begin{bmatrix} H_x \\ H_y \\ H_z \end{bmatrix} \tag{21}$$

An ESR spectrum represents transitions between energy levels, and energy is a scalar value, but the quantity $\bar{g}\cdot\bar{H}$ is a vector. Since the square of the magnitude of a vector is obtained by taking the scalar product of the vector with itself, the vector quantity $\bar{g}\cdot\bar{H}$ may be related to the scalar quantity of energy by

$$(\Delta E)^2 = \beta^2 \, (\bar{H}\cdot\bar{g}) \cdot (\bar{g}\cdot\bar{H}) \tag{22}$$

which leads to

$$(\Delta E)^2 = \beta^2 \, \bar{H}\cdot\bar{g}^2\cdot\bar{H} \, . \tag{23}$$

The elements of the $\bar{g}^2$ tensor, which is a true tensor mathematically speaking, may be obtained by successive rotations of a single crystal along arbitrary xz, yz, and xy planes. For example, a rotation of the crystal about an arbitrary x axis with the magnetic field in the yz plane, and where θ is the angle between the direction of the applied field and the z axis of the crystal, it can be shown that the effective g value (g_{eff}) for this rotation can be described by

$$g_{eff}^2 = (\bar{g}^2)_{yy} \sin^2\theta + 2(\bar{g}^2)_{yz} \sin\theta \cos\theta + (\bar{g}^2)_{zz} \cos^2\theta \tag{24}$$

where g_{eff} corresponds to the center of the pattern. By deriving similar equations for rotations about the y and z axes, the other

elements of the $\bar{g}^2$ tensor may be obtained. Once all of the components are determined, the matrix may be diagonalized to obtain the principle components of the tensor, namely g_{xx}, g_{yy}, and g_{zz}.

It should be noted that even when the ground state of a molecule possesses no orbital angular momentum, field-induced mixing with either filled or unfilled orbitals can lead to significant anisotropy in g. Equation (25) is a simplified equation useful for describing the interactions of the ground state with other electronic states and how these interactions would affect the g value. Assuming the field is along the z axis,

$$g_z = 2.0023 + 2\lambda \sum_n \left(\frac{\langle\psi_o|\bar{L}_z|\psi_n\rangle\langle\psi_n|\bar{L}_z|\psi_o\rangle}{E_{(o)} - E_{(n)}}\right) \qquad (27)$$

where $\psi_o\rangle$ is the ground state wave function, $\psi_n\rangle$ is the state that is mixing in with the ground state, $E_{(o)}$ and $E_{(n)}$ are energies of the respective states, λ is the spin-orbital constant, and $\bar{L}_z$ is an orbital angular momentum operator. Since λ and the numerator are generally positive, if the interaction is primarily with filled orbitals then $E_{(n)} < E_{(o)}$ and there will be a positive g-shift. A negative g-shift, on the other hand, signifies orbital mixing with unfilled orbitals. An example of the qualitative utility of Equation (25) is discussed in conjunction with the radical cations of tetramethyltin and tetramethyllead, page 202.

To mathematically describe hyperfine anisotropy, a dipolar term is added to the spin Hamiltonian where

$$\bar{H}_{dipolar} = - g\beta g_N \beta_N \left[\frac{\bar{S}\cdot\bar{I}}{r^3} - \frac{3(\bar{S}\cdot\vec{r})\ (\bar{I}\cdot\vec{r})}{r^5} \right] \qquad (26)$$

where $\vec{r}$ is the radius vector and r is a scalar distance between the nucleus and a fixed electron. Once the dipolar tensor is added to A, which has been assumed to be a scalar up to this point, the hyperfine interaction term becomes a tensor, $\bar{A}$, which may be described as

$$\bar{A} = \bar{T} + A\bar{1} \qquad (27)$$

where $\bar{T}$ is the dipolar component and $\bar{1}$ is a unit vector. In the strictest sense $\bar{A}$ is not a tensor, whereas $\bar{A}^2$ is a true tensor.

The elements of the $\bar{A}^2$ tensor may be obtained by a procedure very similar to the one outlined for determining the elements of the $\bar{g}^2$ tensor. Once the tensor is diagonalized, the trace of the $\bar{A}$ tensor will correspond to A_{xx}, A_{yy}, and A_{zz}.

If the powder pattern of a radical is observed, then the turning points in the first-derivative pattern correspond directly to the principal values of $\bar{A}$. In this case rotation of the sample in the cavity should not change its ESR spectral appearance.

In either case, once the principal values are known, then the hyperfine tensor, $\bar{A}$, can take on the very simple form

$$\begin{bmatrix} A_{xx} & 0 & 0 \\ 0 & A_{yy} & 0 \\ 0 & 0 & A_{zz} \end{bmatrix} = \begin{bmatrix} A_{iso} & 0 & 0 \\ 0 & A_{iso} & 0 \\ 0 & 0 & A_{iso} \end{bmatrix} + \begin{bmatrix} A_{xx}-A_{iso} & 0 & 0 \\ 0 & A_{yy}-A_{iso} & 0 \\ 0 & 0 & A_{zz}-A_{iso} \end{bmatrix} \qquad (28)$$

where the first term on the right-hand side is the isotropic tensor and second term is the anisotropic part of the tensor. Incidentally, if $\overline{A}$ were not diagonalized, then the off diagonal terms of $\overline{A}$ would not necessarily be equal to zero.

One case often encountered in analyzing anisotropic spectra is where $A_{xx} = A_{yy}$ and $A_{xx} \neq A_{zz}$. In this case the anisotropic term of the tensor takes the form

$$\begin{bmatrix} -B & 0 & 0 \\ 0 & -B & 0 \\ 0 & 0 & +2B \end{bmatrix} \tag{29}$$

where B is called the anisotropic hyperfine coupling constant and the hyperfine tensor is said to be axially symmetric and the following formalisms are generally applied: $A_{\perp} = A_{xx} = A_{yy}$ and $A_{//} = A_{zz}$. The g value is also defined as $g_{\perp} = g_{xx} = g_{yy}$ and $g_{//} = g_{zz}$. It should also be noted that

$$A_{iso} = \frac{1}{3}(A_{//} + 2A_{\perp}), \tag{30}$$

$$B = \frac{1}{3}(A_{//} - A_{\perp}), \text{ and} \tag{31}$$

$$g_{iso} = \frac{1}{3}(g_{//} + 2g_{\perp}) \quad . \tag{32}$$

Just as A_{iso} is directly proportional to the s-spin density on that magnetic nucleus, the anisotropic B parameter is directly proportional to the p-spin density by the simple relation

$$\rho_p = \frac{B}{B_o} \tag{33}$$

where the values of B_o (Table I) are obtained from semi-empirical calculations using atomic wave functions. In this case the value of B_o is obtained by solving the equation below:[52]

$$B_o = \frac{2}{5} h^{-1} g\beta g_N \beta_N \langle r^{-3} \rangle \qquad (34)$$

In the present work, an axially symmetric hyperfine tensor was found appropriate for radicals where there was rapid rotation about only one axis or for radicals where the unpaired electron was primarily located in a single bond.

It should be noted that anisotropic interactions can be removed if the entire molecular system is rotating on two orthogonal molecular axes faster than the ESR time scale. This motional requirement is generally achieved if the radical is generated in the liquid phase or sometimes in the solid state when the radical can rotate quickly enough--especially if the radical is in a cavity in the matrix as in adamantane[58,59] or the matrix is moving quickly itself as in SF_6.[60] Radicals generated in the gas phase, although always isotropic, are complicated by coupling to rotational energy levels. It should be noted that although a high degree of molecular motion can eliminate the observation of anisotropic hyperfine interactions, the anisotropic hyperfine interactions still exist in the radical, that is, the distribution of the unpaired electron in the radical remains essentially independent of molecular motion, but the anisotropic interactions are just averaged to zero by the motion.

TABLE I

SELECTED PROPERTIES OF MAGNETIC NUCLEI[a]

Nucleus	Spin (I)	% Natural Abundance	Nuclear g Factor	A_o (G)	B_o (G)
^{1}H	1/2	99.9844	5.58536	508	--
^{2}H	1	0.0156	0.857387	78	--
^{13}C	1/2	1.108	1.40440	1348	38.3
^{14}N	1	99.635	0.40347	647	19.8
^{15}N	1/2	0.365	-0.56596	-907	-27.8
^{19}F	1/2	100.0	5.25454	18875	628
^{29}Si	1/2	4.70	-1.1095	-1640	-40.8
^{33}S	3/2	0.76	0.42838	1236	35.9
^{35}Cl	3/2	75.53	0.54727	2043	62.7
^{37}Cl	3/2	24.47	0.4555	1701	52.2
^{73}Ge	9/2	7.76	-0.19484	844	17.2
^{79}Br	3/2	50.54	1.3993	11449	292
^{81}Br	3/2	49.46	1.5084	12342	315
^{115}Sn	1/2	0.35	-1.8264	-13756	-229
^{117}Sn	1/2	7.61	-1.9898	-14987	-250
^{119}Sn	1/2	8.58	-2.0818	-15680	-261
^{129}I	5/2	100.0	1.1175	14850	290
^{207}Pb	1/2	22.6	1.16857	29100	232

[a]Taken or calculated from reference 51.

If none of the principal components are the same, then the radical is said to be totally anisotropic and the radical may spectroscopically show three different principal values of the anisotropic hyperfine interaction, termed A_{xx}, A_{yy}, A_{zz}, and three different g values, termed g_{xx}, g_{yy}, g_{zz} (often these values are abbreviated as A_x, A_y, A_z, and g_x, g_y, g_z). The isotropic values are obtained by

$$g_{iso} = \frac{1}{3}(g_x + g_y + g_z) \tag{35}$$

$$A_{iso} = \frac{1}{3}(A_x + A_y + A_z) \tag{36}$$

Although first-order interactions have been assumed up to this point, when for a radical (A^2/H) is greater than the spectral line width by a factor of about 0.1 where H is the magnetic field at that resonance, then a simple first-order analysis is no longer appropriate and a higher-order analysis becomes necessary. This breakdown of the simple first-order pattern, although complicating the ESR spectrum, is not necessarily undesirable since it allows for a firmer identification of the radical and in certain cases allows the relative signs of the coupling constants to be determined.

When the coupling constants become large, the measured spacings between the resonances are no longer equal to A which is the physically significant parameter. Therefore, a more precise analysis is needed to obtain the spectral parameters.[61,62] In this case, the precisely correct equation describing the observed transitions is

$$h\nu = g\beta H + hAM_I + \frac{(I^2 + I - M_I^2)\, hA^2}{D} + \frac{C_3 hA^3}{D^2} + \frac{C_4 hA^4}{D^3} \ldots . \quad (37)$$

The terms C_3 and C_4 in Equation (37) are defined elsewhere.[61] A less exact but very useful form of Equation (37) for a preliminary analysis is

$$h\nu = g\beta H + hAM_I + \frac{(I^2 + I - M_I^2)\, hA^2}{2g\beta H} \quad . \quad (38)$$

Use of Equation (38) is termed a second-order analysis and is easily performed manually. An exact solution of the spin Hamiltonian is usually obtained using standard programs (such as the one described later) and a digital computer. By defining $H_o = (h\nu/g\beta)$ and by converting A from energy units to Gauss, Equation (38) may be rearranged to yield

$$H(I,M_I) = H_o - AM_I - \frac{(I^2 + I - M_I^2)\, A^2}{2H} \quad (39)$$

Using the coupled approximation, I is bounded by I_{total}, $I_{total} - 1$, . . . , 1/2 or 0 where I_{total} is the sum of the absolute values of the M_I's for a group of equivalent nuclei and M_I is the sum of the M_I values for a group of equivalent nuclei with the values $M_I = I_{total}, I_{total} - 1, \ldots, -I_{total}$. An instructive example is a $R\text{-}CH_2\cdot$ type radical for which there are two equivalent spin 1/2 nuclei. In this case, I can take on values of 1 and 0 while M_I takes on values of 1, 0, -1. Taken together, four (I, M_I) combinations are possible, namely (1,1), (1,0), (0,0), and (1,-1). The

line positions for these four cases, correct to second-order, using Equation (39) are $H_o - A - \frac{A^2}{2H}$, $H_o - \frac{A^2}{H}$, H_o, $H_o + A - \frac{A^2}{2H}$ and the intensities of each of these four cases may be determined by an equation given elsewhere.[63]

Whereas the first-order treatment described earlier predicted a 1:2:1 triplet for a $R\text{-}CH_2\cdot$ type radical, the present analysis would predict that if the splitting between the $M_I = 0$ resonances ($A^2/H>$ line width) can be resolved then the observed pattern would be a 1:1, 1:1 quartet.

Of course, it is possible for a radical to show both anisotropic and higher order effects. When both anisotropic hyperfine interactions and higher-order effects are significant, the spectral features are characterized by resonances which are again shifted to lower field while still retaining the line shape characteristic of anisotropic spectra. The only cases which fell into this class of radicals from this work were radicals which possessed an axially symmetric hyperfine tensor; therefore only this case will be discussed in the second-order approximation.

As previously discussed, if the resonances are isotropic, then for a given transition the magnitude of the down-field shift is directly proportional to the square of the magnitude of A_{iso} and is inversely proportional to the magnetic field strength for the transition (Equation 39, page 27). But when the radical exhibits an axially symmetric hyperfine tensor, the two transitions, namely the parallel and perpendicular resonances, must be considered

independently since the shift is different for each component. For the parallel transitions the down-field shift (ΔH) is directly proportional to the square of $A_\perp$ and is inversely proportional to the magnetic field strength for the transition, as given by

$$\Delta H_{//} = (I^2 + I - M_I^2) \frac{A_\perp^2}{2H} . \tag{40}$$

For the perpendicular resonances, the down-field shift is directly proportional to the square of both $A_\perp$ and $A_{//}$ and is inversely proportional to the magnetic field strength for the transition, as given by

$$\Delta H_\perp = (I^2 + I - M_I^2) \frac{A_\perp^2 + A_{//}^2}{4H} . \tag{41}$$

D. Partial Orientation

ESR studies on radicals which show anisotropic hyperfine interactions are conventionally carried out on samples which are either completely oriented, as is the case for single crystals, or randomly oriented solids. Examples of the latter case are glasses which can be considered as liquids of high viscosity and solids in the form of very fine powders. Of course, in principle, there is a vast region between these two extremes in which the solid samples are only partially oriented. The effect of partial orientation is to blend the spectral appearance of randomly oriented samples with those of single crystals, but since the amount of blending is often unpredictable, the ESR spectral appearance of the partially oriented samples

is likewise unpredictable and, consequently, can easily lead to misassignments. In fact, one of the early experimental demonstrations of partial orientation[64] was the result of an initial misinterpretation. Essentially, a complicated ESR spectrum of a frozen solution of a low-spin Co(II) complex in chloroform was interpreted as arising from delocalization of the unpaired electron over the chelate rings.[65] Other authors found that the complex spectra appeared if the sample solution was boiled and disappeared if toluene was added prior to freezing.[66] Fierz and von Zelewsky argued that the real cause of the appearance or disappearance of the complicated ESR spectra was neither the boiling of the solution nor the addition of toluene, but rather dependent upon the degree of randomness of the solid sample.[64] They concluded that, if the sample was composed of crystallites, all of which were sufficiently small, then the contribution from all the crystallites would add together to give an almost random mixture, yielding a smooth absorption envelope. However, if the sample contained a crystallite which exceeded this sufficiently small size, then the absorption envelope would no longer be smooth, and additional resonances would be observed in the ESR spectra. Confirmation of this idea was obtained by Belford and Davis[67] who demonstrated that partial orientation could be generated by grinding a single crystal into a powder even though the crystallites were no larger than about 10^{-5} mm^3.

Several other authors have also documented the effects of partial orientation. In contrast to this early report where the

effects of partial orientation are minimal, a very striking textbook example of partial orientation was reported for the $CF_2 = CFBr^-$ radical anion where a 90° rotation along the sample tube axis could completely discriminate between either the parallel or perpendicular components of the hyperfine tensor.[68] In this particular case and in other cases[69] where partial orientation was observed, the effects of partial orientation assisted the ESR spectral analysis by identifying the resonances belonging to each set of anisotropic components.

To better understand the effects of partial orientation, the two extremes will first be considered, that is, total ordering from a single crystal and random order from a powder sample. This will be followed by a qualitative description of partial orientation.

If all of the radicals in a solid sample are oriented identically in the lattice structure as for a single crystal, all of the radicals will absorb microwave energy at the same fields. Although rotation of the crystal on its axes may change the magnetic field positions at which resonance is achieved, all of the radicals will still resonate in concert.

The spectral characteristics of radicals formed in a single crystal are symmetric line shapes associated with sharp and intense resonances. The symmetric line shape results from the singularity of the field position at which resonance is achieved. Since all of the radicals resonate at the same field positions, the microwave absorption profile resembles a Lorentzian curve as shown in Figure

2a. In general, ESR spectra are recorded as first derivatives of the absorption curve (Figure 2b). Since the integrated area under an absorption pattern is directly proportional to the number of radicals, it follows that if the width of the resonance is increased, as in Figure 2c, such as from some incoherence from a large number of lattice imperfections, the first-derivative pattern intensity will decrease (Figure 2d) although the integrated area under the curve remained constant. An approximate correlation of first-derivative signal intensity (I) to line width (LW)[70,71] is

$$I \alpha 1/(LW)^2 \tag{42}$$

Of course, single crystals are often characterized by few lattice imperfections and thus the resonances are generally sharp, that is, within a narrowly defined field, and intense. The sharper the lines in a single crystal study, the better the definition of the spectrum with all of the components being well-resolved.

Although single crystals have several favorable characteristics, many radicals cannot be generated in single crystals either because the precursor molecule cannot form a regular crystal or the radical once formed would immediately react with a neighboring molecule. Also, single crystal studies are sometimes complicated by a large number of different radicals formed as a result of the irradiation. In other words, when radicals are generated in single crystals, there is often a lack of specificity in radical generation and this fact often translates into the observed ESR pattern being complicated by resonances from several different radicals.

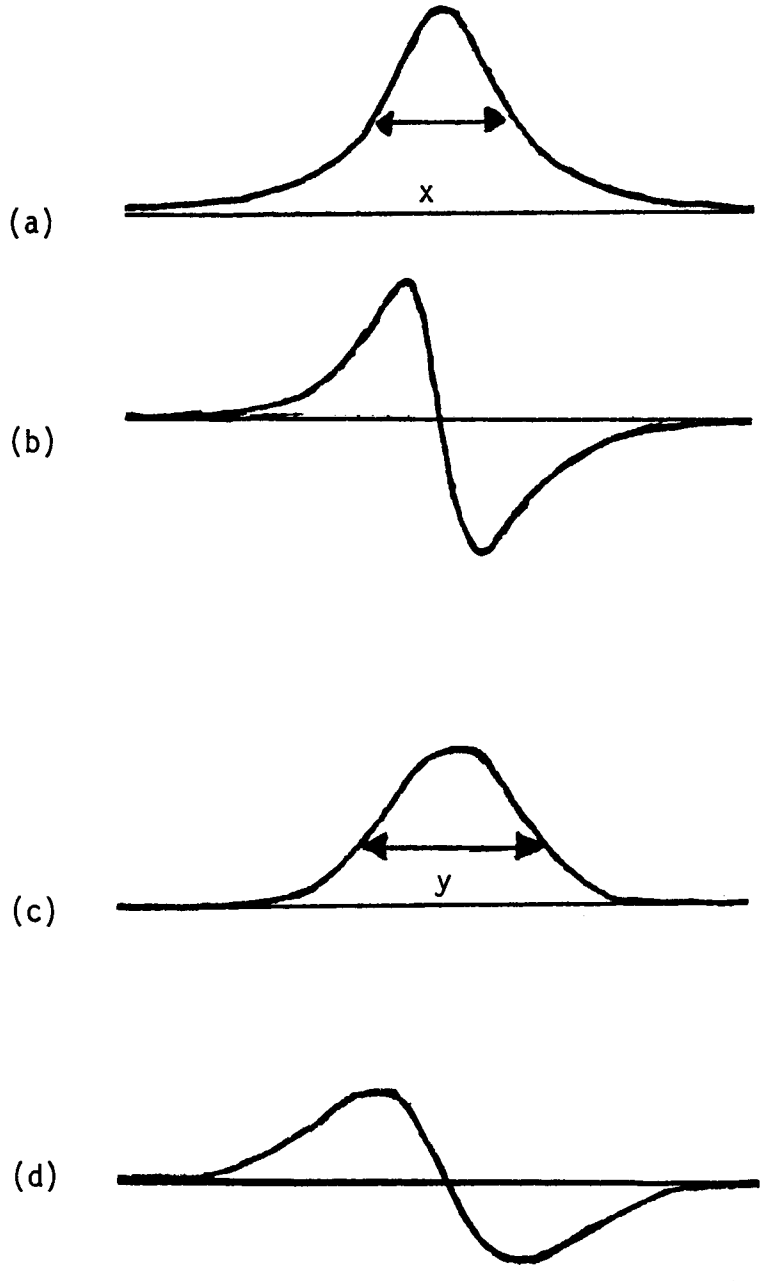

Figure 2. The absorption (a and c) and first derivative curves (b and d) for a resonance with a linewidth of x and y, respectively, are shown where $y > x$. Note the drop in first derivative signal height.

On the other hand, the matrix isolation technique has some advantages over the use of single crystals in terms of more specific radical generation, as previously mentioned, and in isolating the radicals from further reaction. Without some form of a director, the solute molecules in the matrix isolation technique are randomly oriented in the sample. In a randomly oriented sample, it is found that the radicals will resonate between a continuum bounded by the maxima and minima of the hyperfine interaction, assuming for the sake of simplicity an isotropic g factor. Consequently, the absorption pattern is not the simple absorption curve typical of single crystal spectrum but rather consists of an absorption envelope with characteristic features which are related to the g and hyperfine ESR parameters.

The spectral characteristics of radicals formed in randomly oriented matrices often consist of complex lineshapes associated with broad, weak resonances.[70,71] The simplest case of a radical showing an anisotropic interaction would be a radical without any magnetic nuclei (thereby eliminating hyperfine interactions) but having an axially symmetric g tensor. In this case the radical would be characterized by the following absorption pattern, Figure 3a, and first-derivative pattern, Figure 3b, with the two turning points, or peaks, corresponding to $g_{//}$ and $g_{\perp}$. Another simple case showing hyperfine anisotropy is one in which there is an axially symmetric hyperfine interaction with one magnetic nucleus having spin I = 1/2 but no g anisotropy, Figures 3c and 3d. Further

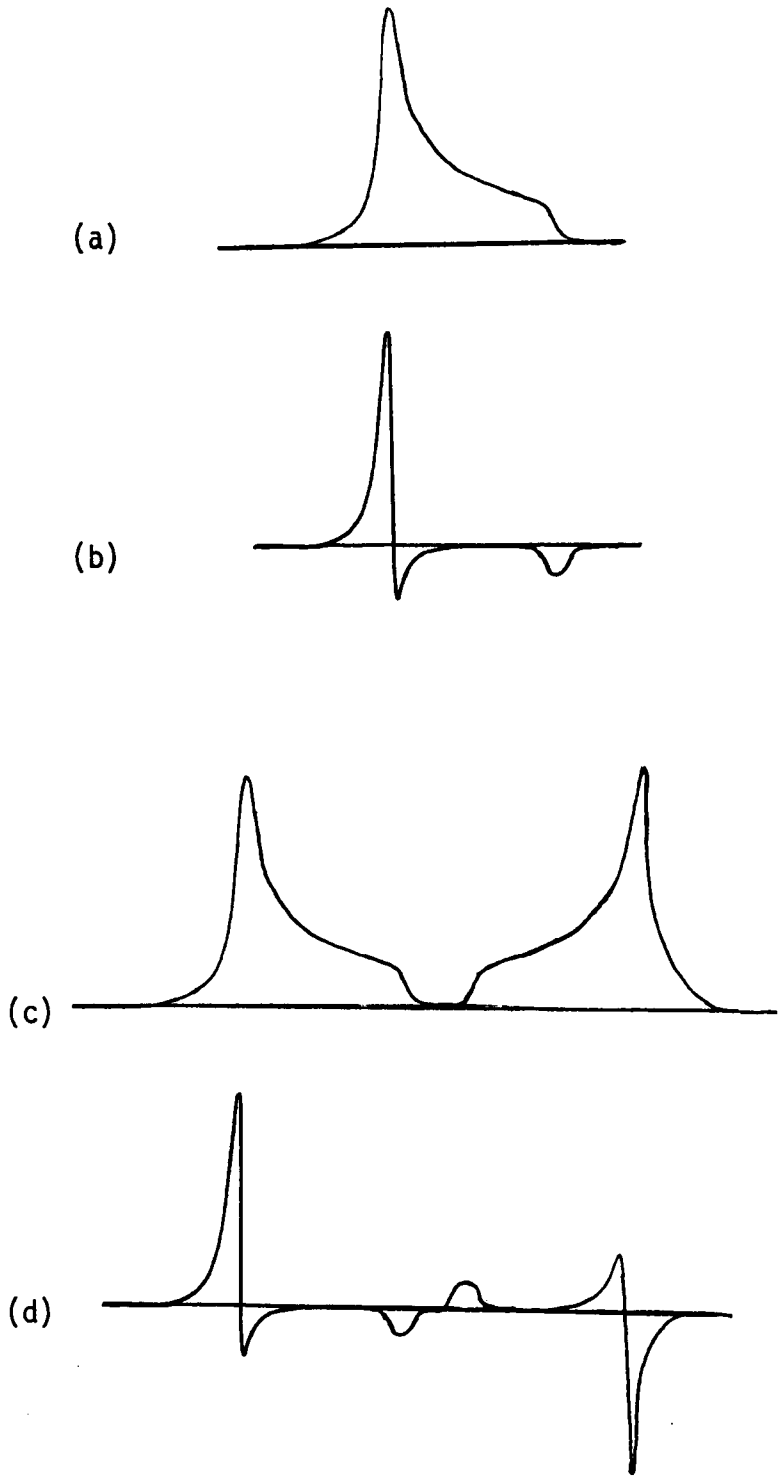

Figure 3. Absorption lineshape (a) and first-derivative curve (b) for a randomly oriented system having an axis of symmetry and no hyperfine interaction ($g_{\perp} > g_{//}$). Absorption lineshape (c) and first-derivative curve (d) for a randomly oriented system having an axis of symmetry and a hyperfine interaction to one nucleus of spin 1/2 where $A_{\perp} > A_{//}$ and $g_{\perp} = g_{//}$.

examples of anisotropic hyperfine interactions quickly become quite complex, and many of these cases are discussed elsewhere.[70,71]

Since the integrated area under the absorption pattern is directly proportional to the radical concentration, the intensity of the features in the first-derivative powder pattern is critically dependent upon the separation between the maxima and the minima of the anisotropic ESR absorption.[71] In contrast to the single crystal line width, which is sometimes less than 1 G, non-oriented samples can have a spread in the anisotropy of over 100 G, especially for halogen-containing radicals. This spread in the anisotropy can very profoundly affect the intensity of the ESR pattern. For example, by use of the approximate Equation (42), page 32, if a single-crystal resonance with a 1 G line width and a randomly oriented radical with a 20 G spread in its anisotropy are compared, then to achieve a comparable observed signal intensity the radical giving rise to the powder pattern would need a 400 times greater radical concentration than in the single crystal. In cases when the spread in the hyperfine anisotropy exceeds 100 G, the radical, although present, may be undetectable in the powder ESR spectrum because its observed first-derivative signal height is lower than the inherent noise level of the spectrometer.

The technique of partial orientation can be applied not only to pure substances but also to solid solutions. In the latter case, orientation of the solute molecules arises not by the crystallization of the precursor molecule with itself, as is the case for pure

substances, but rather through positioning of the solute molecules in the host lattice crystallites. Hence, the important consideration for a successful experiment is how to orient the solute molecule in the host material. One simple technique is to slowly cool the matrix through its freezing point (see Experimental section for details).

Several factors influence the effectiveness of the partial orientation technique. Since the precursor or solute molecule can be viewed as an impurity and impurities generally disrupt crystal formation, the concentration of the solute molecule should be minimized. Exclusion of the solute from the matrix during the crystallization procedure can be minimized by either picking a solvent in which the solute is more soluble or by reducing the freezing time. In addition to factors such as concentration, solvent, and freezing technique, the degree of crystal propagation also determines the degree of orientation produced in the sample. Therefore some element of chance is often involved in obtaining a preferentially oriented sample since a small increase in orientation can bring about a dramatic enhancement in the intensity of the features in a powder pattern. Qualitatively, the effect of partial orientation is more significant the greater the spread in anisotropy. For example, the outermost parallel components of the CF_3Br^- radical anion[7] which was first reported in a randomly oriented sample have a spread in anisotropy of 300 G-330 G and were barely observable; however, in the present study by use of partial orientation these

features were often readily resolved. By comparing the signal height of these outermost resonances of CF_3Br^- in a partially oriented sample with a non-oriented sample having the same CF_3Br concentration and the same γ-irradiation dose, a rough estimate of the enhancement factor due to partial orientation can be made. A comparison of this type revealed that in one instance the enhancement was about a factor of 20. In one extreme case, the enhancement factor turned out to be about 35, but in this case the lineshape changed from the typical parallel lineshape to a symmetric lineshape much like what is observed in single cyrstals. Although the effects of partial orientation are seldom this significant with other solute-matrix combinations, samples which are less oriented often allow different anisotropic features to be maximized by rotation of the sample tube in the magnetic field.

Partially oriented samples, under favorable conditions, possess spectral characteristics of both single crystal spectra, that is, intense resonances which are angularly dependent in the magnetic field, and orientation-dependent powder spectra. In the former instance, the resonances of the angularly dependent anisotropic hyperfine interactions will, upon rotation of the sample in the cavity, shift from one extreme to the other just like typical single crystal samples. On the other hand, for an orientation-dependent powder pattern, the resonance positions defining the envelope remain fixed but the characteristic features will decrease or increase in intensity upon rotation of the sample tube in the

magnetic field. Generally, the more symmetric the lineshape appeared, the more likely the resonances were to shift with rotation of the sample tube as in single crystals. On the other hand, spectra which appeared to possess lineshape features similar to those of typical powder patterns often displayed the orientation-induced enhancement effect. The effect of partial orientation is clearly shown in Figure 4. Note that the maximum intensity of the parallel features falls dramatically with even a small change in angle. Also note that a rotation of the sample tube through 90° maximized the perpendicular components with a corresponding fall in the intensity of the parallel components. Although not shown, the original spectrum was regained after a further rotation of 90°, as expected.

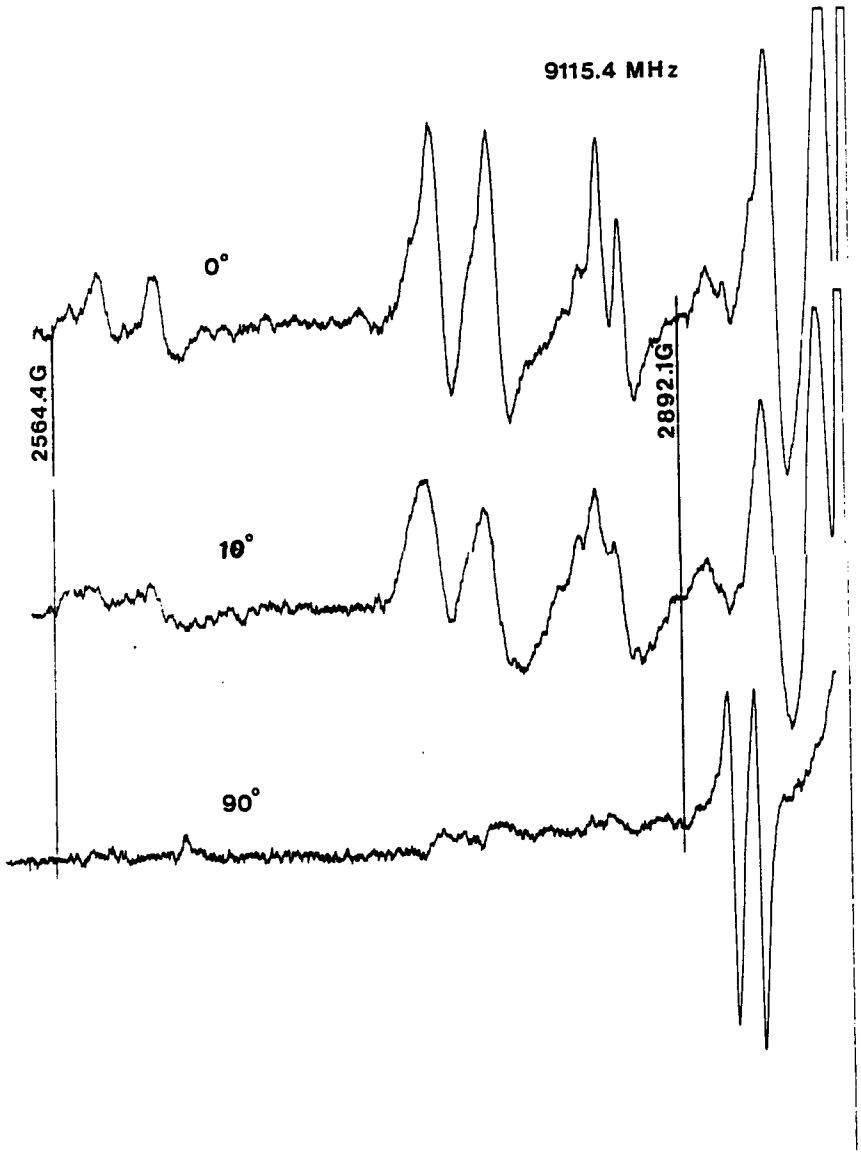

Figure 4. The low-field portion of some first-derivative ESR spectra of a partially oriented sample of CF_3Br^- in TMS-d_{12} at different orientations in the cavity. The complete and analyzed ESR spectra for this radical are shown in Figures 9 and 10, pages 61 and 62.

CHAPTER II

EXPERIMENTAL CONDITIONS

A. ESR Spectrometer and Accessories

The X-band ESR spectra included in this dissertation were obtained with two different ESR spectrometers. Initially, spectra were obtained on a Varian V-4502-15 spectrometer. In the summer of 1982, a new Bruker 200-D spectrometer was installed and used exclusively thereafter. The Bruker spectrometer without computer-signal averaging has about a 20:1 better signal to noise ratio than the older Varian instrument. For each spectrometer, a standard variable-temperature system was used with a rectangular cavity. This consisted of a clear quartz dewar inset which operated between 80 K to 450 K, as shown in Figure 5.

On the Varian instrument, magnetic fields were determined by means of an added Walker/Magnemetrics G-502 NMR gaussmeter using either a Systron-Donner 1037 frequency counter or the newer Systron-Donner model 6054 B frequency counter in the MHz range. The resonating spectrometer frequency at 9.1-9.5 Ghz could be determined during an experiment using either counter; for the Systron-Donner 1037 system a special 1255 A ACTO (transfer oscillator) plug-in unit was needed to obtain the high-frequency range, whereas for the newer Systron-Donner 6054 B counter, the higher frequency range was a standard feature of the equipment. Since the Bruker

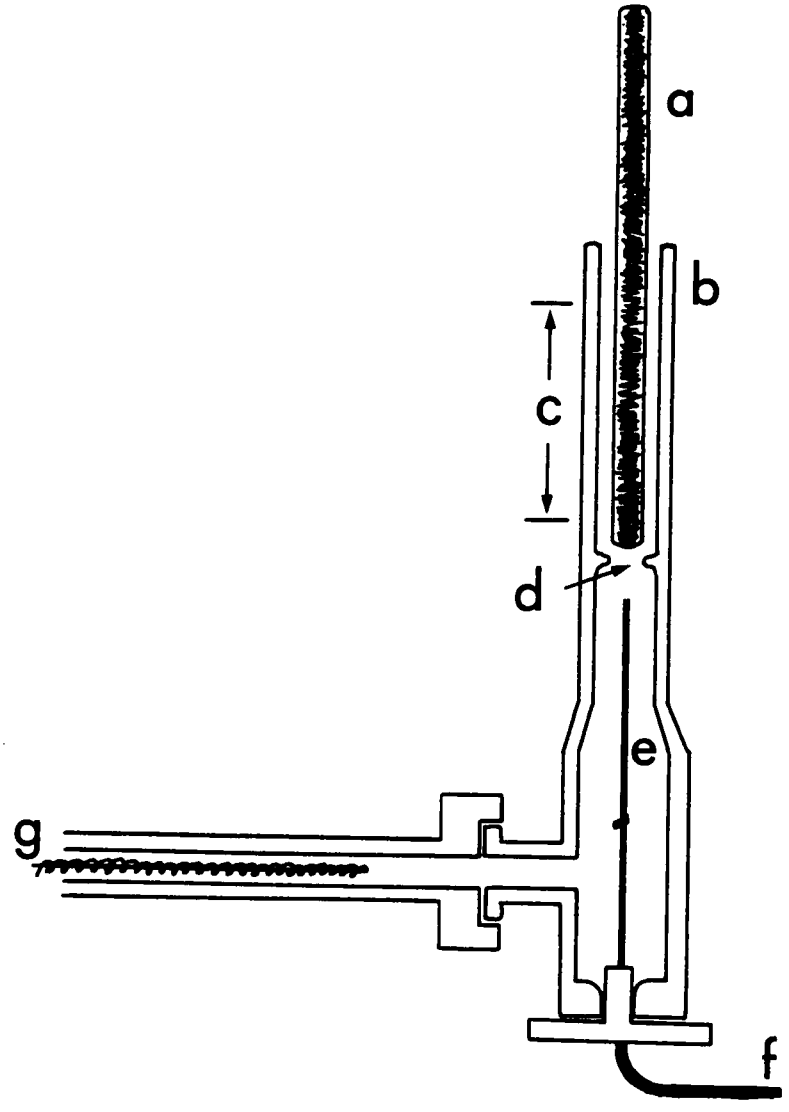

Figure 5. Diagram of ESR quartz insert dewar and peripheral equipment: (a) sample, (b) quartz insert dewar, (c) sensitive region of the cavity, (d) constriction which holds sample tube, (e) thermocouple, (f) to temperature controller, and (g) heater.

spectrometer did not initially come equipped with a field calibration system, the previously described system was also used on the Bruker spectrometer. Once the Bruker ER-035 M modular field calibration unit was installed, it was used exclusively together with one of the high frequency counters. The system was checked with standards such as diphenylpicrylhydrazyl[72] (g_{iso} = 2.0037) and Fremy's salt[73] (g_{iso} = 2.00550, A_{iso} (1 N) = 13.09 G). See Figure 6 for a typical calibration. Also the hydrogen-atom lines can provide an internal standard for most γ-irradiated samples, in quartz tubes although these lines generally decayed around 120 K.

Occasionally in the course of this work it was found necessary to study the temperature-dependence of the ESR spectrum below 80 K. For studies between 3.9 K and 80 K, an Oxford Instruments ESR-900 continuous flow cryostat coupled with a DTC-2 digital temperature controller was used in conjunction with a Minnesota Valley Engineering triple-walled 30 liter liquid helium dewar. This system could easily maintain temperatures above 4.5 K.

All Q-band spectra were obtained using a Strand Labs Inc. spectrometer equipped with a Janis dewar to maintain sample temperatures of about 77 K. This spectrometer was located in the Solid State Division of Oak Ridge National Lab. There was no built-in device to measure the temperature in the cavity and this deficiency led to some initial false starts, probably owing to the temperature being much greater than 77 K. A thermocouple was introduced into the cavity to measure the temperature, but since the thermocouple

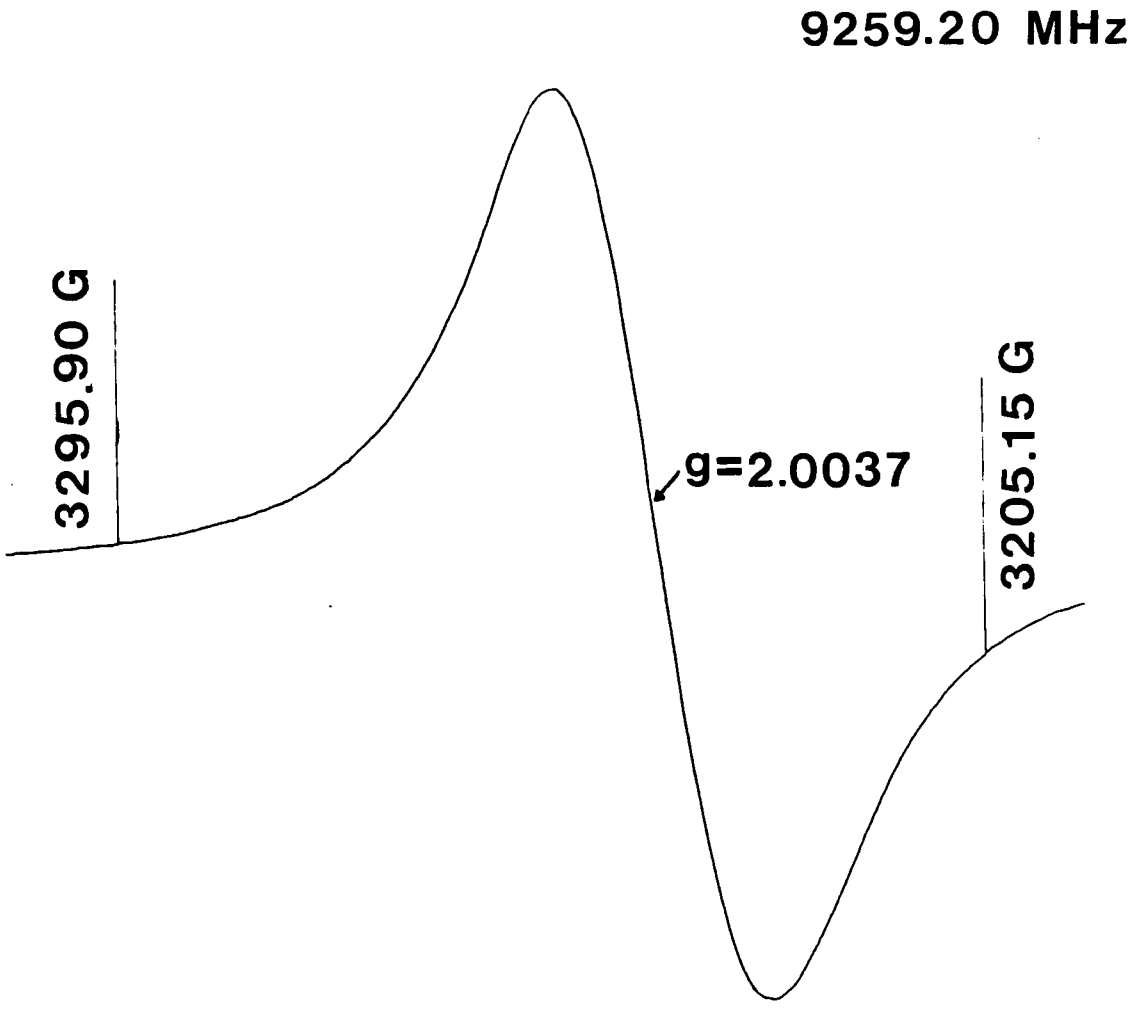

Figure 6. First-derivative ESR spectrum of a sample of DPPH. Sweep with = 100 G, sweep time = 5000 seconds, power level = 29 dB, and modulation = 2.5 G.

was introduced into the cavity through the same hole that the sample was introduced into the cavity, both the temperature and the sample could not be monitored simultaneously. To cool the cavity, filtered liquid nitrogen was poured directly into the cavity. A description of the standard procedure follows. First, the cavity was cooled to near 77 K by introducing the liquid nitrogen, then the temperature was checked. If the cavity was sufficiently cooled, then the sample was introduced and observed spectroscopically. After the sample was removed, the temperature was re-checked to verify that no temperature change had occurred during the course of the examination. The spectrometer frequency was determined by an EIP 548 Band 3-4 frequency counter. Magnetic fields were calculated using a calibration method based upon the magnetic field positions of the hydrogen atom[74] lines, using $g = 2.00233$ and $A_{iso} = 507.8$ and allowing for a second-order shift.

In some instances, it was of interest to expose the samples to either visible or UV light while they were constantly being monitored in the ESR cavity. Visible light, that is, radiation with wavelengths between about 400 to 800 nm, was generated from a 1000 W tungsten lamp which was focused into the cavity with a large lens. Ultraviolet light, on the other hand, was generated from a high pressure mercury arc lamp. Suitable filters purchased from Corning Glass Works were utilized to isolate a particular band in the spectrum.

B. Sample Preparation and Gamma Irradiation Equipment

Only one vacuum system was used during the entirety of this work. A basic diagram is shown in Figure 7. A liquid nitrogen trap was always employed to prevent any back diffusion of gases from the pump oil and to prevent any toxic compounds from entering the work area. The vacuum line was often thoroughly checked and cleaned. From this vacuum system all of the ESR samples were prepared using standard techniques as described elsewhere.[75]

Although no single crystals were used in this work, samples with a high degree of partial orientation were often desired. To promote partial orientation in samples, a device designed to grow single crystals was modified such that instead of lowering samples into a thermostatically cooled bath the samples were simply lowered into a dewar of liquid nitrogen, as indicated in Figure 8. The basic design was that of Dahlgren, Gillbro, Nilsson, and Lund and has been previously described.[76] Thus, to increase the orientation, the rate of sample descension was reduced; however, the only limiting factor of this technique is that the rate of descension cannot be slower than the natural boil-off rate of the liquid nitrogen for that particular dewar.

In the course of this work, all of the samples were γ-irradiated in an Atomic Energy of Canada Limited Gammacell 200 ^{60}Co source. The dose rate was determined by Fricke dosimetry in August 1976 to be 0.24 Mrad/hr[77] where 1 Mrad = 10^4 Gray = 6.24×10^{19}

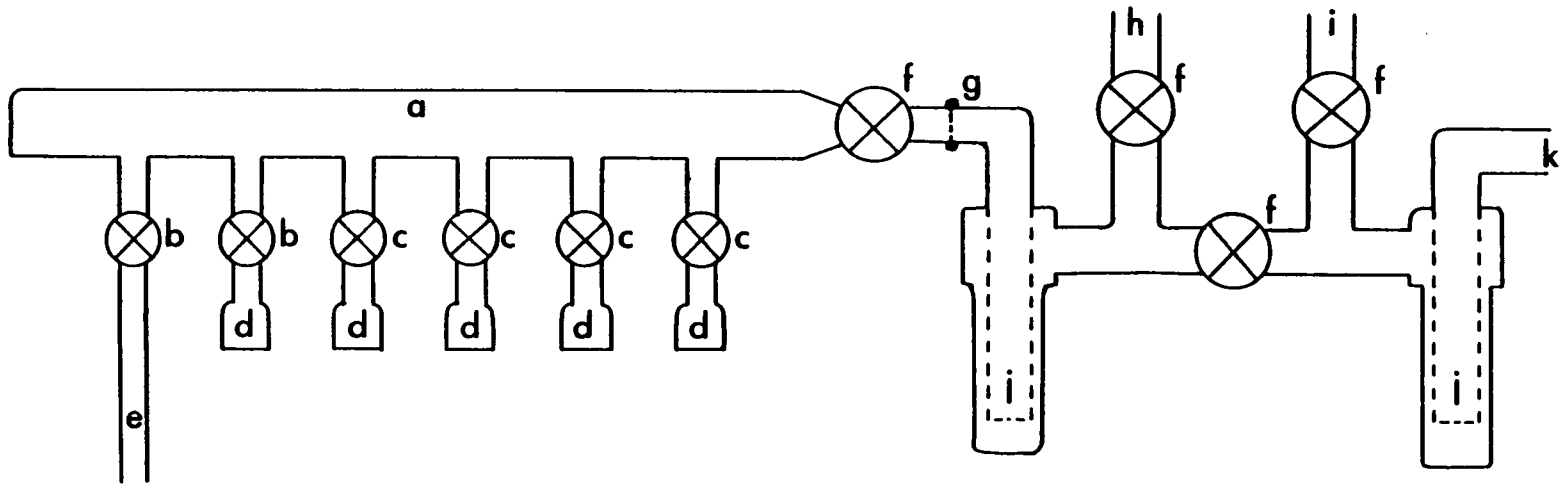

Figure 7. Standard vacuum line: (a) manifold, (b) 2 mm stopcock valves, (c) 4 mm stopcock valves, (d) 12/20 inner joints, (e) to Hg manometer, (f) 8 mm stopcock, (g) 19/24 junction, (h) to Hg diffusion pump, (i) return from diffusion pump, (j) liquid nitrogen trap, and (k) to vacuum pump.

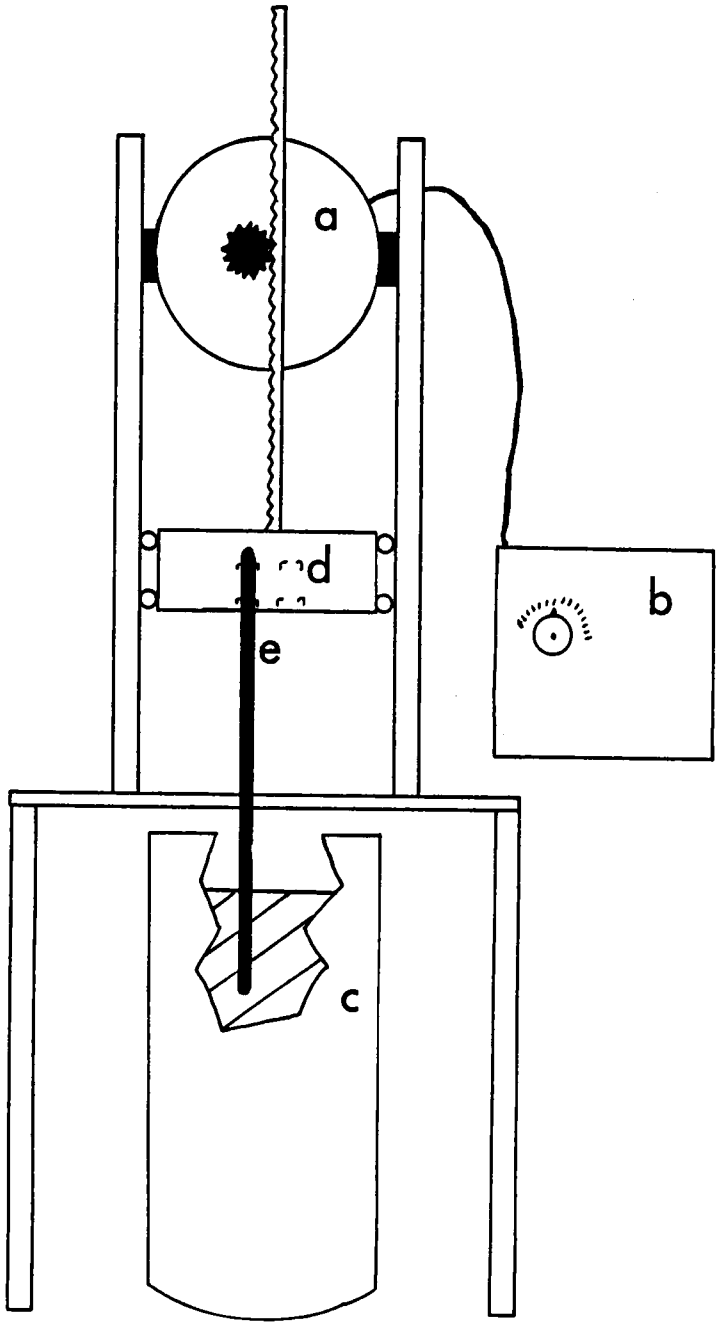

Figure 8. Slow cooling device with the following basic components: (a) step motor, (b) step motor controller, (c) liquid nitrogen dewar, (d) sample holder, and (e) ESR sample tube.

eV/g. Using the known half-life of 5.27 years[31] for ^{60}Co, the dose rate during this work ranged from 0.151 (April 1980) to 0.076 Mrad/hour (May 1984). With just a few exceptions, all samples were γ-irradiated at 77 K. The doses ranged from about 0.1 Mrad to about 5 Mrad with a typical dose being about 1.0 Mrad.

C. Miscellaneous Equipment

Mass-spectroscopic analyses were obtained using a Hewlett-Packard 5980 A Mass Spectrometer with data processing provided by a Hewlett-Packard 5934 A Data System. Mass values are reported accurate to $\pm$ 0.3 AMU. This instrument is located in the Department of Chemistry.

Accurate temperature determinations were often necessary in this research. The Bruker ESR spectrometer has a fully automated temperature sensing system unit, ER 4111 VT. The thermocouple which is mounted in the bottom of the cavity, see Figure 5, page 42, is a chromel-alumel thermocouple with a stated range of 64-999 K. Temperature measurements during an experiment using the Varian ESR instrument were achieved with an Air Products and Chemicals, Inc., Type CGI with a listed range of 1.0 to 280.0 K. A portable battery-operated Omega 2165 A Digital Thermometer was often useful to monitor slush bath temperatures. In each system, the temperature scales were tested with liquid nitrogen (77 K) and icewater (273 K). The Air Products device was also tested with liquid helium (4.2 K).

D. Computer Calculations

Almost all of the computer calculations performed during the course of this work utilized The University of Tennessee, Knoxville's computing facilities. Since the major thrust of this research was experimental in nature and since the programs utilized are standard programs, only a very brief description of the four different programs used will be given.

A standard CINDO program, obtained from Indiana University Chemistry Department through the Quantum Chemistry Program Exchange, was used to perform open-shell calculations either at the complete neglect of differential overlap (CNDO) level or at the intermediate neglect of differential overlap (INDO) level. This program which was originally developed by J. A. Pople[78] is a semi-empirical method of estimating the complete set of molecular orbitals (MOs) in a molecule or a radical where the MOs are built-up from the individual atomic orbitals (AOs) of the atoms in the molecule. For open shell calculations, the spin distribution in the radical is calculated from the nature of the semi-occupied molecular orbital (SOMO). This last piece of information is particularly important since it may be compared with the experimental results. At the CNDO level, molecules composed of hydrogen through chlorine (atomic numbers 1-17) may be calculated while calculations performed at the INDO level are limited to molecules composed of hyrogen through fluorine (atomic numbers 1-9). Valence shell basis functions (1s or 2s, 2p or 3s, 3p, 3d)

are used and up to 35 atoms or 80 basis functions are allowed per molecule or radical.

A short program modified by the author which calculates Cartesian coordinates from bond lengths, valence angles, and dihedral angles was useful to generate the input file for the CINDO program.

A computer program developed by Dr. Kerr allows the exact calculation of the magnetic field positions in an ESR spectrum by the diagonalization of the energy matrix of the full spin Hamiltonian. This program can accommodate up to three groups of non-equivalent nuclei with a total spin multiplicity of less than 51. This program can handle isotropic, axially symmetric, or anisotropic hyperfine and/or g tensors with coincident axes or axes oriented at 90° to one another. The ESR parameters may be refined by one of two methods. First, a fitting procedure was used which involved changing the g and hyperfine parameters until the calculated line positions corresponded, within experimental error, to the experimentally determined line positions. Second, by using the method of Castellano and Bothner-by,[79] a least-squares version of this program was developed that uses the experimental line positions and frequencies as the input data and calculates the best-fit ESR parameters. Dr. Kerr also installed the non-least squares version of this matrix diagonalization program (ESR 101) on the Aspect 2000 computer which is located in our laboratory.

An ESR spectrum simulation program which was developed by R. Lefebvre and J. Maruani was used in this work. This is a general purpose program for simulating high-field ESR spectra for radicals with S = 1/2. Either a Gaussian or Lorentzian line shape or a user-supplied numerical function line shape could be used. The potentially most useful feature of the program is that it allows the simulation of hyperfine patterns not only for radicals with an isotropic hyperfine coupling but also for radicals with either axially symmetric or fully anisotropic g and/or hyperfine tensors. The program is also designed to simulate second order hyperfine patterns. In the present work, the program was only used to simulate first- and second-derivative ESR patterns for radicals with isotropic hyperfine couplings.

E. Chemicals

All of the chemicals used in this research were obtained from either commercial chemical suppliers (see Table II) or received as gifts from other research groups (see Table III).

Of the samples obtained from commercial suppliers, 2-methyltetrahydrofuran was dried over silica gel, followed by several trap-to-trap transfers.

Of the samples supplied by other research groups, most were used without further purification procedures. Impurities were detected in only three samples. In a sample containing trimethylsilyltrimethylstannane ($Me_3SiSnMe_3$), a small amount of tetrahydrofuran (THF) which is presumably a solvent in the synthesis procedure was

TABLE II

CHEMICALS PURCHASED AND SUPPLIERS

Supplier	Compounds
Aldrich Chemical Co., Inc.	Hexa-methyldisilane Methylcyclohexane 2-Methyltetrahydrofuran Tetramethyltin Trichlorofluoromethane 1,1,1-Trichlorotrifluoroethane
Alfa Products, Ventron Division of Thiokol Corporation	Di-t-butylsulfide Hexamethyldisilazane Hexamethyldisiloxane Hexaphenyldigermane Hexaphenyldilead Hexaphenylditin Tetramethylgermanium Tetramethyltin Tin(IV) chloride
PCR Research Chemicals, Inc.	Bromotrifluoromethane Dibromodifluoromethane Hexamethyldisilylthiane Perfluorocyclobutane Perfluoro-1,3-dimethyl cyclohexane (mixture of cis and trans) Perfluoromethyl cyclohexane Trichlorofluoromethane 1,1,2-Trichlorotrifluoroethane
Matheson	Dichlorodifluoromethane 2,2-Dimethylpropane Silane Sulfur hexafluoride Trichlorofluoromethane 1,1,2-Trichlorotrifluoroethane
Norell, Inc.	Tetramethylsilane
Strem Chemicals, Inc.	Tetramethyltin

TABLE III

CHEMICALS RECEIVED AS GIFTS AND SUPPLIERS

Supplier	Compound
K. O. Christe North American Rockwell Corp.	Cesium pentafluorooxysulfide Cesium pentafluorosulfide
Ethyl Corporation Baton Rouge, LA	Tetramethyllead
D. Griller	^{13}C-Trifluorobromomethane ($^{13}CF_3Br$)
J. K. Kochi Houston, Texas	tert-Butyltrimethyltin Ethyltrimethyltin cyclo-Hexyltrimethyltin neo-Pentyltrimethyltin iso-Propyltrimethyltin n-Propyltrimethyltin Tetramethyllead Tetramethyltin and isotopic derivatives
D. M. Lemal Dartmouth College	Octafluorocyclooctatetraene

detected. The THF was identified by its presence in the ESR spectrum since it formed a cation upon γ-irradiation in the Freon-11 matrix.[80] In this instance, the THF solvent was removed by trap-to-trap distillation since the organometal had a much higher boiling point than the THF. A sample of trimethylsilyltrimethylgermane ($Me_3SiGeMe_3$) was thought to be contaminated with small amounts of hexamethyldisilane (Me_6Si_2) and hexamethyldigermane (Me_6Ge_2) but no purification steps were attempted since the spectrum could be analyzed even with the impurities.

A sample of tetramethyllead was received as a 15% blend with toluene. Purification was achieved through several trap-to-trap distillations; however, purification was found to be relatively unnecessary since the toluene impurity did not appear to interfere with the ESR spectrum of the organometal radical cation.

CHAPTER III

RADICAL ANIONS

A. Introduction

Electron capture by neutral diamagnetic molecules can induce quite significant changes in molecular geometry and in certain cases can bring about bond dissociation. This observation is not particularly unexpected since Walsh's rules[3-5] predict that molecular geometries are determined to a great extent by the orbital character of the highest occupied molecular orbital, which, of course, is the orbital that the excess electron enters. For example, electron capture by haloalkanes (R-X) is immediately followed by dissociation into a halide ion (X^-) and a neutral carbon-centered free radical[38] (Equation (10), page 10). In such cases, the electron presumably enters a σ^* antibonding orbital. However, it should be noted that some examples are known in the solid phase where the halide ion and the free radical remain weakly bound;[81] however, even in these cases the existence of the weak bond is possibly the result of the constrictive cage effect of a rigid lattice. In contrast to the immediate dissociative electron-capture process generally characteristic of monohalogenated hydrocarbons, perfluorinated hydrocarbons, in some instances, can stabilize excess electrons without undergoing immediate dissociation.[82-84] It was in this class of compounds that the potential of observing changes in molecular geometry was realized in the

course of this work. For example, neutral octafluorocyclooctatetraene is tub shaped whereas the radical anion is interpreted as being planar.[84] Many perhalogenated hydrocarbons, particularly those with some Cl, Br, or I content, readily capture and stabilize electrons at 77 K, but dissociation of the heavier halide ion becomes a very common decay pathway at higher temperatures.[7,83,85] In some instances the decay of the radical anion into the free radical and the halide ion can be directly monitored by annealing the sample during an ESR experiment.[7] For example,

$$CF_3Cl^- \xrightarrow{\Delta} CF_3\cdot + Cl^- \quad . \tag{43}$$

B. Bromotrifluoromethane Radical Anion

Neutral bromotrifluoromethane (Freon-13B1) is known to be an excellent electron scavenger; in fact, it has found an aerospace application of improving satellite communications.[86] Freon-13B1 has also found an industrial application as a fire retardant where its effectiveness is also thought to be linked to its electron scavenging potential.[87]

The radical anion of CF_3Br was first reported by ESR spectroscopy in 1977, along with the CF_3Cl^- and CF_3I^- radical anions.[7] The authors concluded that in each CF_3X^- radical anion the unpaired electron resides in an a_1 (in C_{3v} symmetry) antibonding orbital with the hypervalent electron being mainly localized between the carbon-halogen bond. Since the observed spectra showed the characteristic line shapes of both parallel and perpendicular features, the spectra

were interpreted by assuming axial symmetry. Hence, the p-orbital composition of the σ* orbital bonds for the heavy halogen could be determined directly. From a comparison of the hyperfine coupling constants, a general trend correlating the decreasing electronegativity of the halogen with an increase in its total s and p spin density was noted.

This conclusion can be explained in terms of a very simple two-center molecular orbital model which considers both bonding and anti-bonding orbitals generated by the interaction of the sp^3 orbital of the CF_3 moiety with mainly the p-orbital of the heavy halogen. The relative positions of the CF_3 and heavy halogen localized orbitals on the energy scale are determined by their relative electronegativities.

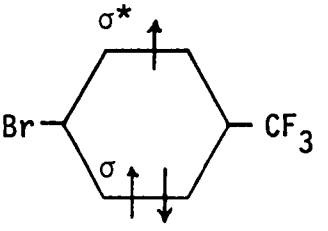

The first two electrons combine to form a σ bonding orbital where the coefficients of this orbital are predominantly associated with the carbon; however, when an excess electron is captured, it enters a σ* antibonding orbital and now the major coefficients of the orbital are derived not from the carbon $2p_z$ orbital but rather from the p_z orbital of the heavy halogen. This model, which has been used to describe the bonding in other σ* radicals,[88] could not be directly tested for both the carbon and the halogen from the data

in the original paper because no carbon-13 hyperfine couplings were reported for the central carbon atom. Nevertheless, a compelling case can be made by comparing the fluorine coupling, which is indirectly indicative of the carbon spin density, with the observed halogen hyperfine coupling.

Subsequent to the original report, the ^{13}C anisotropic hyperfine parameters were determined for the CF_3Cl^- radical.[89] The impetus for the present study was to obtain accurate hyperfine coupling constants to all three different nuclei in the $^{13}CF_3Br^-$ radical and then be able to directly test this simple model. In addition to directly confirming the correlation between the electronegativity of the halogen and the carbon spin density, a careful study of the CF_3Br^- radical was merited because the family of CF_3X^- radicals represent a new class of σ^* antibonding radicals which are relatively stable hypervalent (or excess electron) radicals in contrast to the CH_3X^- radicals which generally dissociate.

Three different lecture bottles of CF_3Br were used without further purification. No differences between any of these different sources were observed. Samples of $^{12}CF_3Br$ were prepared using either TMS-h_{12} or TMS-d_{12} as a matrix. Sample concentrations ranged from about 5 mole % to about 0.1 mole % with the majority being around 2 mole %; yet even over this relatively large range there appeared to be no concentration effect. Partial orientation was induced in the samples by slowly lowering them into liquid nitrogen either by hand or by the mechanical device described earlier. Since

the signal was often very weak, large total irradiation doses (4.0 Mrad) were used to generate a sufficient number of radicals to obtain a suitable signal-to-noise ratio. Poor signal level was more often a problem for samples showing very little partial orientation.

The initial effort for this project was to optimize the procedure for generating partially oriented samples which could give resolvable ESR spectra. Since the use of TMS-d_{12} as a matrix reduces the line width slightly, thus giving better resolved ESR spectra, all of the spectra described in this section used TMS-d_{12} as a solvent. However, the effects of partial orientation are essentially the same for either TMS-h_{12} or TMS-d_{12} and it was in TMS-h_{12} that the earlier attempts at favorable partial orientation were performed.

Initially, the sample tubes were lowered over a 3-5 minute period by hand into liquid nitrogen, but in these cases the observed spectra after γ-irradiation resembled those previously reported. However, when the mechanical device was used to lower the samples into liquid nitrogen over a 1-2 hour period, highly resolved spectra were subsequently obtained showing a considerable angular dependence as the sample tube was rotated in the cavity of the ESR spectrometer. In these cases the samples evidently possessed a high degree of partial orientation. In fact, under certain optimum conditions of sample preparation, rotation of the sample tube through 90° could completely discriminate against either the parallel, as shown in Figure 9, page 61, or perpendicular, as seen in Figure 10, page 62, components. Slowly cooling the samples with the mechanical

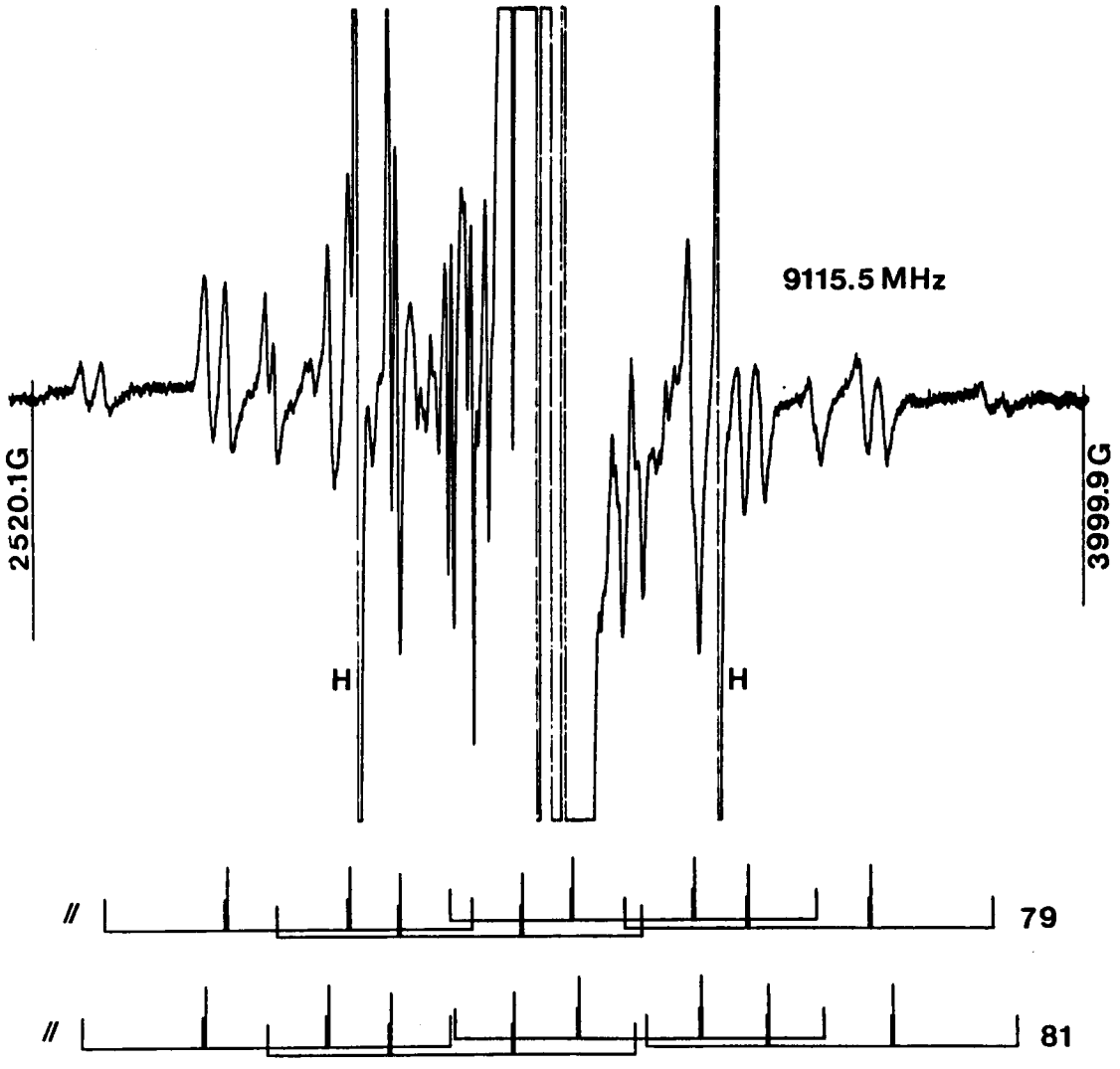

Figure 9. First-derivative ESR spectrum of a γ-irradiated 2 mole % solid solution of CF_3Br in TMS-d_{12}, parallel features. The sample was oriented to maximize the parallel features which are defined by the lower stick diagram.

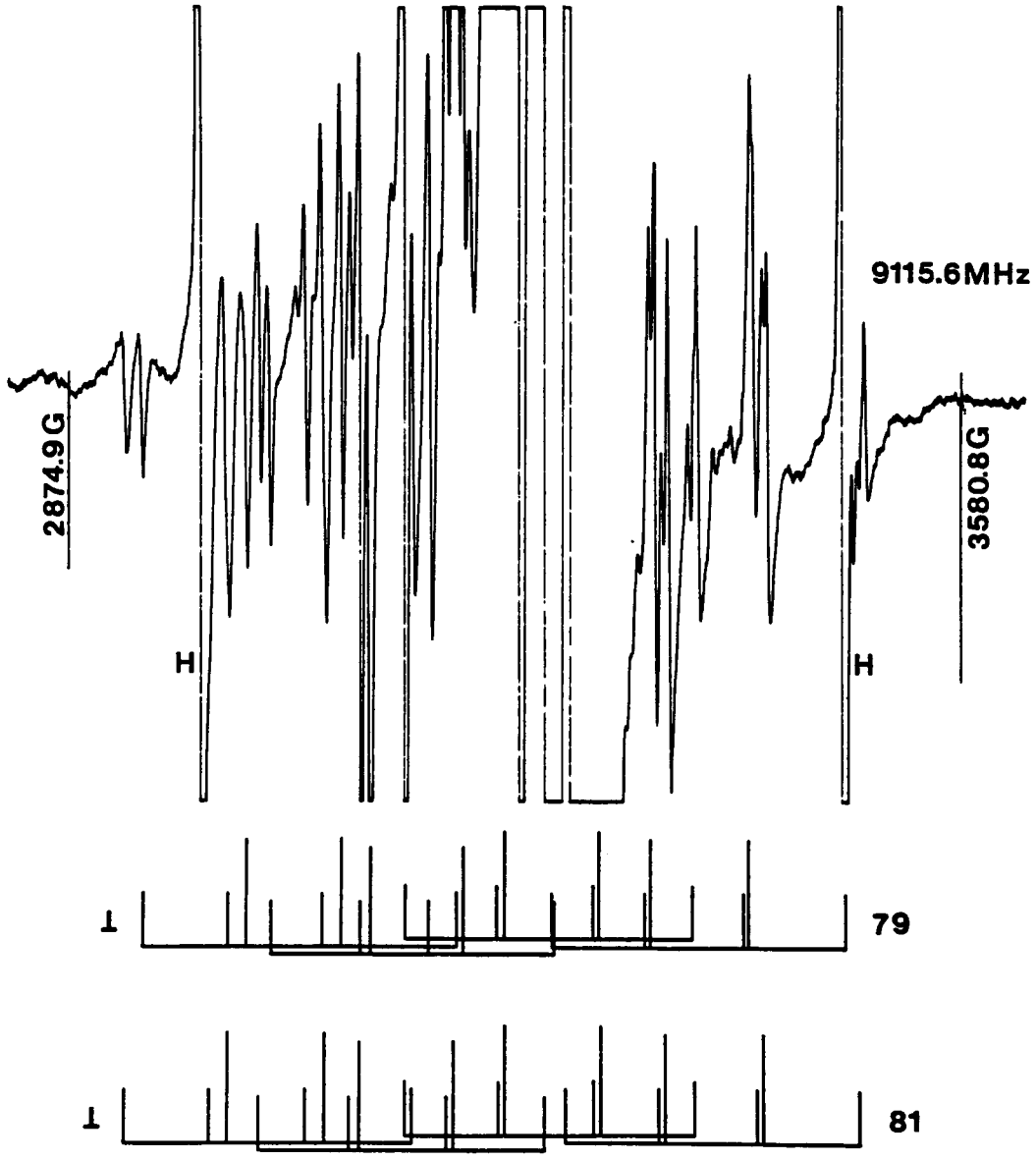

Figure 10. First-derivative ESR spectrum of a γ-irradiated 2 mole % solid solution of CF_3Br in TMS-d_{12}, perpendicular features. The sample was oriented to maximize the perpendicular features which are defined by the lower stick diagram.

device over a time greater than 2 hours generally produced samples which were too highly oriented for detailed analysis, the ESR spectra as shown in Figure 11 (page 64) presumably being complicated by resonances of several different lattice sites. Thus a balance had to be maintained between too little orientation and too much. Another technique used to generate partial orientation was to cool the sample to the matrix melting point (-27°C) in an EtOH-N_2 slush bath maintained at approximately -26°C. After equilibration, the ethanol was further cooled slowly by the addition of more liquid nitrogen and in so doing, the TMS froze gently. This technique did not significantly increase the degree of partial orientation observed in the sample; in fact, the spectra were virtually identical to those obtained by quenching the samples.

The analysis of the ESR spectra of $^{12}CF_3Br^-$ as shown in Figures 9 and 10 are indicated by the stick diagrams in the lower portion of each figure.

The CF_3Br^- radical was found to be unstable above 130 K in the TMS matrix at which temperature it decayed without a trace of any detectable product radicals. This observation contrasts with the decay sequence established for CF_3Cl^- in a neopentane matrix where the loss of the radical anion resonances were marked by the growing in of resonances attributed to the $CF_3\cdot$ radical, as shown below.

$$CF_3Cl^- \xrightarrow{\Delta} CF_3\cdot + Cl^- \qquad (44)$$

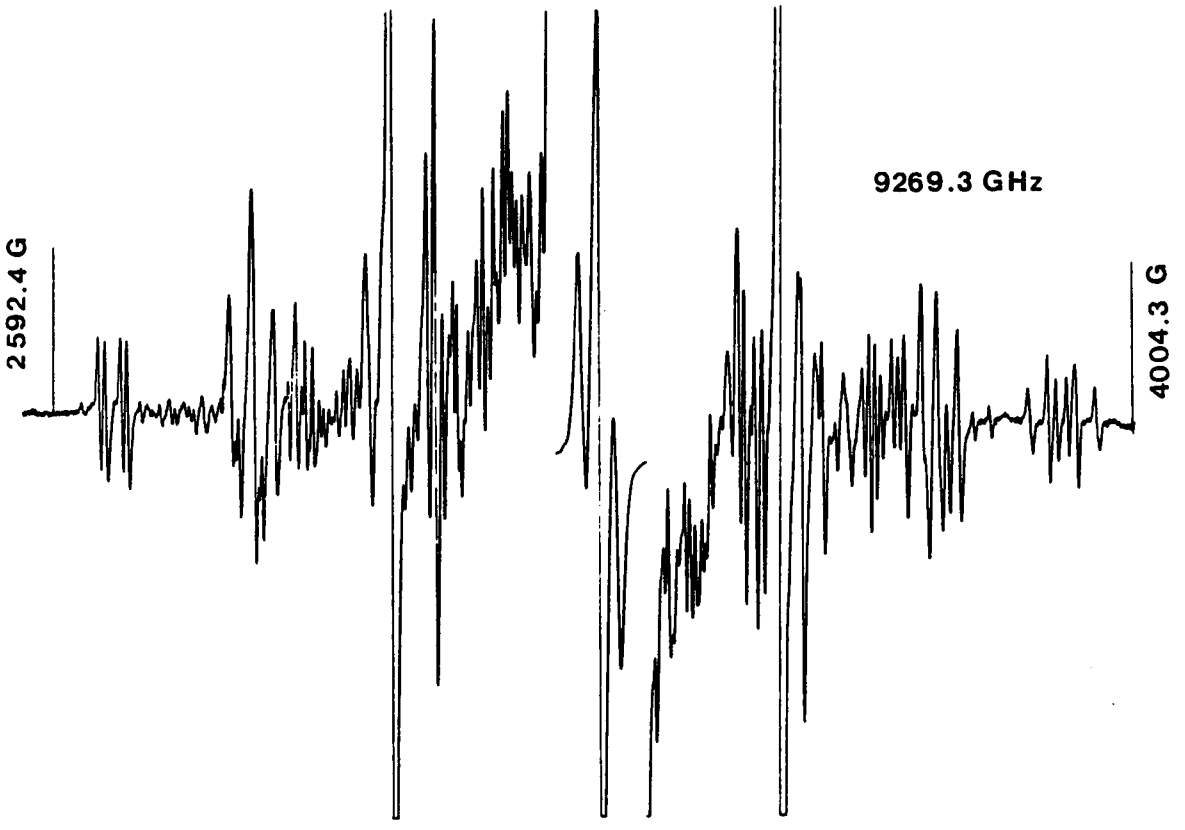

Figure 11. First-derivative ESR spectrum of a γ-irradiated 2 mole % solid solution of CF_3Br in TMS-d_{12}. The sample prior to γ-irradiation was slowly crystallized over a 4-hour period.

Directly exposing the γ-irradiated sample with either visible or UV light did not change the ESR spectral appearance. Even at the decay temperature, the radical still exhibited the same anisotropic pattern as at 83 K. However, the hyperfine coupling constants did show a slight temperature dependence. This temperature dependence was examined between 4.2 to 130 K with the use of the Oxford liquid helium system.

While cooling the sample from 130 K, the general spectral appearance remained relatively unchanged, until the sample was cooled to below 10 K, at which point the spectral appearance became quite complex. See Figure 12, page 66. Table IV is a compilation of the temperature dependent hyperfine parameters between 20 and 130 K.

One sample which showed favorable partial orientation was stored in liquid nitrogen for over 2 months. Interestingly, upon rerunning the sample, the anisotropic hyperfine coupling parameters measured at the same temperature had slightly increased while the $g_{\perp}$ and $g_{//}$ remained unchanged.

A ^{13}C enriched sample of $^{13}CF_3Br$, supplied by D. Griller but synthesized at DuPont by P. J. Krusic, B. E. Smart, and E. R. Wonchoba was incorporated into a TMS-d_{12} matrix on a standard vacuum system by Dr. T. F. Williams while visiting the Division of Chemistry, National Research Council of Canada. This $^{13}CF_3Br$/TMS-d_{12} mixture was slowly lowered with the mechanical device into liquid nitrogen over a 2-hour period, and the polycrystalline sample was subsequently γ-irradiated for a dose of about 4.0 Mrad. This sample

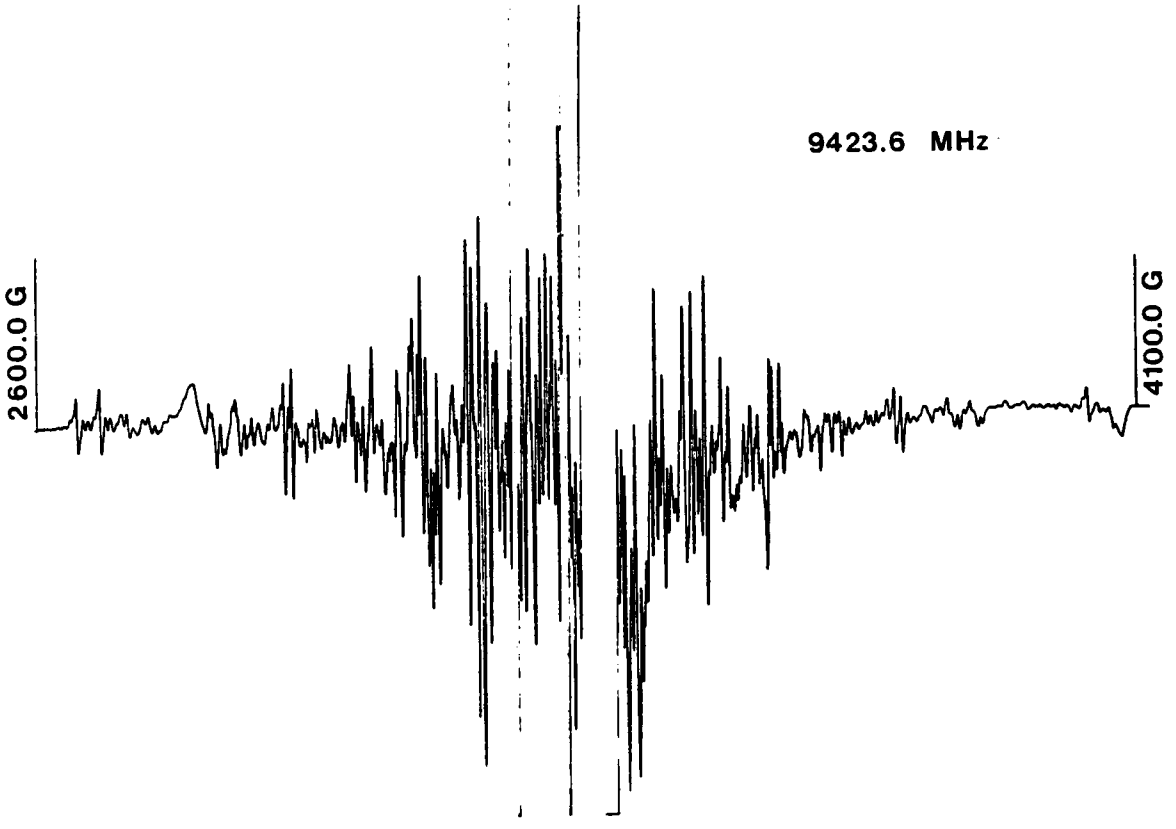

Figure 12. First-derivative ESR spectrum of a γ-irradiated 2 mole % solid solution of CF_3Br^- in TMS-d_{12} at 4.4 K. Annealing this sample to 100 K resulted in the observed pattern becoming essentially the same as Figure 9, page 61.

TABLE IV

TEMPERATURE DEPENDENCE OF THE ^{19}F AND ^{81}Br HYPERFINE COUPLING CONSTANTS BETWEEN 120 TO 4.2 K

Temperature	$g_\perp$	$g_\parallel$	$A_\parallel$ (G)		$A_\perp$ (G)	
			(3 ^{19}F)	^{81}Br	(3 ^{19}F)	^{81}Br
120 K	2.01891	2.00482	172.3	263.5	79.5	114.9
80 K	2.01851	2.00422	180.3	270.5	80.4	115.3
45 K	2.0182	2.0043	183.5	280.6	80.1	115.6
35 K	2.0186	2.0043	186.2	284.5	80.2	115.1
10 K	2.0181	2.0043	186.8[a]	283.9	79.8[a]	114.8
4.2 K	2.0188	2.0043	186.1[a]	284.7	78.8[a]	113.2

[a]Since the three fluorines are not equivalent at this temperature, the reported values represent the average hyperfine coupling constant.

exhibited quite strong partial orientation effects. The spectral resolution and signal level were carefully optimized to obtain the clearest spectra by varying the temperature, microwave power, and angular position of the sample tube in the cavity. The parallel hyperfine pattern, Figure 13, page 69, or the perpendicular hyperfine pattern, Figure 14, page 70, could be separately optimized. A rotation of the sample tube through 90° caused the observed hyperfine pattern to alternate between the parallel and perpendicular patterns.

The analysis of the ESR spectrum of $^{13}CF_3Br^-$ is straightforward since in the low and high-field wings of the spectrum the observed pattern is similar to the non-carbon-13 enriched sample (compare Figures 9 and 10, pages 61 and 62). The appropriate analysis is shown by the stick diagrams in the lower portion of Figures 13 and 14.

Since several anisotropic hyperfine couplings were greater than 100 G, the least squares fit program was utilized to obtain accurate hyperfine coupling constants for both the $^{12}CF_3Br^-$ and $^{13}CF_3Br^-$ radicals. First, the anisotropic parameters, $g_{//}$, $g_{\perp}$, $A_{//}$ (^{19}F), $A_{\perp}$ (^{19}F), $A_{//}$ ($^{79,81}Br$), and $A_{\perp}$ ($^{79,81}Br$) were fit very accurately to the data of the $^{12}CF_3Br^-$ radical. It should be noted that the experimental line positions used as input data for the least-squares program were not taken from Figures 9 and 10 where the precision of measurement is low but rather were taken from expansions of small segments of the spectrum where the field

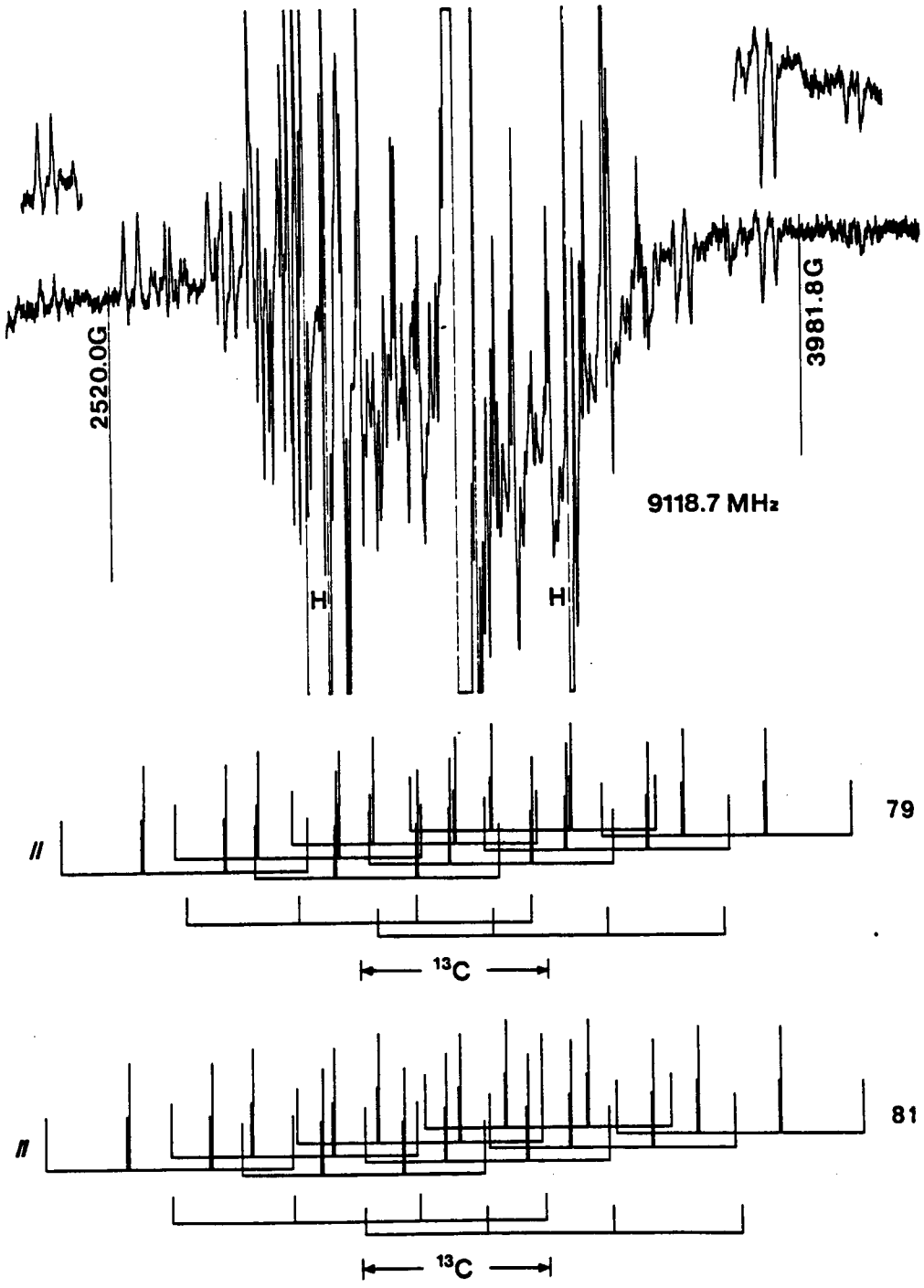

Figure 13. First-derivative ESR spectrum of a γ-irradiated sample of $^{13}CF_3Br$ in TMS-d_{12}, parallel features. The sample was oriented to maximize the parallel components which are defined by the lower stick diagram. The upper inset has a gain of two times stronger.

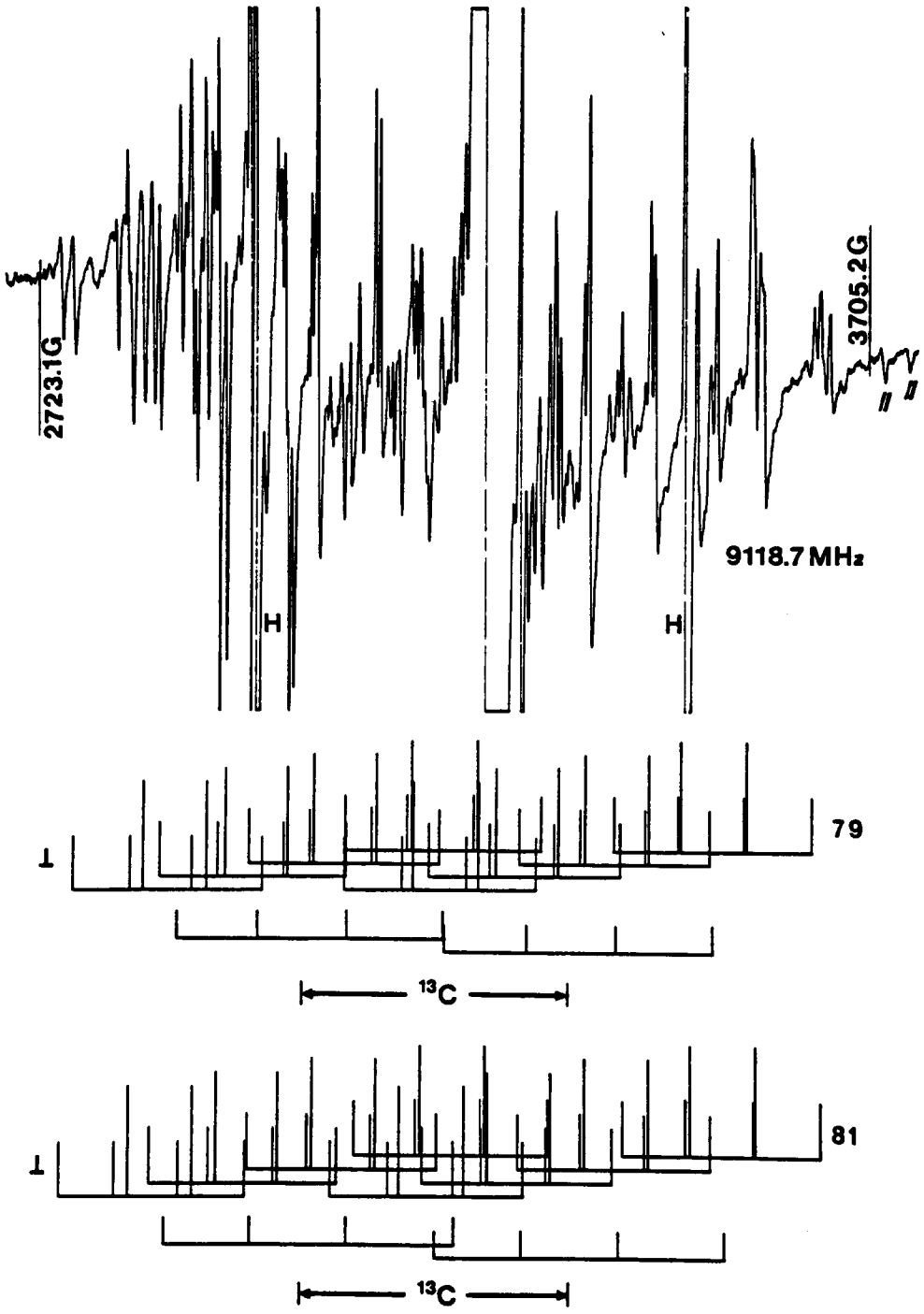

Figure 14. First-derivative ESR spectrum of a γ-irradiated sample of $^{13}CF_3Br$ in TMS-d_{12}, perpendicular features. The sample was oriented to maximize the perpendicular components which are defined by the lower stick diagram.

positions of the lines could be measured precisely. Then, using these best-fit values, only the anisotropic parameters, $A_{//}$ (^{13}C) and $A_{\perp}$ (^{13}C), were fit to the data of the $^{13}CF_3Br^-$ radical. This procedure, although not exactly rigorous,[90] was necessitated since the signal-to-noise level of the ESR spectra of the isotopically enriched sample was inferior to the non-carbon-13 enriched sample, owing to the larger number of lines in the former case. In none of the computer fits was an additional term in the Hamiltonian involving a quadrupole moment coupling to bromine needed to fit the data.

Using the data obtained in this work with the data already reported or obtained from other workers, Table V was constructed.

In addition to affording a direct test of the simple two-center bonding model, the present study has yielded supporting evidence for a few assumptions made by the original authors.

First, although not explicitly stated in the original report, the reasonable assumption of the hyperfine couplings all being of the same sign was made. If for the $^{13}CF_3Br^-$ radical this assumption is used, then the total spin density is 1.34; however, if any of the anisotropic couplings are of opposite sign, then the spin density distribution would become less reasonable. For example, if $A_{//}$ (^{13}C) and $A_{\perp}$ (^{13}C) were of opposite sign, then the B (^{13}C) would change from 28.5 G ($\rho(P_z) = 0.747$) to 120 g which represents a $2p_z$ orbital spin density on carbon of 6.26; likewise, if $A_{//}$ (^{79}Br) and $A_{\perp}$ (^{79}Br) were of opposite sign then the B (^{79}Br) value would change from 31 G ($\rho(p_z) = 0.16$) to 58 G which represents a p_z orbital spin density on

TABLE V

COMPARISON OF A FEW RADICALS OF THE FORM CF_3X

Radical	T (K)	$g_{//}$	$g_{\perp}$	Nucleus	Hyperfine Couplings $A_{//}$ (G)	Hyperfine Couplings $A_{\perp}$ (G)	Spin Densities[a] ρ_s	Spin Densities[a] ρ_p
$^{13}CF_3$	77	2.0024	2.0042[b]	^{13}C	318	247[c]	.219	.615
				^{19}F	264	84[c]		
$^{13}CF_3Cl^-$	101	2.0021	2.0070	^{13}C	389.8	326.6	.259	.5875
				^{19}F	196.76	86.4	.0066	.0583
				^{35}Cl	44.28	18.45	.0128	.1356
				^{37}Cl	36.06	15.01	.0128	.1356
$^{13}CF_3Br^-$	121	2.0036	2.0212	^{13}C	403	317	.256	.747
				^{19}F	172	78.5	.006	.050
				^{79}Br	244	106	.013	.158
				^{81}Br	264	115	.013	.158
$^{12}CF_3I^-$	98	2.0002	2.0483	^{19}F	144.6	67.2	.0049	.0414
				^{129}I	373.1	178.8	.0164	.2234

[a]Orbital spin densities calculated using the atomic values in Table I, page 25.

[b]Average of g_{yy} and g_{zz}.

[c]Average of A_{yy} and A_{zz}.

bromine of 0.31 yielding a total spin density of about 1.5. Therefore, the assumption of the same sign is consistent with the present data.

Also, the CF_3X^- radicals were assumed to be rotating about their C_3 axis because such a rotation readily explained the fact that the three fluorines in each case were observed to be magnetically equivalent. That the CF_3 group could undergo rapid rotation about its C_{3v} axis has been established in the literature for other similar radicals.[91,92] Nevertheless, a direct test of this assumption was obtained from the low temperature experiment. If CF_3Br^- were not rotating at 100 K, which corresponds to the temperature at which Figures 9 and 10, pages 61 and 62, were obtained, then cooling the radical should not significantly affect the observed hyperfine pattern. This situation corresponds to a case where the anisotropic components would have to be fortuitiously equivalent. If, on the other hand, the CF_3Br^- were rotating fast on the ESR time scale at 100 K, then cooling the sample to very low temperatures (~4.2 K) may cause the rotation to slow or even stop, in which case the observed ESR pattern would change. The fact is that the observed ESR pattern did become considerably more complex below about 10 K at which temperature the fluorines appear to become non-equivalent; therefore, the low temperature experiment provides convincing evidence that the CF_3Br^- rotates rapidly above about 10 K and confirms the earlier assumption.

As previously noted, the determination of the anisotropic hyperfine parameters allows a direct test of the sample two-center bonding model which for σ* orbitals predicts that the substitution of increasingly less electronegative heavy halogens in the CF_3X^- radical will result in a shift of the spin density from the carbon to the halogen. As indicated in Table V, the s-spin density of the carbon only decreases very slightly from $\rho(2s) = 0.259$ to $\rho(2s) = 0.256$ while the halogen p-spin densities increase, as predicted, from $\rho(3p_z) = .136$ to $\rho(4p_z) = 1.58$ for the series $^{13}CF_3Cl^-$ to $^{13}CF_3Br^-$. The carbon $2p_z$-spin density, however, does not seem to follow this anticipated trend since it increases from $\rho(2p_z) = 0.588$ to $\rho(2p_z) = 0.747$ on exchanging Cl with Br in the CF_3X^- radical. This latter experimental observation is, at face value, directly <u>opposite</u> to the prediction of the simple two-center bonding model.

Several factors may be responsible for this apparent deviation from the predicted trend, such as accounting for the excess spin density and/or allowing for slight changes in geometry.

The term excess spin density is applied to radicals where the sum of the absolute spin densities from each atom assumes a value greater than unity. In the present case the total spin densities are 1.18 and 1.34 for the $^{13}CF_3Cl^-$ and $^{13}CF_3Br^-$ radical anions, respectively.

A seemingly attractive way of explaining the excess spin density would be to suggest that the theoretical estimates of the

atomic parameters, A_o and B_o, are too low. This being the case, the orbital spin densities would be artifically inflated. For example, using the B_o parameter for ^{13}C which is estimated to be 38.3 G, the carbon $2p_z$-spin density for $^{13}CF_3Br^-$ is estimated to be 0.747, but if a value of, say, 45 G is used, then the estimated carbon $2p_z$-spin density drops to 0.637. However, inaccuracies in atomic values alone cannot account for the apparent increase in spin density in the carbon $2p_z$-orbital on comparing $^{13}CF_3Cl^-$ and $^{13}CF_3Br^-$ because it is carbon in both radicals that is being compared. On the other hand, underestimated atomic values could be responsible for some over estimation of the spin density on a particular atom in the molecule, but an over estimate of 0.34 is admittedly quite unlikely.

Although there are several other examples of carbon centered σ^* radicals which would be very helpful for comparison, anisotropic ^{13}C data have not been reported for any of these radicals. Fortunately, two nitrogen-centered σ^* radicals suitable for comparison have been reported, namely the N-chloro[93] and N-bromo[94] succinimide (NCS and NBS respectively) radical anions. For these latter radicals the σ^* orbital is thought to be mainly localized between the nitrogen and the heavy halogen as shown below.

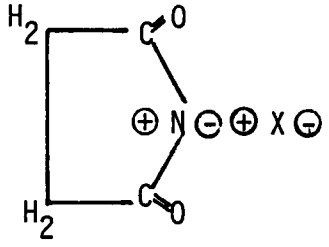

For ready comparison, part of Table V, page 72, has been reproduced in Table VI along with the s- and p-spin density distributions reported for the NCS and NBS radical anions. The appropriateness of the comparison is evidenced by several criteria. First, the central atom s-spin densities and the heavy halogen s- and p-spin densities of the NCS and NBS radical anions parallel the distribution trends of the $^{13}CF_3Cl^-$ and $^{13}CF_3Br^-$ radical anions. Also, when the bromine atom is the heavy halogen in the σ^* radical anion then the excess spin density is greater than when the chlorine atom is in the σ^* bond. Likewise, the $g_{//}$ and $g_{\perp}$ values follow the same shifts upon replacement of the chlorine for bromine. Of key importance though from Table VI is that although the $2p_z$-spin density on the nitrogen is less than the corresponding carbon $2p_z$-spin density, the central atom $2p_z$-spin density increases from 0.374 for NCS to 0.416 for NBS upon substitution of the less electronegative, heavier atom. Thus, the NCS and NBS radical anions, just like the $^{13}CF_3Cl^-$ and $^{13}CF_3Br^-$ radical anions, seem to not follow the trends predicted by the simple two-center model.

Although the simple two-center molecular orbital model has been found to be very adequate to explain the bonding of many diatomic σ^* radicals such as KrF and XeF[95] and FCl^-, KBr^- and FI^-,[96] its failure to adequately predict the spin density trends in the present work and the NCS and NBS radical anions is undoubtedly linked to the fact that the simple model does not allow for any spin polarization by the heavy halogens or for any changes in geometry, assuming complete orbital following.[97]

TABLE VI

SPIN DENSITY COMPARISON FOR A FEW σ* RADICALS

Radical Anion	Nucleus	Spin Densities[a] ρ_s	ρ_p	Reference
N-chlorosuccinimide	^{14}N	0.099	0.374	93
	^{35}Cl	0.033	0.610	
N-bromosuccinimide	^{14}N	0.085	0.416	94
	^{81}Br	0.030	0.699	
Trifluorochloromethane	^{13}C	0.259	0.588	102
	^{35}Cl	0.128	0.136	
Trifluorobromomethane	^{13}C	0.256	0.747	This Work
	^{81}Br	0.013	0.15	

[a]Orbital spin densities calculated using the atomic values found in Table I, page 25.

Spin polarization is a mechanism whereby the spin of the unpaired electron in the SOMO polarizes the electrons in filled molecular orbitals,[53] the effect being to produce a slight unpairing of electrons resulting in an increase in the absolute value of the total spin density. Of course, the algebraic sum of the spin densities cannot exceed unity. Therefore, spin polarization may be one of the factors contributing to the excess spin density characteristic of the σ^* radicals reported in Table VI.

Changes in geometry would in principle result in changes in λ^2 which is the ratio $\rho p/\rho s$. Using the equations derived by Coulson,[98] an estimate of the geometry about the central carbon atom may be made by processing the data in Table VI. The value of λ^2 for $^{13}CF_3Cl^-$ is (.588/.259) 2.27 which leads to $\theta = 111°$ and $\phi = 107.5°$[99] while the value of λ^2 for $^{13}CF_3Br^-$ is (.747/.256) 2.92 which may be solved to yield: $\theta = 109.7°$ and $\phi = 109.3°$.[99] Although the angular differences are relatively small, the calculations do seem to indicate that while the CF_3Br^- radical anion is almost exactly pyramidal (i.e. $\theta \sim 109.5°$), the CF_3Cl^- radical is somewhat distorted from pyramidality. This slightly distorted structure for CF_3Cl^- was reflected by a CNDO/2 calculation which was minimized with respect to total energy to yield $\theta = 114°$ and $\phi = 104.6°$.[83] (No CNDO/2 calculations were performed for the CF_3Br^- since the computer program was not parameterized for third-row elements.)

Thus, although the measure in halogen p-orbital spin density with decreasing electronegativity is consistent with the simple

two-center bonding model, this model is not adequate to explain slight changes in orbital hybridization, and therefore in the geometry.

In addition to providing a more thorough characterization of the spin distribution, the data from the ^{13}C enriched samples clearly demonstrate that these radicals are, indeed, genuine radical anions and not merely radical adducts, as is the case for the corresponding CH_3X^- species.[81,100,195] The ESR data support this statement in three ways. First, if the $^{13}CF_3Br^-$ were merely an adduct, in which case the radical could be described as a $CF_3\cdot$ group being perturbed by a bromide ion, then the ^{13}C and ^{19}F hyperfine couplings in the hypothetical adduct would be expected to be essentially unchanged from the $CF_3\cdot$ radical hyperfine couplings. As shown in Table V, page 72, however, there is a significant difference between the ^{13}C and ^{19}F anisotropic hyperfine couplings in the $^{13}CF_3\cdot$ free radical and the $^{13}CF_3Br^-$ radical anion. In conjunction with this point, the anisotropic g values for the hypothetical adduct would be expected to be the same as or close to the value for the $^{13}CF_3\cdot$ radical. Once again, a comparison of $^{13}CF_3\cdot$ and $^{13}CF_3Br^-$ reveals a significant difference in their g values. Finally, adducts which are typically observed in rigid lattice structures readily break apart on annealing whereas genuine σ^* radicals are generally more stable and do not have to be generated in constrictive rigid solids. Certainly the TMS matrix may not be considered as a rigid solid since it is well known to have a high

degree of plasticity.[83] Taken together, these three considerations establish that the $^{13}CF_3Br^-$ is a genuine σ^* radical.

Having characterized the CF_3Br^- through its hyperfine coupling constants, attention will now be turned to the temperature dependence of the hyperfine parameters. As indicated in Table IV, page 67, upon cooling from 80 K to 10 K, the bromine and fluorine parallel hyperfine couplings increase while the corresponding perpendicular couplings remained essentially unchanged. There are a few possible explanations for this apparent change.

First, a seemingly reasonable postulate would presume that at 80 K CF_3Br^- populates one or more vibrationally excited states but that as the temperature is lowered, the relative populations of the different excited vibrational modes will shift to the ground state. The lowest energy vibrational modes for CF_3Br and presumably also for CF_3Br^- are the ν_1 (453 cm^{-1}) and ν_6 (537 cm^{-1}). Since a standard Boltzmann distribution equation (Equation (45)) may be used to describe the relative populations of the ground ($N_{i,o}$) and the first excited vibrational state ($N_{i,1}$) for the i^{th} normal mode of vibration, the proposed importance of excited vibrational state may be checked.

$$\frac{N_{(i,1)}}{N_{(i,o)}} = \exp\ (-\Delta E_i/KT) - 1 \qquad (45)$$

Using the vibrational energies 453 cm^{-1} (ν_1) and 537 cm^{-1} (ν_6) and the temperatures 80 and 10 K, the ratio of $N_{(i,1)}/N_{(i,o)}$ was so small

that in each case the population of the vibrationally excited state was negligible. A recent study on the temperature dependence of the $^{13}CF_3\cdot$ radical,[101] which in many respects is structurally similar to the present case, showed that there was no appreciable temperature effect in the range from 200-300 K. Thus, it seems unreasonable that vibrational excitation is responsible for the observed changes.

A second postulate would allow the CF_3 group to precess to a greater extent at higher temperature (120 K) but at lower temperature (10 K) the precessional motion would either stop or become smaller.

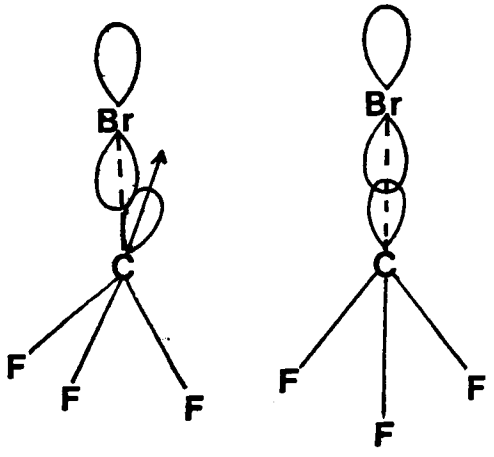

When there is no precessional motion such as at low temperature (10 K) and when the magnetic field is parallel to the C-Br bond, the interaction between the magnetic field and the carbon $2p_z$ orbital is at a maximum. However, when the CF_3 group is precessing and when the magnetic field is parallel to a line passing through the carbon and the bromine (dashed line), the interaction between magnetic field and the carbon $2p_z$ orbital will be underestimated. The amount of the underestimate would sensibly follow the simple

relation P sin θ where P is the maximum $2p_z$ interaction and θ is the angle of the precession.

C. Tetrafluoroethylene Radical Anion

Tetrafluoroethylene was first examined by ESR spectroscopy in 1962.[102] In this study, pure C_2F_4 was γ-irradiated and observed at 77 K. However, instead of generating the radical anion of C_2F_4, the authors suggested that a free radical was formed. In 1977, by using the technique of matrix isolation, clear evidence of the C_2F_4 radical anion was obtained in two different matrices,[103] namely tetramethylsilane (TMS) and 2-methyltetrahydrofuran (MTHF). In the TMS matrix, the second-order isotropic pattern was interpreted as consistent with coupling to four equivalent fluorines (A_{iso} (4F) = 94.3G). At high gain and by optimizing the signal-to-noise ratio, the isotropic carbon-13 hyperfine coupling (A_{iso} ($2^{13}C$) = 48.7 G) was detected in natural abundance. Whereas isotropic spectra were obtained in a tetramethylsilane (TMS) matrix, axially symmetric anisotropic spectra were obtained in an MTHF matrix and were interpreted as consistent with coupling to four equivalent fluorines ($A_{//}$ ($4^{19}F$) = 135.9 G and $A_{\perp}$ ($4^{19}F$) = 74.4 G). Since the anisotropic spectra of the $C_2F_4^-$ in MTHF were characterized by quite broad resonances, a second experimental determination of the axially symmetric hyperfine coupling parameters was later reported[104] ($A_{//}$ ($4^{18}F$) = 124.1 G and ($A_{\perp}$ ($4^{19}F$) = 78.75 G) using perdeuterated methylcyclohexane (MCH-d_{14}) as a matrix. This latter sample utilized

the technique of slow cooling thereby inducing partial orientation to obtain sharp, clearly defined resonances whose relative intensities varied with orientation of the sample tube in the cavity.

Although the identity of the radical which gives rise to the observed ESR spectra has not been questioned, the geometry of the radical anion and the orbital that the unpaired electron occupies has been widely discussed.[104-106] Both planar (D_{2h}) and pyramidal (C_{2h}) structures can be considered for this radical. In the former case, the unpaired electron may occupy either a π^* or σ^* orbital. These three possible cases will be considered next.

In a π^* orbital, the unpaired electron occupies an orbital which is antisymmetric to the plane of the molecule, as shown in Figure 15a, page 84. One way to test the reasonableness of the π^* model is to compare the $C_2F_4^-$ ESR hyperfine parameters with other known examples of π type radicals. Such a comparison is given in Table VII, page 85. The data reveals that the isotropic fluorine hyperfine coupling of 94.3 G for $C_2F_4^-$ is much larger than other known examples of simple π type radicals. In a recent study, however, the authors found that by accounting for second-order Jahn-Teller effects and using the INDO approximation,[108] the isotropic ^{13}C and ^{19}F hyperfine coupling constants could be explained assuming an essentially π^* orbital. A similar argument was used to explain the isotropic ^{13}C and ^{19}F hyperfine couplings for the perfluorobenzene radical anion[109] and the ^{1}H and ^{19}F hyperfine couplings in $CH_2CF_2^-$.[110]

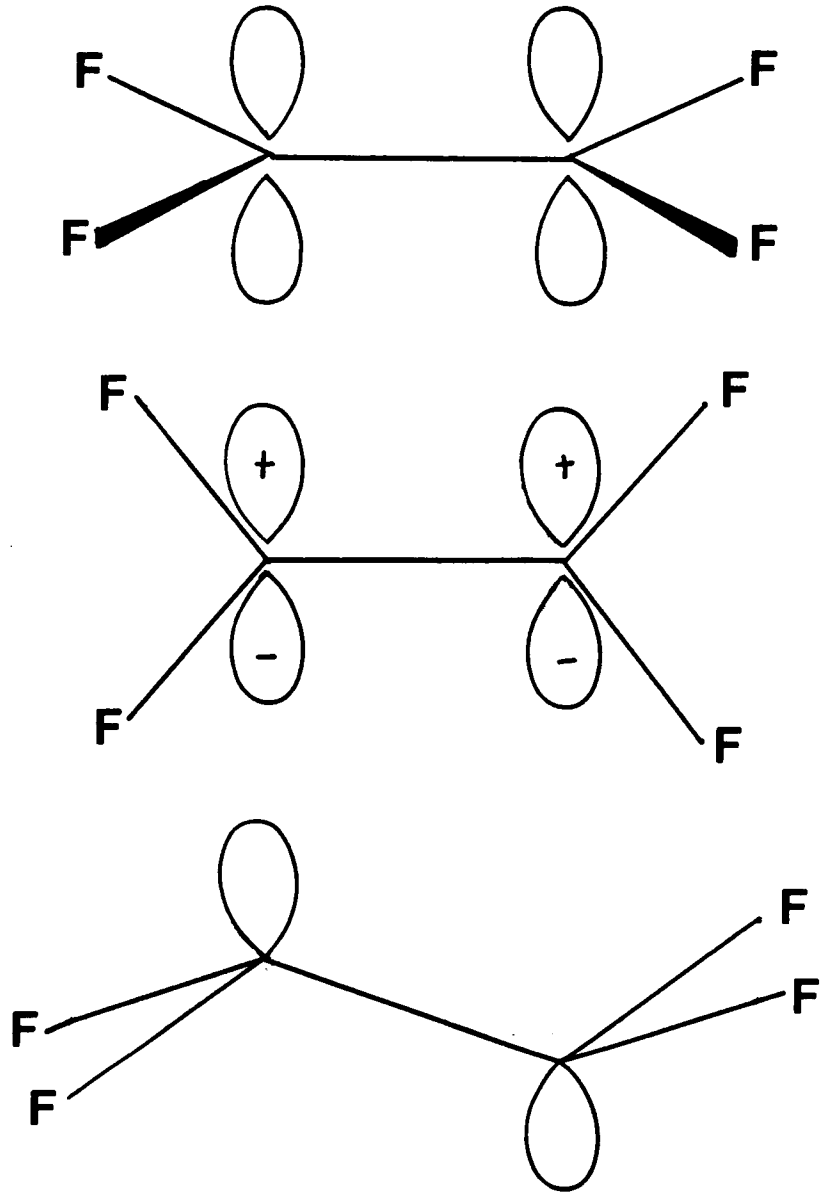

Figure 15. Three structures for $C_2F_4^-$: (a) planar π^*, (b) planar σ^*, and (c) pyramidal chair structure.

TABLE VII

COMPARISON OF THE ANISOTROPIC HYPERFINE COUPLING CONSTANTS FOR $C_2F_4^-$ WITH OTHER π TYPE RADICALS

Radical	Hyperfine Coupling (G)						Reference
	$A_{//}(^{13}F)$	$A_{\perp}(^{13}F)$	$A_{iso}(^{13}F)$	$A_{//}(^{13}C)$	$A_{\perp}(^{13}C)$	$A_{iso}(^{13}C)$	
$C_2F_4^-$	124.2	78.75	94.3	64.5	43.0	48.7	This Work
CCl_2F	193	29	83.7				107
CH_2F			64.3			54.8	
CCl_2CF_3						67.3	a
CH_3						38.5	

[a]This work, page 281.

If the radical were to retain a planar structure and the unpaired electron were to occupy a σ* orbital, then the orbital of the unpaired electron would occupy a symmetric orbital to the plane of the molecule, as shown in Figure 15, page 84. The choice of a σ* orbital such as the $5b_{2u}$ orbital[111] as the SOMO appears to satisfy the requirements imposed by the ^{19}F and ^{13}C coupling constants. While the ^{19}F coupling is consistent with other known examples of fluorine containing σ radicals, the low value of the ^{13}C coupling can be straightforwardly explained because there is no direct contribution to the carbon 2s-orbitals in the $5b_{2u}$ orbital.[103] An MX-α calculation indicated that the unpaired electron could occupy a diffuse Rydberg Ag type orbital, but the authors pointed out that in the solid phase the orbital may be perturbed by the matrix.[112] Incidentally, a recent theoretical study has demonstrated that although a Rydberg type orbital may be of lower energy, only valance orbitals are possible in the condensed phase.[99] In consideration of the ESR results, although the experimental evidence points toward the $5b_{2u}$ orbital, the experimental evidence does not rule out a small distortion from planarity into a chair structure.

A structure in which the radical becomes pyramidal at each carbon center, which was considered and discussed by the original authors, is the structure favored by several other authors.[113-116] In this model the radical is non-planar with C_{2h} symmetry, as shown in Figure 15c, page 84. Theoretical calculations which were performed at different levels of approximation and which were minimized

with respect to energy, each predicted the distorted C_{2h} structure. However, it should be noted that the experimentally determined hyperfine coupling constants did not closely agree with the theoretical estimates.[114]

From the reported experimental data obtained for the $C_2F_4^-$ radical, a definitive choice between either the planar π^* or σ^* or the pyramidal chair structure is not possible. Thus, the impetus for the present study was to obtain more experimental data, namely the anisotropic ^{13}C hyperfine couplings and the temperature dependence of the hyperfine coupling constants between 125 and 4.2 K, in the hope of being able to definitively distinguish between these two models. Although the effect of temperature on the observed hyperfine coupling constants have been reported using an MTHF matrix,[104] the use of this matrix generally results in very broad resonances; hence, the results were not very definitive. Thus, a low temperature study of the anisotropic pattern with MCH-d_{14} matrix which yields sharp anisotropic resonances could be helpful to define the temperature dependence of the hyperfine interactions.

Turning now to the experimental aspects of this study, the $^{12}C_2F_4$ was obtained from PCR which had d-limonene as a polymerization inhibitor and was used as received. Samples of between 1-2 mole % in perdeuterated methylcyclohexane (MCH-d_{14}) were prepared. Since MCH-d_{14} can form either a glassy or polycrystalline-type matrix depending upon the rate of cooling, controlling the rate of cooling was vital to a successful experiment. Favorable partial

orientation was generally observed in samples which were lowered over a 10-16 hour period into liquid nitrogen using the mechanical device previously described. Radiation doses ranged between 1.0-2.0 Mrad with differences in amount of signal being the only difference between the results for lowest and highest doses. One sample which showed favorable partial orientation upon standing 1 week in liquid nitrogen lost its favorable partial orientation characteristics. This effect was not checked, however, because every time thereafter the samples were immediately observed after γ-irradiation and not re-examined later.

In favorable cases, the amount of partial orientation was sufficiently great to yield symmetric line shapes for the resonances whose field positions were dependent upon the angular position of the sample in the cavity. More usually, however, rotation of the sample tube would cause either the parallel or perpendicular features to be intensified at the expanse of the other anisotropic component. For example, at a certain orientation the parallel components were enhanced, as shown in Figure 16, page 89, but rotation of the sample tube 90° intensified the perpendicular components, as shown in Figure 17, page 90. Spectra very similar to these have already been reported.[104]

Changes in the hyperfine coupling constants with temperatures between 4.4 K and 70 K were monitored on a sample for which, fortuitously, clearly resolved parallel and perpendicular features were obtained at a single orientation in the cavity. This latter

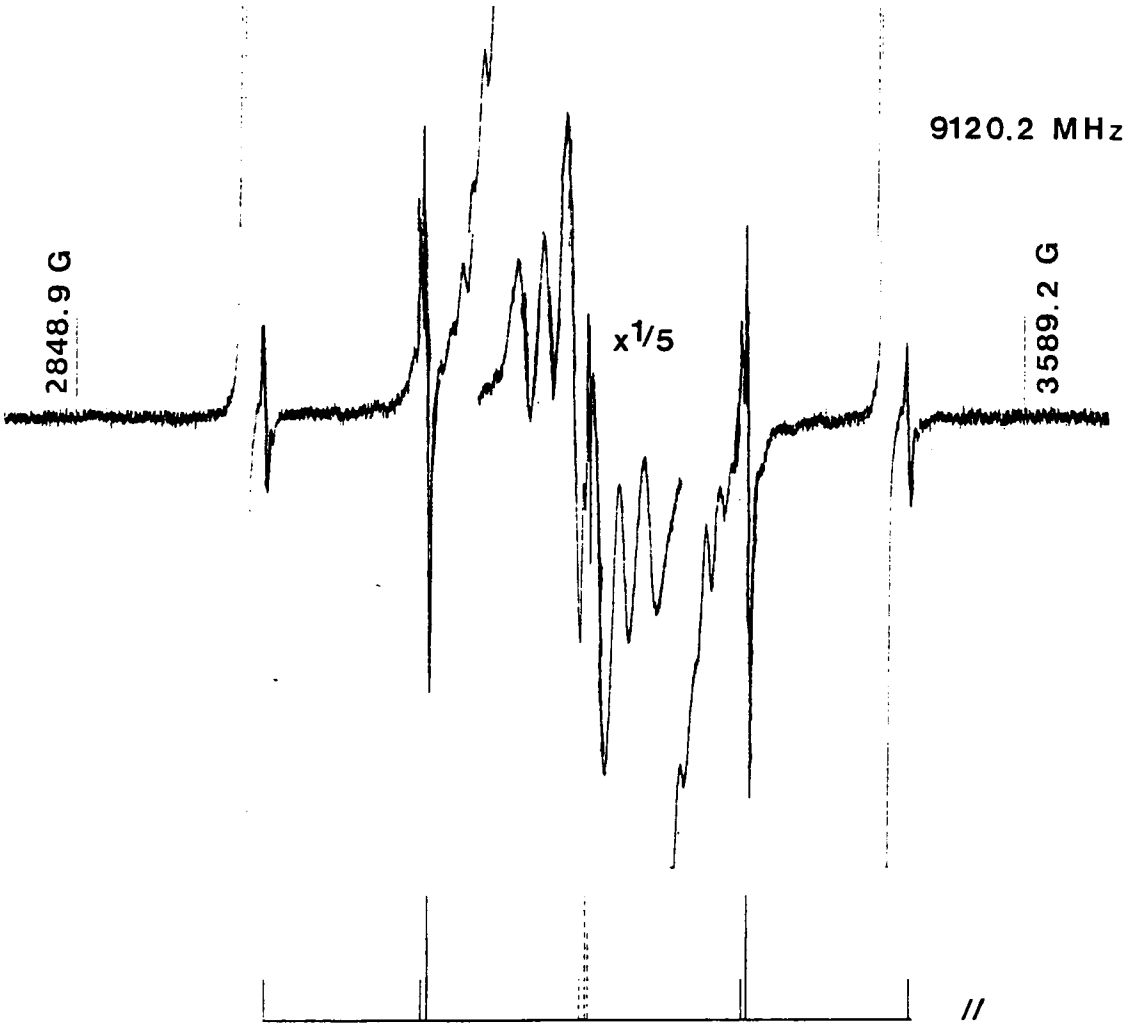

Figure 16. First-derivative ESR spectrum of a γ-irradiated 1 mole % solid solution of C_2F_4 in MCH-d_{14} at 90 K. The parallel pattern is defined by the stick diagram.

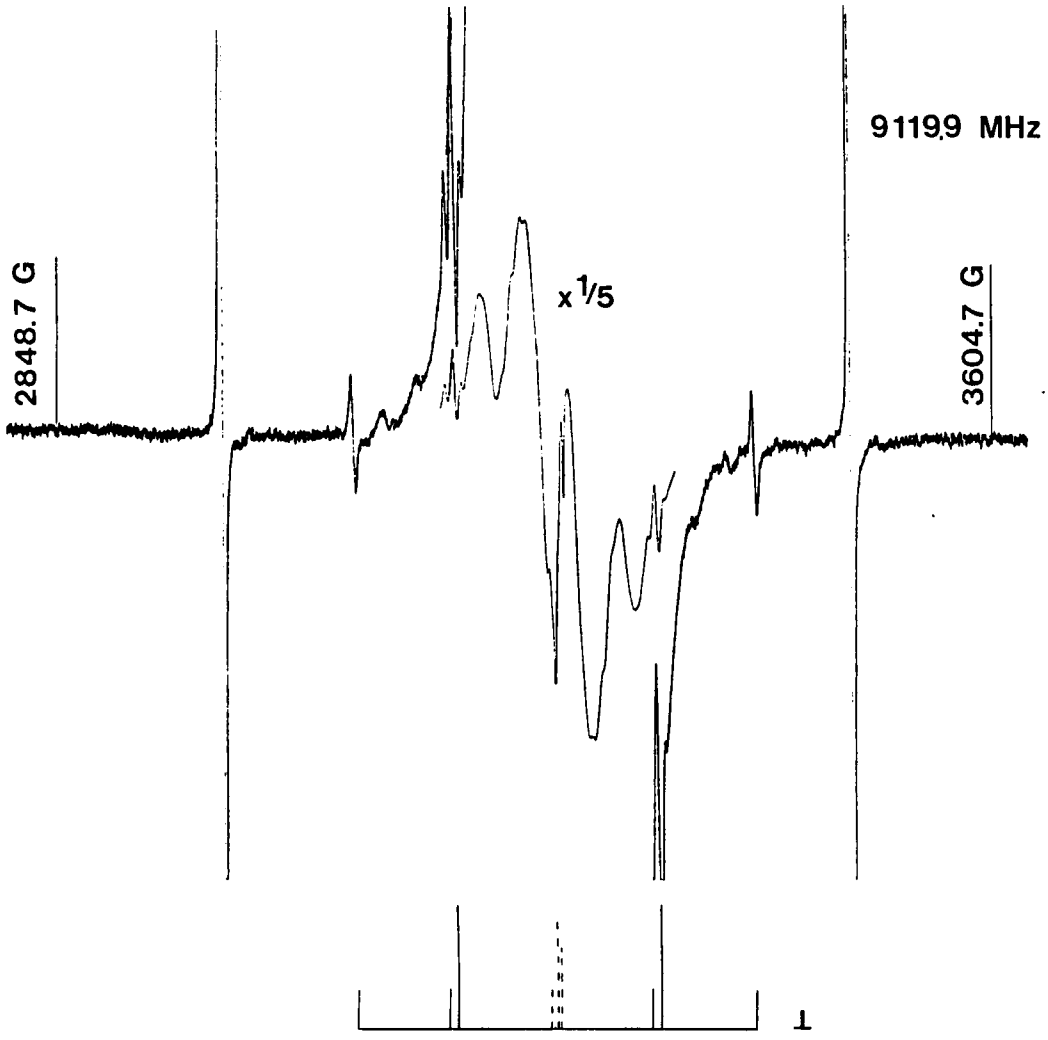

Figure 17. First-derivative ESR spectrum of a γ-irradiated 1 mole % solid solution of C_2F_4 in MCH-d_{14}. The perpendicular pattern is defined by the stick diagram.

property of this particular sample allowed simultaneous monitoring of both the parallel and perpendicular hyperfine features without rotation of the sample tube. Between 70 and 45 K there was virtually no change in either the spectral appearance or the hyperfine parameters, as shown by Table VIII, page 92, and Figures 18 and 19, pages 93 and 94. At 35 K, however, the parallel components seemed to change from a quintet pattern into a triplet of triplets with $A_{//}$ ($2^{19}F$) = 128 G and $A_{//}$ ($2^{19}F$) = 120 G but the perpendicular components seemed to remain unchanged, as shown in Figure 20, page 95. This change in the parallel components is confirmed by the change in the second-order pattern. Since maintaining a temperature of about 4 K was difficult for an extended period of time, the lowest temperature spectra were obtained by sweeping only one-half of the field at a time. These partial sweeps are shown in Figures 21 and 22, pages 96 and 97. These spectra confirm the trend previously described for the parallel components; that is, a breakdown of the parallel components into an apparent triplet of triplets. In addition to the apparent non-equivalence of the four fluorines as manifested in the parallel features, the perpendicular hyperfine pattern also becomes more complex at low temperature. This complication of the perpendicular pattern may also reflect a similar inequivalence of the four fluorines or the loss of axial symmetry in the fluorine hyperfine tensor.

It should be noted that the microwave levels used, 10-20 dB, during this low temperature experiment did not seem to cause any

TABLE VIII

THE EFFECT OF TEMPERATURE ON THE $C_2F_4^-$ HYPERFINE COUPLING CONSTANTS BETWEEN 100 TO 4.4 K

Temperature (K)	$A_{//}$ (G)	$A_{\perp}$ (G)
100	124.5 (4)[a]	78.6 (4)
70	124.7 (4)	78.4 (4)
45	124.2 (4)	78.9 (4)
35	128.6 (2) 122.3 (2)	81.1 (2) 74.6 (2)
10	132.1 (2) 123.9 (2)	82.5 (2) 73.2 (2)
4.4	138.9 (2)[b] 117.6 (2)[b]	-- --

[a]The number in the parenthesis corresponds to the number of equivalent nuclei with that hyperfine coupling.

[b]Tentative analysis.

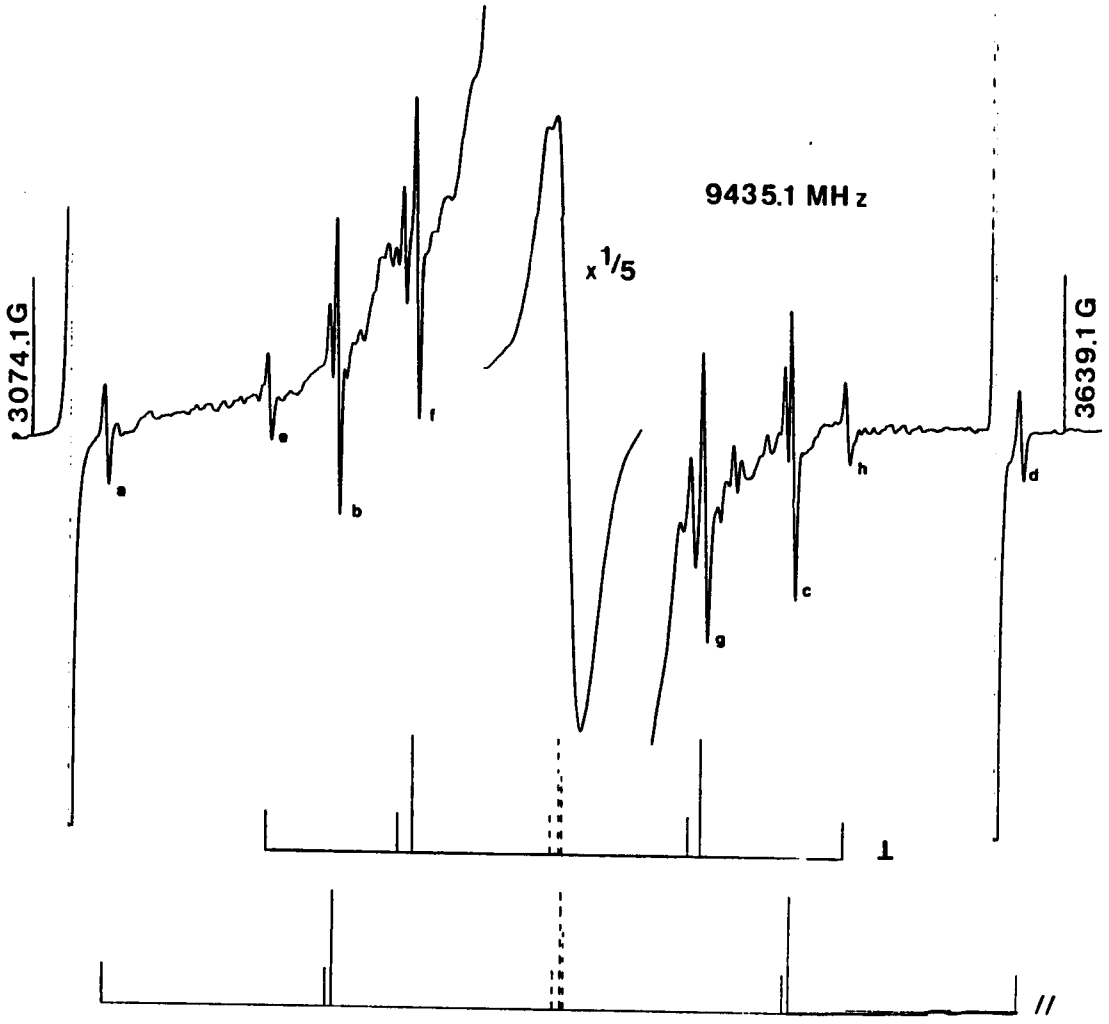

Figure 18. First-derivative ESR spectrum of a γ-irradiated 1 mole % solid solution of C_2F_4 in MCH-d_{14} at 70 K. The observed resonances which are observed and which change with temperature are labeled a-h.

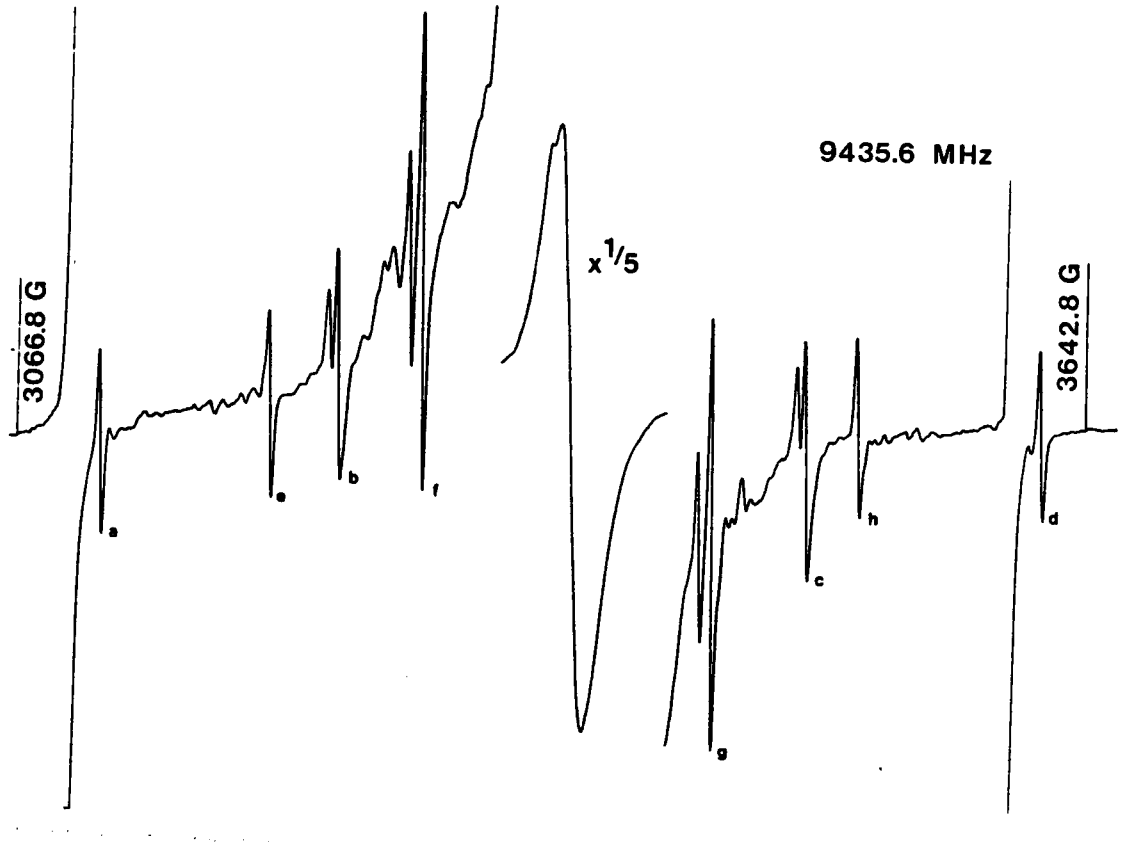

Figure 19. First-derivative ESR spectrum of a γ-irradiated 1 mole % sample of C_2F_4 in MCH-d_{14} at 45 K. The features marked with letters (a-h) are defined in Figure 18, page 93.

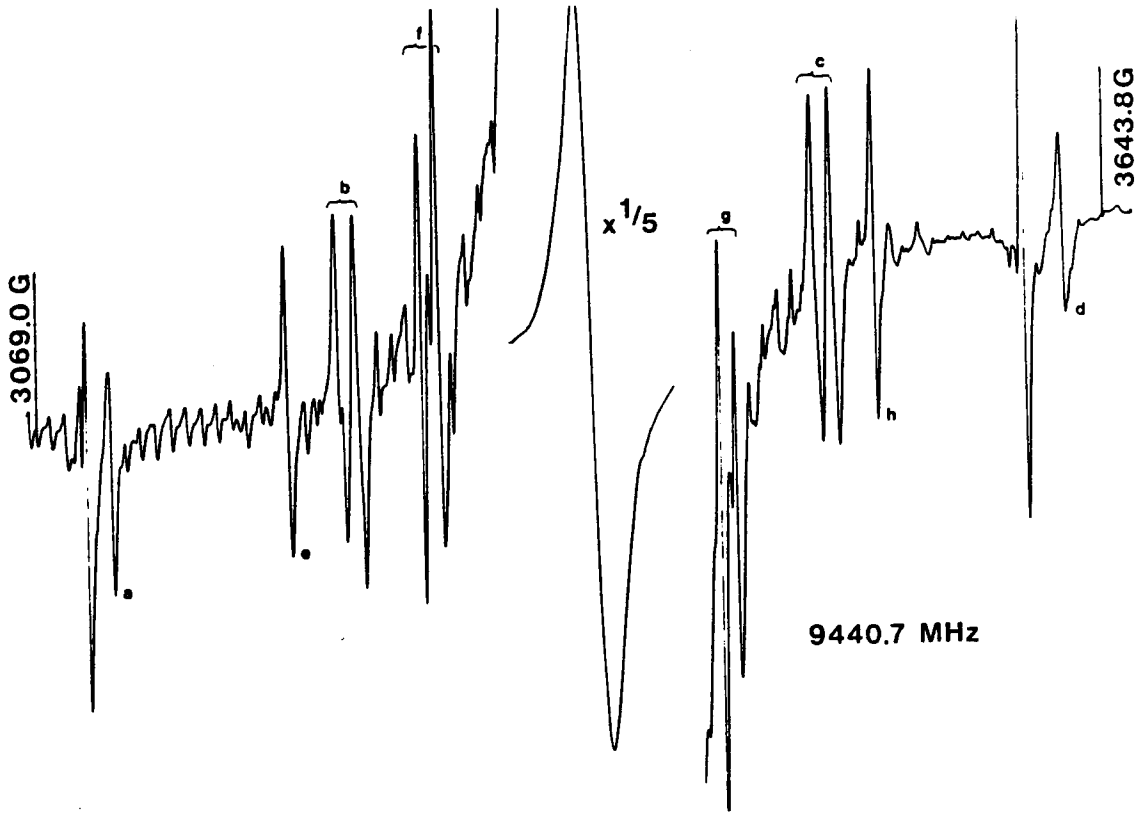

Figure 20. First-derivative ESR spectrum of a γ-irradiated 1 mole % solid solution of C_2F_4 in MCH-d_{14} at 10 K. The small oscillating resonances on the low-field side are instrumental in origin. The feature marked with letters (a-h) are defined in Figure 18, page 93.

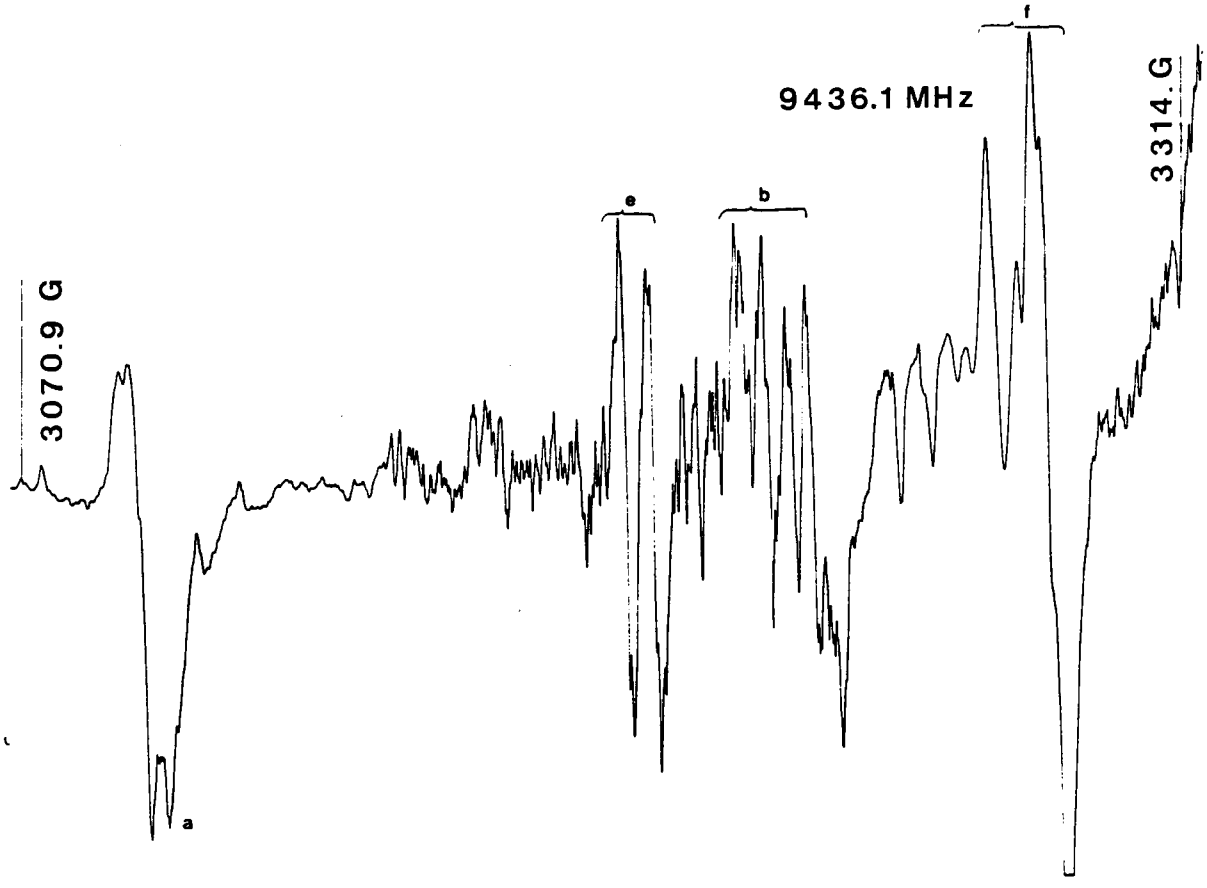

Figure 21. Low-field portion of a first-derivative ESR spectrum of a γ-irradiated sample of C_2F_4 in MCH-d_{14} at 4.2 K. The features marked with letters are defined in Figure 18, page 93.

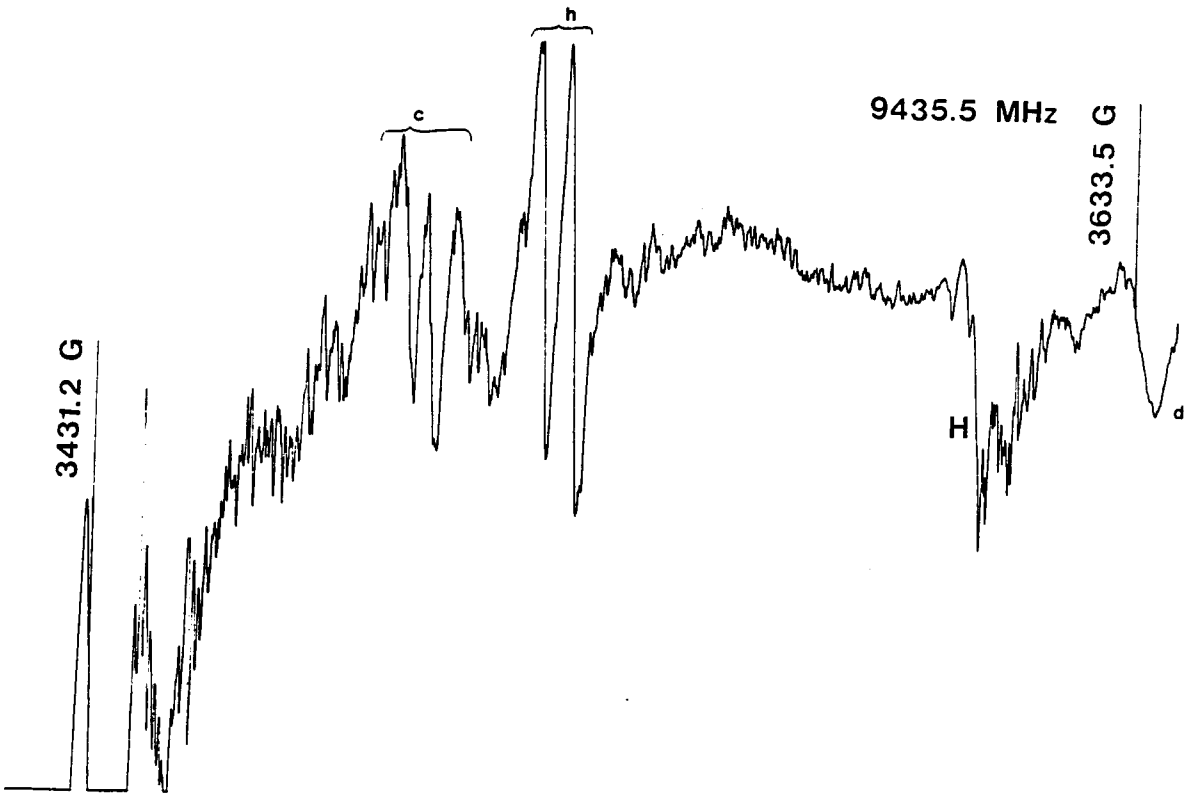

Figure 22. High-field portion of a first-derivative ESR spectrum of a γ-irradiated sample of C_2F_4 in MCH-d_{14}. The features marked with lower-case letters (c, h, and d) are defined in Figure 18, page 93. The feature marked with a capital H is the high-field hydrogen atom resonance.

noticeable distortion in the $C_2F_4^-$ radical resonances due to saturation. Also, all of the thermal changes below 35 K were observed to be fully reversible.

In addition to the low temperature study, the anisotropic spectrum of the $^{13}C_2F_4^-$ radical was obtained. The ^{13}C enriched sample of $^{13}C_2F_4$ was synthesized by Dr. J-T Wang. Just as in the previous study, MCH-d_{14} was used as the matrix with the $^{13}C_2F_4$ being approximately 1 mole %. The sample mixture was slowly lowered into liquid nitrogen over a 16-hour interval thereby forming a polycrystalline sample. After γ-irradiation of the sample, the resulting ESR spectra were characterized by symmetric line shapes for the resonances whose magnetic field positions were dependent upon the angular position of the sample tube in the cavity. This orientational dependence was utilized to obtain almost complete discrimination between either the parallel, as shown in Figure 23, page 99, or the perpendicular, as shown in Figure 24, page 100, anisotropic features by rotation of of the sample reported for this matrix, the resonances in this case actually represent the parallel and perpendicular components of the hyperfine tensor.

The hyperfine coupling constants for this radical were refined using the least squares program previously described. The results of this analysis are listed in Table IX.

The effect of temperature on the hyperfine coupling constants in the present work seem to be slightly different from the low temperature results obtained in a MTHF matrix. In the MTHF matrix,

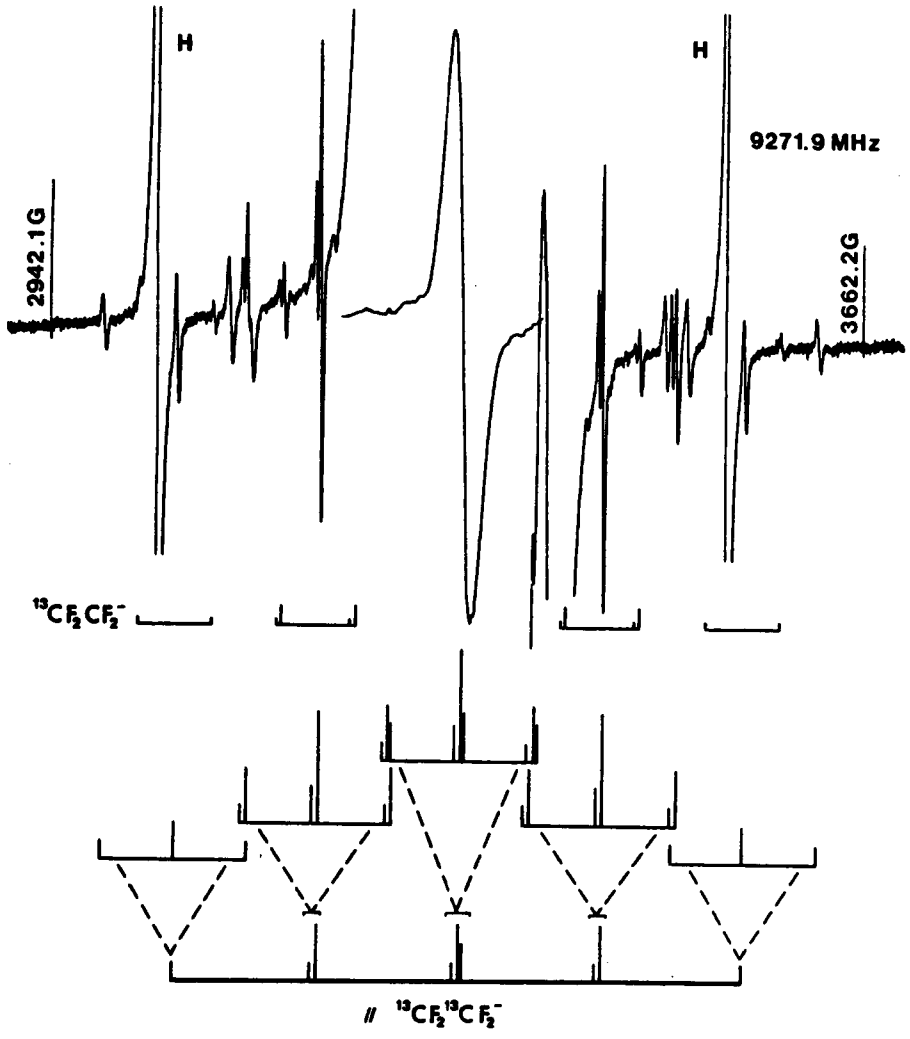

Figure 23. First-derivative ESR spectrum of a γ-irradiated 1 mole % solid solution of ^{13}C-enriched $^{13}C_2F_4$ in MCH-d_{14} at 90 K, parallel features. The features which correspond to the parallel components are defined by the lower stick diagram.

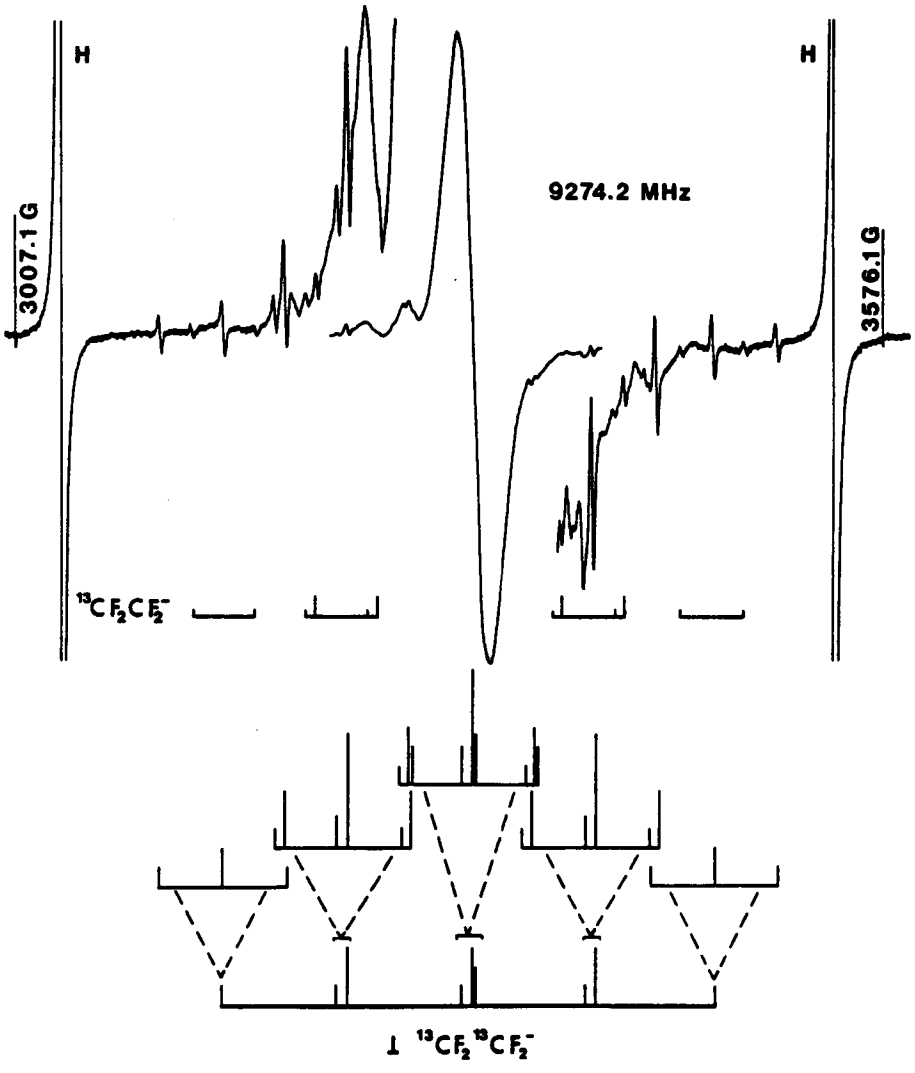

Figure 24. First-derivative ESR spectrum of a γ-irradiated 1 mole % solid solution of ^{13}C-enriched $^{13}C_2F_4$ in MCH-d_{14} at 90 K, perpendicular features. The features which correspond to the perpendicular components are defined by the lower stick diagram.

TABLE IX

ANISOTROPIC HYPERFINE PARAMETERS FOR $^{12}C_2F_4^-$ AND $^{13}C_2F_4^-$ IN MCH-d_{14} AND ORBITAL SPIN DENSITIES

Radical Anion	Temp. (K)	$g_{//}$	$g_{\perp}$	Nucleus	Hyperfine Couplings $A_{//}$ (G)	Hyperfine Couplings $A_{\perp}$ (G)	Spin Densities[a] ρ_s	Spin Densities[a] ρ_p	Reference
$^{12}C_2F_4^-$	100	2.0022	2.0033	^{19}F	124.2	78.75	.005	.024	This Work
$^{13}C_2F_4^-$	100	2.0024	2.0035	^{13}C	64.5	43.0	.040	.187	This Work
				^{19}F	123.6	79.1	.005	.023	This Work

[a]Orbital spin densities calculated using the values from Table I, page 25.

the $A_{//}$ (4F) coupling was said to increase to 138 G while the $A_{\perp}$ (4F) coupling was said to decrease to about 63 G. The differences between these two low temperature studies may be simply a natural result of the poorer resolution characteristic of the MTHF matrix. In any event, a possible interpretation of the observed facts will be given and how this relates to the question of the anion's structure will be postulated.

First, it must be recognized that irrespective of the question regarding a planar or chair structure, the four fluorines are not magnetically equivalent in the stationary radical. Although the fluorines are equivalent with respect to symmetry, their anisotropic hyperfine interactions are <u>not</u> equivalent with respect to the magnetic field in every direction. Specifically, for a planar π^* radical, although the four fluorines would be expected to be equivalent when the field is parallel to $2p_z$ orbitals, rotation would still be needed to obtain an axially symmetric hyperfine tensor by averaging the x and y hyperfine components which are perpendicular to the $2p_z$ orbitals. An example of this point is the $C_2F_4^+$ π radical[116] where although the parallel components are well-defined, sharp resonances, the perpendicular components which are unobserved are presumably anisotropically smeared due to a lack of rotation. For a planar σ^* radical or the pyramidal chair structure, the trans-fluorines are equivalent in the magnetic field since they are geometrically parallel in pairs, as shown in Figure 15, page 84. Thus, for the four fluorines to be spectroscopically equivalent either

some motion must interchange the non-equivalent pairs or, if there is no motion, then the anisotropic interactions of the non-equivalent pairs must be fortuitously equivalent. This latter possibility can be immediately rejected since such a case would predict that the four fluorines would remain spectroscopically equivalent independent of temperature which is clearly incorrect, as shown by Table VIII, page 92. Therefore the radical must be undergoing some kind of motion which averages together the two sets of fluorines. This averaging could result from a vibrational motion or from a rotation of the entire molecule. If the averaging were the result of rotation, then assuming a non-constrictive environment the axis of rotation would be expected to be along the axis with the lowest moment of inertia.

In order for a vibrational motion to give rise to the observed experimental results, the vibrational mode would have to symmetrically interchange the two equivalent pairs fast above 45 K but gradually slower below this temperature. Within the framework of the planar π^* or the σ^* model, no such vibrational mode exists. Within the framework of the chair structure, there is also no such mode, but an umbrella inversion type mode could lead to a near-equivalence in the four fluorines.

Although this umbrella inversion mode is well-known to occur in NH_3, it is energetically unfavored for both NF_3 and N_2F_4.[118] Also, theoretical calculations predict this barrier to be quite high.[114] Hence, it can be reasonably asserted that the spectroscopic changes observed below 35 K are not the result of vibration.

Within the framework of a rotational model, the effects of temperature can be rationalized in the following way. At temperatures above 45 K, rotation about an axis causes the non-equivalent pairs to exchange quickly resulting in an averaging of the anisotropic hyperfine interactions which results in the four fluorines being spectroscopically equivalent. Lowering the temperature, however, slows the rotation and now the averaging is incomplete and the anisotropic hyperfine interactions of the four fluorines begin to split apart into the two sets of magnetically equivalent pairs. With further cooling, one would expect that the partial averaging would become even less and the differences between the hyperfine interactions of the two pairs would become even greater. This last observation is qualitatively what is observed, as shown by Table VIII, page 92.

Therefore it seems reasonable that rotation of the radical about an axis causes the four fluorines to be spectroscopically equivalent. This conclusion, however, does not discriminate between either the planar or chair structures because both structures possess rotation axes which could average the four fluorines.

From the ^{13}C enriched sample, $^{13}C_2F_4$, the anisotropic hyperfine interactions to the ^{13}C nuclei were determined. As listed in Table IX, page 101, the parallel components of both the ^{13}C and ^{19}F anisotropic hyperfine tensors are larger than the perpendicular components. Given that the radical anion is rotating about a particular axis, this experimental result implies that more spin density is directed parallel to the axis of rotation than perpendicular to this axis. The planar π^* and σ^* models and the pyramidal chair structures will be evaluated in light of this implication.

The first case to be considered will be the pyramidal chair structure. The lowest moment of inertia for rotation for the chair structure is shown below:

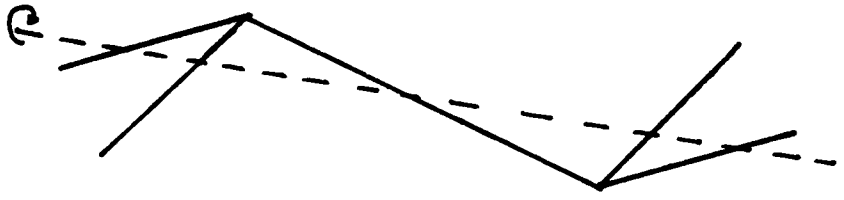

Using the orbital description, as obtained from high level ab initio calculations, of the $CF_3\cdot$ radical as a point of comparison, the largest principal value of the ^{19}F tensor would be expected to be co-linear to the axis of rotation. This being the case, the parallel component of the ^{19}F axially symmetric hyperfine interaction would then be expected to be greater than the perpendicular hyperfine interaction. This prediction, as noted earlier, corresponds to the experimentally determined data, Table IX (page 101). Extending the above argument to the ^{13}C axially symmetric hyperfine tensor,

the principal value would be expected to be perpendicular to the axis of rotation thereby yielding a perpendicular ^{13}C hyperfine coupling greater than the parallel coupling. Since this latter prediction is contrary to the experimental results, the appropriateness of a chair structure to describe $C_2F_4^-$ must be questioned. It should be noted that by extending this simplified argument to the other two orthogonal axes of rotation, in neither case does the largest principal value of the ^{13}C and ^{19}F tensor lie along the axis of rotation.

The next case to be considered is the planar σ^* model. Using the known neutral molecular geometry (R(C-C) = 1.319 Å, R(C-F) = 1.311 Å, <FCC = 123.76°), the rotation having the lowest moment of inertia is a rotation along the C-C bond which, using the Mulliken convention, is defined as the Z axis. The molecular orbital of the unpaired electron as determined by an INDO calculation which used the neutral molecular geometry is shown below. The pertinent numerical output is graphically shown below.

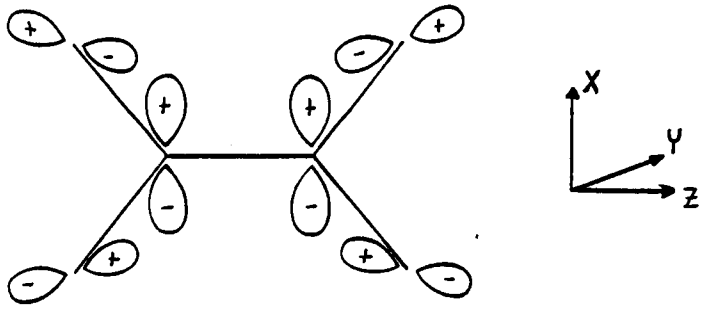

Although the INDO calculation correctly predicts that the largest principal value of the fluorine tensor should lie along the Z axis, the calculation incorrectly predicts that the principal value of the

^{13}C tensor would be along the Y axis. It should be noted that if allowances are made for small distortions from the neutral equilibrium geometry (R(C-C) = 1.18 Å, R(C-F) = 1.46 Å and LFCC = 117°), the lowest moment of inertia becomes the Y-axis. The molecular orbital of the unpaired electron as determined by an INDO calculation using this latter geometry is shown below

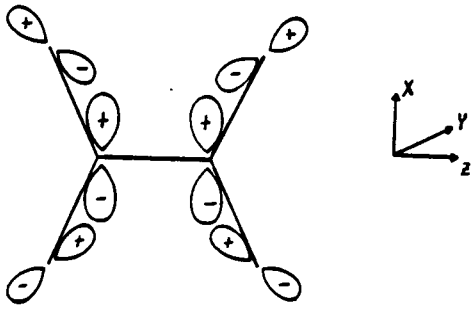

In this case, as diagrammatically shown above, the largest principal values of both of the ^{13}C and ^{19}F tensors lie along the axis of rotation, the X-axis. Thus, this structure if correct would aptly explain the experimental results.

The final case to be considered is the planar π^* model. Using the known molecular geometry, the moments of inertia for the three orthogonal axes may be evaluated. The rotation with the lowest moment of inertia is along the C-C bond (Z axis). The rotation with the highest moment of inertia is the one perpendicular to the plane of the molecule (Y-axis). While a hypothetical change in the structure could result in the X-axis having the lowest moment of inertia, the Y-axis would still remain the axis with the largest

moment of inertia.

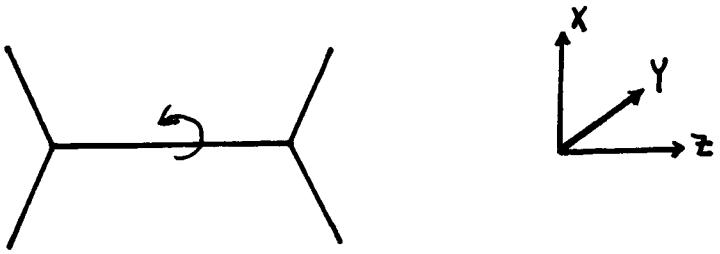

Since the largest principal components of the ^{13}C and ^{19}F tensors must lie along the axis of rotation, within the framework of this model, a rotation about either the X- or Z-axes would be inappropriate. However, a rotation about the Y-axis which corresponds to the highest rotational moment of inertia could explain the observed results.

In summary, three possible descriptions of the structure and the orbitals that the unpaired electron in $C_2F_4^-$ may occupy have been discussed. The present low temperature study allows a further confirmation of the rotational nature of the radical anion. Since the largest principal components of the ^{13}C and ^{19}F tensors lie along the same axis, then the anisotropic ^{13}C data appears to be inconsistent with the pyramidal chair structure where the largest values are perpendicular to each other. The experimental result may be explained within the framework of a planar π^* radical if rotation is allowed about the axis with the greatest moment of inertia. If the assumption that a radical preferentially rotates about its axis which has the lowest moment of inertia is valid, then by allowing for slight geometric distortions in the radical anion from

the neutral molecule, an INDO calculated SOMO for a planar σ^* radical fits the experimental data. Although the experimental results appear to favor a planar structure with a σ^* orbital being somewhat more reasonable, an ultimately decisive choice of either the structure or the orbital will probably not be possible without higher level computer calculations.

D. Octafluorocyclooctatetraene Radical Anion

Our interest in trying to generate the radical anion of octafluorocyclooctatetraene (OFCOT) was triggered by a visit of David M. Lemal[119] to The University of Tennessee, Knoxville, Chemistry Department. It was thought that OFCOT might be a suitable electron scavenger and that the structure of the OFCOT radical anion, if it could be determined, might provide some interesting insights into π bonding when compared with the hydrogen analog, the cyclooctatetraene (COT) radical anion.[120,121] Upon electrochemical reduction, the neutral tub-shaped COT molecule changes to an aromatic π radical. In like manner, the OFCOT neutral molecule, which also possesses a tub-shaped equilibrium geometry,[122] might be expected to distort to an aromatic π structure upon electron capture. Thus, the determination of any structural modification and/or detecting a drive toward aromaticity were the goals of this investigation.

Several different matrices were tried in a search to find a suitable matrix in which to generate the radical anion. The neutral OFCOT was introduced directly into the ESR tubes without further

purification. Except in the case of hexamethylethane (HME) which is a solid at room temperature, the OFCOT solid was degassed at 77 K before the matrix material was vacuum transferred into the ESR tube. When the HME matrix was used, both solids were introduced into the ESR tube and then degassed. After the sample was prepared, the contents were melted in an oil bath to promote the mixing of the two solids. In all of the different matrices, the OFCOT appeared to be soluble. All samples were γ-irradiated at 77 K.

Initially, it was thought that HME would be a suitable matrix for radical anion generation and detection, since a very well-resolved isotropic spectrum of the perfluorobenzene radical anion was observed in this matrix. A 1 mole % sample of OFCOT was mixed with HME and at 77 K received a dose of 0.65 Mrad. At low temperature, the ESR spectrum in Figure 25, page 111, consists mainly of the expected free radicals derived from the matrix. However, at higher gain a weak set of features was obtained outside the matrix signal. These weak features which at 90 K were not well resolved sharpened up significantly at 135 K giving an apparent 246 G doublet of nonets with a splitting of 8.8 G, as shown in Figure 25. Interestingly, upon warming to 165 K these weak features disappeared but upon returning to 135 K the features returned minus a slight amount of decay. Further attempts to identify this radical were not explored, but these results are included here for completeness.

Since it was feared that heating the sample of OFCOT and HME in the hot oil could have caused the OFCOT to degrade, a 1:1 mixture

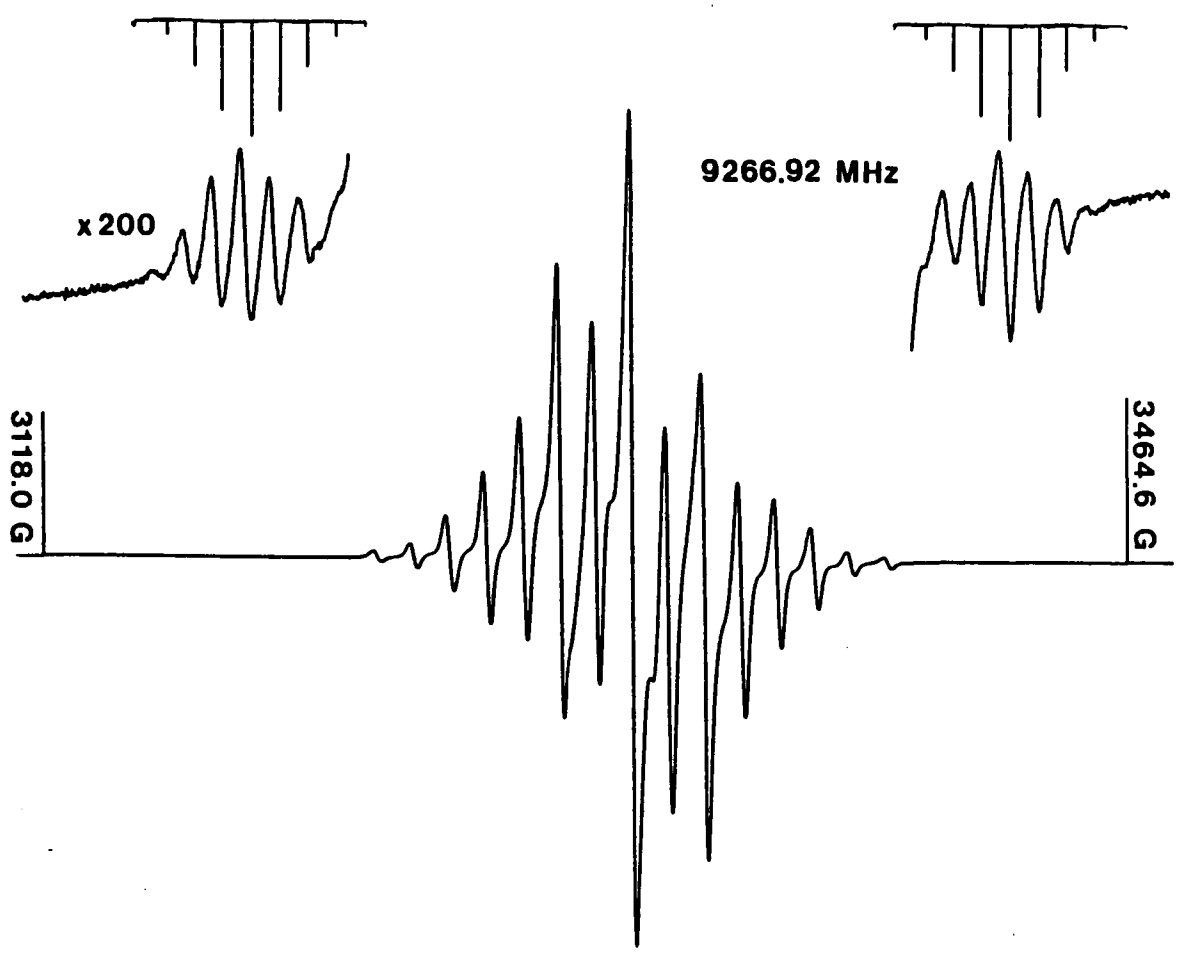

Figure 25. First-derivative ESR spectrum of a γ-irradiated 1 mole % sample of OFCOT in HME. The features marked with the stick diagrams are discussed in the text.

of tetramethylsilane (TMS) and HME was tried as a solvent since TMS is a liquid at room temperature. However, these results essentially paralleled those of the pure HME matrix, the only difference being the appearance of a more intense triplet pattern derived from the $R\text{-}CH_2\cdot$ type radical of TMS and the poorer resolution of the outer weak features described above.

A 1% by weight sample of OFCOT in MCH-d14 was prepared and γ-irradiated; however, only matrix radicals were observed.

The successful approach to obtain easily interpretable spectra of the OFCOT radical anion was to use MTHF as a matrix. A 0.3% by weight (0.1 mole %) sample of OFCOT in MTHF was exposed to a 0.65 Mrad dose of γ-irradiation. Since MTHF produces a clear glassy-type matrix, the color of the sample after γ-irradiation was easily observed as being a dark reddish-blue or magenta color (λ_{max} = 360-385 nm).[123] At low temperature (80 K) a dominant seven-line pattern was observed with a splitting of about 18 G which was identified as the MTHF free radical.[124,125] Evidence for the trapped electron[126] was sought for in this sample by optimizing the conditions for its observation, such as minimizing the γ-irradiated sample's exposure to visible light since this "bleaches" or induces the decay of the trapped electron, and also by minimizing the power level in the cavity since the higher power settings tend to saturate the trapped electron resonance. Nevertheless, there was no ESR spectral evidence suggesting the presence of a trapped electron as shown in the lower portion of Figure 26, page 113. In contrast, a pure MTHF

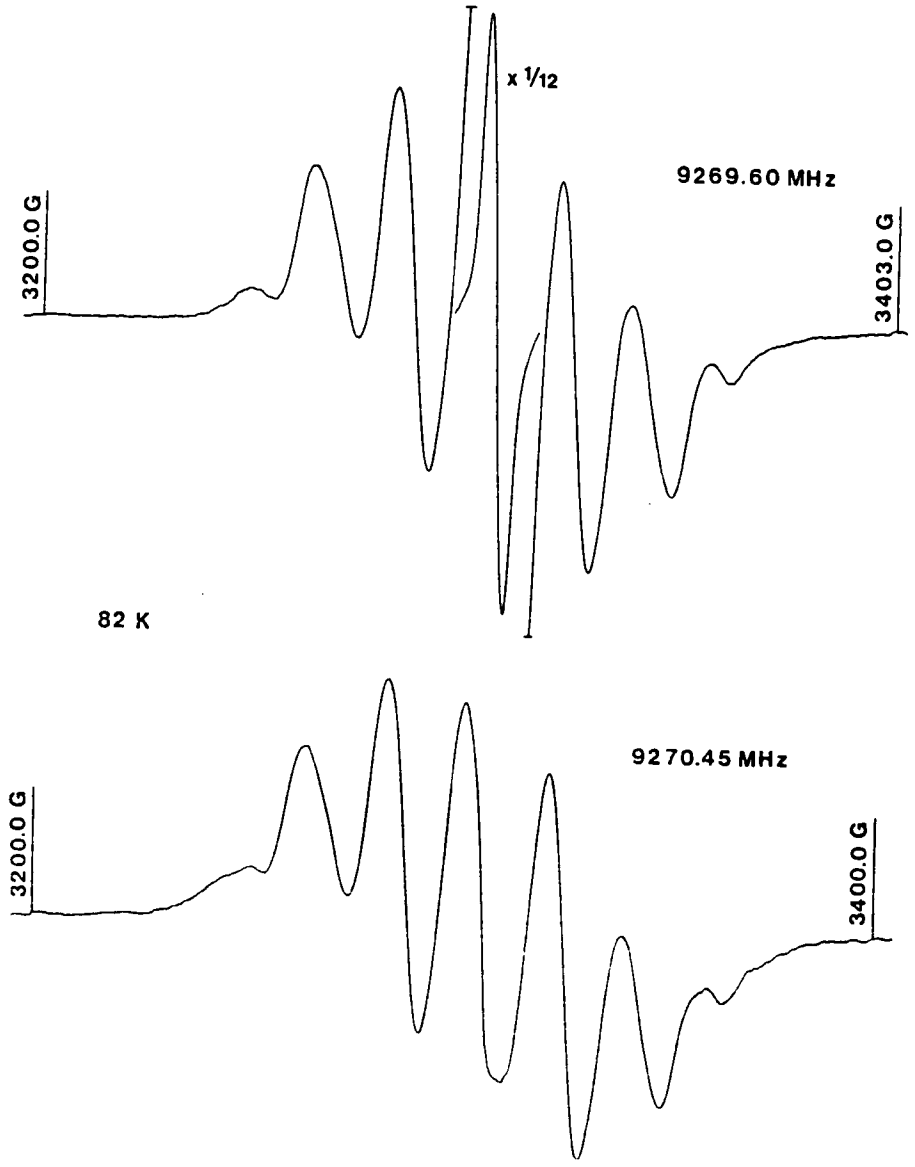

Figure 26. First-derivative ESR spectra of samples of pure MTHF (upper spectrum) and of a 0.1 mole % solution of OFCOT in MTHF (lower spectrum) recorded under the same conditions at low microwave power (55 dB) and 82 K after exposure to ^{60}Co γ radiation for identical doses (0.5 M rad) at 77 K.

sample which was also exposed to an identical γ-irradiation dose (0.65 Mrad) and also observed under exactly the same experimental conditions exhibited both an extremely intense resonance from trapped electrons, as shown in the upper portion of Figure 26, and a seven-line pattern from the MTHF matrix, just like the OFCOT/MTHF sample. The color of this sample was dark blue which is characteristic of trapped electrons in glasses.

Since the sample which contained the OFCOT did not give evidence for a trapped electron, a reasonable conclusion is that the OFCOT must capture the electrons. Since the MTHF free radical is thought to be produced by the positive hold, and since the presence of OFCOT would not be expected to perturb this process, the observation of the MTHF free radical in both systems is quite reasonable. The difference in color between the OFCOT/MTHF and pure MTHF samples is further evidence suggesting that OFCOT can readily capture electrons. As is often the case, differences in the microwave power level can quite drastically change the observed spectral pattern. Based upon the author's limited observations, free radicals often began to power saturate around 10-15 dB (20-63 mW) where as radical anions and cations do not seem to saturate so easily and can often be more favorably observed between 0-5 dB (200-63 mW). Of course there can be exceptions to this general rule. For example $(CH_3CN)_2^{-}$[127] readily power saturates whereas $Me_3PbCH_2\cdot$[128] does not.

If instead of 61 dB (158 mW), the power level is changed to 5 dB (63 mW) for the OFCOT sample, then weak features are observed

on both the low and high field sides of the MTHF free radical resonance width of about 125 G, indicating that possibly another radical is present but is buried beneath the dominant MTHF free radical resonances. However, a similar power intensification on the pure MTHF sample only results in a saturation of the trapped electron with no evidence of this other pattern. These observations are shown in Figure 27, page 116.

Either temporarily warming the pure MTHF sample to 95 K or bleaching with visible light resulted in the disappearance of the trapped electron signal. Both of these procedures are well-known methods of removing trapped electrons. After removal of the trapped electron, the sample was a straw-yellow color. Similar treatment of the OFCOT/MTHF sample, however, did not change its spectral appearance, nor its color.

Warming the OFCOT/MTHF sample to around 100-130 K resulted in the irreversible loss of the MTHF free radical and exposed signals which were previously buried, as shown in the upper portion of Figure 28, page 117. This ESR spectral change, however, was not followed by a color change; that is, the sample still retained its original magenta color. Similarly, warming the pure MTHF sample to between 100-103 K resulted in the irreversible loss of the MTHF free radical, but now the only signals remaining were from the γ-irradiated Suprasil tube as shown in the lower portion of Figure 28. The sample in this case was now transparent.

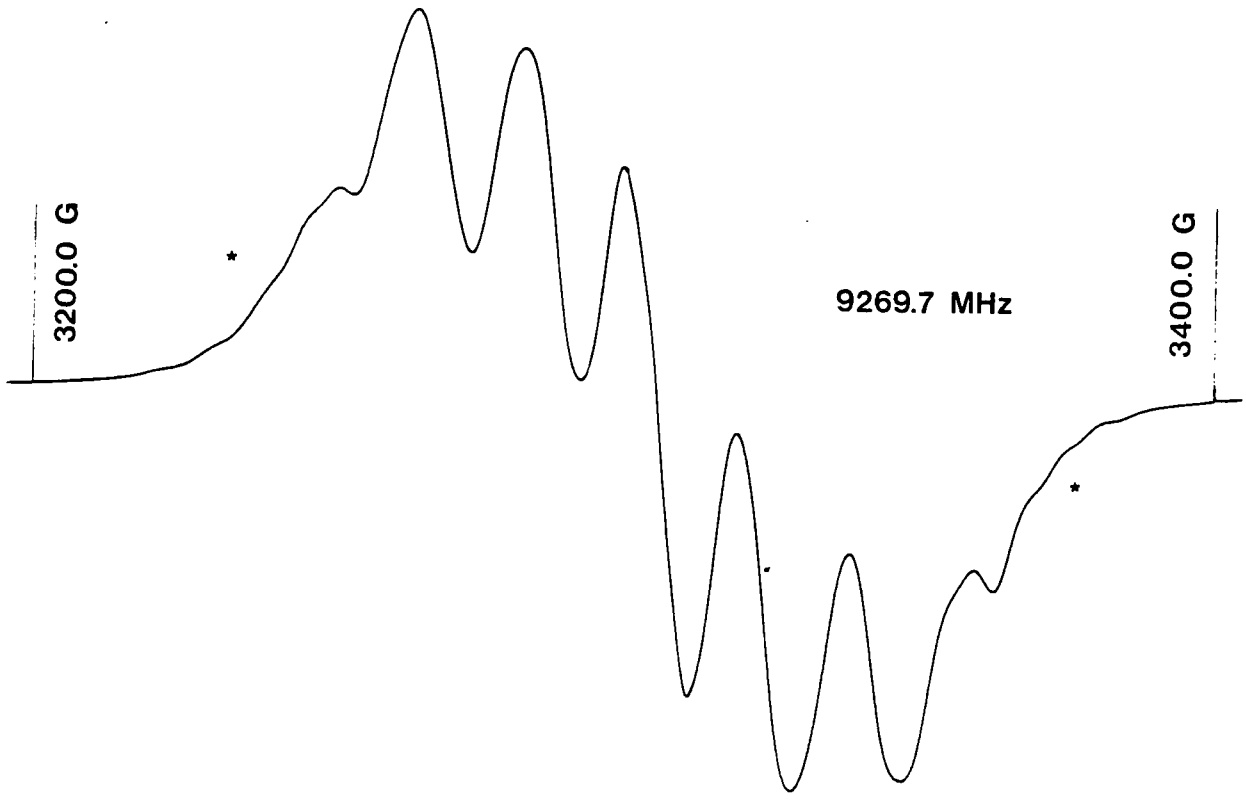

Figure 27. First-derivative ESR spectrum of a γ-irradiated 1 mole % solid solution of OFCOT in MTHF at 83 K and high spectrometer power. The regions marked with asterisks correspond to the outermost lines of the OFCOT radical anion.

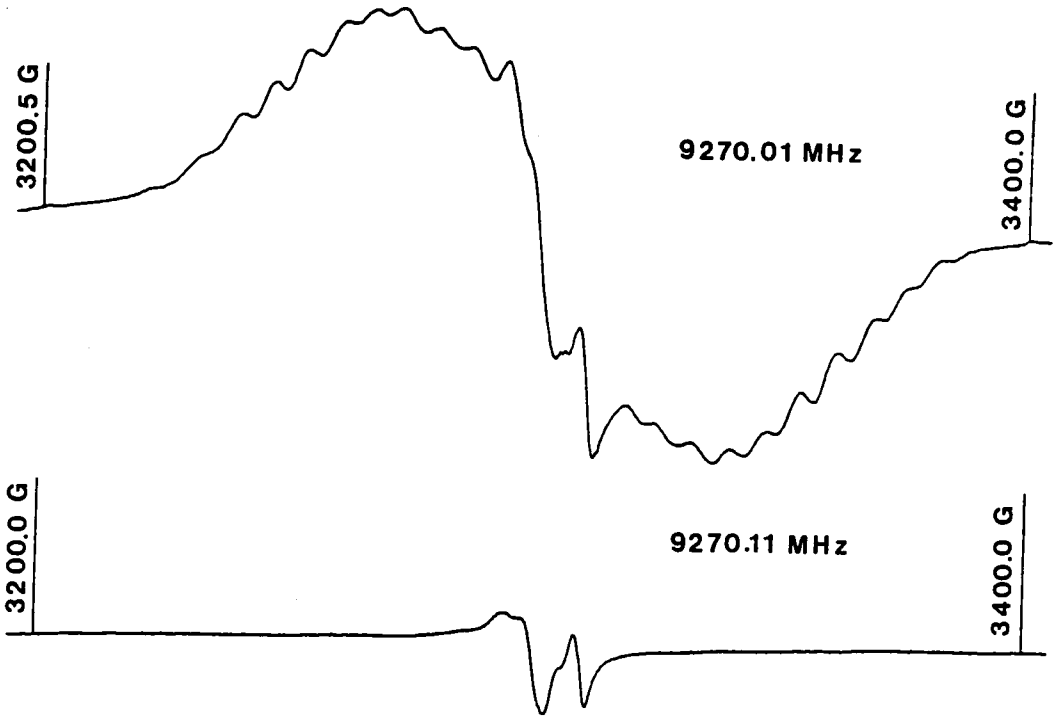

Figure 28. First-derivative ESR spectra of γ-irradiated samples of a 0.1 mole % solution of OFCOT in MTHF (upper spectrum) and of pure MTHF (lower spectrum) recorded under the same conditions (microwave power of 10 dB) at 82 K after the samples had been treated identically to thermal annealing at 103 K and recooled.

Attention will now be focused upon the thermal changes of the OFCOT/MTHF sample. Although the low-temperature pattern of this radical shows a tantalizing amount of symmetry, it has defied all of the author's attempts at analysis. Upon warming, portions of the pattern begin to coalesce around 110 K. At 120 K, an apparent seven-line pattern is formed but is replaced with a much different pattern at 130 K. In this temperature region and above, the sample became quite "lossy" and the microwave power had to be reduced. With further warming to 138 K, the broad anisotropic features began to be replaced with an isotropic looking pattern. Just a 4° increase in temperature was sufficient to complete the transition to an essentially isotropic simple nine-line binomial pattern. These spectral changes are depicted in Figure 29, page 119, and were completely reversible. An optimum spectrum of the nine-line pattern was obtained at 145 K. This temperature seemed to be a good compromise between favorable resolution and radical decay which was quite significant around 150 K or above. Figure 30, page 120, shows both the first-derivative and second-derivative spectra obtained at this temperature. A computer simulation of the second-derivative pattern, shown in the lower portion of Figure 30, using the parameters of A_{iso} (8 F) = 10.92 G, g_{iso} = 2.0049, and a line width of 4.9 G, is in excellent agreement with the observed spectrum.

After the sample was warmed to 145 K, it was recooled back to 80 K and the observed spectra were identical to those taken before warming; also the sample color was still magenta. If the sample

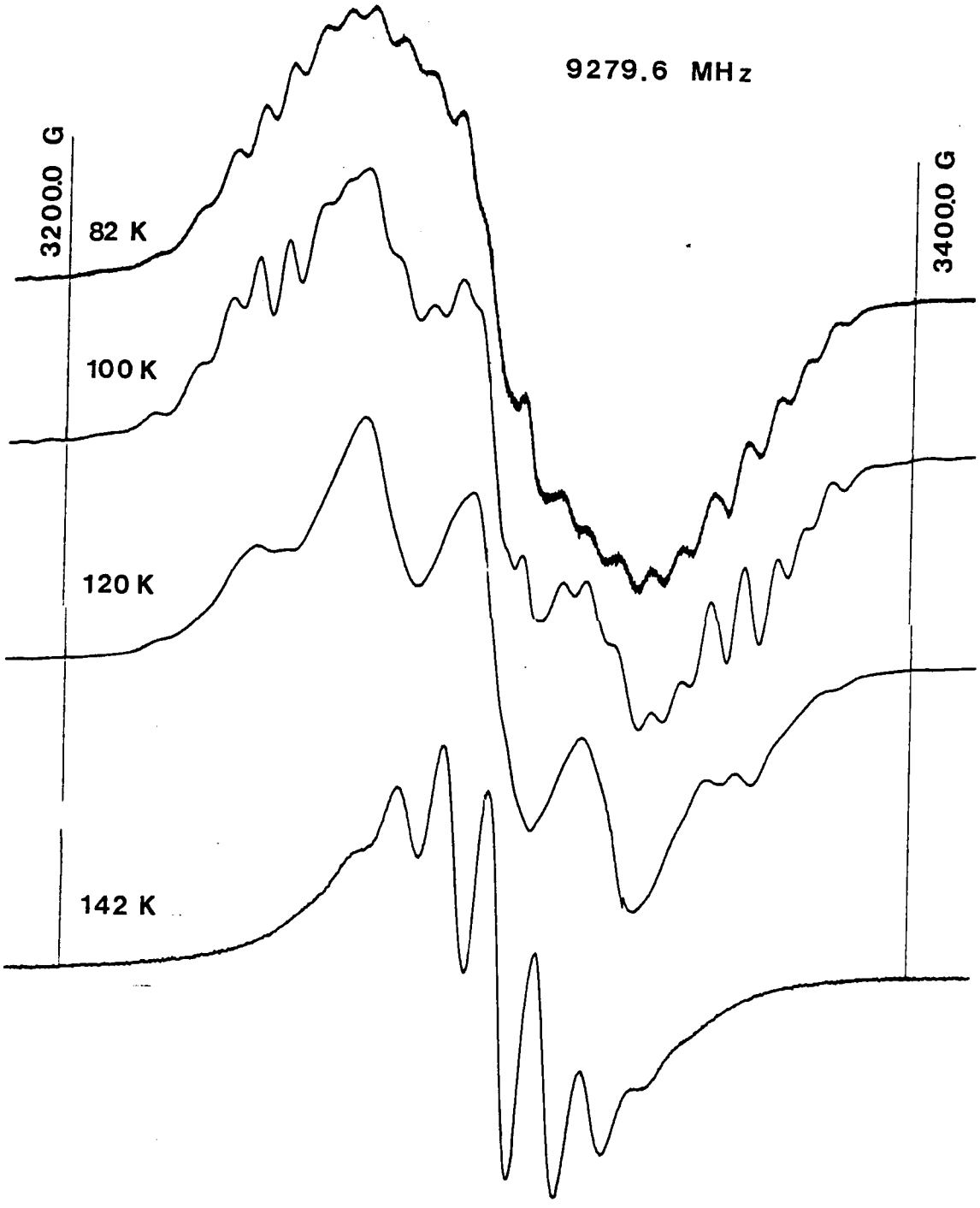

Figure 29. First-derivative ESR spectra of a 0.5 mole % γ-irradiated solid solution of OFCOT in MTHF from 83 K (upper) to 143 K (bottom).

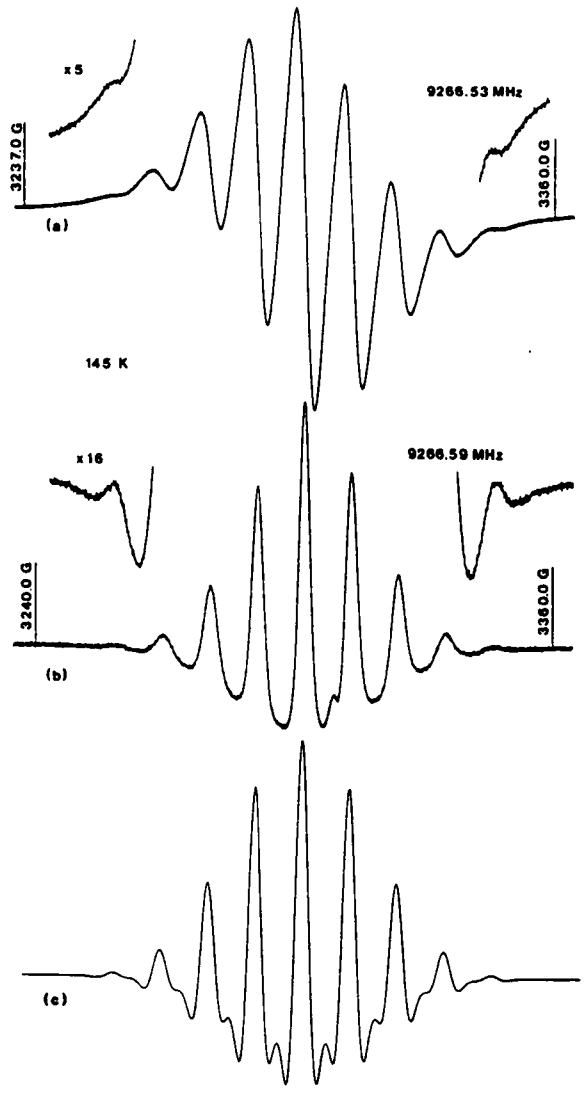

Figure 30. First-derivative (a) and second-derivative (b) ESR spectra of a solid solution of 0.1 mole % OFCOT in MTHF recorded at 145 K after γ-irradiation (dose of 0.5 Mrad) at 77 K. The second-derivative spectrum (c) was obtained by computer simulation using the parameters in the text and a linewidth of 4 G.

was maintained at a temperature of 150 K or more for a few minutes then the isotropic pattern decayed quickly and irreversibly, and the sample turned transparent. The weak resonances observed in the HME matrix were not observed in this matrix.

It should be noted that the OFCOT radical anion could have been produced in the HME or HME/TMS matrix, but since the spectral extent of the matrix radicals (~230 G) exceeded that of the OFCOT (87.36 G), it could have simply been obscured.

Using the INDO program which was previously described, the calculated electronic distribution of the SOMO for the OFCOT radical anion was determined assuming a regular octagonal (D_{8h}) geometry with C-C and C-F bond lengths of 1.38 and 1.35 Å, respectively. These bond lengths were taken as the appropriate averages of the bond lengths in the neutral molecule. Further refinement of the INDO data by energy minimization procedures was not attempted.

The INDO calculations indicated that the unpaired electron occupies one of the essentially doubly-degenerate E_{2u} "nonbonding" π orbitals diagrammatically shown below.

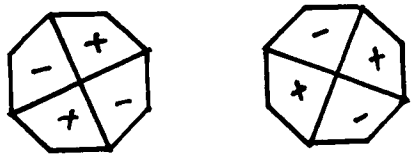

The π character of the SOMO is borne out by the calculation in three ways. First, the spin density distribution is uniformly distributed throughout the entire framework. Also, the majority of the spin density (8 * .116 = .928) is localized in the $2p_z$ carbon orbitals

in contrast to the fluorine $2p_z$ orbitals which contain a much lower spin density (8 * .009 = .072). Finally, the calculation predicts 2s-orbital spin densities of only 0.0029 and 0.0002 on carbon and fluorine, respectively. This latter prediction, which was the only one that could be directly tested in this experiment, was certainly found to be qualitatively correct since $A_{iso}(^{19}F)$ = 10.92 G corresponds to a 2s fluorine spin density of 0.0006.

Parallel to the observation of a nearly isotropic, binomial nine-line pattern for the OFCOT radical anion is the previously reported isotropic nine-line pattern of the COT radical anion. This similarity of patterns, however, does not of itself establish a planar π structure for the OFCOT radical anion. Indeed, the perfluorobenzene radical anion is characterized by six equivalent fluorines and yet it is apparently not a simple π type radical.[129,109]

As is often the case, the structure of a novel radical can be determined by comparison with other known radicals whose structures are established. In the present study, the OFCOT radical anion contains nine π electrons which is just one electron short of the ten electrons needed for aromaticity as predicted by the Huckel 4n+2 rule where n = 2. Thus it could be argued that the electronic structure of the OFCOT radical anion should resemble the radical cations of fluorinated aromatic molecules or other fluorinated molecules which are one electron short of the complement needed for Huckel aromaticity. This assertion is supported by the INDO calculations which, while assuming a planar structure, predicted a simple π radical.

For π radicals, probably the most useful method of correlating the isotropic hyperfine coupling (A_{iso}) of the fluorine atom with the carbon $2p_z(\pi)$ spin density (ρ_c) is the very simple McConnell equation of the form,[130-132]

$$A_{iso} = Q^F_{eff} \cdot \rho_c \quad ,$$

where Q^F_{eff} is an empirical parameter. Just as for hydrogen-containing aromatic radical ions, the constancy of the Q^H_{eff} parameter can be used to correlate isostructural radicals. Likewise, if the Q^F_{eff} parameter is found to be relatively constant for other "electron deficient" radicals whose structures are known, then a strong argument can be made concerning the structure of the OFCOT radical anion. This argument is particularly valid for fluorinated radicals since even the slightest change in 2s spin density will dramatically change the observed hyperfine coupling constant. For example, a spin density of 0.01 in a hydrogen 1s orbital amounts to a hyperfine coupling of only 5 G but the same spin density in a fluorine 2s orbital gives rise to a hyperfine coupling of 188 G. In other words, the fluorine coupling should be very sensitive to structural variations which would alter the 2s spin density on fluorine. Table X, page 124, summarizes the Q^F_{eff} values obtained from several different perfluoro radicals using either the calculated McLachlan or INDO spin densities. Although Q^F_{eff} values obtained from positions of low carbon spin density could easily be in error, the spread in the values is actually quite small with most falling between 90 and 104 G. This finding is in good agreement with other authors who

TABLE X

COMPILATION OF $\underline{Q}^{F}_{eff}$ VALUES[a] FOR FLUORINATED AROMATIC RADICALS AND THE OCTAFLUOROCYCLOOCTATETRAENE RADICAL ANION

Parent Compound	Radical Ion	Ring Position	ρ^{b}_{C}	$\underline{a}^{c}_{F}$/G	$\underline{Q}^{F}_{eff}$/G	Reference
Fluorocyclooctatetraen	C_8H_7F	1 (1)	0.1187	12.9	108.7	135
Pentafluorocyclopentadiene	C_5F_5		0.200	16.3	81.5	133
Perfluorobenzene	$C_6F_6^+$		0.124	15.9	128.2	130
Perfluoronaphthalene	$C_{10}F_8^+$	1 (4)	0.178	18.5	103.9	130
			0.195	19.0	97.4	132
		2 (4)	0.048	4.6	95.8	130
			0.050	4.8	96.0	132
Perfluoroanthracene	$C_{14}F_{10}^+$	1 (4)	0.089	9.2	103.4	130
		2 (4)	0.035	3.6	102.9	130
		9 (2)	0.212	19.0	89.6	130
Perfluoropyrene	$C_{16}F_{10}^+$	1 (4)	0.142	13.8	97.2	130
		2 (2)	-0.034	(-)3.4	100.0	130
		4 (4)	0.084	7.0	83.3	130
Perfluorocyclooctatetraene	$C_8F_8^-$		0.1159	10.92	94.2	d

[a] $\underline{Q}^{F}_{eff}$ is defined in the text.

[b] Spin densities on carbon calculated by the McLachlan method for the radical cations[19,21] and by the INDO method for $C_8F_8^-$[d].

[c] Experimental fluorine hyperfine coupling constants.

[d] This work.

used data from both perfluoro and partially fluorinated radicals and estimated Q^F_{eff} as 98.2 and 107.4 G. Thus, the value of 94.2 G obtained for $C_8F_8^-$ is certainly consistent with these other radicals. Since the structures of the perfluoro aromatic radicals and the C_5F_5 radical are undoubtedly planar and since the Q^F_{eff} parameter is consistent in all of the radicals, Table X, the OFCOT radical anion is, likewise, planar. The fact that the isotropic g-values of these radicals are all grouped within a narrow range is further evidence that these radicals are all isostructural. Therefore, the ESR evidence supports an aromatic planar structure for the OFCOT radical anion.

E. Perfluoromethylcyclohexane and Perfluoro-1,3-dimethylcyclohexane Radical Anions

The radical anion of perfluoromethylcyclohexane (PFMCH) was observed during a search to find a suitable matrix in which to observe the radical cation of tetramethyltin (Me_4SN) that is from a γ-irradiated 1 mole % solution of Me_4Sn dissolved in PFMCH. The observed ESR spectra, although showing evidence for the Me_4Sn^+, were characterized by a clearly defined parallel pattern which had a spread of about 1100 G. A spectrum similar to that obtained in the present study had been reported before[136] but was not analyzed and only tentatively assigned to the PFMCH radical anion.

The formation of the radical anion of PFMCH upon γ-irradiation is not particularly surprising since several examples are known

where saturated perfluorocarbons capture electrons[82,83] and since gas phase studies have established that many perfluorocarbons have a positive electron affinity.[137] However, in previous ESR studies these perfluorocarbon radical anions were prepared in TMS and neopentane matrices. The clear identification of the radical anion therefore became the objective of this minor project. The project was further extended to perfluoro-1,3-dimethylcyclohexane (PFDMCH) to test the proposed model for the PFMCH radical anion.

All of the samples included in this study were either pure PFMCH or PFDMCH or samples of these which included trace amounts of Me_4Sn (about 1 mole %). All of the chemicals were used as received and samples were prepared by standard procedures. Since the previously mentioned perfluorocarbon radical anions were observed in tetramethylsilane (TMS) or in neopentane, it was thought that the PFMCH radical anion might be more clearly detected in these matrices. To this end, a 1 mole % sample of PFMCH in TMS was prepared. However, the only radical observed after γ-irradiation was the $Me_3SiCH_2\cdot$ free radical.

As previously mentioned, a broad and obviously anisotropic spectrum with a spectral extent of about 1100 G was obtained at 80 K after γ-irradiation of a 1 mole % sample of Me_4Sn in PFMCH. The incorporation of Me_4Sn, or any organometal for that matter, resulted in an enhancement of the radical anion spectrum, and except for the absence of resonances from the cation, the spectra were essentially identical to those without the organometal. The reason for this is

that probably the organometal acts as a positive hole scavenger, thus reducing the likelihood of annihilation reactions, such as Equation (5), page 7.

In an attempt to establish the origin of this radical anion, a pure sample of PFMCH was examined. Since the radical giving rise to the broad spectrum did not power saturate, a suitable spectrum of the radical with a good signal-to-noise ratio was obtained at 10 dB (20 mW) power level, as shown in Figure 31, page 128. As indicated by the stick diagrams, the parallel components can be analyzed as a large doublet of triplets of doublets. Further proof of this analysis together with a tentative analysis of the perpendicular components will be given later. Warming the sample to 110 K results in the splitting for the set of smaller doublets becoming less distinct with the introduction of an asymmetry such as to indicate an apparent increase in the intensity of the inner component. Further warming to 120 K increases this trend toward a complete smearing of the smaller doublets. Recooling the sample to 80 K regenerates the original spectrum. Further cooling the sample below 80 K to 20 K resulted in a gradual deterioration in the resolution of the spectra but there was no significant quantitative change from the 83 K spectrum. Raising the temperature above 125 K resulted in the rapid decay of the above described features. When a cation trap such as Me_4Sn was included in the matrix, then the decay of the subject radical was marked by the growing in of the $\cdot CH_2SnMe_3$ radical.

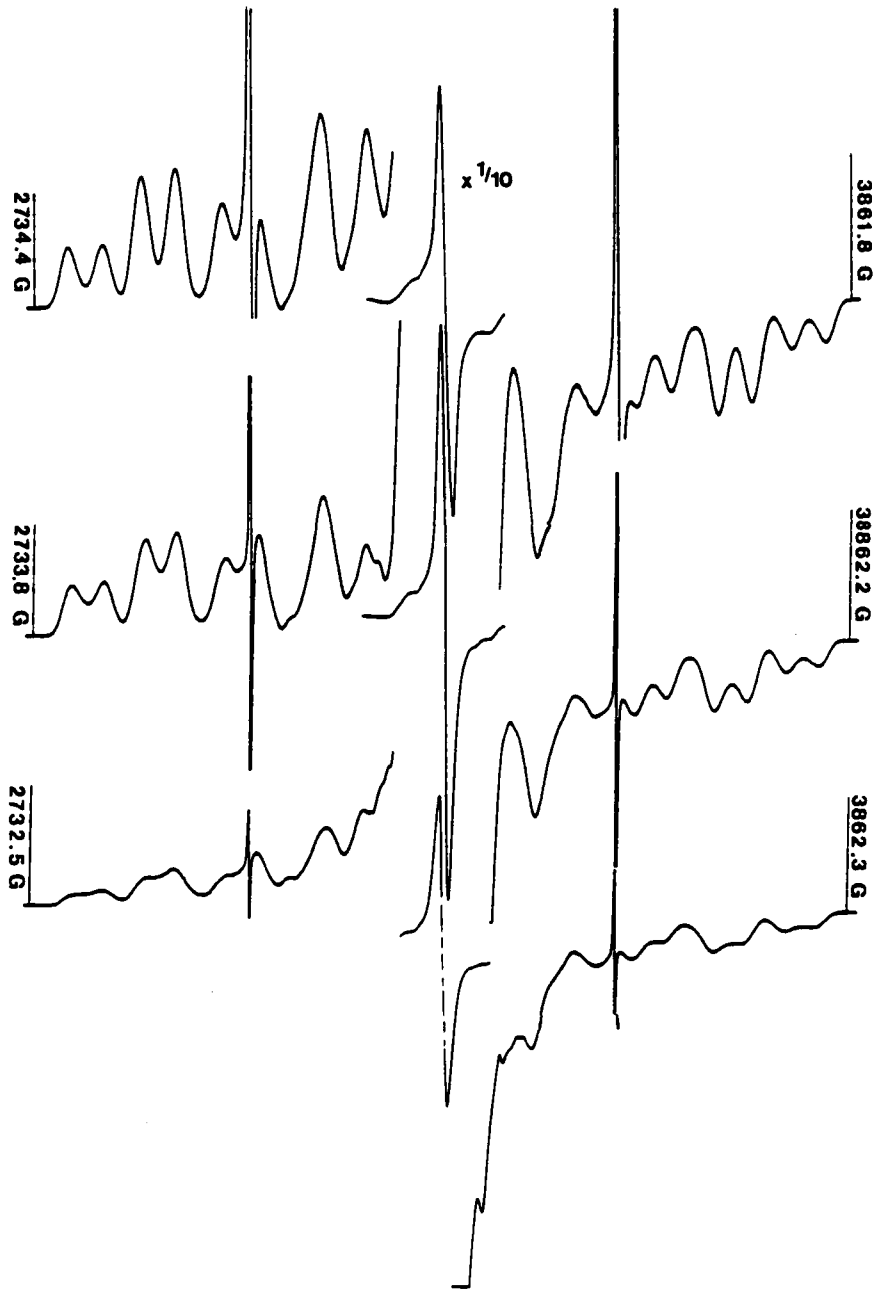

Figure 31. First-derivative ESR spectra of pure PFMCH at temperatures ranging from 81 K (upper) to 120 K (bottom).

As indicated by the stick diagram in Figure 31, page 128, the parallel features in the wings can be definitely assigned as a triplet of doublets, but a natural question is whether the separation between these two sets arises from either a doublet or triplet splitting. Since the center portion of the spectrum is dominated by a very intense resonance which does not appear to be part of this pattern, the observation of the inner component of a triplet could well be masked. Therefore, two analyses must be considered for the parallel pattern. First, the large parallel splitting between the wing features could arise from two equivalent fluorines giving a triplet with $A_{//}$ (2F) ~400 G or the large splitting could result from an interaction with just one fluorine yielding a doublet with $A_{//}$ (1F) ~800 G.

In addition to the clearly defined parallel features located in the wings of the spectrum, two sets of two resonances (marked with an asterisk (*) in Figure 31) are located inside the hydrogen resonances. These inner features are not part of the parallel pattern because the splitting between the sets differ from those of the parallel couplings. However, these features have decay rates and power saturation properties which are identical to those of the parallel features. Therefore, it is reasonable to consider that these resonances also arise from the same radical species and constitute part of the associated perpendicular pattern. Additional perpendicular resonances could well be masked by the intense center resonance as in the situation described for the parallel pattern.

Consequently, at first sight, the analysis of the perpendicular pattern also suffers from a similar ambiguity.

In order to resolve this problem, two alternate assignments may be made. First, if the parallel pattern is a triplet of triplets of doublets, then the perpendicular pattern ought to be characterized by a triplet ($A_\perp$ (2F) = 160 G) of triplets ($A_\perp$ (2F) = 61 G) of doublets ($A_\perp$ (1F) < 10 G). Alternatively, if the parallel pattern is a doublet of triplets of doublets, then the perpendicular pattern would also be a doublet ($A_\perp$ (1F) = 320 G) of triplets ($A_\perp$ (2F) = 61 G) of doublets ($A_\perp$ (1F) < 10 G).

A correct analysis must also be consistent with the predicted second-order shifts. A second-order calculation, using the trial parameters of the second analysis, predicts that the resonances would all be shifted to lower field. However, a similar calculation for the first analysis predicts that, in addition to the parallel components in the wings being shifted to lower field, the center component (M_I = 0) of the parallel pattern would be split into two where one of the components (I = 1, M_I = 0) would be shifted to lower field by $\sim A^2/H$ whereas the other component (0,0) would not be shifted (see earlier discussion, page 27). The observation of this shifted component (1,0) would provide convincing evidence for the first analysis, whereas the failure to observe this component would suggest that the second analysis may be correct. An argument similar to this was used to establish that a radical obtained from the γ-irradiation of a pure sample of trimethylphosphite was a "dimer

cation" ($(CH_3O)_3P\text{-}P(OCH_3)_3^{+\cdot}$) with anisotropic hyperfine couplings of $A_{//}$ ($2^{31}P$) = 727 G and $A_{\perp}$ ($2^{31}P$) = 618 G[138] instead of a monomer radical cation with couplings of $A_{//}$ ($1^{31}P$) ~1450 G and $A_{\perp}$ ($1^{31}P$) ~1240 G.

The triplet of triplets of doublets analysis will be considered first. Using the ESR matrix diagonalization program previously described and the trial parameters, the second-order shifts of each of the resonances can be estimated. A stick diagram representing this analysis is labeled A and is shown in Figure 32, page 132. While the stick diagram very faithfully reconstructs the wing features of the parallel pattern, some of the second-order shifted resonances, namely, the ones marked with an ↓, are not observed although there were no interfering resonances to obscure their observation. The absence of these expected resonances provides convincing evidence to reject this analysis.

The doublet of triplets of doublets analysis will now be considered. Again, using the ESR program and the appropriate trial parameters, the second-order pattern may be calculated. The stick diagram labeled B in Figure 32 graphically represents the numerical output of the computer program. In this case, the only resonances not observed are the ones located within the range of the intense center resonance. Therefore, this analysis is consistent with the observed spectrum. Further refinement of the hyperfine parameters yields: $A_{//}$ (1F) = 798 G, $A_{//}$ (2F) = 106 G, $A_{//}$ (1 F) = 46 G, $A_{\perp}$ (1F) = 320 G, $A_{\perp}$ (2F) = 61 G, $A_{\perp}$ (1F) < 10 G, $g_{//}$ = 2.0035, and $g_{\perp}$ = 2.0023.

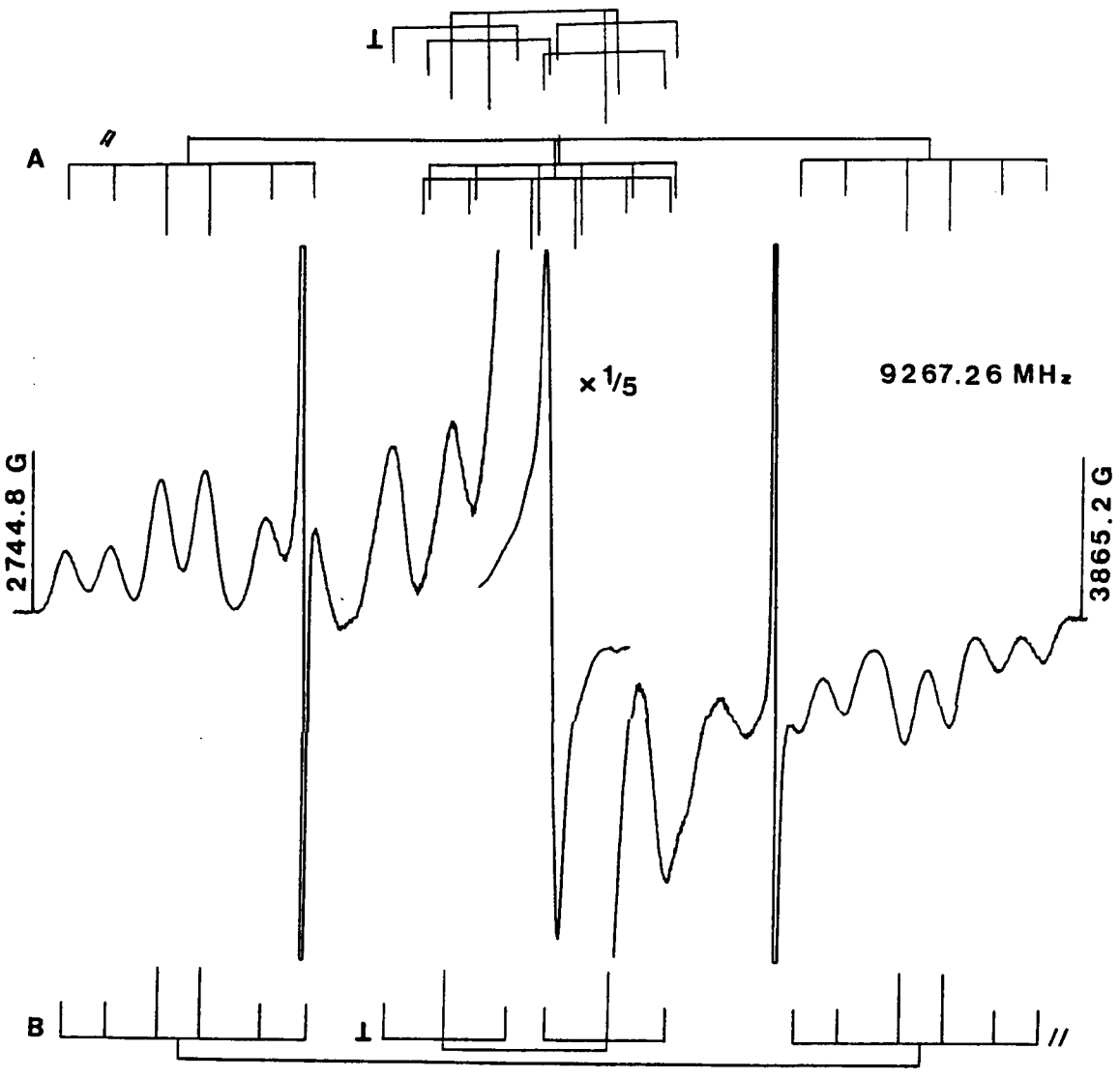

Figure 32. First-derivative ESR spectra of pure PFMCH at 81 K. The upper (labeled A) and lower (labeled B) stick diagrams correspond to two alternative analyses.

Since the data seem to indicate a very strong and highly anisotropic coupling to just one fluorine nucleus, a reasonable assumption is that the unpaired electron is located in a σ^* orbital which lies principally along one C-F bond. From the nature of the substructure which is discussed below, it is taken to be the unique C-F bond at the CF_3 substituted position. Assuming that this C-F bond is in the axial position, the next two strongly coupled nuclei are the β-axial fluorines on the cyclohexane ring, and the smallest resolved coupling probably arises from the conformationally locked β-axial fluorine of the CF_3 group as shown in the structure below. The assumption of a preferred conformation for a CF_3 group below 115 K is reasonable since this effect has been noted in other fluorinated radical anions.[92,139]

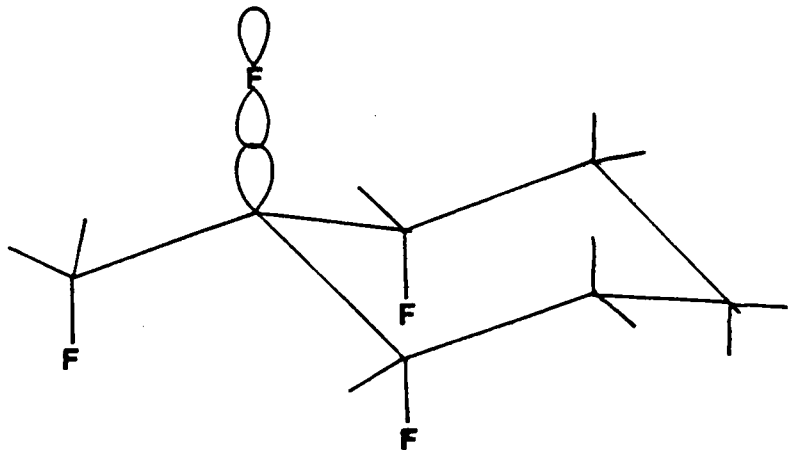

If the assignment of the hyperfine couplings to the aforesaid nuclei is correct, then the observed hyperfine pattern would be expected to be unaffected by substitution on the ring in the 3-position, taking the CF_3 group to be substituted at the one equitorial position. This arises because there are now two sites for

electron capture which are similar to that in the monosubstituted compound. Therefore, the radical anion of perfluoro-1,3-dimethylcyclohexane (PFDMCH), shown above, would be expected to yield ESR spectra identical to those described for the PFMCH radical anion.

A pure sample of PFDMCH was prepared following standard procedures. No attempt was made to separate the two isomers, that is the cis and trans-PFDMCH. As shown by a comparison of Figures 33, page 135, and 32, page 132, the spectrum of the PFDMCH radical anion at 85 K is virtually indistinguishable from that of the PFMCH radical anion with the perpendicular component being slightly better resolved in the latter case. Moreover, samples of PFDMCH containing organometal solutes again yielded solute cation spectra similar to those obtained from organometal solutions in PFMCH.

To demonstrate that the proposed orbital description for the PFMCH radical anion is a reasonable one, a search of the literature was made to find other similar radicals. One particularly suitable example is the perfluoro-tert-butyliodide radical anion ($(CF_3)_3CI^-$).[139] The appropriateness of this example may be seen in several ways. First, the structures of $(CF_3)_3CI$ and the CF_3 substituted end of PFMCH are essentially very similar, as shown below (the bold lines on PFMCH merely indicate the region of comparison). A detailed analysis of the iodine anisotropic hyperfine couplings established that the iodine nucleus possesses a 0.38 $5p_z$ spin density where the $5p_z$ orbital of iodine is along the C-I bond. This fact closely corresponds to the PFMCH radical anion where a similar analysis

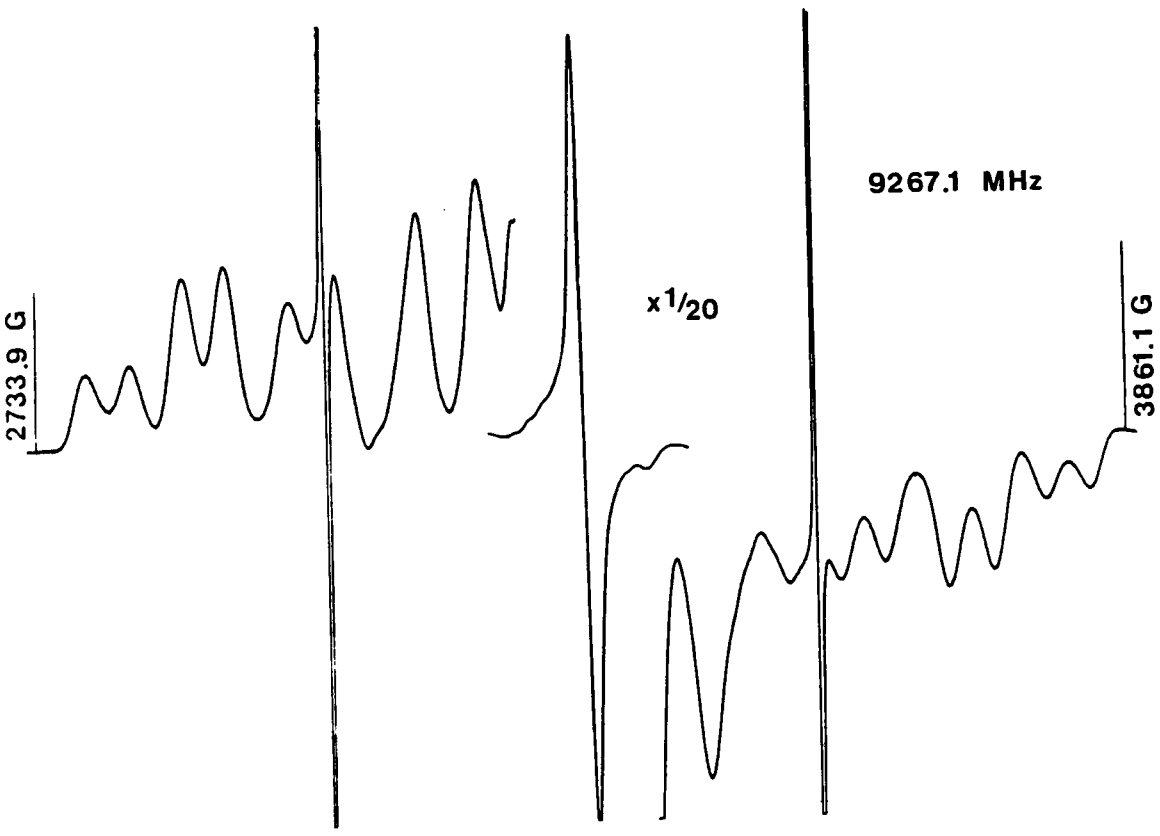

Figure 33. First-derivative ESR spectrum of a γ-irradiated pure sample of perfluoro-1,3-dimethylcyclohexane at 100 K. The analysis is the same as shown for the PFMCH radical anion.

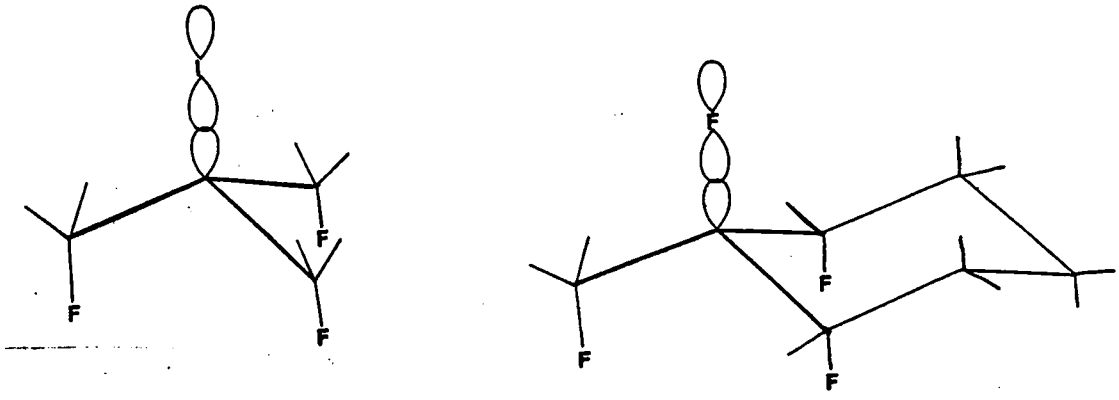

revealed a 0.26 $2p_z$ spin density in the unique apical fluorine orbital. The fact that a greater amount of spin density is localized in the less electronegative iodine $5p_z$ orbital than in the fluorine $2p_z$ orbital, follows the trend expected when the electron occupies an antibonding orbital.

In $(CF_3)_3CI^-$, hyperfine coupling to only three of the nine fluorines in the t-butyl group were resolved. This fact was taken to imply that $(CF_3)_3CI^-$ adopts a preferred conformation in which the C_{β}-F axial bond from each CF_3 group is aligned parallel to the C-I bond. This result parallels the finding in the present case that the CF_3 group adopts a locked conformation. Interestingly, the $A_{//}$ coupling of 46 G observed to the axial fluorine of the CF_3 group of the PFMCH radical anion is nearly the same as the $A_{//}$ coupling of 43.2 G to the axial fluorine of the CF_3 group in $(CF_3)_3CI^-$. Table XI, page 137, compares the hyperfine coupling constants for $(CF_3)_3CI^-$ and the PFMCH and PFDMCH radical anions. Taken together, these considerations indicate that the proposed σ^* orbital description is a reasonable one.

TABLE XI

COMPARISON OF A FEW σ* RADICAL ANIONS

Radical Anion	$g_{//}$	$g_{\perp}$	Hyperfine Coupling Constants (G) $A_{//}$	$A_{\perp}$
PFMCH	2.0035	2.0023	798 (1F) 106 (2F) 46 (1F)	320 (1F) 61 (2F) a
PFDMCH	2.0037	2.0022	793 (1F) 107 (2F)	318 (1F) 62 (2F)
$(CF_3)_3CI$	1.9631	2.1651	458.0 (1I) 43.2 (3F)	174.8 (1I) 38.9 (3F)

[a]Unresolved.

As previously mentioned, a spectrum which is similar to the ones reported in the present work has been reported,[136] but the spectrum was not analyzed. In this previous report, it was noted that this radical when warmed to temperatures above 140 K dissociated to produce a tertiary free radical by loss of the axial fluorine (adjacent to the CF_3 group) as a fluoride ion. Attempts to duplicate this result were unsuccessful, but this may have been related to the different phases that a PFMCH solid may have. If the proposed model is correct for the $PFMCH^-$ radical, then an obvious conclusion is that the unpaired electron has become localized in a relatively small part of the total molecule. This result is quite different than that observed for the perfluorocyclopropane, -cyclobutane, and -cyclopentane radical anions[82,83] since in each of these examples the unpaired electron enters a SOMO which is evenly distributed throughout the entire molecular framework. Also, studies on the perfluorocyclohexane, although tentative, seem to indicate that a binomial distribution of at least nine unresolved line groups is present.[83] If this result is being properly interpreted then the unpaired electron is being at least somewhat distributed throughout the entire framework. Apparently the introduction of the CF_3 group provides enough of a perturbation to the system to constrain the unpaired electron to a localized section of the radical framework.

F. Sulfur Tetrafluoride and Sulfur Tetrafluorooxide Radical Anions

One of the most useful principles routinely used to aid the prediction of radical structure and hence the interpretation of ESR spectra is the isoelectronic principle.[140,141] This principle predicts that if two molecules have the same number of atoms and the same number of valence electrons, then they will have the same geometry. Possibly no keener test of this principle can be found in the literature than in the correct identification of the 41-electron isoelectronic family of PF_5^-,[142] SF_5,[143,149] AsF_5^-,[144] and SeF_5[145] which all adopt a square pyramidal (C_{4v}) structure, since for all these radicals the apical fluorine rather unexpectedly yielded a very

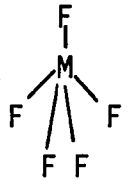

small hyperfine interaction. For the radicals PF_5^- and SF_5, the hyperfine coupling to the apical fluorine was not resolved and this fact led to their initial misidentification as PF_4[146] and SF_4^+.[147] The unusual semi-occupied orbital (SOMO) of these radicals has sparked interest in not only other members of the 41-electron family but also in other similar inorganic isoelectronic families.

The initial effort in this project was performed by a co-worker, J-T Wang, who obtained a promising result. He observed that a clear quintet pattern with appropriate second-order splittings,

indicative of four equivalent fluorine nuclei, was obtained when a $Cs^+SF_5^-$ salt was γ-irradiated. Early attempts to detect the magnetic ^{33}S nuclei which has a natural abundance of only 0.76% were unsuccessful. Yet, without the detection of the ^{33}S resonances, a compelling proof of the radical's identity could not be made.

While the author was investigating the $Cs^+SF_5^-$ salt, another salt, $Cs^+SF_5O^-$, was similarly examined. Both of the salts, $Cs^+SF_5^-$ and $Cs^+SF_5O^-$, utilized in this project were obtained through Karl O. Christe[148] and were synthesized by the reported procedures.[150,151] Since the samples were received in quartz sample tubes, the samples were not opened but were used as received. The samples were γ-irradiated at 77 K.

Paralleling the earlier ESR studies, a γ-irradiated sample of the $Cs^+SF_5^-$ salt showed spectroscopic evidence for coupling to four equivalent fluorine nuclei. Considering the ^{33}S low natural abundance (0.76%) and its nuclear spin of 3/2, ^{33}S satellites are generally at least a factor of 500 times lower in intensity than the main spectrum from ^{32}S which has no nuclear spin. Consequently, to obtain clearly resolved spectra from ^{33}S containing radicals in natural abundance, all of the experimental parameters had to be precisely optimized, such as sample position in the cavity, modulation amplitude, microwave power, temperature, cumulative dose, and mode of presentation--either first or second derivative.

As seen in Figure 5, page 42, the sensitive region of the cavity is quite large; consequently, positioning the sample within

the active region of the cavity was relatively trivial, yet important. Although increasing the modulation amplitude resulted in more intense resonances, the resonances also broadened undesirably when the modulation was greater than about 12.5 G. Thus, a modulation amplitude of 12.5 G was utilized. The radical giving rise to the observed quintet pattern was not saturated by high power, and the best compromise between machine stability and signal level seemed to be at 4 dB (79 mW). Since there appeared to be a slight amount of decay of the radical when the sample was maintained at temperatures above 330 K, and since the spectral features did not seem to sharpen up any above 300 K, there was no advantage in warming the samples to above 300 K. Therefore, all of the reported spectra were taken at 300 K. Other parameters being the same, it was observed that the signal of the quintet pattern became more intense with a larger cumulative dose. Thus, a final cumulative dose of about 4.0 Mrad was given to each sample. Although all of the other factors are vitally important, the most important key to obtaining well resolved ^{33}S satellite lines was the use of the second-derivative presentation. Since the ^{33}S satellites are approximately 500 times less intense than the main lines of the ^{32}S containing radicals the gain setting must be increased by a factor of about 500 to obtain comparable signal amplitudes. Whereas the baseline was markedly distorted when the first-derivative presentation was used, the baseline remains relatively flat for a second-derivative presentation outside the quintet pattern. This fact made necessary the use of the second-derivative presentation.

Although a clearly defined pattern at high gain could be obtained with a single scan, 30 scans were taken and computer averaged using the Aspect 200 computer to reduce the instrumental noise.

The lower portion of Figure 34, page 143, presents an example of a spectrum which was obtained after optimizing all of the above-mentioned parameters. This was taken at low gain while the upper portion of Figure 34 was taken at much higher instrumental gain and reveals those features not observed at lower gain. The lower trace is readily analyzed as a quintet pattern showing the appropriate second-order hyperfine splitting pattern from four equivalent nuclei of spin I = 1/2 which, considering the composition of the sample, may undoubtedly be assigned to four equivalent fluorine nuclei. The weak resonances detected at higher gain clearly constitute a partial replica of the more intense quintet pattern. A careful analysis reveals the presence of four almost equally spaced partial replicas indicating a hyperfine interaction with a nucleus of spin I = 3/2. Given the relative intensity of these weak features (about 500 to 1) and their hyperfine pattern, the weak features are confidently assigned to the result of an additional hyperfine interaction to ^{33}S. This analysis is defined by the upper stick diagram in Figure 34 where the solid lines represent resonances which are detected while the dashed lines show those lines unobserved due to overlap with the more intense pattern.

A least-squares fit of the patterns in Figure 34 was attempted in order to precisely fix the hyperfine coupling constants and the

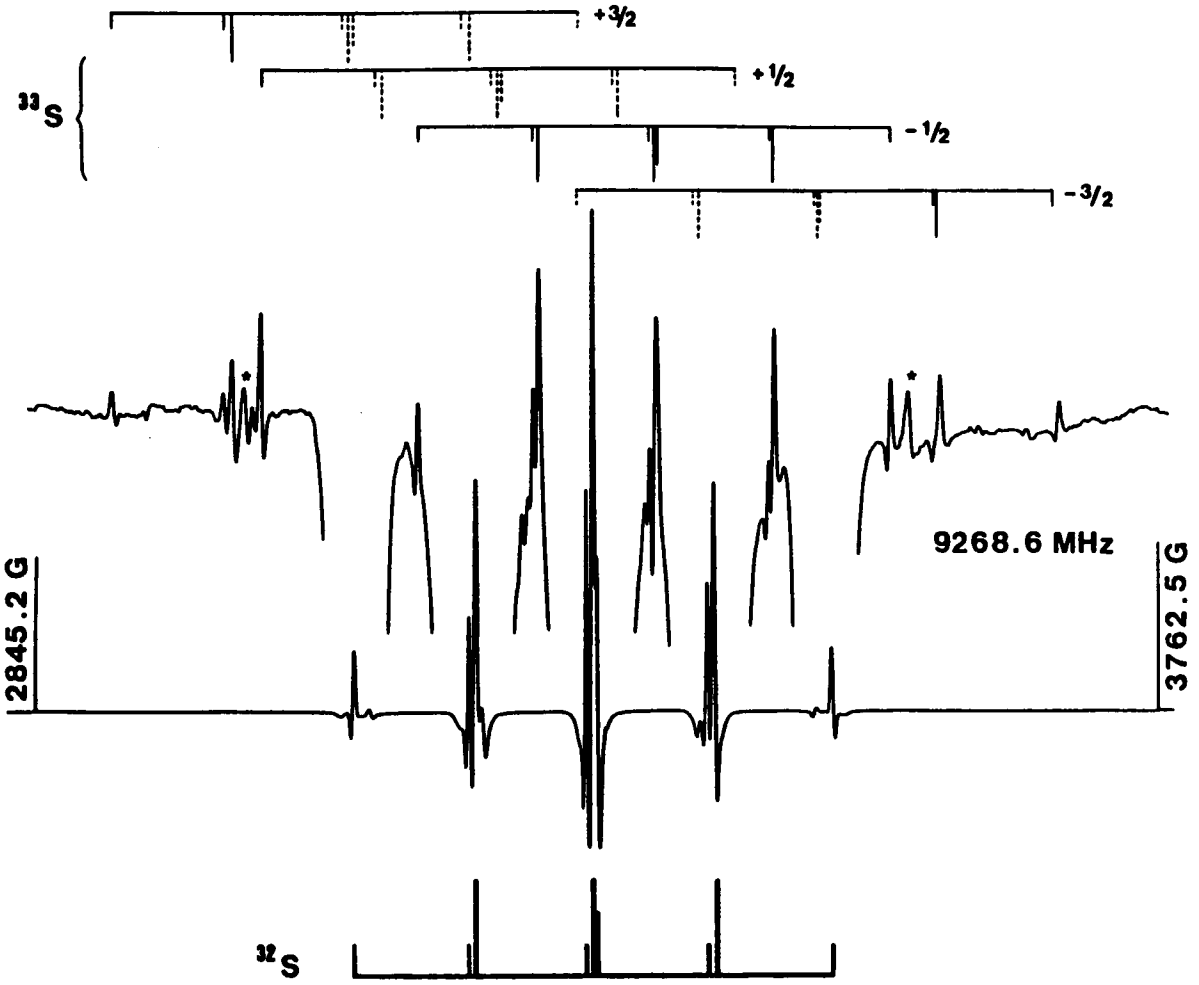

Figure 34. Second-derivative ESR spectra (lower) of a γ-irradiated (dose 2 Mrad) pure sample of $CsSF_5$ at 300 K. The upper trace resulted from signal averaging 30 scans at 500 times the gain of the lower trace. The lower stick diagram defines a hyperfine interaction to four equivalent fluorines while the upper diagram defines an additional hyperfine interaction to a sulfur-33 nucleus. The two lines marked with asterisks apparently do not belong with the pattern.

g-value. For the $^{32}SF_4^-$ pattern, the hyperfine coupling and the g-value were estimated to be A_{iso} (4F) = 97.5 G and g_{iso} = 2.0045. A least-squares fit of the upper trace which allowed all three independent parameters to vary yielded A_{iso} (4F) = 98.2, A_{iso} (^{33}S) = 127.4, and g_{iso} = 2.00665. The slightly different fluorine A_{iso} value is simply due to experimental error since the accuracy of determining the field positions for the upper spectrum is less than the lower spectrum. Using the already determined g_{iso} and A_{iso} (4F) values, a least-squares fitting procedure was used to obtain the ^{33}S coupling. This procedure gave A_{iso} (^{33}S) = 128.5 G. These latter values will be assumed to be the most accurate.

The spectrum obtained from γ-irradiating the $Cs^+SF_5O^-$ salt was also characterized by a quintet pattern at low gain, as shown in Figure 35, page 145. An optimization procedure was also performed on this radical paralleling the previously described procedure. This radical was characterized by the same trends as were observed in the previous example. Since the line width was slightly greater for this radical, a modulation amplitude of 25 G was utilized. At very high gain a few barely resolved resonances were observed, but with the aid of signal-averaging these resonances could be dramatically clarified.

The lower quintet pattern indicated by the lower stick diagram was analyzed as arising from four equivalent fluorides. A least-squares fit of the resonances yields A_{iso} (4F) = 189.5 and g_{iso} = 2.00274. In the previous example, several resonances could be

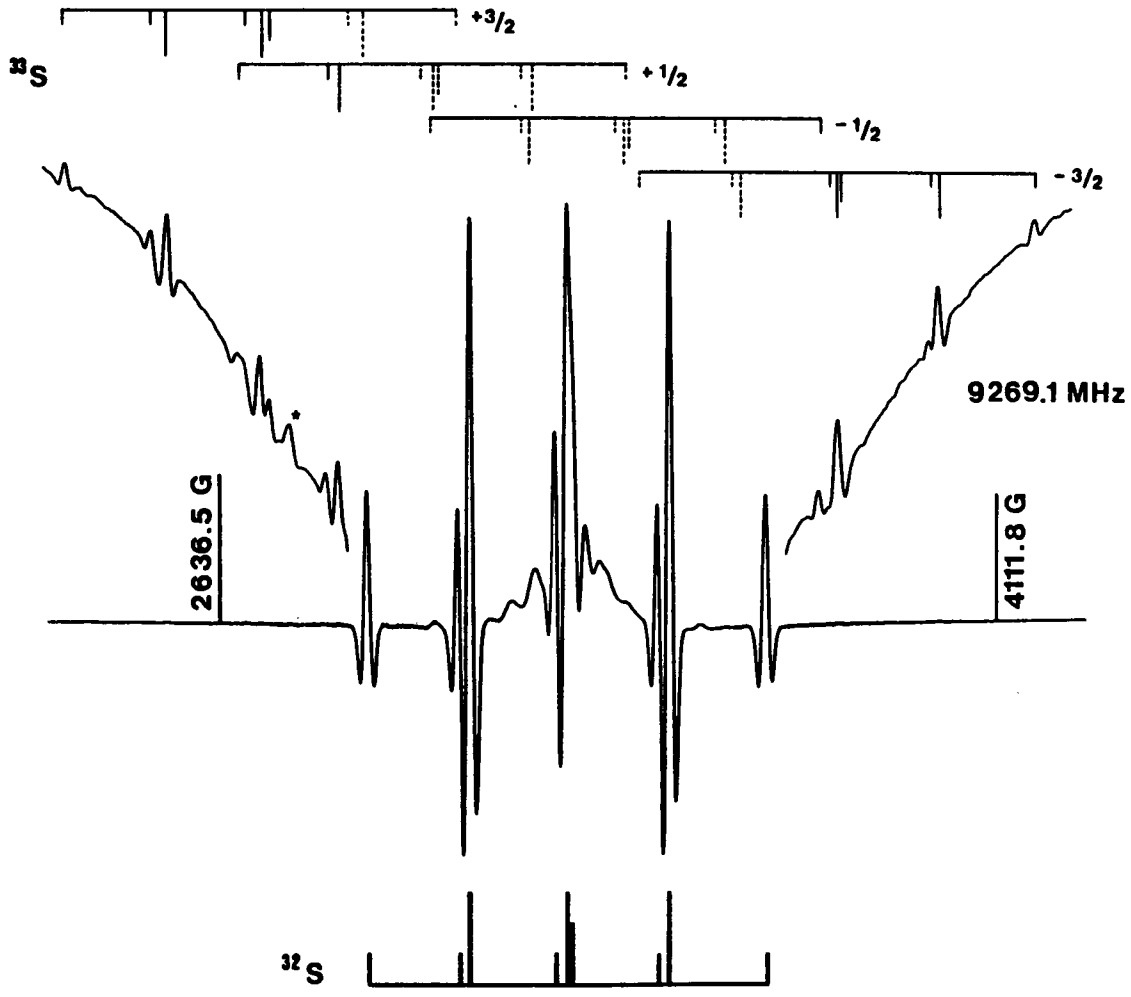

Figure 35. Second-derivative ESR spectra (lower) of a γ-irradiated (dose 2.5 Mrad) pure sample of $CsSF_5O$ at 300 K. The upper trace resulted from signal averaging 30 scans at 500 times the gain of the lower trace. The lower stick diagram defines a hyperfine interaction to four equivalent fluorines while the upper diagram defines an additional hyperfine interaction to a sulfur-33 nucleus.

detected between the resonances of the more intense radical, but in this case extraneous signals prohibited such observations. Nevertheless, a clear quartet-of-quintets pattern was readily obvious at high gain with the quintet patterns being replicas of the main quintet pattern. Following the least squares analysis procedure described for the previous results, the ^{33}S hyperfine coupling was found to be 362.6 G.

Neither of these two samples were photo-bleached by visible light. The observed radicals were extremely stable; in fact, after being stored at room temperature for several months they showed very little decay, but after about a year of storage the radicals had decayed somewhat. The radicals which were observed in the γ-irradiated $Cs^+SF_5^-$ and $Cs^+SF_5O^-$ salts are undoubtedly SF_4^- and SF_4O^-, respectively. Proof of these identities follows from an argument based upon the result of electron capture by the salt and from a comparison with the spin density distribution in other isoelectronic species. Following this initial discussion, a more detailed analysis of their structure will be given.

It is known, for example, that γ-irradiation of $K^+PF_6^-$[142] and $K^+AsF_6^-$[144] salts is followed by the generation of the PF_5^- and AsF_5^- radical anions. A reasonable mechanism for the above process is that the negative ion first captures an electron and then loses a fluoride ion, as shown below in Equations (46) and (47). This is entirely analogous to the well-known process of dissociative electron capture by neutral molecules.[38]

$$PF_6^- + e^- \rightarrow [PF_6^{2-}] \rightarrow PF_5^- + F^- \quad (46)$$

$$AsF_6^- + e^- \rightarrow [AsF_6^{2-}] \rightarrow AsF_5^- + F^- \quad (47)$$

In these examples no coupling was observed to the potassium nucleus of the stable cation although it possesses a non-zero nuclear spin. Likewise, no hyperfine interaction was observed to the cesium nucleus although it possesses a nuclear spin of 7/2 in a 100% natural abundance. Similar reasonable mechanisms may be written for the present investigation, that is

$$SF_5^- + e^- \rightarrow [SF_5^{2-}] \rightarrow SF_4^- + F^- \quad (48)$$

$$SF_5O^- + e^- \rightarrow [SF_5O^{2-}] \rightarrow SF_4O^- + F^- \quad (49)$$

Incidentally, MO calculations on SF_5^{2-} and SF_5O^{2-} at the INDO level revealed that the SOMO is in each strongly anti-bonding between the sulfur and the unique apical fluorine and is weakly bonding to the other ligands as shown below:

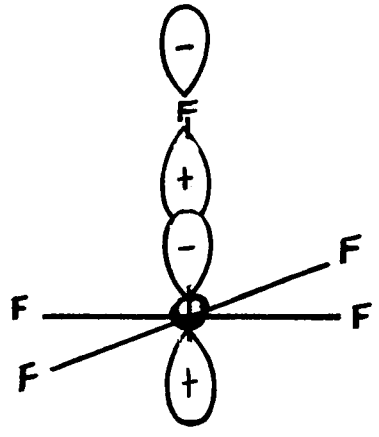

Given that the starting compounds are relatively free of contaminants, it is hard to imagine a reasonable radiation mechanism

that would produce radicals possessing four equivalent fluorines and one sulfur nucleus other than the proposed species. For example, in order to produce SF_4^+, the SF_5^- ion would have to be ionized and then spontaneously eject a fluoride ion.

$$SF_5^- \rightsquigarrow SF_5 + e^- \quad (50)$$

$$SF_5 \rightarrow SF_4^+ + F^- \quad (51)$$

Such a process seems quite unlikely, especially since SF_5 is known to be relatively stable.[143,149]

Probably the most compelling argument for the identity of these radicals follows from a comparison with their isoelectronic counterparts combined with an understanding of the anti-bonding orbital that the unpaired electron enters.

The 41 electron isoelectronic family, namely PF_5^-, SF_5, AsF_5^-, and SeF_5, serves as an instructive example. In Table XII, page 149, the unpaired electron s-orbital spin densities are given. Three observations are readily obvious. First, in all four radicals the apical fluorine has either a very low or an unresolved coupling. Second, there is a decrease in both the central atom and ligand fluorine 2s character in passing from the anion to the neutral radical. This same effect has been observed in many other isoelectronic families. Exchanging the central atom with a heavier congeneric atom results in an increase of the central s-spin density along with a decrease in the ligand 2s-spin density. This observation reflects the antibonding nature of the orbital since in antibonding orbitals the spin density tends to shift to the nucleus with the lower electronegativity.

TABLE XII

COMPARISON OF FOUR 41-ELECTRON PENTAFLUORIDE RADICALS[a]

Radical	Hyperfine Interaction (G)		Central Atom s-Spin Density
	Central Atom	Fluorine	
PF_5^-	1354.4	197.6	0.37
SF_5	306.8	143.0	0.32
AsF_5^-	1762	187.0	0.52
SeF_5	1877	118.0	0.39

[a]Table taken from reference 154.

Table XIII, page 151, displays a comparison between the SF_4^- radical and the $ClF_4\cdot$ radical[152,153] which is the only other known example of a 35-electron species. The ClF_4 radical was thought at one time to be ClF_5^+,[154] but subsequent convincing arguments supporting the original identification of the radical as ClF_4 were reported.[155] As seen in Table XIII, the 2s fluorine spin density decreases in the series SF_4^-/ClF_4 paralleling the PF_5^-/SF_5 and AsF_5^-/SeF_5 examples in Table XII, page 149. It should be noted, however, that the central atom spin density apparently increases in the SF_4^-/ClF_4 series contrary to the other examples. The reason for this apparent inversion of the expected central atom spin density distribution may simply be the result of inaccuracies in the empirically-computed atomic values.

As a final consideration, it should be noted that although the SF_4^+ radical was previously rejected on the grounds that its production was unlikely given the starting material, a further proof against it being the observed radical will be given. Since SF_4^+ would be a 33 electron radical, other known 33 electron radicals, such as SiF_4^-,[156] PF_4,[157] and AsF_4[158] should be compared with the present results. In each of these three examples, the radicals adopt a C_{2v} structure where the fluorine nuclei are equivalent in pairs. This inequivalency in the fluorines was certainly not observed in the present study; therefore, the SF_4^+ radical is ruled out as the species giving rise to the present results.

TABLE XIII

COMPARISON OF THE SF_4^- AND $ClF_4\cdot$ RADICALS

Radical	g_{iso}-Value	Hyperfine Interactions (G)		s-Spin Density[a]		Reference
		Central Atom	Fluorine	Central Atom	Fluorine	
SF_4^-	2.0045	128.5	97.5	.1039	.0052	This Work
ClF_4	2.0117	288.2 (^{35}Cl) 240.0 (^{37}Cl)	78.6	.1411	.0042	

[a]The s-orbital spin densities were calculated using the atomic values in Table I, page 25.

Table XIV, page 153, was constructed in order to help correlate the SF_4O^- data with other known 41 electron examples. Since the observed spectra for this radical are consistent with four equivalent fluorine nuclei, the oxygen is assumed to be in the apical position. In each of the examples given both the central atom and the fluorine 2s-orbital spin density increase with the replacement of the oxygen ion for a fluorine. This latter observation is not particularly surprising given that it is an antibonding orbital and that an oxygen ion (O^-) is undoubtedly much less electronegative than a fluorine atom. As also noted in Table XIV, both PF_4O^{2-} and AsF_4O^{2-} have two forms, that is, the unique oxygen can either occupy the apical or basal positions. The SF_4O^- radical, however, appears to preferentially position the oxygen in the apical position. It should be noted in passing that in sulfuranyl ($ROSF_4$) radicals the oxygen preferentially adds to the basal position,[159] but this fact may simply be the result of a steric effect, as shown below:

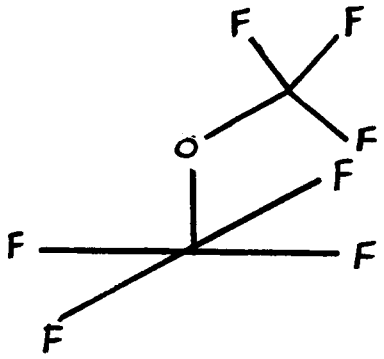

As shown, when, for example, the substituted group is OCF_3 in the apical position, there is more steric crowding than when the

TABLE XIV

COMPARISON OF SOME 41 ELECTRON RADICALS TO SF_4O^-

Radical	s-Spin Density[a] Central Atom	Fluorine	Reference
SF_5	.2476	.0076 (4)[b] <.00005 (1)	154
$SF_4O^-_{ap}$	.2934	.0105 (4)	This Work
PF_5^-	.2857	.0105 (4) .0002 (1)	155
$PF_4O^{2-}_{ap}$	.2928	.0112 (4)	155
$PF_4O^{2-}_{ba}$	.2619	.0118 (1) .0093 (2)	155
AsF_5^-	1827 G	.0097 (4) .0003 (1)	155
$AsF_4O^{2-}_{ap}$	1854 G	.0102 (4)	155
$AsF_4O^{2-}_{ba}$	1650 G	.0116 (1) .0082 (2)	155

[a]Orbital spin densities were calculated using the atomic values found in Table I, page 25.

[b]Figures in parentheses indicate number of equivalent nuclei having identical hyperfine interactions.

OCF_3 group is in the basal position. This argument is even more applicable when the substituted group is OC_2F_5 or OSF_5.

Since only the isotropic hyperfine couplings were obtained for the SF_4^- and SF_4O^- radicals, the experimental data do not give complete structural information. Consequently, a resort to computer calculations must be made. Several theoretical studies have been reported on the structures of ClF_4,[160-162] which is the isoelectronic counterpart of SF_4^-. Initially the ClF_4 free radical was thought to be planar with D_{4h} symmetry but later calculations criticized this conclusion and suggested instead that a C_{4v} structure was more likely. No theoretical calculations have been reported on the structure of either the SF_4^- or the SF_4O^- radicals.

INDO calculations for these two radicals were performed by R. L. Hudson.[163] The INDO program used was parameterized for second row elements and used either a k value of 1.0 or 0.75. While retaining C_{4v} symmetry, the total energy of the molecule was minimized by varying the bond lengths and the angle α defined as the angle between the plane of the four fluorines and the S-F bond. For k = 1.0, the minimum in energy for SF_4^- was found to be at α = 11.0° and R(S-F) = 1.75 Å. Likewise, the minimum in energy was achieved for SF_4O^- at α = 12.40, R(S-F) = 1.74 Å, and R(S-O) = 1.66 Å.

The results of the INDO produced spin densities are summarized in Table XV, page 155, along with the experimental values. Although the calculated values do not agree exactly with the experimental parameters, the fit is certainly sufficient to suggest that the C_{4v} model is correct.

TABLE XV

COMPARISON OF THEORETICAL INDO CALCULATIONS
WITH EXPERIMENTAL RESULTS

Radical	Experimental s-Spin Density		k-Value	Calculated s-Spin Density	
	Sulfur	Fluorine		Sulfur	Fluorine
SF_4^-	.1039	.0052	1.0	.1935	.0079
			0.75	.1239	
SF_4O^-	.2934	.0105	1.0	.2525	.0098
			0.75	.1703	

Although the INDO program predicts that the principal eigenvectors of the SOMO are s-orbitals, significant p-orbital participation, particularly along the C_4 axis, is also predicted. This being the case, the fact that the observed spectra in randomly oriented powders are characterized by isotropic lineshape indicates that the anisotropic hyperfine interactions must be averaging to zero. This latter conclusion implies that both SF_4^- and SF_4O^- are tumbling faster than the ESR time scale. This type of rotational freedom in a salt matrix has been reported for several other radicals of this type.

In summary, these studies have established the identity and orbital nature of the novel radical anions, SF_4^- and SF_4O^-. The SF_4^- radical is of particular interest in that it represents only the second example of a 35 electron radical of this type reported in the literature.

CHAPTER IV

RADICAL CATIONS

A. Introduction

As a natural consequence of their extremely reactive tendency, there were no examples of saturated organic radical cations established in the ESR literature prior to 1979. For the same reason, sparingly few examples of saturated organometallic radical cations were characterized prior to this same data. The turning point came when it was realized that well-resolved spectra of radical cations could be formed and stabilized in matrices composed of Freons.

Although Hamill and Shida established through a series of optical studies that aromatic radical cations could be readily generated and stabilized in certain chloroalkane matrices in 1966, the first use of a Freon matrix technique to generate radical cations was due to Grimison and Simpson in 1968.[165] However, the application of this technique in the field of ESR did not come about until 1972 with the report of the pyridine radical cation by Kato and Shida.[166] The first identification of a saturated hydrocarbon radical cation was the hexamethylethane radical cation in 1979.[167,168] The identification of saturated organometallic radical cations using this technique soon followed with the identification of the hexamethyldisilane[169] and then later the hexamethyldigermane radical cation.[170] Subsequent to these initial reports, a vast number of saturated and

unsaturated organic radical cations as well as a few examples of organometallic radical cations have been successfully identified by ESR using the Freon matrix isolation technique.[171,172]

The formation of the radical cations of these organometallic species is not particularly surprising since these species, especially those of the group IVB metals, are well known as excellent electron donors.[173,174] The one-electron oxidation of these species involves a rate-limiting process in which the electron is transferred from an outer-sphere orbital, sensibly forming the radical cation of the parent species.[175] However, the direct ESR spectroscopic observation of these parent cation radicals under liquid phase conditions could only be inferred owing to their extremely short lifetimes. The radical invariably observed by ESR spectroscopy following charge transfer was not the parent cation radical but rather a free radical formed by the dissociation of one of the organometal ligands.[175] A reasonable reaction sequence is as follows:

$$R_4M \xrightarrow{\text{oxidation}} [R_4M^+] \rightarrow R\cdot + R_3M^+ \qquad (52)$$

It is the ligand structure of this primary organometallic radical cation that is the central focus of this chapter.

The organization of the following sections will roughly parallel the organization utilized in the previous chapter. One exception is that the sample preparation procedures will in general be omitted because for practically all of the samples the method of preparation was essentially the same, namely: small amounts (0.1-5.0

mole %) of the diamagnetic organometal were dissolved in one of several different halocarbons and sealed under vacuum in a standard ESR tube. Typically, the liquid solution was quenched in liquid nitrogen to form a polycrystalline solid solution. Cation formation of the organometal following γ-irradiation can be ascribed in each case to the result of the positive charge transfer mechanism previously described.

Often in this section the organometal radical cations described were prepared in several different halocarbon matrices. In general, the same radical cation was generated independent of the type of matrix utilized, but the ESR spectral characteristics of the radical cation were often very different. A few generalizations will be made concerning the general characteristics of each of the different matrices utilized, using as a basis of information the findings of others but mainly the author's somewhat limited observations. This discussion is summarized in Table XVI (page 160).

Fluorotrichloromethane (Freon-11) proved to be the most generally useful matrix because of its excellent solubility properties with the precursor and of the generally high spectral resolution obtained for the radical cation. Typically, the initial matrix radical (probably $CFCl_3^-$) does not obscure the radical cation signal below 145 K. At 145 K or above, a matrix radical (Figure 36, page 161), identified as the $CFCl_2\cdot$ radical ($A_{//}$(1 F) = 165 G, $A_{//}(2^{35}Cl)$ = 19 G, $g_{//}$ = 2.0041 and $g_{\perp}$ = 2.0033) undoubtedly formed by the loss of a chloride ion, begins to become more prominent in the spectrum. If

TABLE XVI

SUMMARY OF HALOCARBON MATRICES USED TO GENERATE RADICAL CATIONS

Matrix	Maximum Temperature Before Cation Decay (K)	Matrix Radical Signal		Typical Cation Resolution
		80 K or Below	Near Cation Decay Temperature	
$CFCl_3$	155	Weak	Weak	Better than Average
CF_3CCl_3	145	Very Weak	Very Intense	Average
$CF_2ClCFCl_2$	120	a	Weak	Slightly Better than Average
$CFCl_3$:CF_2BrCF_2Br[d]	83	a	Weak	Poor
CCl_4	210	Very Strong	Strong	Average
CF_3CF_2Cl	110	Weak	a	Poor
CF_2Cl_2	b	c	Very Strong	d
$CBrCl_3$	180	Moderate	Strong	Average
$CF_3C_6F_{11}$	120	Weak	a	Below Average
1,3-$(CF_3)_2C_6F_{10}$	120	Weak	a	Below Average
CF_2ClCF_2Cl	105	Strong Singlet	Weak	Average

[a]Too weak to be observed in this work.

[b]Cation not observed at 80 K.

[c]Parent anion not observed.

[d]No basis for judgement.

[e]This mixture forms a glass.

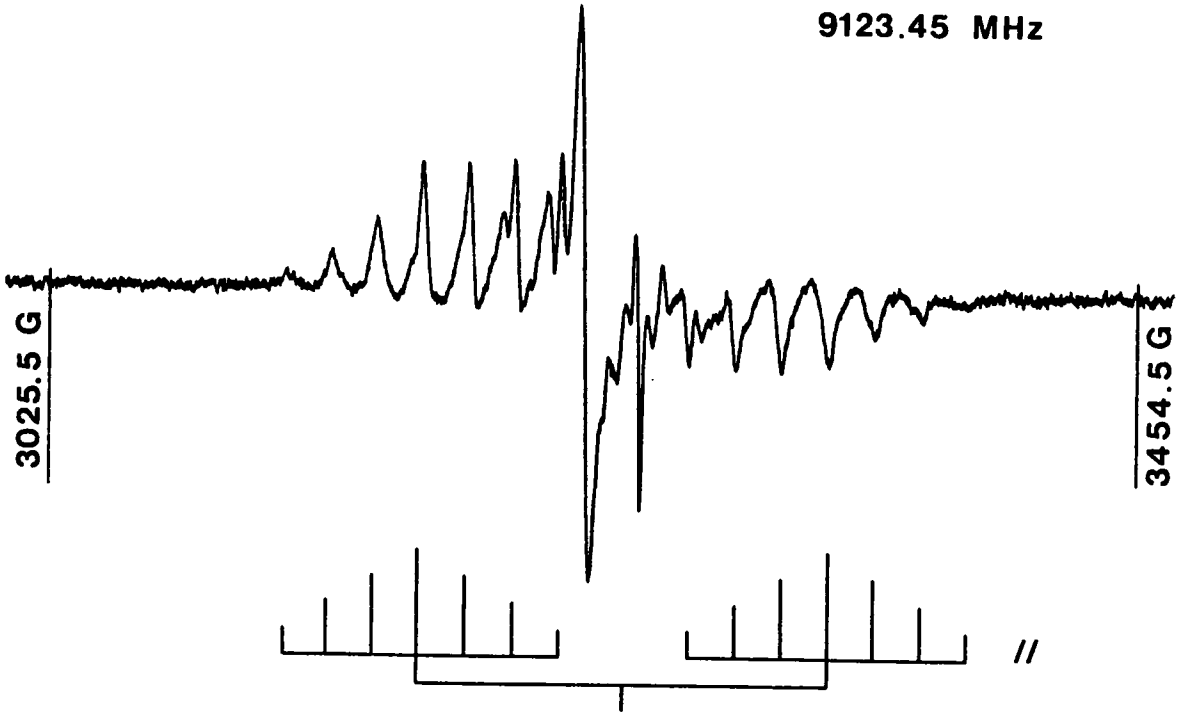

Figure 36. First-derivative ESR spectrum of a γ-irradiated pure sample of $CFCl_3$ at 160 K. The analysis of the parallel pattern is indicated by the lower stick diagram.

the cation radical signal is still strong, then the matrix radical may still go undetected. The radical cations will, in general, decay above 155 K, but the matrix radical does not decay until around 165 K.

1,1,1-Trichlorotrifluoroethane (CCl_3CF_3) and the 1,1,2-trichlorotrifluoroethane ($CFCl_2CF_2Cl$), with slang names of the "symmetric" and "unsymmetric" matrix, respectively, were both used extensively in this work. Radical cation generation in the CCl_3CF_3 matrix appeared to be particularly efficient since the first-derivative ESR signal of the organometal radical cations generated in this matrix were typically an order of magnitude greater than the signal intensity from, for example, Freon-11 although the samples were exposed to comparable doses. The signal from the matrix radical (probably $CCl_3CF_3^-$) is very weak, but shows a very sharp transition at 145 K. At this temperature, the radical cation decays and this change is accompanied by the growing in of the $CF_3CCl_2\cdot$ free radical which is characterized by an extremely intense isotropic signal ($A_{iso}(1^{13}C)$ = 67.3 G, $A_{iso}(3F)$ = 18.5 G, $A_{iso}(2^{35}Cl)$ = 4.2 G, and g_{iso} = 2.0077). The resolution of the hyperfine patterns in this matrix, however, were generally inferior to Freon-11. The $CFCl_2CF_2Cl$ matrix was also very efficient at generating radical cations but not quite as much as CCl_3CF_3. Although the resolution was slightly better in this matrix than in CCl_3CF_3, the cation was often stable only to about 108 K. In some instances with this matrix, the radical cation decayed via a bond breaking mechanism. For example, the t-butyltrimethyltin radical cation dissociates in this matrix to form the t-butyl

radical and the metal cation. This ability of the matrix to induce chemical reactions has proved to be quite rewarding in other instances outside of this work.[176] These secondary radicals generally decayed at 120 K and were replaced with a relatively weak non-analyzable matrix radical.

Perfluoromethylcyclohexane (PFMCH) was also useful for generating radical cations in high yields, but this matrix has a large number of resonances which may obstruct the detection of weak radical cation resonances; also the spectral resolution was quite poor in this matrix. However, the poorer resolution in this matrix may be the result of unresolved superhyperfine interactions between the radical cation and the matrix and is not the result of restricted molecular motion. Experimental evidence supporting the idea that molecular motion is allowed is that the $\cdot CH_2SiMe_3$ free radical is observed at 140 K in this matrix to have so much motion that the resonances become sharp enough to observed the ^{13}C and ^{29}Si hyperfine interactions in natural abundance. The spectral characteristics of the radical cations generated in the perfluoro-1,3-dimethyl cyclohexane (PFDMCH) were identical to the results obtained in the PFMCH matrix.

Carbon tetrachloride (CCl_4) was occasionally useful for obtaining a higher temperature spectrum of the radical cation than could be obtained in other matrices since this matrix did not soften until about 210 K. Unfortunately the matrix radical is quite intense and often obscured the radical cation signals. A similar situation was observed for the bromotrichloromethane (CCl_3Br) matrix.

A Freon mixture composed of $CFCl_3$ and 1,2-dibromotetrafluoroethane ($CBrF_2CBrF_2$) in a 1:1 ratio was occasionally employed when the photochemical aspects of the radical cation needed to be characterized because this mixture formed a clear glass. Although the matrix radical signals are very weak, this matrix was not very useful since temperatures below 83 K were required.

B. Tetramethylsilane and Tetramethylgermane Radical Cations

The original interest in trying to generate the radical cations of tetramethylsilane and tetramethylgermane was a natural extension of the successful detection and characterization of the hexamethyldisilane and hexamethyldigermane radical cations,[170] and this was in fact suggested to us in a private communication by J. K. Kochi.

Photoelectron spectroscopy studies have established that the highest occupied orbitals of the Group IVB tetramethyl derivatives are the triply degenerate t_2 orbitals of T_d symmetry.[173,177] Consequently, the radical cations would be expected to distort from their original T_d symmetry to a lower symmetry as a natural consequence of the Jahn-Teller effect.[178-180,184] Of particular focus in this section are the radical cations formed from tetramethylsilane (Me_4Si) and tetramethylgermane (Me_4Ge) and their Jahn-Teller distortions upon oxidation.

After γ-irradiation of a sample containing 8 mole % of Me_4Si in trichlorofluoromethane (Freon-11), a spectrum (Figure 37, page 165)

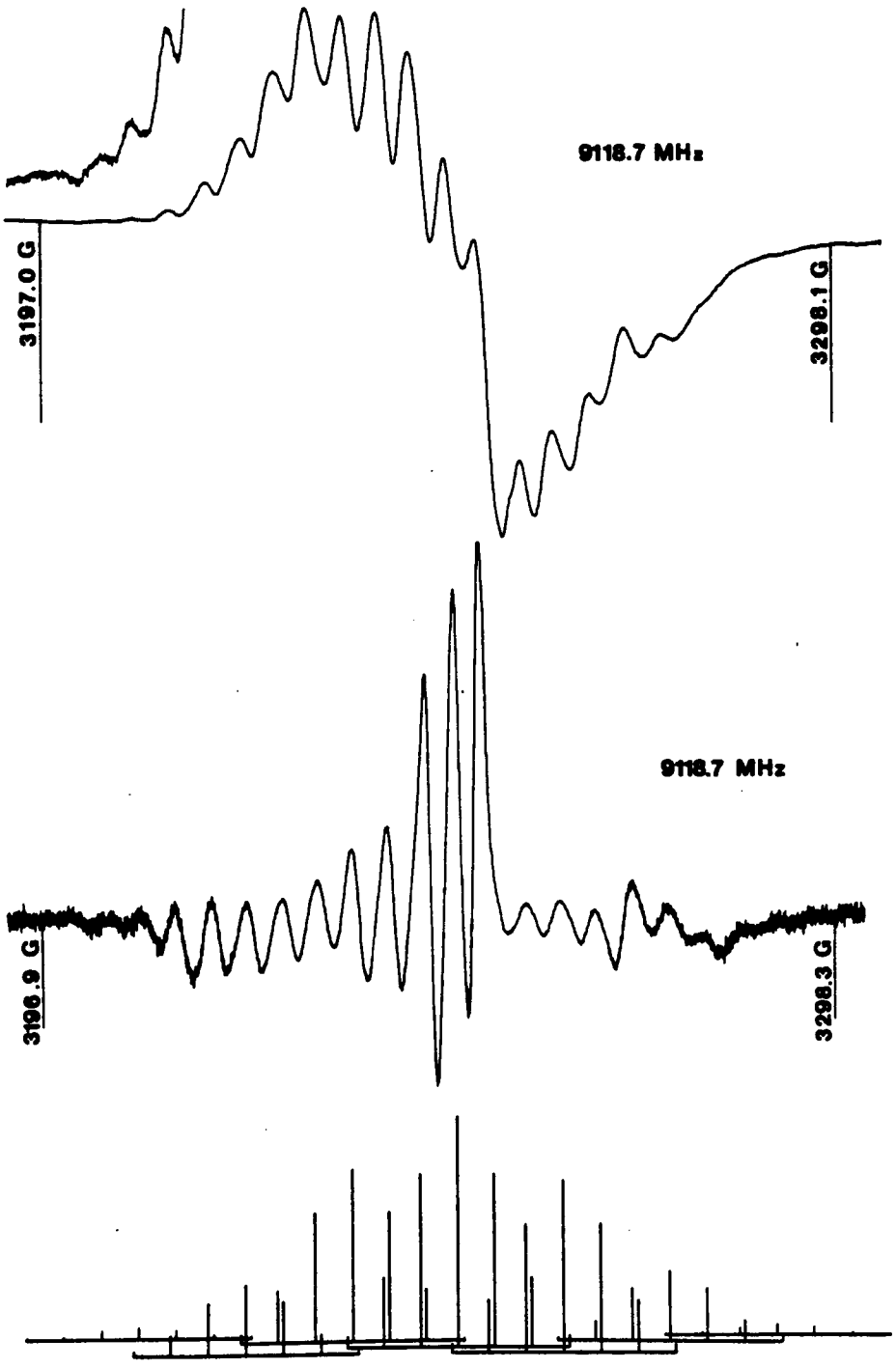

Figure 37. First-derivative (upper) and second-derivative (lower) ESR spectra of a γ-irradiated (dose 1 Mrad) solid solution of 8 mole % $(CH_3)_4Si$ in $CFCl_3$ at 90 K. The stick diagram reconstruction consisting of a septet of septets shows the line components assigned to the tetramethylsilane radical cation.

characterized by at least 19 almost evenly spaced resonances, was observed at 90 K. Warming the sample from its optimum resolution temperature of about 90 K to 130 K resulted in a broadening of the resonances. Interestingly, the 19 line resonance pattern seemed to coalesce into a broad singlet upon further warming to ~142 K or above. Recooling the sample below this high temperature (142 K) resulted in the reappearance of the 19 line pattern, but the spectrum was slightly obscured by decay radicals probably produced at the higher temperature.

The observed pattern was not bleached with visible light. Also, identical results were obtained from a γ-irradiated 1 mole % sample of Me_4Si in Freon-11.

Confirmation that the resonances observed in the above experiment arise from the methyl protons and not from some kind of matrix interaction was obtained by replacing deuterium (^2H or D) for the protons (^1H) in the methyl groups. Such a substitution would be expected to result in the collapse of the 19-line pattern if only protons were coupling while if a matrix interaction were to apply, then at least some of the resonances would be expected to remain unchanged. In fact, the ESR spectrum of a γ-irradiated 1 mole % sample of $(CD_3)_4Si$ in Freon-11 was characterized by an intense singlet centered at g = 2.0056 (Figure 38, page 167) at 130 K. At temperatures below 130 K, the singlet was found to be not as intense and was obscured slightly by what appears to be other radicals.

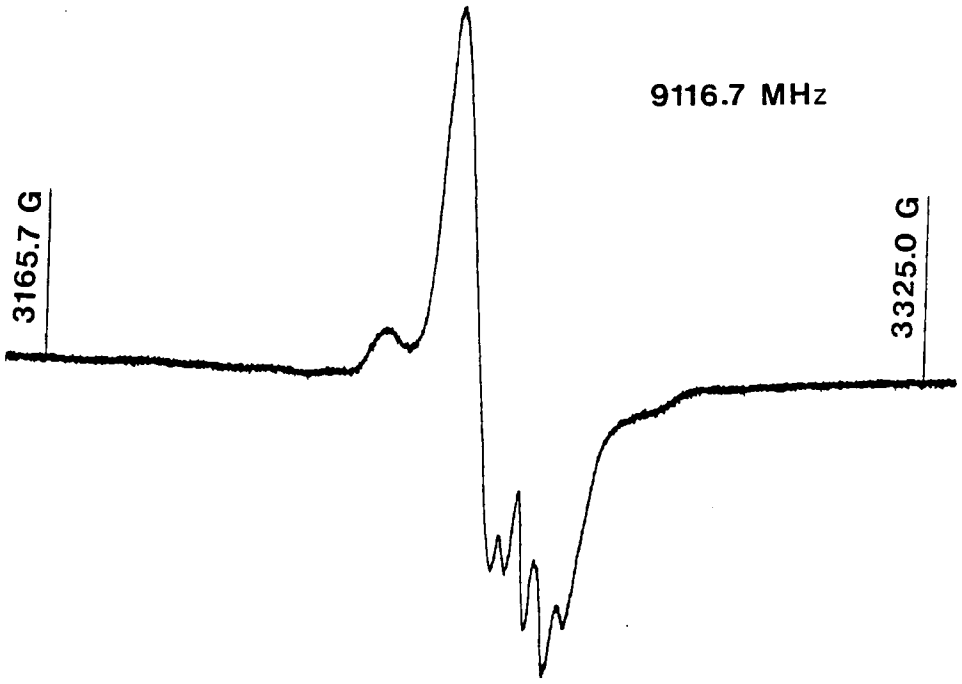

Figure 38. First-derivative ESR spectrum of a γ-irradiated solid solution of 1 mole % of $(CD_3)_4Si$ in $CFCl_3$ at 90 K.

Just as for the Me_4Si experiment, γ-irradiation of a 8 mole % sample of Me_4Ge in Freon-11 resulted in the observation (Figure 39, page 169) of a pattern characterized by at least 17 resonances at 85 K. As is readily obvious from Figure 39, the high-field portion of the ESR spectrum is obscured by other resonances. Warming the sample above 85 K to 132 K was accompanied by a gradual loss of some resolution. Further warming to 150 K resulted in the partial coalescence of the hyperfine pattern into a very broad singlet with still some resolution. The radical was not "bleached" by visible light at 120 K.

One mole percent samples of both Me_4Si and Me_4Ge in perfluoromethylcyclohexane (PFMCH) were prepared and exposed to γ-irradiation. In each case the resultant spectrum, in addition to resonances from the matrix radical, consisted of a very intense broad singlet at 80 K. For the Me_4Si and Me_4Ge samples in PFMCH, the g-factors were computed as 2.0049 and 2.0176 respectively. Above 115 K the singlet irreversibly decayed accompanied by the growing in of the $\cdot CH_2MMe_3$ radical, but a discussion of this decay radical will be deferred to Chapter V.

The singlet which was obtained from the sample of $(CD_3)_4Si$ in Freon-11 may be interpreted as establishing that the apparent 19-line hyperfine pattern which is obtained for the Me_4Si^+ also in Freon-11 arises from coupling to the protons of the organometal cation. Although the corresponding $(CD_3)_4Ge$ in Freon-11 experiment was not performed, the observed 17-line pattern may, by analogy, be assigned to the methyl protons of the organometal.

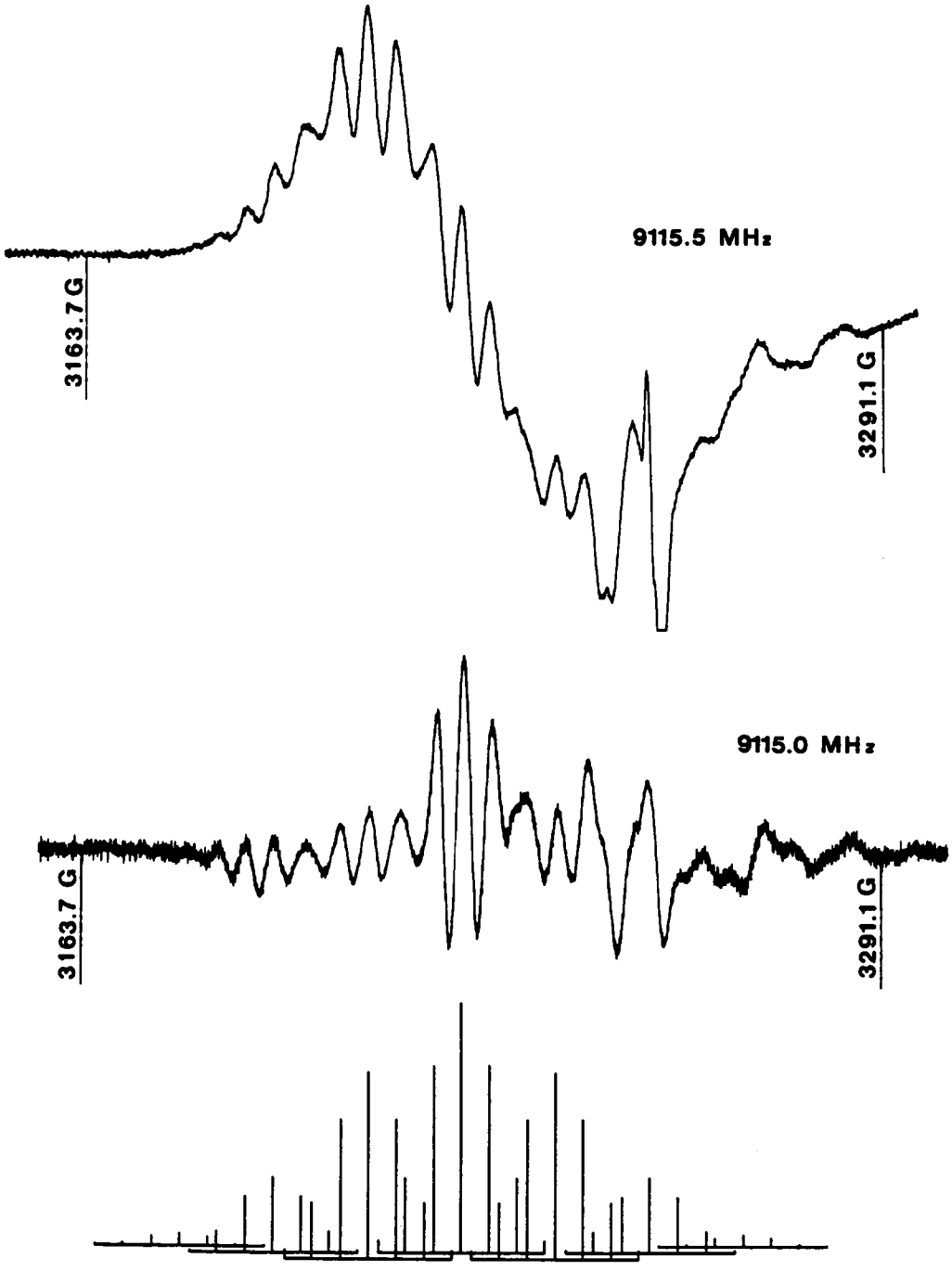

Figure 39. First-derivative (upper) and second-derivative (lower) ESR spectra of a γ-irradiated (dose 1 Mrad) solid solution of 8 mole % $(CH_3)_4Ge$ in $CFCl_3$ at 85 K. The stick diagram reconstruction consisting of a septet of septets shows the line components assigned to the tetramethylgermane radical cation. The high-field region is obscured due to extraneous radicals.

If the methyl groups are freely rotating and are giving rise to an isotropic hyperfine interaction as was the case for the hexamethyldisilane and hexamethyldigermane radical cations, then a 13-line binomial pattern would be expected for the 12 equivalent protons of a tetrahedrally coordinated radical. However, the observed spectrum of these compounds is not a 13-line pattern but is instead characterized by at least a 19- or 17-line pattern. Consequently, without any further analysis, the evidence confirms the prediction that both Me_4Si^+ and Me_4Ge^+ distort from T_d symmetry. Also, it should be noted that not only is a tetrahedrally symmetric radical ruled out, but any distortion which retains four equivalent methyl groups is also ruled out such as for radicals with D_{2d} or D_{4h} symmetry. Distortions to C_{2v} or C_{3v} symmetry, on the other hand, could give rise to many more than just 13 lines in the spectrum and, thus, these distortions should be considered.

A careful analysis of the observed spectra from the Me_4Si and Me_4Ge samples reveals that they may be reduced to a septet of overlapping septet patterns as depicted by the stick diagrams in the lower portion of Figures 37 and 39 (pages 165 and 169). Confirmation of a septet-of-septets pattern was obtained by computer simulations of the observed patterns. The spectra of both radical cations were straightforwardly simulated. The observation that some of the components, particularly in the Me_4Ge^+ spectrum (see Figure 40, page 171), appeared to be broadened greatly supported the septet-of-septets analysis. This analysis, of course, requires that the methyl groups

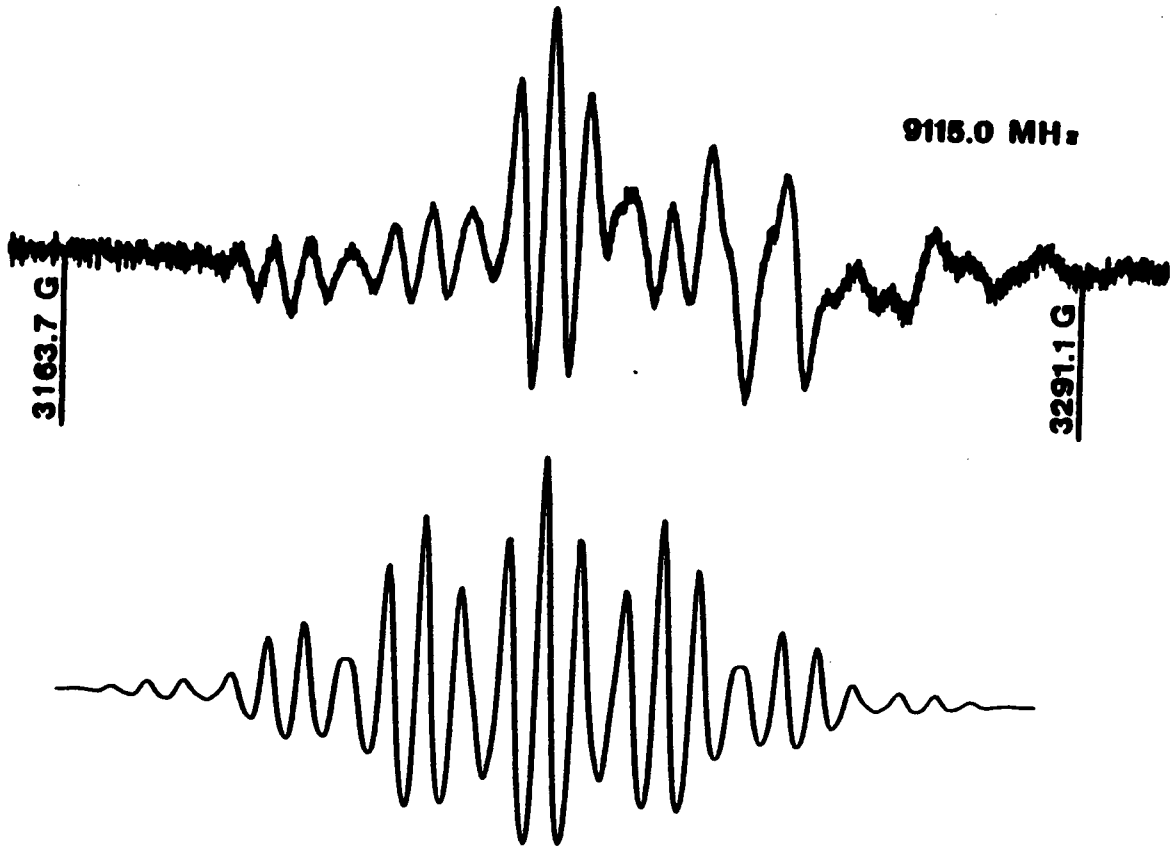

Figure 40. The second-derivative ESR spectrum (upper) of Figure 39, page 169, is reproduced along with a computer simulation which used the parameters listed in the text.

be equivalent in pairs and this implies that the organometal radical cation distorts into a structure possessing C_{2v} symmetry, as shown below:

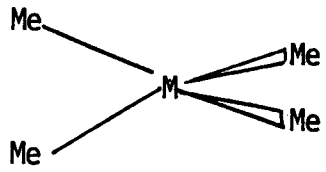

Initial theoretical and photoelectron studies have predicted that tetrahedrally shaped neutral molecules like methane (CH_4) will undergo a Jahn-Teller distortion to either a C_{3v} or D_{2d} structure following one electron oxidation. However, the partially deuterium enriched methane radical cation ($CH_2D_2^+$) which was recently characterized by ESR spectroscopy[181] appears to adopt a C_{2v} structure with the unpaired electron probably occupying a $^2B_1$ orbital. Ab initio configuration interaction (CI) calculations which were carried out at the 6-31 G* basis set UHF level predict[181,182] that the C_{2v} structure has the lowest energy in agreement with the experimental results. The D_{2d} structure was calculated as being only about 900 cm^{-1} above the C_{2v} structure. Incidentally, the $BH_4\cdot$ radical[183] which is isoelectronic with CH_4^+ is also thought to adopt a C_{2v} structure. In light of these findings, the C_{2v} structure proposed for Me_4Si^+ and Me_4Ge^+ seems quite reasonable.

The fact that the hyperfine pattern for the Me_4Si^+ appears to coalesce at higher temperature (> 140 K) may suggest that the methyl ligands are beginning to exchange and are, consequently, smearing the hyperfine splittings. If this interpretation is correct, then the

potential energy well of the locked C_{2v} structure must not be very deep. One possible motion for exchange is that the methyl groups may swing together in pairs alternating between two C_{2v} structures as shown below. Incidentally, the non-deuterium enriched methane radical cation (CH_4^+) appears to be undergoing at 4 K a dynamic Jahn-Teller or fluxional behavior[181] much like that described above.

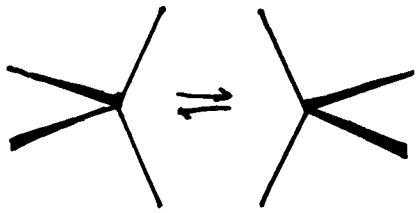

The fact that a broad singlet was also observed for the Me_4Si^+ in the PFMCH matrix at 80 K is not necessarily indicative of a ligand exchange mechanism at low temperature but may be the result of the poorer resolution characteristic of this matrix.

Although the Me_4Ge^+ also began to coalesce into a singlet at 150 K in Freon-11, the smearing in this case could arise from the g anisotropy and not necessarily from an exchange mechanism. That the Me_4Ge^+ would be expected to have some g anisotropy is reasonable since the hexamethyldigermane radical cation[170] exhibited significant g anisotropy ($g_{//} = 2.0023$, $g_{\perp} = 2.0441$).

In summary, upon ionization Me_4Si and Me_4Ge distort to a structure possessing C_{2v} symmetry in contrast to the C_{3v} structure of the neopentane radical cation.[185] In the case of Me_4Si^+, the potential well is not very deep and the radical cation at higher temperature may oscillate between two equivalent C_{2v} structures.

C. Tetramethyltin Radical Cation

Since electrochemical studies have demonstrated that tetraalkyl tin compounds readily undergo one-electron oxidation, it was natural to try and extend the present ESR work on Me_4Si^+ and Me_4Ge^+[186] to Me_4Sn^+ which would be the cation from the next member of the Group IVB organometals. Of course, the detection of a radical in a successful ESR experiment involves more stringent requirements than simply those of generation.

The primary goal of this project was to observe the parent organometallic cation and to characterize the ligand structure of this intermediate. Consequently, to realize this goal, the initial study of Me_4Sn was extended in three ways. First, three isotopically substituted forms of Me_4Sn were utilized, namely $(CD_3)_4Sn$, $(^{13}CH_3)_4Sn$, and $(^{13}CD_3)_4Sn$. Secondly, the organometal radical cation was generated in several different matrices to check the possible effect of a matrix interaction with the radical cation. Thirdly, the samples were examined using a Q-band spectrometer to confirm the X-band analysis.

After the initial stages of this work were completed but before the results were published,[187] another author published[188] his results on the radical cation of $(CH_3)_4Sn$ and later on SnH_4.[189]

The following discussion will be organized in the following way. First, the experimental results of $(CH_3)_4Sn$ and $(CD_3)_4Sn$ in the many different matrices will be presented at X- and Q-band, followed by a discussion of these results pertaining to the structure of the

organometal radical cation. Next, the experimental results of $(^{13}CH_3)_4Sn$ and $(^{13}CD_3)_4Sn$ in the several matrices utilized will be presented and then discussed briefly. The final section will propose two models pertaining to the structure of the Me_4Sn radical cation.

Figure 41, page 176, presents a typical spectrum obtained from γ-irradiation of a 2 mole % solid solution of $(CH_3)_4Sn$ in Freon-11. A spectrum very similar to Figure 41 was obtained from samples where the concentration of $(CH_3)_4Sn$ was varied from less than 0.05 mole % to 15 mole %. The signal level obtained for comparable γ-irradiation doses appeared to be independent of the organometal concentration, although this effect was not precisely measured. The ESR spectrum was characterized by a well-resolved 1:3:3:1 quartet which was analyzed as the set of perpendicular components resulting from hyperfine coupling to three protons ($A_\perp(3H)$ = 13.7 G and $g_\perp$ = 2.045). At higher gain, a partial replica of the more intense quartet pattern was observed to lower field and was assigned to the perpendicular satellite feature resulting from hyperfine coupling to the naturally abundant magnetic isotopes of tin ($A_\perp(^{117,119}Sn)$ = 78 G). The high-field component of the tin isotope was not observed since this region of the spectrum is obscured by other resonances. Further evidence suggesting that these low-field features are tin satellites was obtained by noting their simultaneous decay with the main pattern at about 160 K and their identical power saturation properties, namely a maximum signal level at 0 dB (200 mW). All of these above mentioned features were assigned to the radical cation of $(CH_3)_4Sn$, as will be justified later.

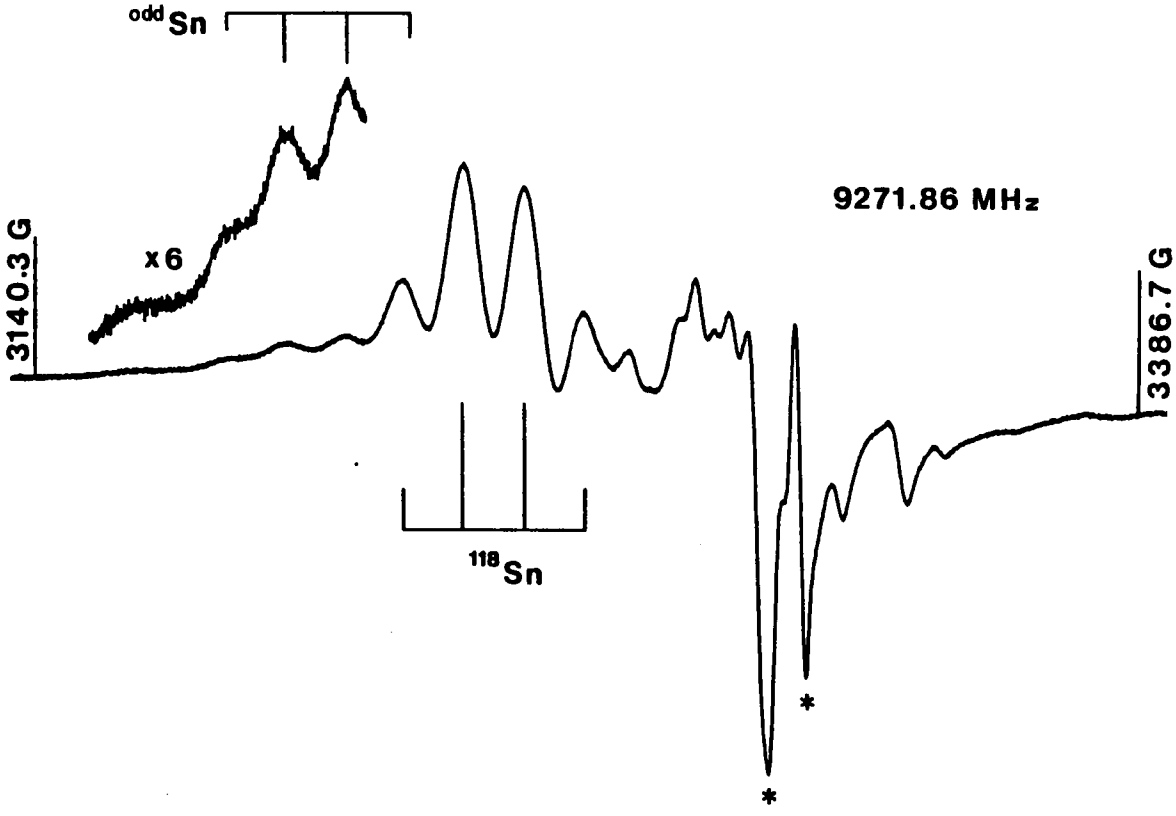

Figure 41. First-derivative ESR spectrum of a γ-irradiated 2 mole % solid solution of $(CH_3)_4Sn$ in $CFCl_3$ at 90 K. The lower quartet stick diagram shows the line components assigned to the perpendicular features of the radical cation. At higher gain additional resonances appear which are labeled by the upper quartet stick diagram and are assigned to an additional hyperfine coupling to the magnetic isotopes of tin.

If a γ-irradiated sample was maintained at temperatures below 90 K, then several photochemical changes were observed but in none of the photochemical experiments did the quartet features assigned to the $(CH_3)_4Sn^+$ change in any way. The features marked with asterisks were readily bleached with filtered visible light (range λ = 340-610 nm), but no detectable radical grew in. Exposure of the original γ-irradiated sample to UV light resulted once again in the disappearance of the features marked with the asterisks but, in this case, it was accompanied by the appearance of an isotropic-looking quartet pattern ($A_{iso}(3H)$ = 22.9 G and g_{iso} = 2.0032) which undoubtedly can be assigned to the methyl radical. This transformation with UV light is clearly shown in Figure 42, page 178). The resulting spectrum revealed the growth of another feature centered at g = 1.9873 which is marked with an arrow (↑) in Figure 42. The spectrum obtained from the same sample after being stored for 24 hours in the dark at 77 K revealed that even at 77 K there had been a significant loss of methyl radicals with time, but the features assigned to $(CH_3)_4Sn^+$ were relatively unchanged in intensity. This experiment was repeated several times with other samples and in each case the results were qualitatively the same but in each case the quantitative transformation to the methyl radical was slightly different. A sample of $(CH_3)_4Sn$ in Freon-11 which had not been exposed to γ-irradiation did not show any of the photochemical changes described above.

Annealing the sample to about 110 K resulted in the thermal decay of the features labeled with asterisks in Figure 42. Also,

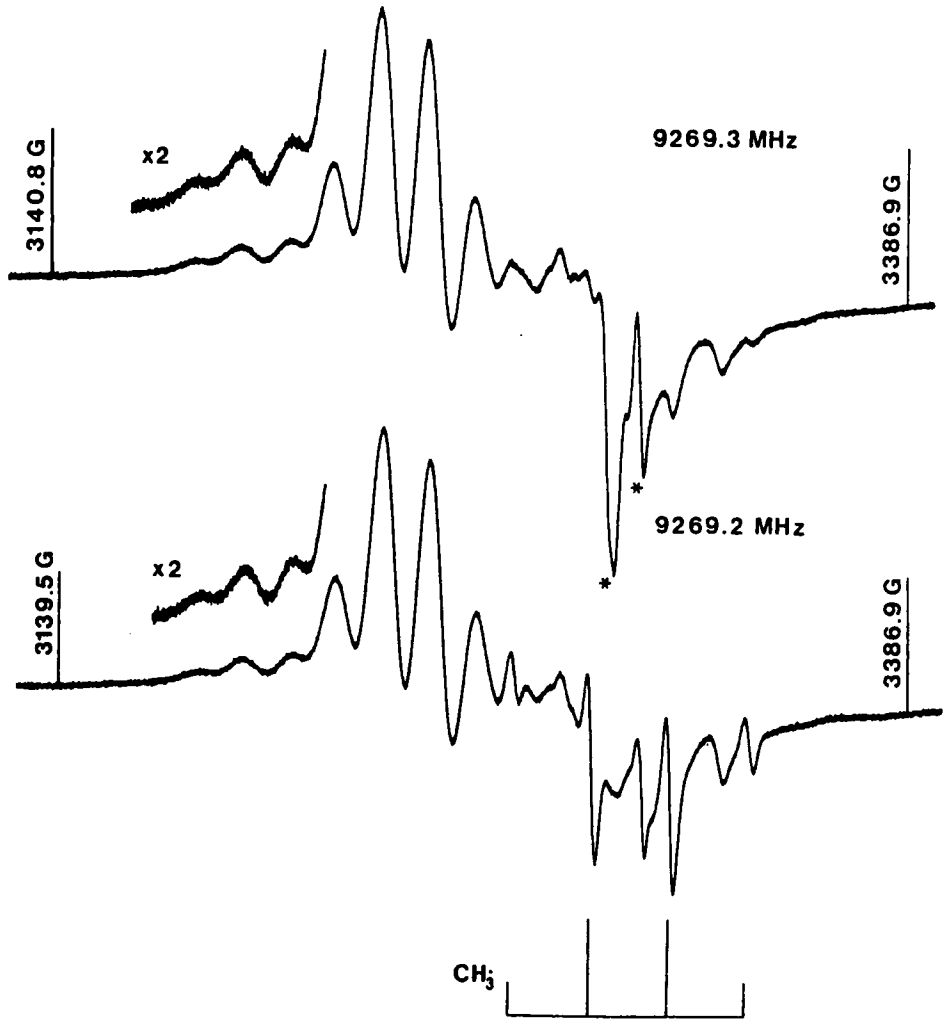

Figure 42. First-derivative ESR spectrum of a γ-irradiated 5 mole % sample of $(CH_3)_4Sn$ in $CFCl_3$ at 80 K before exposure to UV light (upper) and after 5 minutes of exposure (below).

once a sample was annealed above about 120 K, exposure of the sample to UV light did not produce any methyl radicals.

In an attempt to confirm the analysis for Me_4Sn^+, further experiments were carried out using a Q-band spectrometer and using the isotopically substituted $(CH_3)_4Sn$ in Freon-11.

A γ-irradiated 1 mole % sample of $(CH_3)_4Sn$ in Freon-11 was observed using a Q-band spectrometer. Although the resolution was inferior to the X-band spectra, the Q-band spectra confirmed the quartet pattern and the low-field tin satellite resonance (Figure 43, page 180). To check that the radical of interest had survived the manipulations required to obtain the Q-band spectrum, a spectrum of the γ-irradiated sample was taken at X-band a few hours before the Q-band observation and then the following day. Comparison of the before-and-after X-band spectra revealed that there was virtually no difference between them and they closely resembled Figure 41, page 176.

Evidence that the hyperfine splitting arises from interaction with the methyl protons and not through a matrix interaction was achieved by use of the 99% deuterium-enriched $(CD_3)_4Sn$. A 2 mole % sample of $(CD_3)_4Sn$ in Freon-11 was prepared and γ-irradiated. At 80 K the observed spectrum (Figure 44, page 181) was characterized by an intense singlet at $g_1 = 2.0447$ and a singlet at low field which was assigned to the low-field tin satellite resonance (A_1 ($^{117,119}Sn$) = 78.3 G). In addition to the above features, several resonances were observed in the "free spin" region ($g \sim 2.0023$) of the spectrum just

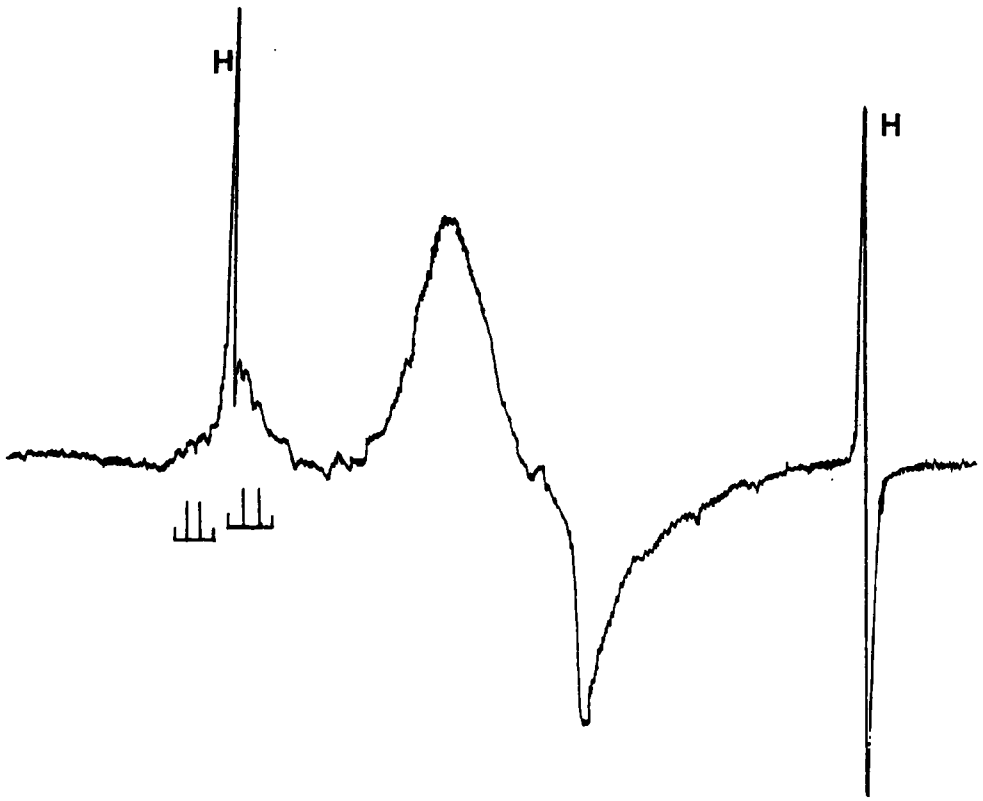

Figure 43. Q-band ESR spectrum of a γ-irradiated 2 mole % solid solution of $(CH_3)_4Sn$ in $CFCl_3$ at about 77 K.

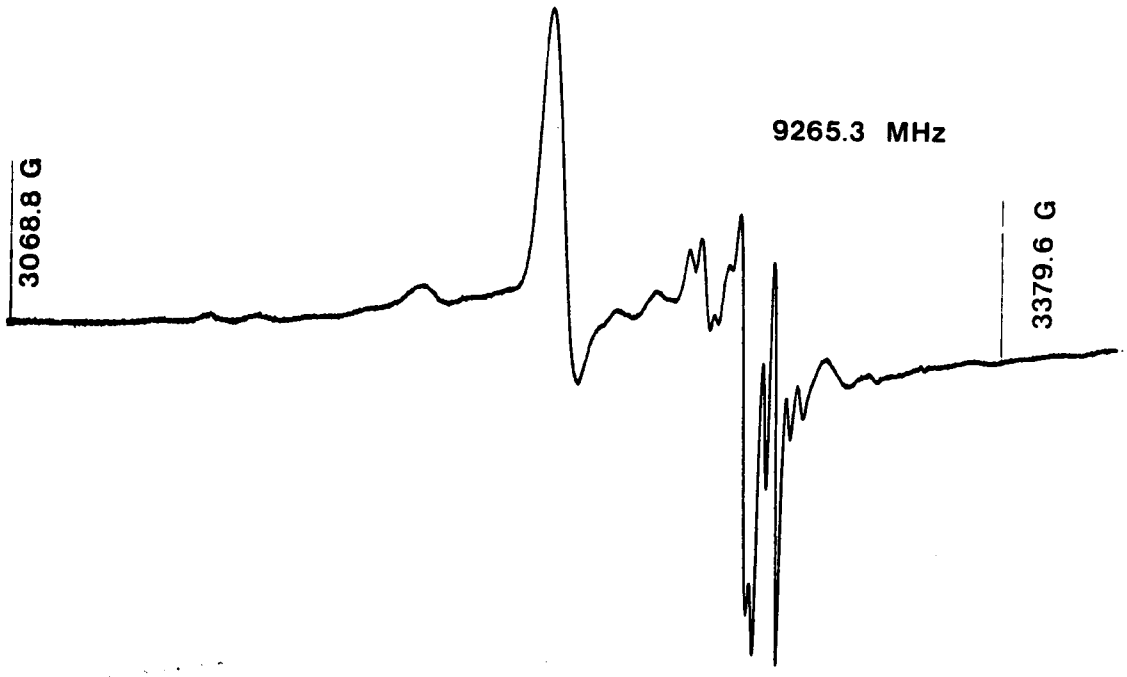

Figure 44. X-band ESR spectrum of a γ-irradiated 2 mole % solid solution of $(CD_3)_4Sn$ in $CFCl_3$ at 100 K. Compare with Figure 41, page 176.

as with $(CH_3)_4Sn$. Interestingly, the two unanalyzed features which were marked with asterisks in Figure 42, page 178, were also observed in the present case, thus establishing that these features do not arise from any hydrogen couplings. Annealing the sample to 110 K resulted (as for the $(CH_3)_4Sn$ sample) in the irreversible decay of the unidentified features marked with asterisks in Figure 42. The organometal radical cation decayed at about 160 K.

The effect of low temperature on the spectrum of $(CD_3)_4Sn^+$ was also examined. As the temperature of the γ-irradiated sample was cooled to below 60 K, the signals assigned to $(CD_3)_4Sn^+$ grew more intense and the signals in the free spin region became poorer resolved. These two factors allowed the high-field tin satellite perpendicular feature to become clearly resolved against the background signals. Figure 45, page 183, shows an optimum low temperature spectrum of $(CD_3)_4Sn^+$ taken at 10 K.

Again in an attempt to positively confirm the analysis, a γ-irradiated sample of $(CD_3)_4Sn$ in Freon-11 was observed using a Q-band spectrometer. In addition to confirming the assigned g_1 value, Figure 46, page 184, confirms the position of the high field tin satellite resonance.

Since there are two naturally abundant isotopes of tin (^{117}Sn = 7.67% and ^{119}Sn = 8.68%) having different <u>nuclear</u> g values (g_N = -0.9949 (^{117}Sn) and g_N = -1.0409 (^{119}Sn)), it might be expected that two resonances on each side of the non-magnetic isotope peak should appear instead of just the one satellite resonance which is observed.

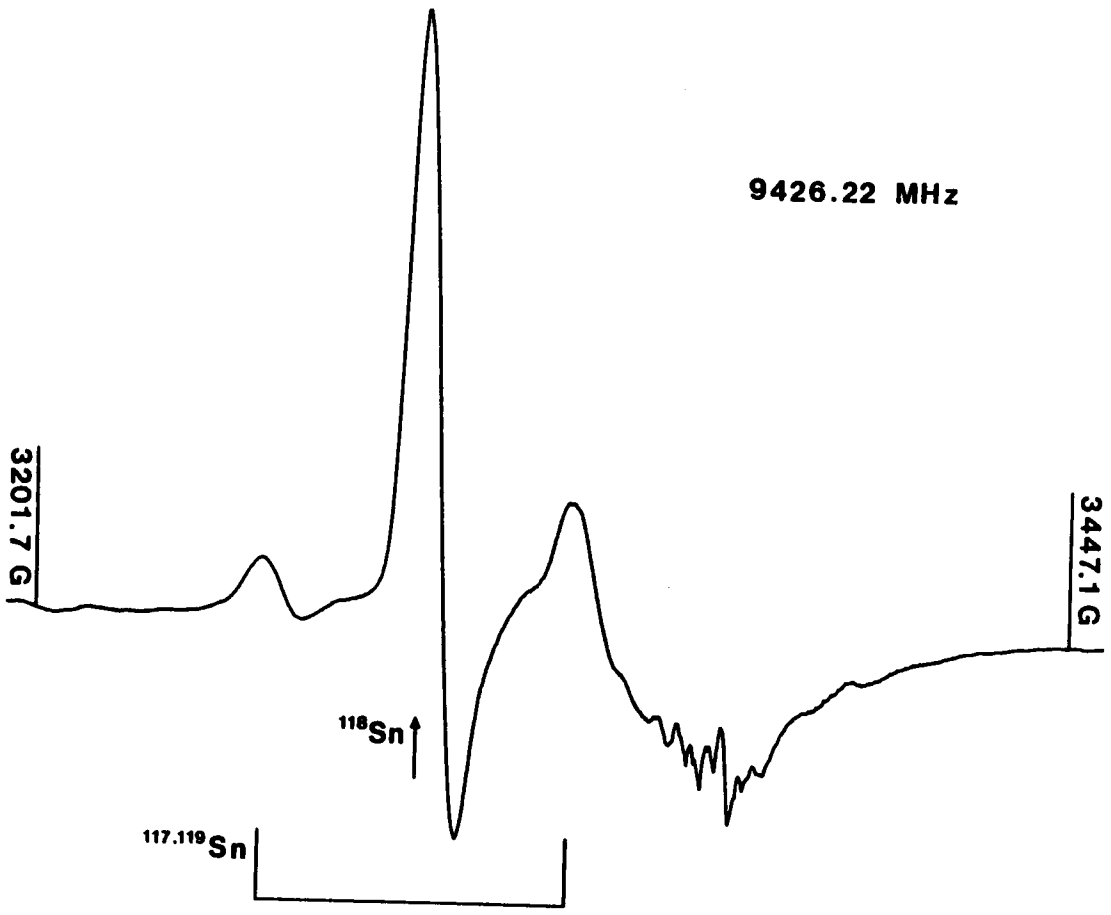

Figure 45. X-band ESR spectrum of a γ-irradiated 2 mole % solid sample of $(CD_3)_4Sn$ in CCl_3 at 10 K.

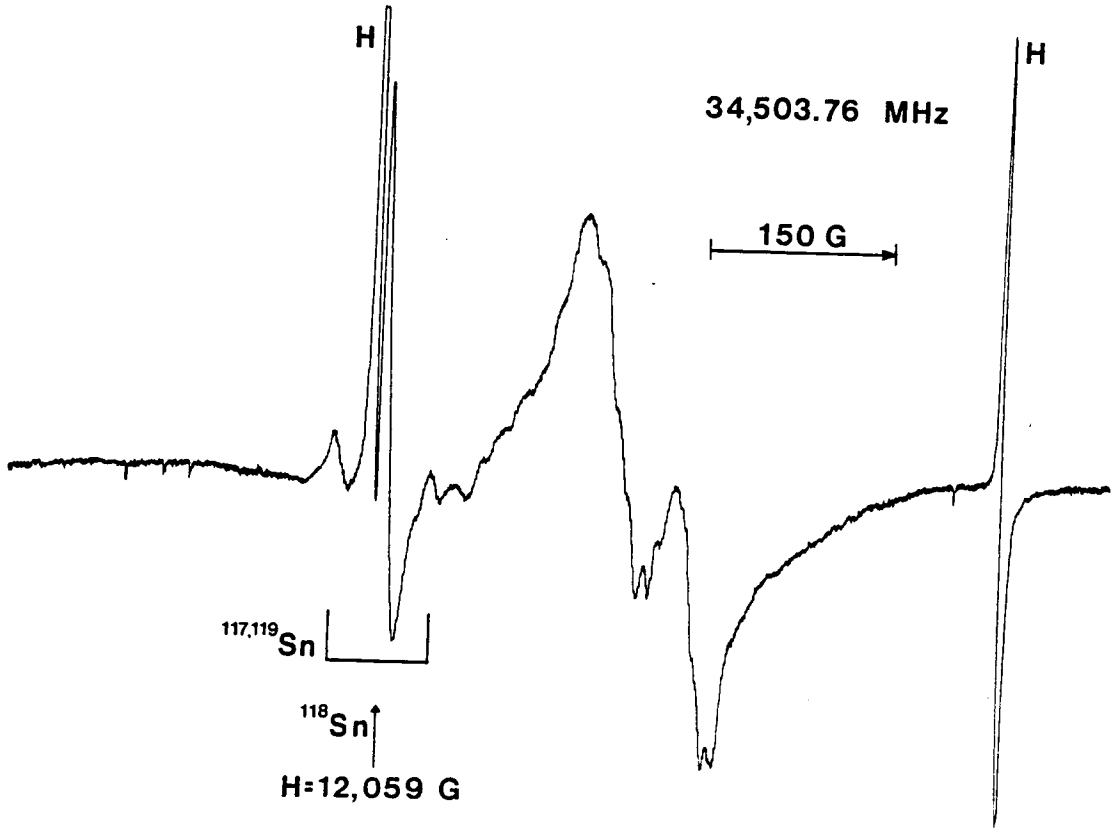

Figure 46. Q-band ESR spectrum of a γ-irradiated 2 mole % solid solution of $(CD_3)_4Sn$ in $CFCl_3$ at about 77 K.

However, for tin (^{117}Sn or ^{119}Sn) hyperfine couplings on the order of about 100 G or less, the separation between the two satellite resonances is calculated to be about 2.3 G which is less than the natural linewidth of the individual components and, therefore, only one broadened feature is observed. The amount of broadening is predictable and can be used as an independent test to establish that the low-field resonances observed in each of these studies arises from the tin satellite resonances. For example, the width of the main line resonance of $(CD_3)_4Sn^+$ at half-maximum height in Freon-11 is 8.4 G and the corresponding point on the low-field resonance is 10.5 G, yielding an increase of 2.1 G. Given that the tin coupling constant is 78 G, the expected increase in linewidth is 2.0 G which is in almost exact agreement with that observed in the spectrum.

Although the resolution was poor, the observed spectrum (Figure 47, page 186) of a γ-irradiated 1 mole % sample of $(CH_3)_4Sn$ in $CFCl_2CF_2Cl$ was similarly characterized by a quartet pattern ($A_1(3H)$ = 13.5 G and g_1 = 2.0446). Once again, on the low-field side of the main line pattern, a weaker replica pattern was observed and was assigned to a tin hyperfine interaction ($A_1(^{117,119}Sn)$ = 89.4 G. Confirmation that the pattern arises from proton coupling was obtained by substituting the deuterium-enriched compound for the protiated compound and following the same procedures. The observed spectrum of $(CD_3)_4Sn^+$ in $CFCl_2CF_2Cl$ is clearly defined by an intense singlet with g_1 = 2.0447 and a tin satellite resonance at low-field (A_1 ($^{117,119}Sn$) = 89 G).

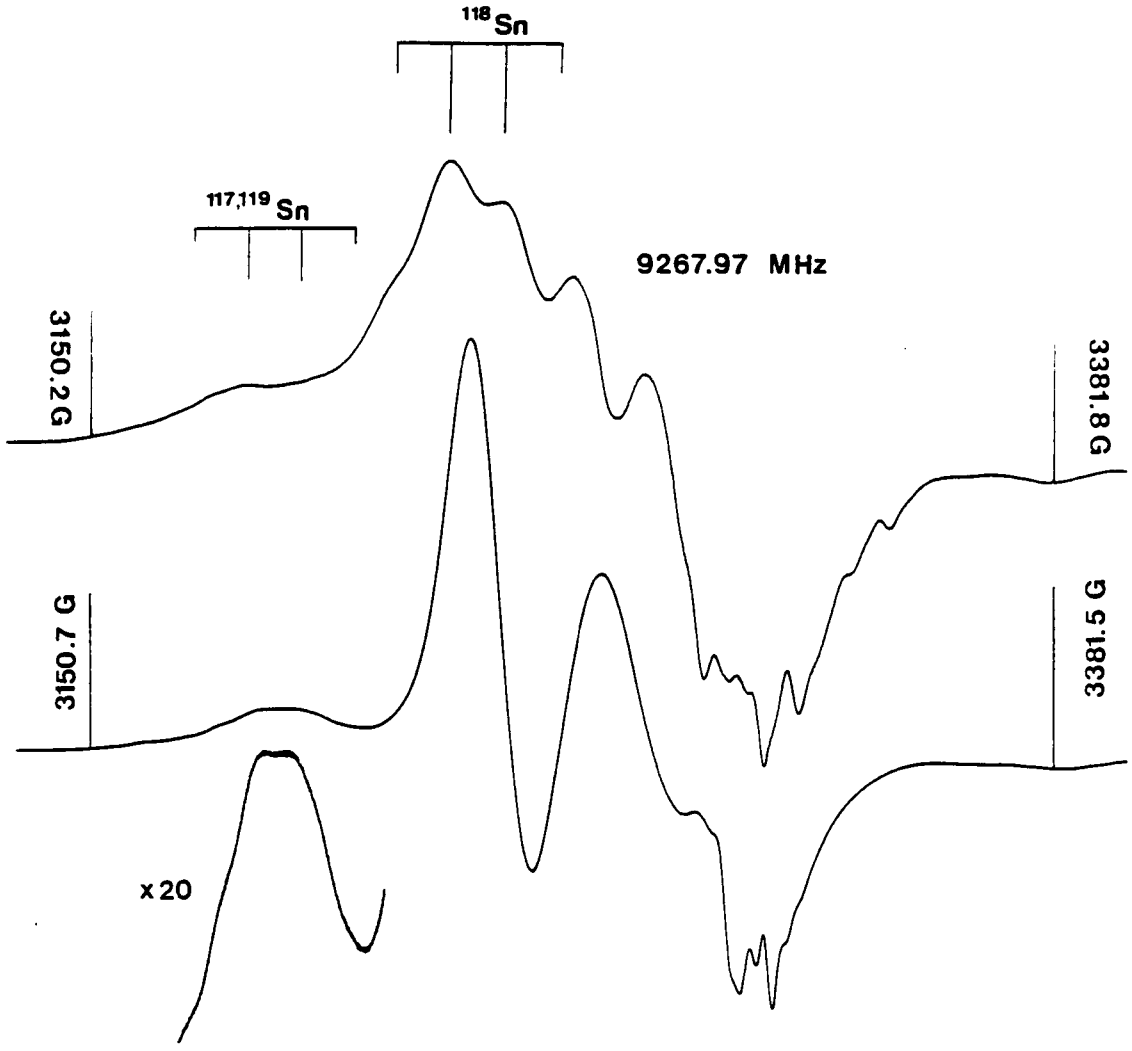

Figure 47. First-derivative ESR spectra of γ-irradiated samples of either $(CH_3)_4Sn$ (upper) or $(CD_3)_4Sn$ (lower) in CCl_2FCF_2Cl at 83 K.

Paralleling the results in the Freon-11 matrix, UV photolysis of a γ-irradiated sample of $(CH_3)_4Sn$ in $CFCl_2CF_2Cl$ resulted in the appearance of resonances which were assigned to the methyl radical with no apparent disappearance of the features assigned to $(CH_3)_4Sn^+$. Also, warming the γ-irradiated sample to 110 K resulted in the rapid decay of $(CH_3)_4Sn^+$ without any methyl radical formation.

Instead of the simple quartet splitting which is observed for $(CH_3)_4Sn^+$ in Freon-11, the observed spectrum (upper portion, Figure 48, page 188) of a γ-irradiated 1 mole % sample of $(CH_3)_4Sn$ dissolved in CCl_3CF_3 was characterized by at least a 5-line pattern. That some of the hyperfine pattern arises from proton couplings was established from the observation (lower portion, Figure 48) of the corresponding spectrum from a γ-irradiated 1 mole % sample of $(CD_3)_4Sn$ in the same matrix. For each sample the low-field feature at higher gain is assigned to satellites resulting from hyperfine coupling to the magnetic isotopes of tin ($A_1(^{117,119}Sn)$ = 96 G).

In order to analyze these two spectra, attention will be first focused on the isotopically labeled $(CD_3)_4Sn$ results. Although $(CD_3)_4Sn^+$ in Freon-11 (Figure 44, page 181, and Figure 45, page 183) is characterized by a single smooth and narrow (~ 8 G line width) resonance, the corresponding resonance in this matrix appears to be split into at least three resolved components and possibly four with a coupling of 9.2 G. This splitting may be assigned to a hyperfine interaction with a chlorine nucleus (I = 3/2), with $A_1(^{35}Cl)$ = 9.2 G, and is shown by the lower stick diagram. Turning to the $(CH_3)_4Sn^+$

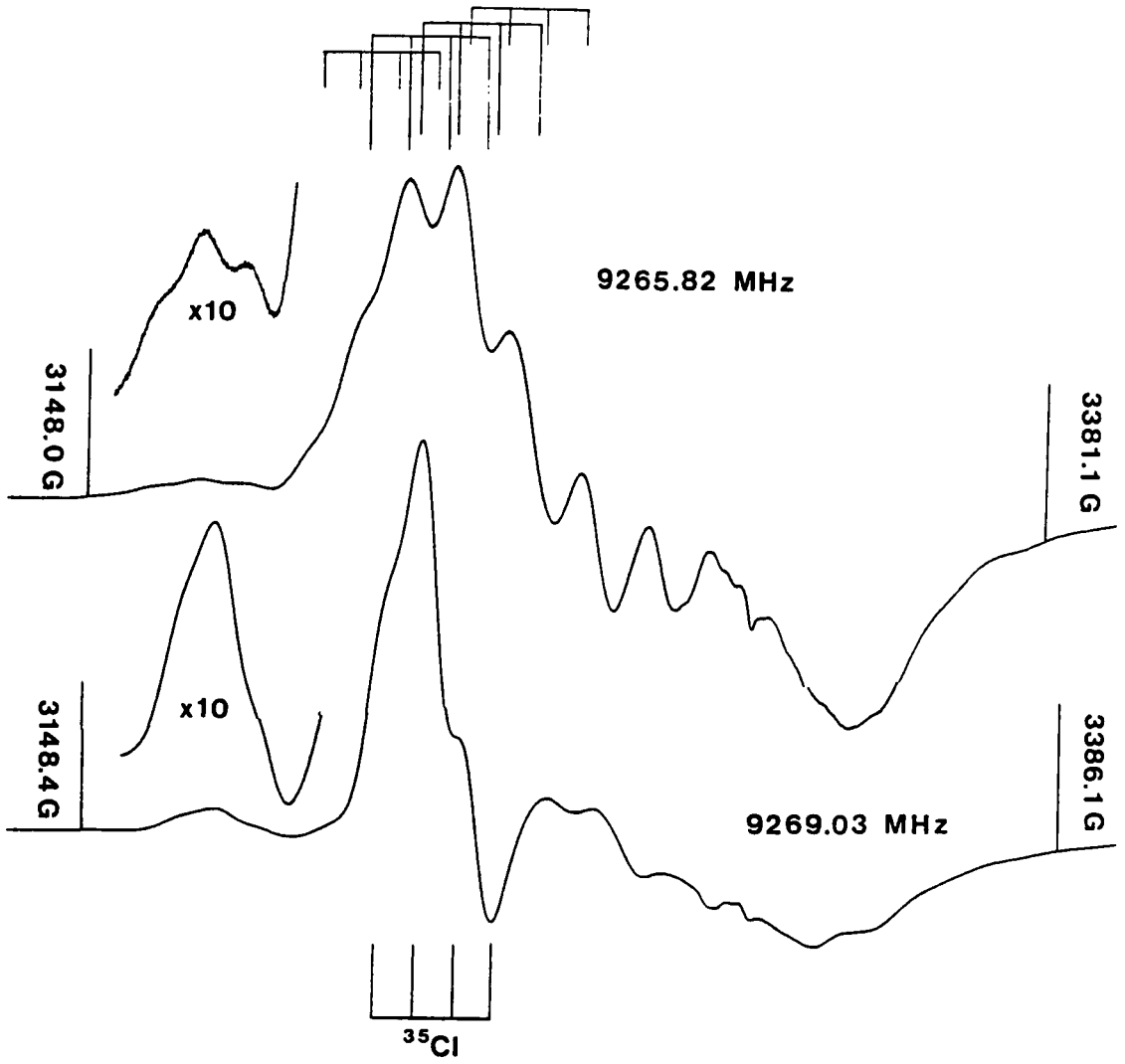

Figure 48. First-derivative ESR spectra of γ-irradiated samples of either $(CH_3)_4Sn$ (upper) and $(CD_3)_4Sn$ (lower) in CCl_3CF_3 at 85 K. The lower stick diagram defines the chlorine hyperfine interaction while the upper stick diagram shows the additional proton hyperfine coupling expected for three equivalent protons.

spectrum, the spacings are assigned to an overlapping quartet of quartets hyperfine pattern ($A_1(^{35}Cl)$ = 9.2 G and $A_1(3H) \sim 8$ G) and is shown by the upper stick diagram. Based on this analysis, g_1 = 2.0477. Evidence supporting this analysis was obtained in two ways. First, the five features assigned to $(CH_3)_4Sn^+$ appeared to decay together at 145 K. Secondly, the five features were intensified together as the power was increased. Photo-bleaching the sample with either visible or UV light resulted in only minor changes in the spectrum with no detectable production of methyl radicals.

The ESR spectrum (Figure 49, page 90) of a γ-irradiated sample of a 5 mole % sample of $(CH_3)_4Sn$ in CCl_4 at low temperature, 80 K, was dominated by an intense singlet centered at g = 2.013 and by a broad resonance centered at g = 2.139, both from matrix radicals. As shown by the stick diagram on Figure 49, page 190, some features were observed which could be assigned to $(CH_3)_4Sn^+$. Warming the sample above about 115 K resulted in the irreversible decay of the two initially strong features. By further warming to 163 K (Figure 50, page 191), the quartet pattern ($A_1(3H)$ = 13.6 G and g_1 = 2.0444) and the tin satellite resonance ($A_1(^{117,119}Sn)$ = 92 G) were clearly defined. Above 180 K, the resolution of the quartet pattern deteriorated, but the radical did not decay until 215 K.

In an attempt to generate $(CH_3)_4Sn^+$ in a non-heavy halogen matrix, a 1 mole % solid solution of $(CH_3)_4Sn$ in perfluoromethylcyclohexane (PFMCH) was prepared and γ-irradiated. In addition to evidence for $(CH_3)_4Sn^+$, the observed ESR spectrum (Figure 51, page

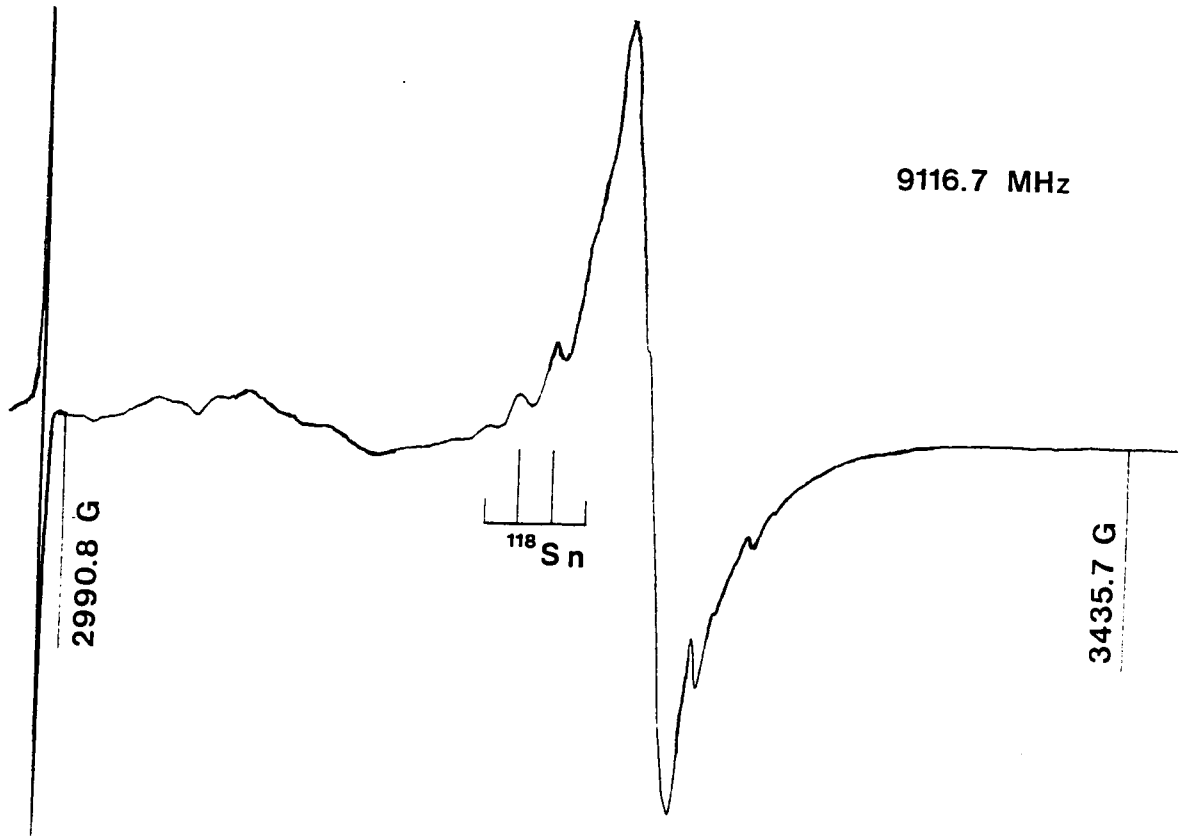

Figure 49. First-derivative ESR spectrum of a 1 mole % solid solution of $(CH_3)_4Sn$ in CCl_4 at 80 K.

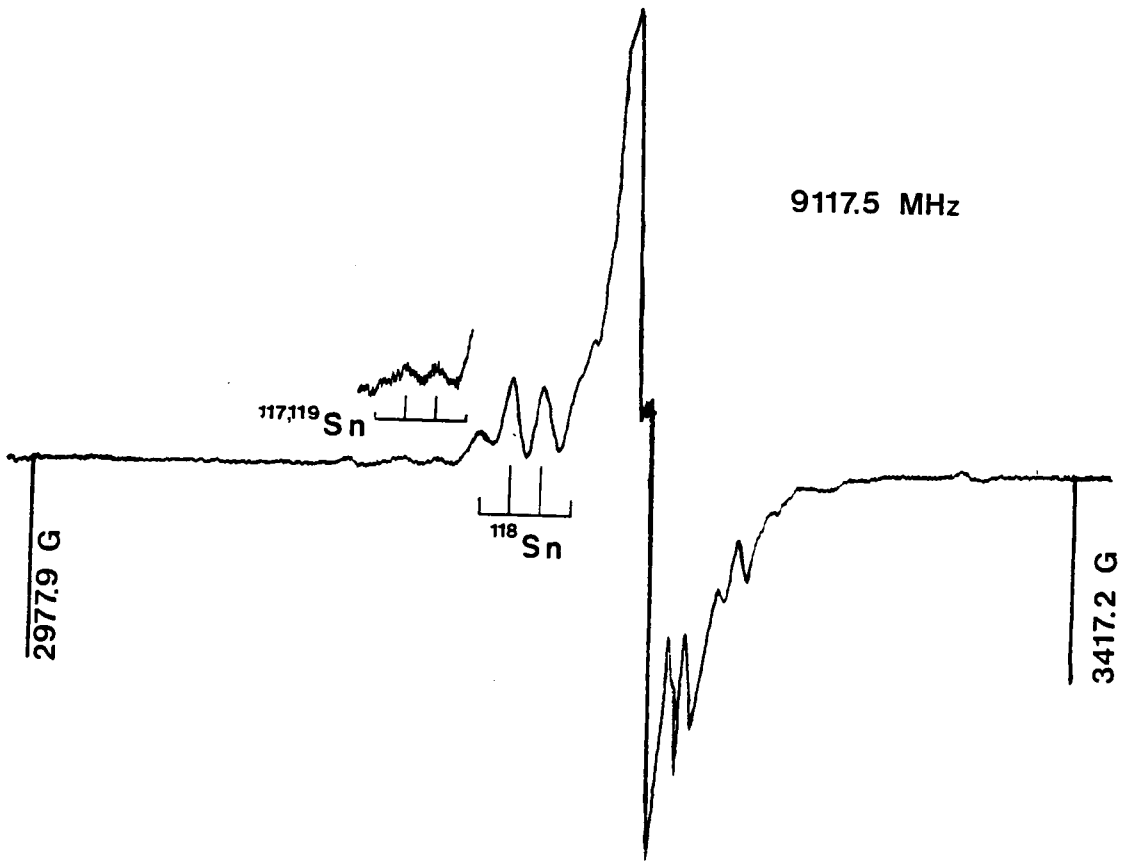

Figure 50. First-derivative ESR spectrum of a 1 mole % solid solution of $(CH_3)_4Sn$ in CCl_4 at 163 K.

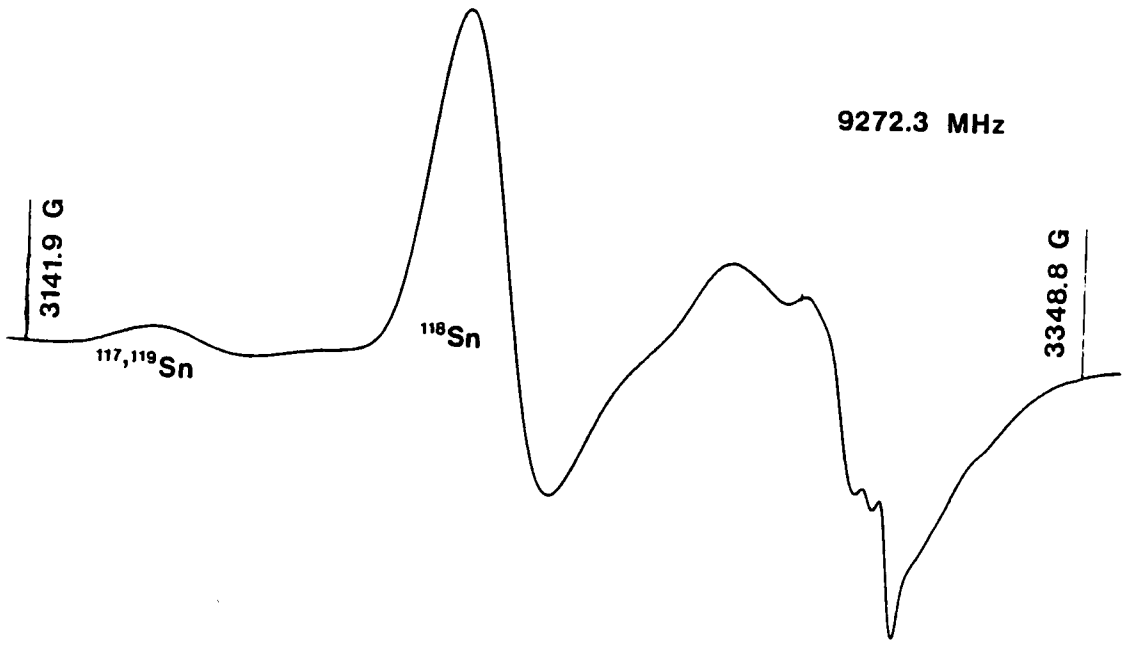

Figure 51. First-derivative ESR spectrum of a 1 mole % solid solution of $(CH_3)_4Sn$ in PFMCH.

192) showed evidence for the PFMCH radical anion (this radical is discussed in Chapter III, section E). Although the quartet splitting is not well-resolved in this matrix, the slight inflections in the perpendicular feature which are indicated by the stick diagram located in the lower portion of Figure 51, page 192, correspond to a hyperfine coupling of 13.5 $\pm$ .5 G and a g value of about 2.048. Again, a replica pattern of the main resonance was observed on the low-field side and was assigned to a tin-isotope hyperfine interaction ($A_1(^{117,119}Sn)$ = 114 G. These results obtained while using the PFMCH as the matrix were reproduced when perfluoro-1,3-dimethylcyclohexane was used as the matrix. Warming the sample to 115 K resulted in the rapid and irreversible decay of the features assigned to $(CH_3)_4Sn^+$ accompanied by the growing in of a triplet pattern which was assigned to the $Me_3SnCH_2^{\cdot}$ neutral radical. This latter radical will be discussed later (Chapter V, Section B).

In order to check the photochemical behavior of $(CH_3)_4Sn^+$, a glassy matrix was needed to allow greater penetration of visible light. To that end, a 1:1 mixture of Freon-11 and CF_2BrCF_2Br was employed as the matrix with a 1 mole % amount of $(CH_3)_4Sn$ being dissolved in it (Figure 52, page 194). After γ-irradiation, the sample was put into a liquid nitrogen ESR dewar which was then placed into the cavity. These transfers were made while allowing the very minimum amount of exposure to room light. As expected the parameters closely resembled those obtained in pure Freon-11 ($A_1(3H)$ = 13.5 G,

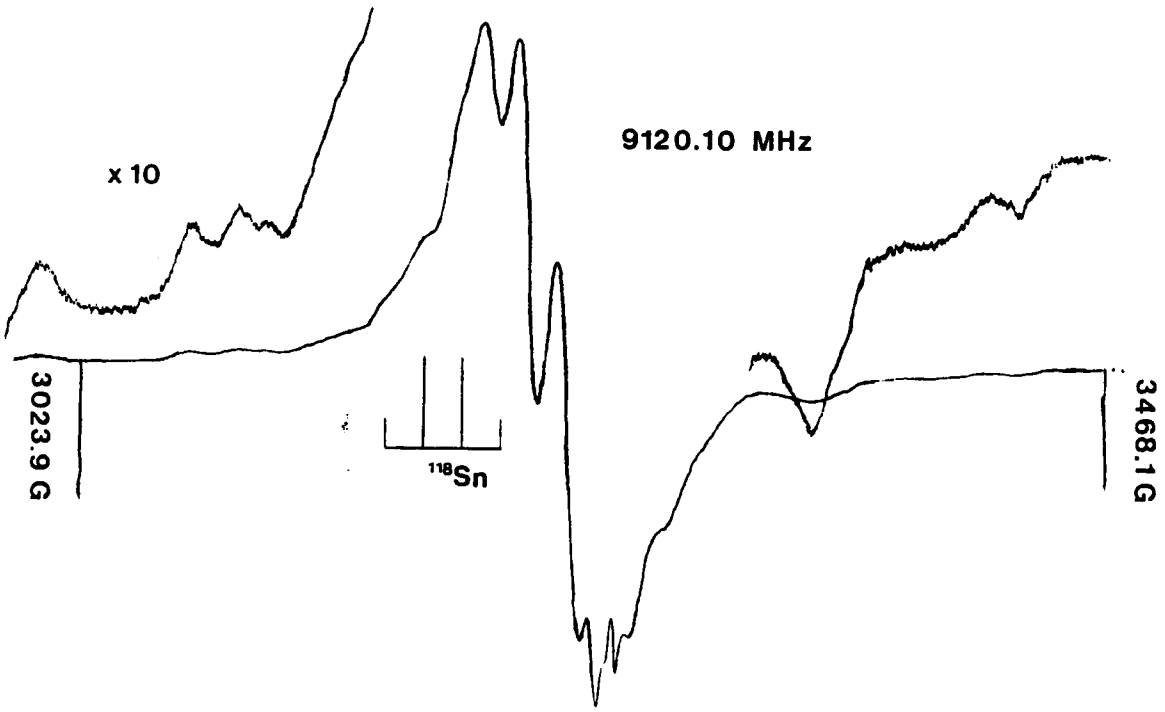

Figure 52. First-derivative ESR spectrum of a γ-irradiated sample of $(CH_3)_4Sn$ in a Freon glass (1:1; CCl_3F:CF_2BrCF_2Br) at 77 K.

$A_{\perp}(^{117,119}Sn)$ = 78.8 G, and $g_{\perp}$ = 2.044. Exposing the sample to visible light using a Corning filter #4308 (λ = 340-610 nm) resulted in the decay of the two features previously described in conjunction with Figure 42, page 178. Although there were resonances which were assigned to the methyl radical before exposure to visible light, no further growth of these resonances was detected even though the sample was exposed for 21 minutes. Exposure of this sample for just 2 minutes of UV light resulted in the rapid formation of the methyl radical.

The spectrum of a γ-irradiated 1 mole % solid solution of $(CH_3)_4Sn$ in $CBrCl_3$ was characterized by a broad but intense quartet splitting ($A_{\perp}$(3H) = 13.6 G) centered at $g_{\perp}$ = 2.0427 as indicated by the stick diagram in the lower portion of Figure 53, page 196. Careful examination of the low-field edge of the main perpendicular resonance yielded evidence suggestive of a weak unresolved resonance. This hump was tentatively assigned to a tin satellite feature ($A_{\perp}(^{117,119}Sn) \sim 90$ G) and its position is designated by the stick diagram.

Several other matrices were utilized such as SF_6, CF_3CF_2Cl, CF_2Cl_2, but in these cases only matrix radicals were detected.

Unfortunately, in none of the different matrices was a clearly defined parallel pattern observed for $(CH_3)_4Sn^+$ or $(CD_3)_4Sn^+$. Nevertheless, an upper limit of the tin parallel hyperfine coupling can be set by the following argument. If a first-order analysis is appropriate, then the tin satellite resonances would be equally

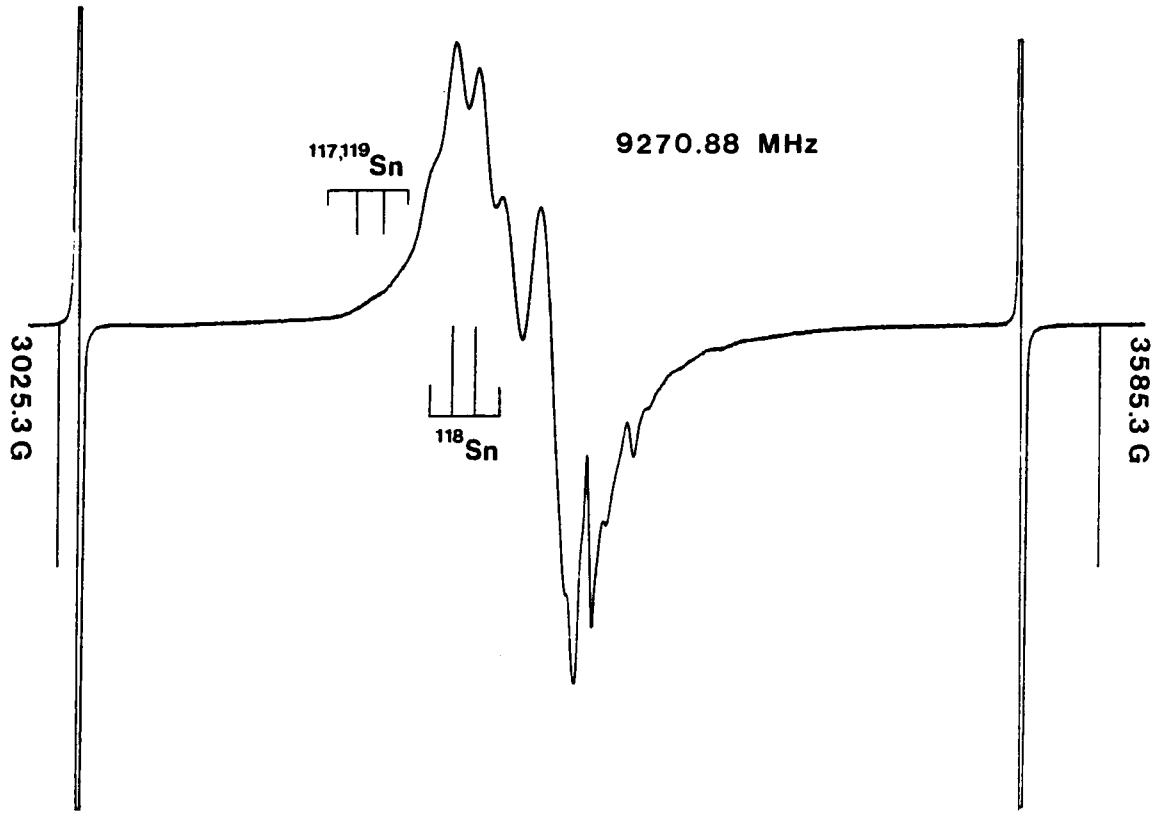

Figure 53. First-derivative ESR spectrum of a γ-irradiated solid solution of $(CH_3)_4Sn$ in $CBrCl_3$ at 88 K.

displaced on either side of the main resonance, that is from the non-magnetic isotopes. Thus, for a first order analysis, the $^{117,119}Sn$ hyperfine coupling may be obtained by simply doubling the distance from the main resonance to, say, the low-field satellite resonance, as shown in the upper diagram below. If a higher-order analysis is appropriate, then the satellite resonances will <u>not</u> be equally displaced about the main resonance because the higher order effects will shift the satellite resonances to lower field (as shown in the lower diagram below), but the main resonance will not be shifted. The net result is that the distance from the satellite resonance to the non-magnetic isotope resonance (I=0) is no longer equal to one-half of the coupling constant.

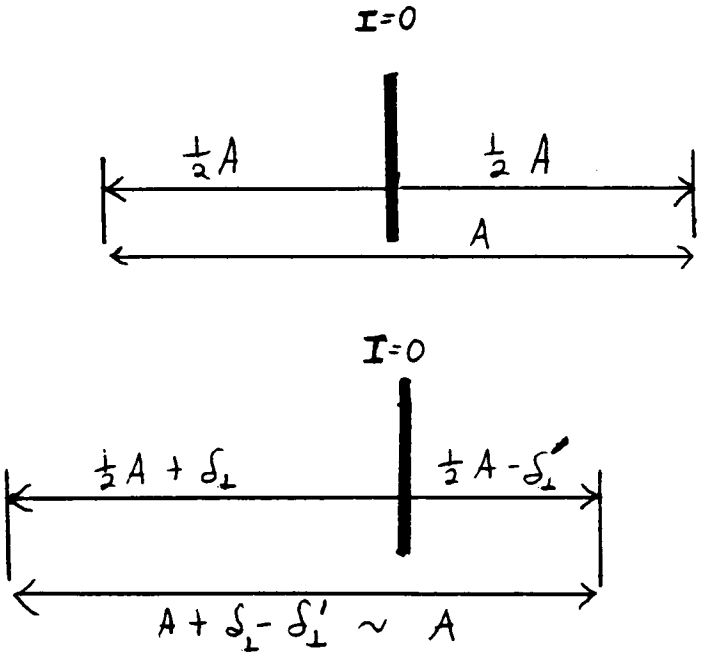

A useful equation may be obtained by solving Equation (41), page 29, for $A_{//}^2$ as

$$A_{//}^2 = \frac{4H\,\delta_1}{I^2 + I - M_I^2} - A_1^2 \qquad (53)$$

As shown by the equation above, a value of $A_{//}$ may be estimated without even observing any parallel resonance if the other parameters in Equation (53) are known. A precise measurement of Figure 45, page 183, reveals that within the accuracy of the measurements (ΔH_{error} < 2.0 G) the distance from the low-field satellite resonance to the main resonance is equal to the spacing from the high-field satellite resonance to the main resonance. Since a down-field second-order shift was therefore not detected, this implies that δ_1 must be less than the accuracy of the measurements. Using δ_1 < 2.0 G, A_1 = 78 G, and H = average of the low and high-field magnetic positions (~ 3200 G), an upper limit to $A_{//}$ may be estimated as less than 250 G. That the second-order shift is negligible and thus $A_{//}$ is small may also be established by a close examination of the Q-band spectrum (Figure 46, page 184). Equation (53) would predict that if δ_1 were significant, then the spacing between the low-field satellite and the main features should be smaller in the Q-band experiment where the magnetic field, H, is ~ 12,500 G instead of the 3200 G used in X-band. In the Q-band experiment, however, this spacing is not observably smaller. Also in this experiment both the low and high field resonances were observed and yielded a hyperfine coupling of A_1 ($^{117,119}Sn$) = 78 G. Therefore, although the tin parallel hyperfine

coupling was not directly observed, a value of $A_{//} < 250$ G may be confidently assigned.

As noted in Table XVII, page 200, which summarizes the experimental results using the different matrices, the ESR spectra of $(CH_3)_4Sn^+$ may in general be characterized by three parameters, that is, a hyperfine coupling to 3 protons ($A_1(3H) \sim 13$ G), a significant g_1 shift ~ 2.044), and a tin isotope coupling ($A_1(^{117,119}Sn) \sim 80$ G). The significance of each of these three parameters and how they relate to the ligand structure of $(CH_3)_4Sn^+$ will be considered next.

Since the hexamethyldimetal (i.e., $Me_3MM'Me_3^+$, where MM' = SiSi,[169,170] SiGe,[187] SnSn,[190] and GeGe[170]) radical cations and the tetramethylsilane and tetramethylgermane radical cations[186] have all been interpreted as possessing freely rotating methyl groups, it seems very reasonable to assume that the methyl groups in $(CH_3)_4Sn^+$ are also freely rotating. By making this assumption, the only way that there can be hyperfine coupling to just three protons is by constraining the unpaired electron density to one unique methyl ligand.

That the trimethyltin moiety is planar or very near planar may be established by the following arguments. Assuming the maximum $A_{//}$ value of 250 G estimated earlier, the 5s and 5p spin densities may be estimated as $\rho(5s) = 0.0093$ and $\rho(5p) = 0.24$. If $A_{//}$ and A_1 are of opposite sign, then $\rho(5s) = 0.0171$ and $\rho(5p) = 0.172$. It should be noted that the apparent 5s spin density is primarily the result of spin polarization and does not reflect direct occupancy of

TABLE XVII

COMPARISON OF THE TETRAMETHYLTIN RADICAL CATION
IN SEVERAL DIFFERENT MATRICES

Matrix	g_1	Hyperfine Coupling Constants (G) A_1 (3H)	$A_1(^{117,119}Sn)$
$CFCl_3$	2.0447	13.7	78
CCl_3CF_3	2.0451	11.0	96
$CFCl_2CF_2Cl$	2.0496	13.5	89.4
CCl_4	2.0444	13.6	92
PFMCH	2.048	13.5	114
Freon Mixture ($CFCl_3$:CF_2BrCF_2Br)	2.0441	13.6	84
$CBrCl_3$	2.0427	13.6	~90

the unpaired electron in the 5s orbital. Two very instructive examples to demonstrate this point are the methyl[191] and t-butyl radicals[192] which are both undoubtedly planar or very near planar with the unpaired electron occupying a carbon $2p_z$ orbital, yet these radicals possess a net 2s spin density of $\rho(2s) = 0.031$ for the methyl radical and $\rho(2s) = 0.037$ for the t-butyl radical. The correlation between these radicals is further strengthened by the fact that while the planar methyl and t-butyl radicals possess $2p_z$ and 2s spin densities of 1.0 and about 0.034 (respectively), the Me_3Sn group posseses $5p_z$ and 5s spin densities of 0.24 and about 0.0093 where the decrease in the $5p_z$-spin density is proportionately matched by a decrease in the 5s-spin density. Assuming that the actual 5s spin density is vanishingly small, the ratio of $\rho(5p)/\rho(5s)$ which may be used to estimate bond angles[141] predicts that the trimethyltin group is planar. The anisotropic tin hyperfine parameters also establish that, at most, about 25% of the total spin density is on the tin nucleus and that the trimethyltin group may be approaching the limit of the diamagnetic trimethyltin cation which is known to be planar.[200] If, on the other hand, the trimethyltin portion of $CH_3\text{-}SnMe_3^+$ were to approximate the trimethyltin radical,[201] the tin isotope coupling should approach the known trimethyltin radical hyperfine parameters ($A_\perp(^{119}Sn) = 1350 \pm 20$ G and $A_{//}(^{119}Sn) = 1950 \pm 50$ G). Clearly such a comparison is inappropriate since the latter couplings are enormously larger than those detected in the present study. It should be noted that the significant $g_\perp$ shift

indicates that the unpaired electron is localized near to the tin atom and that the reason for the low tin coupling is not that the unpaired electron density is removed from the tin atoms.

Taken together, a simple interpretation of the hyperfine splitting patterns suggests that the organometal undergoes a significant change in configuration from T_d to C_{3v} symmetry following the loss of the outer-sphere electron to form a trigonal pyramidal structure as shown below.

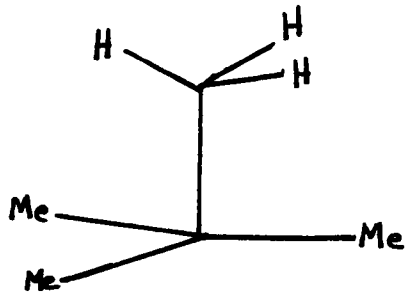

The molecular orbital may be approximated as simply being built up from a $2p_z$ orbital on the carbon of the unique methyl ligand and a Sn $5p_z$ orbital but most of the spin density is in the carbon $2p_z$ orbital.

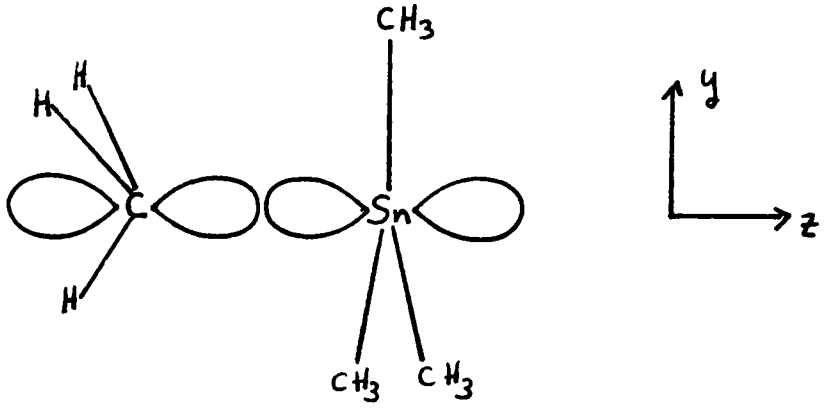

Consider the situation with the magnetic field perpendicular to the cylindrical z-axis. For example, when the field is parallel to the x axis (i.e., perpendicular to the plane of the paper) the $2p_z$ orbital is allowed to interact with those orbitals of the appropriate symmetry which are in the yz-plane, giving rise to orbital angular momentum. This interaction gives rise to $g_\perp$ shifts. The allowed types of interaction can be qualitatively seen by simply rotating the $2p_z$ orbital 90° and seeing which orbitals overlap most easily. For example, the modified $2p_z$ orbital can readily overlap with the filled d orbital on tin as shown below on the left, but would not be expected to overlap with say a $6p_z$ tin orbital, as shown below on right.

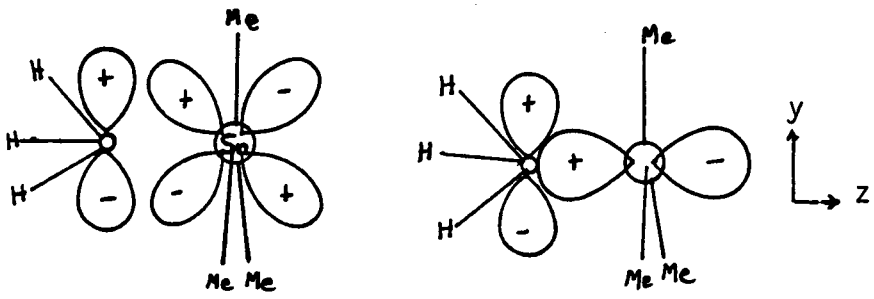

A magnetic-field induced 2p orbital interaction might be expected with the $5p_y$ orbital.

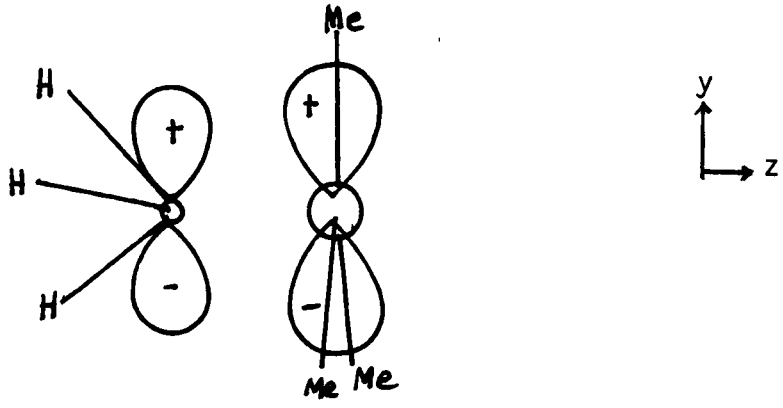

However, since the lobes of the tin $5p_y$ orbital are parallel to the y axis while two of the lobes of the tin $4d_{yz}$ orbital are directed along the C-Sn bond, the lobes of the $5p_y$ orbital would be presumed to be farther away from the unique carbon $2p_z$ orbital than the lobes of the $4d_{yz}$ orbital. Hence, the contribution to the $g_\perp$ shift of the $5p_y$ orbital would be expected to be smaller than from the filled $4d_{yz}$ orbital, since the amount of overlap for the $4d_{yz}$ orbital with the modified $2p_z$ orbital is much greater than the overlap with the $5p_y$ orbital. Because the $4d_{yz}$ orbital is filled, the $g_\perp$ shift would then be expected to be positive which, in fact, is supported by the experimental results with $\Delta g_\perp = +0.0424$.

When the field is along the z axis, the $2p_z$ orbital is unaffected by rotation about this axis, and no orbital angular momentum is generated. This case corresponds to $g_{//}$.

In summary, the ionized tetramethyltin radical cation is thought of as approximating a trigonal pyramidal structure where the unpaired electron spin density is primarily localized along the unique carbon-tin bond with most of the spin density being localized on the carbon in a $2p_z$ orbital.

Up to this point nothing has been stated concerning the structure of the unique ligand. A natural question arises concerning whether the unique methyl ligand retains its tetrahedral configuration about the carbon or does it distort to a planar structure. If the methyl ligand group retains its tetrahedral shape, then the proton hyperfine coupling of 13.7 G is straightforwardly explained in

terms of a positive spin density in the 1s hydrogen orbitals of the unique methyl group. If, on the other hand, the methyl group is planar thereby approximating a methyl radical, then the proton hyperfine coupling of 13.7 G may be explained simply as a reduced spin density on the carbon nucleus. In an attempt to resolve this ambiguity, two 90 atom % ^{13}C enriched tetramethyltin compounds were synthesized, namely $(^{13}CH_3)_4Sn$ and $(^{13}CD_3)_4Sn$. The experimental results of these compounds in Freon-11 and in PFMCH will be discussed next.

The observed ESR spectrum of a γ-irradiated 1 mole % solid solution of $(^{13}CH_3)_4Sn$ in Freon-11 at 83 K closely resembled the non-^{13}C enriched $^{12}(CH_3)_4Sn$ spectra also observed at 83 K. This comparison is shown in Figure 54, page 206. When a sample of $(^{13}CH_3)_4Sn$ in PFMCH was γ-irradiated, the observed hyperfine pattern (Figure 55, page 207) was again similar to the one obtained from a sample which was prepared using $(^{12}CH_3)_4Sn$ as the solute. Turning to the ESR results using $(^{13}CD_3)_4Sn$ as the solute and Freon-11 as the solvent, the ESR spectra of the γ-irradiated sample with the ^{13}C enriched organometal were in many respects identical to the non-^{13}C enriched organometal sample, as shown in Figure 56, page 208. Several other experiments were performed using these ^{13}C enriched organometals, but these results will be presented later.

The analysis of these spectra, at first sight, appears to be straightforward. By virtue of the fact that the observed perpendicular pattern is qualitatively unchanged between the ^{13}C and ^{12}C

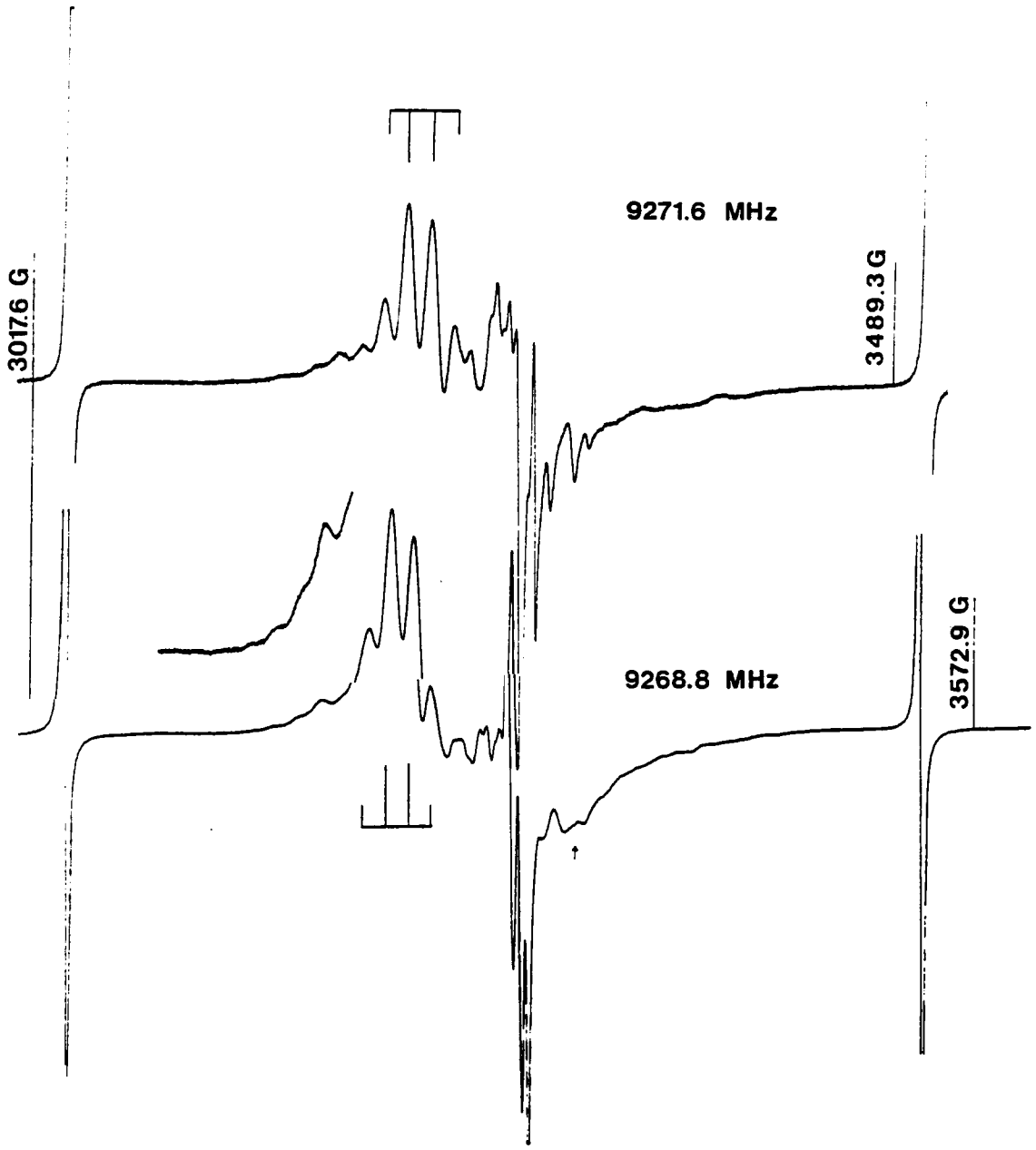

Figure 54. First-derivative ESR spectra comparing the difference between samples of $(CH_3)_4Sn$ (upper) and $(^{13}CH_3)_4Sn$) (lower) in $CFCl_3$ at 83 K.

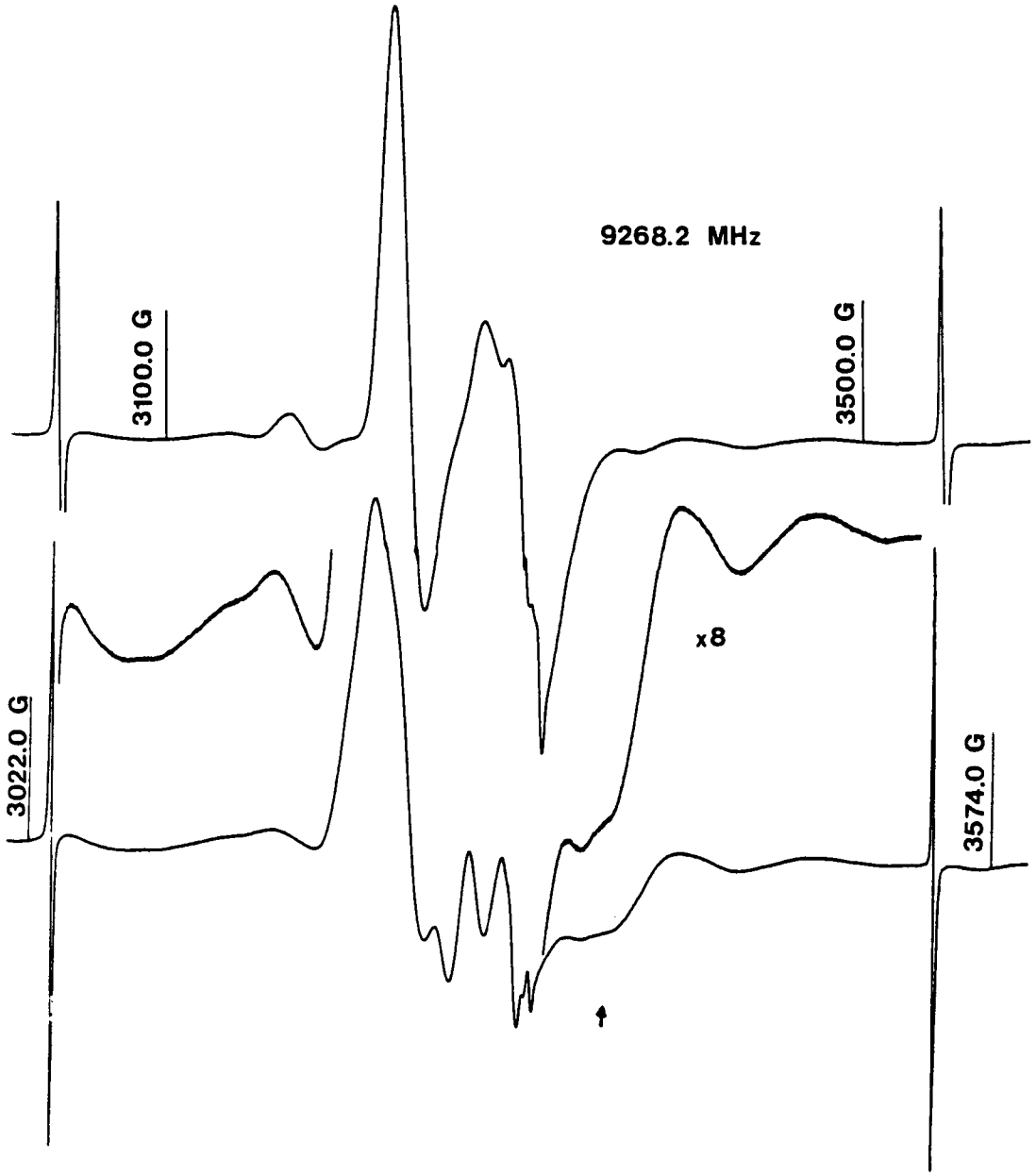

Figure 55. First-derivative ESR spectra comparing the difference between samples of $(CH_3)_4Sn$ (upper) and $(^{13}CH_3)_4Sn$ in PFMCH.

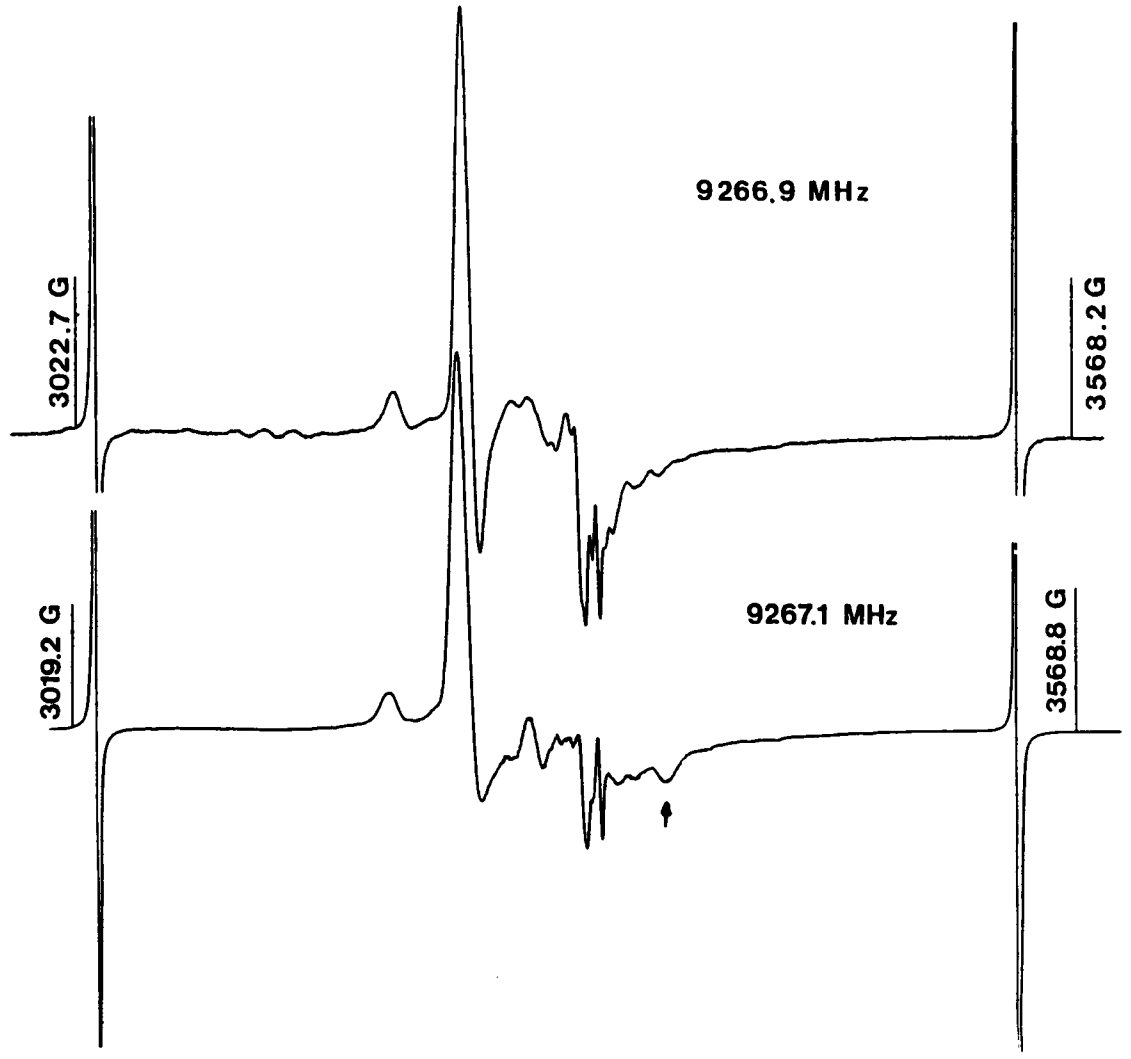

Figure 56. First-derivative ESR spectra comparing the difference between samples of $(CD_3)_4Sn$ (upper) and $(^{13}CD_3)_4Sn$ (lower) in $CFCl_3$.

samples, a reasonable assumption is that the ^{13}C perpendicular hyperfine coupling is merely too small to be resolved, that is, $A_{\perp}(^{13}C)$ < linewidth ~ 4 G. Using this assumption, the analysis of the ^{13}C spectra directly follows the analysis previously described for the ^{12}C spectra. Evidence supporting this assumption is that in each case the features assigned to the perpendicular resonance were slightly broadened as would be the case from a small unresolved coupling.

However, it should be noted that an alternative explanation may be given for the apparent similarities between the ^{13}C and ^{12}C spectra. If the unique methyl group is pyramidal, then the ^{13}C anisotropic hyperfine interaction in the methyl group might be expected to be similar to other tetrahedrally-shaped carbon radicals, such as $^{13}CF_3\cdot$ and $^{13}CF_3Br^-$ where $A_{\perp}$ ~ 300 G and $A_{//}$ ~ 400 G (the actual values are listed in Table V, page 72). This being the case, the spread in the anisotropy may smear the ^{13}C hyperfine interaction in the powder pattern to such an extent that the ^{13}C interaction would not be detected. A situation similar to the described case was noted for the isotopically enriched acetonitrile monomer radical anion $(CD_3{}^{13}CN^-)$[193] where the ^{13}C hyperfine interaction was unobserved in a randomly oriented sample but was observed from a highly oriented sample. If this explanation applies in the present case, then the observed resonances must originate solely from the less-abundant ^{12}C species. Since the carbon-13 enrichment is 90 atom %, the methyl group which forms the unique carbon-tin bond in the radical cation

will statistically have a 90% probability of being ^{13}C and a 10% probability of being ^{12}C, assuming that there is no preference for either isotope to form the unique carbon-tin bond. Thus, the anisotropic hyperfine pattern which is observed in the ^{13}C enriched sample may simply arise from the 10% of the ^{12}C in the sample, thereby explaining the similarities between the two samples.

If the above argument that the ^{13}C hyperfine interaction is anisotropically broadened is valid, then the following predictions can be made. First, since the observed pattern from the ^{13}C enriched sample would actually be arising from the 10% ^{12}C in the sample, the observed pattern should be a factor of about 9 times weaker than the corresponding pure ^{12}C sample. Secondly, since it is the $^{12}CH_3$ group in each case that would be giving rise to the observed pattern, the hyperfine couplings and the $g_\perp$ value should be identical[90] for the two spectra.

Turning now to the observed experimental results, although the spectra from the ^{13}C enriched sample are slightly weaker in each of the three cases, they do not appear to be a factor of 9 times weaker (compare the upper and lower scans in Figures 54, 55, and 56, pages 206, 207, and 208). The hyperfine and $g_\perp$ values for these radical cations were measured from several spectra and are collected in Table XVIII, page 211. Note in particular the differences observed in the $g_\perp$ values. These comparisons of intensities and $g_\perp$ values seem to argue against the idea that the ^{13}C hyperfine interaction is anisotropically broadened and is therefore not observed.

TABLE XVIII

HYPERFINE COUPLING CONSTANTS FOR THE TETRAMETHYLTIN RADICAL CATION

Radical	Hyperfine Coupling Constants (G)	
	A_1 (3H)	A_1 (^{117,119}Sn)
$(CH_3)_4Sn$	2.0447	78
$(CD_3)_4Sn$	2.0452	78.3
$^{13}(CH_3)_4Sn$	2.0474	79
$(^{13}CD_3)_4Sn$	2.0484	78

Whereas the qualitative similarities between the ^{13}C enriched samples and the non-enriched samples have been stressed up to this point, a careful examination of the two hyperfine patterns reveals that additional features are present in the ^{13}C enriched samples. These additional features are most clearly defined by an examination of the spectra from $(^{13}CD_3)_4Sn^+$ and $(^{12}CD_3)_4Sn^+$. In this case, an additional feature is located on the high-field side of free spin and is marked with an arrow ($\uparrow$) in Figure 56, page 208, and is likewise marked in the spectra from the $(^{13}CH_3)_4Sn$ samples (Figures 54, page 206, and 55, page 207). Evidence which suggests that this additional feature arises from the same radical that is giving rise to above-mentioned perpendicular features was obtained by a power saturation study and by thermal annealing.

For an annealing experiment with $(^{13}CD_3)_4Sn$ in Freon-11, the initial spectrum before warming was taken (Figure 57, page 213) and readily conformed to the analysis given earlier. Note the presence of the additional peak which is marked with an arrow ($\uparrow$) on the high-field side of free spin. Warming the sample from 80 K to 145 K resulted in only minor changes in the spectra. As expected, warming above 145 K to 155 K resulted in the appearance of several resonances which were assigned to the matrix radical ($CFCl_2\cdot$). Warming to 161 K was followed by a further intensification of the matrix radical signals accompanied by a slight amount of decay of the features assigned to $(^{13}CD_3)_4Sn^+$ (upper portion of Figure 58, page 214). While maintaining the sample temperature at 165 K for about 20 minutes,

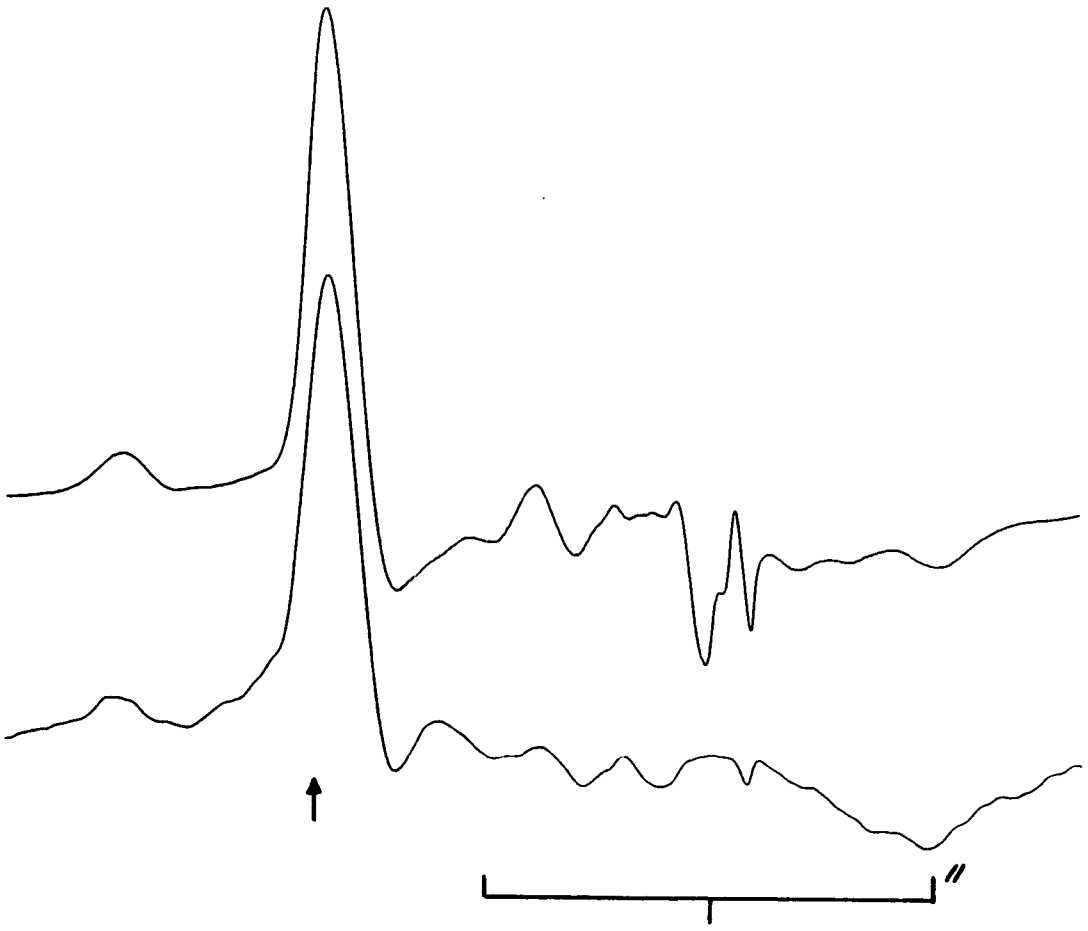

Figure 57. First-derivative ESR spectra of a γ-irradiated 0.5 mole % sample of $(^{13}CD_3)_4Sn$ in Freon-11 at 85 K. The origin of the lower spectrum is described in the text.

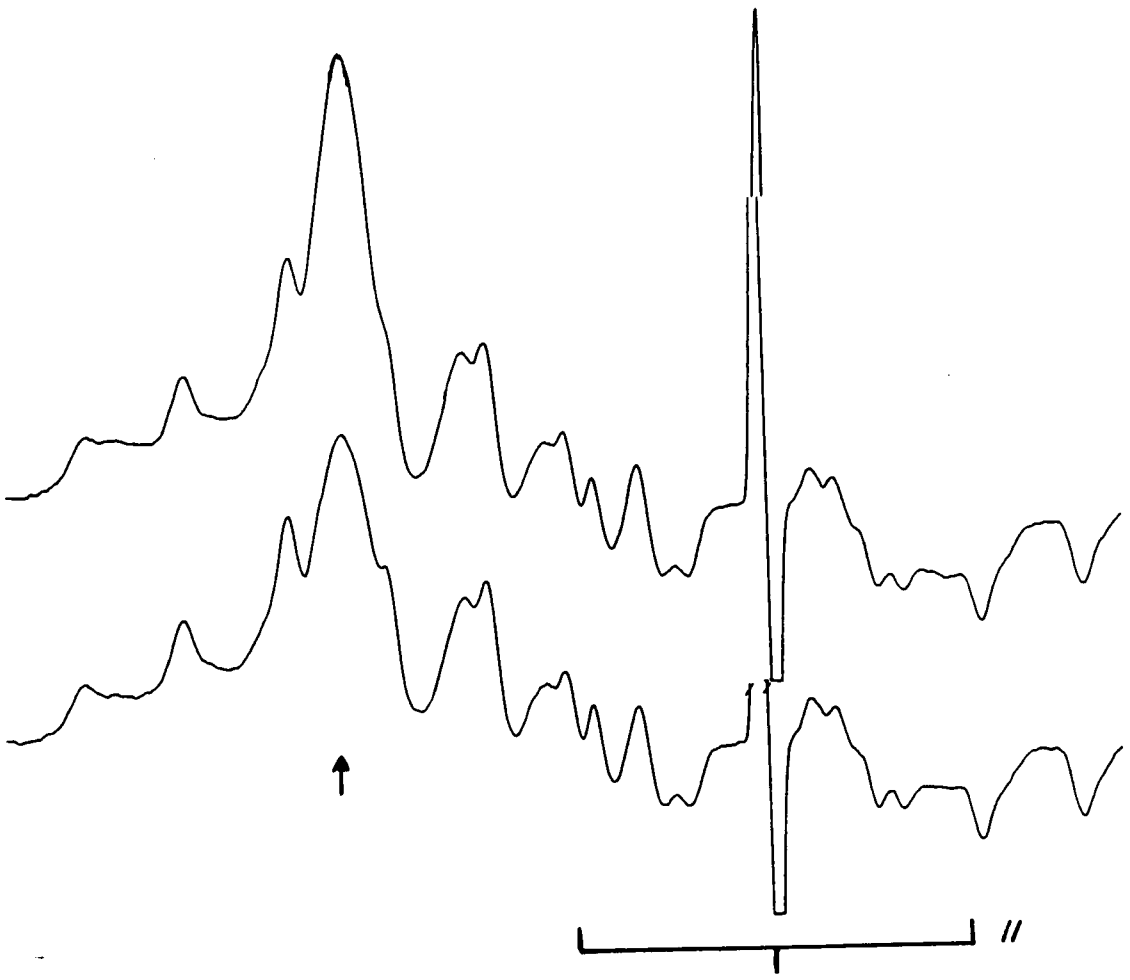

Figure 58. First-derivative ESR spectra of a γ-irradiated 0.5 mole % sample of $(^{13}CD_3)_4Sn$ in Freon-11 at 165 K. The lower trace was taken after annealing at 165 K for 20 minutes.

the features assigned to $(^{13}CD_3)_4Sn^+$ continued to slowly decay, but the matrix radical signals appeared to remain constant (lower portion of Figure 58, page 214). The lower portion of Figure 57 shows the result of a computer subtraction of the upper and lower portions of Figure 58. As is shown from a comparison of the subtracted spectrum (lower portion of Figure 57) to the initial spectrum (upper portion of Figure 57), the feature marked with an arrow (↑) decayed at the same rate as the features already assigned to $(^{13}CD_3)_4Sn^+$. It should be noted that the feature marked with an arrow (↑) showed similar power saturation properties as the lower-field perpendicular resonances.

Taken together, the results seem to indicate that the peak marked with an arrow (↑) arises from the same radical that gives rise to the well-defined perpendicular features. However, since the peak is positioned somewhat close to free spin, one must consider that this peak may simply arise from an impurity or from a dissociation product with a large ^{13}C hyperfine coupling. In this case, the simultaneous decay of the additional peak with the perpendicular peak would be considered coincidental. However, an argument that the peak arises from dissociation products is not very probable considering that neither of the two reasonable dissociation products, $^{13}\cdot CH_2SnMe_3$ and $\cdot SnMe_3$, would give rise to such a peak.

Attention will now be focused on a possible interpretation of the hyperfine interaction giving rise to this additional peak. Since there is a danger of ascribing too much significance to a

single peak, the interpretation offered in the following section must be considered somewhat speculative.

This additional peak could be considered to be the high-field component of a doublet of the parallel component. Since the parallel component of a non-^{13}C labeled compound has not been resolved in the Freon-11 matrix or in any other matrix, fixing the ^{13}C parallel hyperfine coupling constant cannot be done without assuming $g_{//} \sim 2.0023$. This analysis corresponds to $A_{//}(^{13}C) \sim 70$ G and is shown by the stick diagram in the lower portion of Figure 57, page 213.

Coming back to the earlier question of the two possible structures, planar or somewhat pyramidal, of the unique methyl group in Me_4Sn^+. These two cases will be considered and evaluated in light of the tentative analysis.

Various types of methyl radicals are known to be stabilized on solid surfaces.[81,194-196] In some cases, the methyl radical proton hyperfine coupling constant remains at about 23 G while in other cases the coupling falls somewhat below this normal value--hence their names, normal (n-CH_3) and abnormal (a-CH_3) methyl radicals, respectively. Table XIX, page 217, summarizes the experimental results for normal and abnormal methyl radicals. Although the ^{13}C hyperfine couplings of the methyl radical adducts appear to correspond to the tentative analysis in the present case, the proton hyperfine coupling constant of only 13.7 G is significantly different from those reported in Table XIX.

TABLE XIX

HYPERFINE COUPLING CONSTANTS AND SPIN DENSITIES FOR VARIOUS METHYL RADICALS[a]

Environment	Nucleus	$A_{//}$ (G)	$A_{\perp}$ (G)	ρ_s	ρ_p
n-$^{13}CH_3$ on PVG	^{13}C	~83	16	0.034	0.71
	^{1}H	~23	23		
a-$^{13}CH_3$ on PVG	^{13}C	77	8	0.028	0.72
	^{1}H	18	20		
Iodine Ion Adduct in CD_3CN	^{13}C	87 ± 2	9	0.031	0.82
	^{1}H	20	20		
$^{13}CH_3$ in Sodium Acetate	^{13}C	82.7	15.25	0.034	0.71
Methyl Group in Me_4Sn^+	^{13}C	~70	<4	0.022	0.59

[a]Taken from Reference 195.

The other possibility is that the unique methyl ligand adopts a somewhat pyramidal structure. In order to get a general idea of the appropriate spin distribution for a radical of this type a CNDO/2 calculation[78] was desired, but the CNDO/2 program was not parameterized for atoms with atomic numbers greater than 17 (chlorine). Thus, a calculation was performed on Me_4Si^+, where the radical was constrained to a C_{3v} trigonal planar geometry. The program gave a spin density distribution which reproduced with remarkable accuracy all of the values derived from the observed hyperfine coupling constants for Me_4Sn^+. A similar calculation using a planar unique methyl group were vastly different from the experimental results. These different cases are compared in Table XX, page 219.

In summary, these studies have established that the tetramethyltin radical cation adopts a C_{3v} structure. While the ESR results allowed only a tentative conclusion concerning the pyramidal structure of the unique methyl ligand, there is little doubt regarding the near planar geometry about the trimethyltin moiety.

D. Alkyltrimethyltin Radical Cations

In the previous study on the tetramethyltin radical cations, it was concluded that the unpaired spin density was likely to lie preferentially between one of the four methyl ligands and the tin nucleus while the remaining three methyl groups became coplanar with the tin nucleus. In the present study, a series of alkyltrimethyltin radical cations (RMe_3Sn^+) were examined. It was thought that these

TABLE XX

COMPARISON OF CALCULATED AND EXPERIMENTAL SPIN DENSITIES

	ρ_s[a]			ρ_p[a]	
	Metal	Unique Carbon	Hydrogen	Metal	Unique Carbon
Experimental	0.0093	0.022	.028 (3H) <.006 (9H)	0.24	0.59
Calculated with:					
Planar Methyl Group	0.0302	0.0009	.009 (3H) .013 (9H)[b]	0.532	0.288
Pyramidal Methyl Group	0.0081	0.028	.032 (3H) ~.0002 (9H)[b]	0.181	0.670

[a]Assuming A and B are of the same sign.

[b]Average values.

radical cation species might provide further insight into the structure of the unique ligand found in the previous study.

In addition to better defining the ligand structure of organometal radical cations, it was hoped that this study might provide some insights into the known chemical properties[197] of these more complex organometals.

In the first section below, the ESR results for the t-butyltrimethyltin radical cation ($t\text{-}BuMe_3Sn^+$) are presented along with a discussion concerning a simple model which has proved helpful for interpreting the ESR results of $t\text{-}BuMe_3Sn^+$. In the following sections, the ESR results of several other alkyltrimethyltin radical cations are presented and in each case discussed in light of the proposed model for the $t\text{-}BuMe_3Sn^+$. In the final section, all of the results will be reviewed.

Although the ESR spectrum was not analyzed correctly at first,[198] the best characterized radical cation in this section is probably the $t\text{-}BuMe_3Sn^+$. The correct analysis of the X-band spectrum of $t\text{-}BuMe_3Sn^+$ was made possible by the analysis of its Q-band spectra. The Q-band ESR spectrum of a γ-irradiated 1 mole % solid solution of $t\text{-}BuMe_3Sn$ and Freon-11 in a quartz tube (2 mm O.D. and about a 1.6 mm I.D.) is shown in Figure 59, page 221. The intense features in Figure 59 are assigned to a perpendicular quartet pattern ($A_\perp(3H)$ = 44 G and $g_\perp$ = 2.031). Using a higher gain, a weak resonance at low-field was detected and assigned to a tin satellite ($A_\perp(^{117,119}Sn)$ = 89 G). Although not shown, an identical Q-band spectrum to Figure 59 was

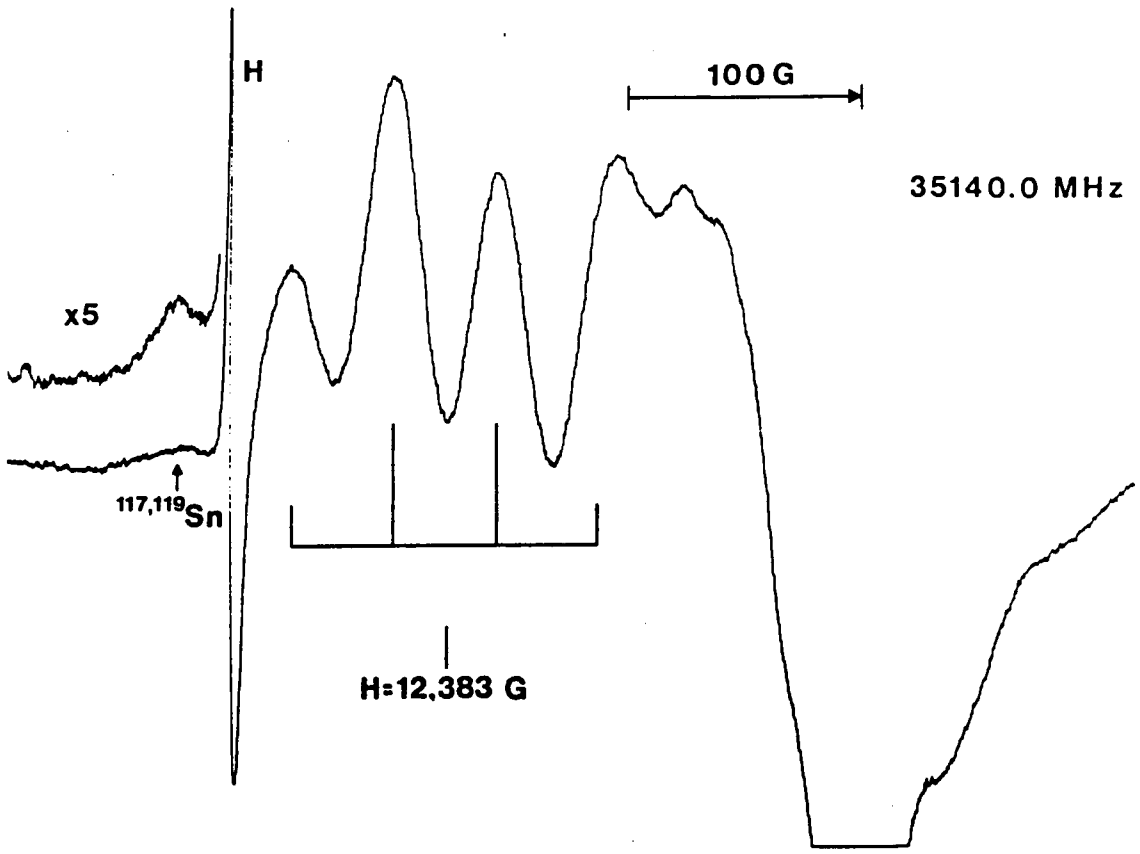

Figure 59. First-derivative Q-band ESR spectrum of a γ-irradiated 1 mole % sample of t-$BuMe_3Sn$ in $CFCl_3$ at ~77 K.

obtained when a CCl_3CF_3 matrix was utilized. Since the Q-band spectrometer used in this study was located in another laboratory, X-band ESR spectra were taken the day before and the day after the Q-band observations. This was done in order to detect any decay of the parent cation due to the manipulations necessary to obtain the Q-band spectra. In all cases, the X-band ESR spectra were virtually identical before and after the Q-band experiment, but unexpectedly the X-band spectra showed more fine detail than the Q-band spectra. Indeed, additional substructure which should have been within the resolution capabilities of the Q-band spectrometer was observed in the same sample, with Freon-11 as the matrix, using the X-band spectrometer. Although the additional substructure could be observed using the small quartz sample tube (2 mm O.D., 1.6 mm I.D.) used for the Q-band experiment, a better signal-to-noise ratio could be obtained from a sample prepared in a standard X-band ESR quartz tube (4 mm O.D./3 mm I.D.) using a similar concentration of the organometal as was previously described.

As shown by the stick diagram in the upper portion of Figure 60, page 223, the pattern may be analyzed as a quartet of septets ($A_1(3H)$ = 44 G, $A_1(6H)$ = 7.6 G, g_1 = 2.031). Just as in the Q-band spectra, a weaker feature was observed on the low-field side of the main quartet pattern. This weaker feature displayed a substructure similar to the more intense resonances, and was assigned to a satellite resulting from additional hyperfine coupling to the magnetic isotopes of tin ($A_1(^{117,119}Sn)$ = 89 G). It should be noted

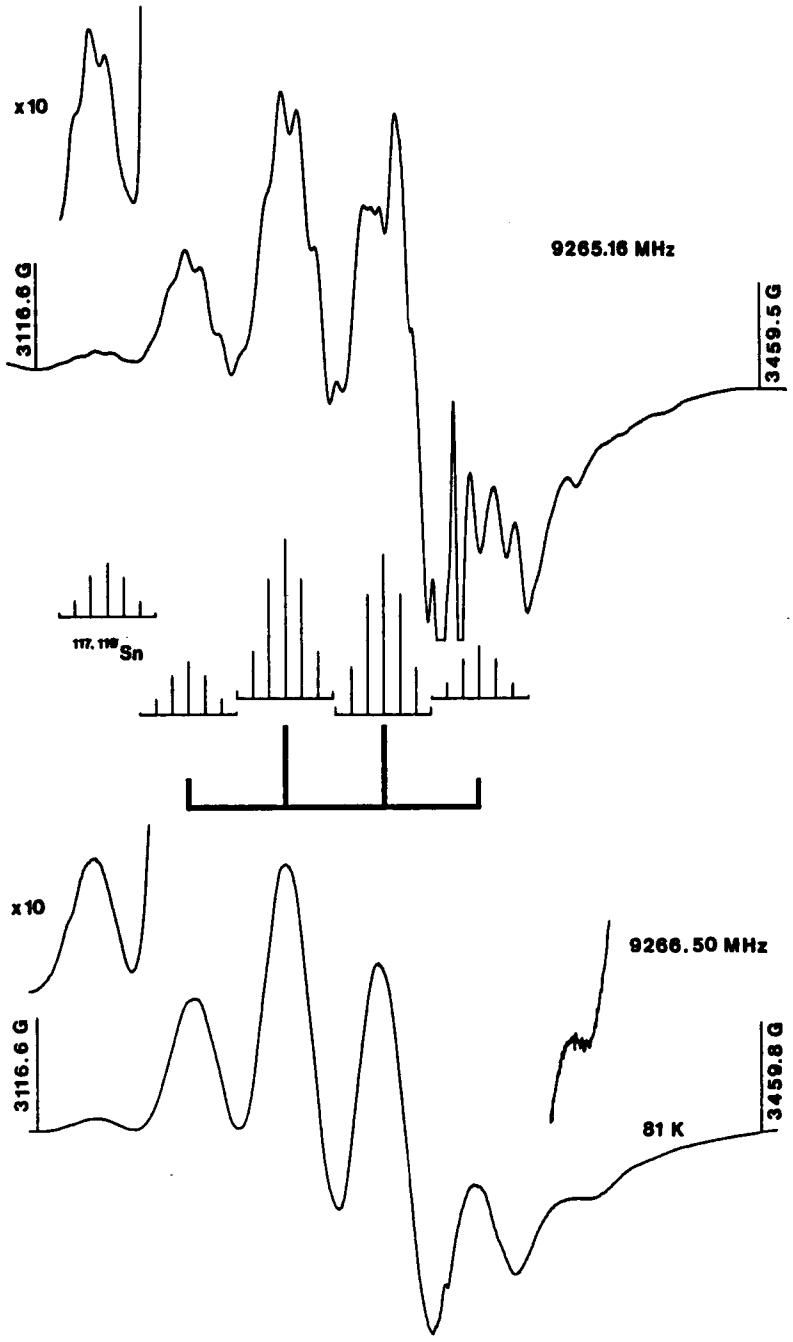

Figure 60. First-derivative ESR spectra of γ-irradiated 1 mole % samples of t-$BuMe_3Sn$ in $CFCl_3$ (upper) and in $CFCl_2CF_2Cl$ (bottom) at high spectrometer power levels (0 dB = 200 mW).

that although only two components of the large quartet pattern are clearly observed in the X-band experiment, in contrast to the three components observed in the Q-band experiment, this difference may be anticipated since the spectral patterns of differing g values are spread apart a factor of about 3.5 times greater at Q-band than at X-band. The net effect in the Q-band experiment is to shift the quartet pattern to the low-field side of resonances which have g values near free spin (2.0023).

Further evidence establishing that the main quartet pattern arises from hyperfine interaction with three equivalent protons and not from g anisotropy was obtained from the ESR observation of a γ-irradiated 1 mole % solid solution of t-butyltrimethyltin in $CFCl_2CF_2Cl$. At high incident microwave power (0 dB = 200 mW), the t-$BuMe_3Sn^+$ is significantly enhanced relative to the background matrix radical, thus allowing the quartet pattern (A_1(3H) = 44G, g_1 = 2.031) and the low- and high-field tin satellite resonances ($A_1(^{117,119}Sn)$ = 89 G) to be unobscured, as shown in the lower portion of Figure 60, page 223. Although not nearly as well resolved as in Freon-11, a substructure with a spacing of about 7.6 G was also noted in this matrix.

The interpretation of the observed low-temperature ESR spectra of t-$BuMe_3Sn^+$ is greatly assisted by recalling the tetramethyltin radical cation results. First the small perpendicular tin isotope coupling of 89 G suggests that the trialkyltin moiety is planar. Also, although the g_1 shift is not as large as was found for

$(CH_3)_4Sn^+$, the $g_\perp$ shift is certainly significant, indicating that the unpaired electron is again localized in a tin-carbon bond to one of the alkyl groups. Since there are two types of ligands in t-$BuMe_3Sn^+$, namely t-butyl and methyl, the identity of this particular alkyl group must be established.

Assuming that the other three ligands form a planar configuration at tin and do not give rise to a resolvable hyperfine coupling, then there are two possible cases. In the first case, one of the three methyl ligands could become the stereochemically unique ligand leaving the bonds to the t-butyl and the other two methyl groups to lie in the plane with the tin nucleus. In this case, however, the ESR spectrum should closely resemble the results found for the tetramethyltin radical cations. This first possibility can be immediately rejected since the ESR spectra of $(CH_3)_4Sn^+$ and t-$BuMe_3Sn^+$ are vastly different. For example, the quartet splitting in $(CH_3)_4Sn^+$ is 13.7 G with no substructure, whereas the quartet splitting in t-$BuMe_3Sn^+$ is 44 G with a substructure coupling of 7.6 G. In the other case, the t-butyl group could become the stereochemically unique ligand leaving the bonds to the three methyl groups to lie in a plane with the tin nucleus. In this case the ESR spectra could be expected to reflect hyperfine coupling to more than just three protons. Indeed, the observed ESR pattern clearly shows a significant hyperfine interaction with three protons and a minor coupling with possibly another six protons, thereby accounting for a total of nine protons. Therefore,

the evidence suggests that the t-butyl group becomes the stereochemically unique ligand.

Assuming the above analysis is correct, the positive hole in the radical cation can be thought of as being accommodated between the central carbon of the t-butyl group and the tin nucleus, as shown below:

$$Me_3C- \; -^{+\cdot}- \; -SnMe_3$$

Given the fact that the positive hole in the radical cations of hexamethylethane[167,168] and hexamethyldistannane[190] are known to be localized principally between the two central atoms,

$$Me_3C- \; -^{+\cdot}- \; -CMe_3 \qquad\qquad Me_3Sn- \; ^{+\cdot}- \; -SnMe_3$$

the singly occupied molecular orbital of the t-$BuMe_3Sn^+$ should reflect the orbital of the hexamethylethane (HME) radical cation on the t-butyl side while it should be similar to the hexamethyldistannane ($Me_6Sn_2^+$) radical cation on the trimethyltin side.

The septet ESR pattern ($A_{iso}(6H)$ = 29 ± 0.2 G) for the HME radical cation is interpreted as arising from one strongly coupled proton from each methyl group. Assuming the preferred conformation where the C-CH_3 bonds are all staggered (shown below), the relatively large coupling to the axial protons may be rationalized by invoking the W-plan where each of the six strongly coupled protons fit into a 1-1/2 V arrangement.

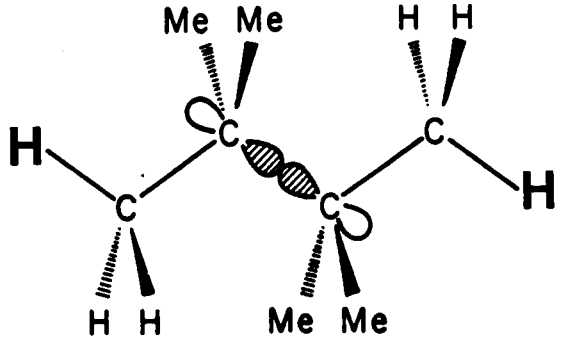

The qualitative predictions of the W-plan were supported by an INDO calculation[169] which for the staggered geometry estimated a large hyperfine interaction to the 6 axial hydrogens. In this same report on the HME radical cation, partially resolved substructure was observed on the septet pattern and was interpreted as arising from hyperfine interaction with the other 12 hydrogens (A (12H) = 4.2 G). This assignment was also supported by the INDO calculations.[169] Incidentally, since these initial reports, the assumption of a locked conformation and the applicability of the W-plan has proved to be useful for explaining the ESR results for a number of saturated, branched and unbranched, hydrocarbon radical cations. Therefore, in the present case, the t-butyl group is by analogy assumed to adopt a locked conformation in which the large quartet hyperfine splitting of 44 G arises from the three axial protons while the smaller 7.6 G coupling arises from the other six hydrogens. Interestingly, the ratio of the hyperfine coupling constants increases from the HME radical cation to the t-$BuMe_3Sn^+$ for both the β-axial protons (44/29 = 1.5) and the β-equatorial protons (7.6/4.2 = 1.8).

Turning now to the hexamethyldistannane radical cation ($Me_6Sn_2^+$), the ESR results reveal an intense perpendicular feature centered at $g_\perp$ = 2.110 with a slight substructure corresponding to a coupling of about 3.4 G and a perpendicular tin isotope coupling of about 100 G.[190] For this radical cation the small perpendicular tin isotope hyperfine coupling was used to establish that each trimethyltin moiety was very near planar and that the positive hole may be thought of as being equally shared by both tin nuclei. The substructure which consisted of at least 11 equally spaced resonances was used to establish that the methyl groups are freely rotating. Therefore, in the present case, the trimethyl tin portion of t-$BuMe_3Sn^+$ would be expected to be planar and contribute to a significant $g_\perp$ shift, as was suggested earlier. Although a hydrogen hyperfine coupling of 3.4 G was detected for the protons in $Me_6Sn_2^+$, the non-observation of these protons in the Me_3Sn moiety of t-$BuMe_3Sn^+$ may merely reflect a slightly lower spin density on the tin nucleus than is found in $Me_6Sn_2^+$. For example, if the perpendicular tin isotope couplings are used as a crude estimate of the spin density on the tin nucleus, then the spin density drops from nominally 50% in $Me_6Sn_2^+$ ($A_\perp$ = 100 G) to about 44% in t-$BuMe_3Sn^+$ ($A_\perp$ = 89 G) and the proton couplings would also be expected to drop from 3.4 G to about 3.0 G where this latter value is just at the typical resolution capabilities of solid-phase ESR.

Taken together, these considerations point to a reasonable structure of t-$BuMe_3Sn^+$, as shown below.

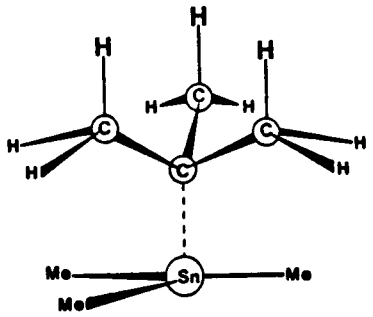

Additional support for the above mentioned structure was obtained by studying the spectral changes as a function of temperature.

The study of the reversible thermal changes was particularly informative in the Freon-11 matrix, since in this matrix the window of observation typically extends to about 155-160 K. Three significant spectral changes were noted when a γ-irradiated sample of t-$BuMe_3Sn$ in Freon-11 was warmed from 85 to 120 K. First, the septet substructure appeared to smear to such an extent that the substructure was no longer resolved. Secondly, although the large quartet splitting was still resolved at 120 K, the troughs between the peaks became much less significant. Finally, the overall signal amplitude was significantly reduced by this thermal change. All three thermal changes were 100% reversible when the sample was re-cooled to 85 K. Warming to 145 K further extended the trends previously discussed to such an extent that the entire region of the perpendicular feature was marked by a broad undefined hump where the highest point roughly corresponded to $g_1 = 2.031$. Once again it should be noted that this thermal change was 100% reversible. Further warming to 156 K resulted

in the appearance of at least five unobscured evenly spaced resonances with a spacing of about 19.1 G. Additional resonances belonging to a 10-line pattern may have been present except that the region where they would be expected to appear was obscured by the matrix type radicals. Re-cooling the sample from 156 K to 85 K resulted in the regeneration of the initial quartet of septets pattern, although a slight amount of decay was noted. Warming above 156 K resulted in the quick irreversible decay of t-$BuMe_3Sn^+$. These thermal changes are shown in Figure 61, page 231.

As previously mentioned, the t-$BuMe_3Sn^+$ can also be formed using CF_3CCl_3 as a matrix but in this matrix the septet substructure is unresolved. Although the window of radical cation observation is smaller in this matrix than in Freon-11, the effect of temperature on t-$BuMe_3Sn^+$ was also examined in this matrix. These thermal changes are shown in Figure 62, page 232, and they essentially parallel the thermal changes noted in Freon-11.

By virtue of the fact that the above described thermal changes are essentially reversible, these changes probably reflect some kind of motional change and not a chemical change since the latter effect is generally not thermally reversible. Since the methyl groups of the t-butyl moiety are interpreted as being locked at 85 K, a simple interpretation of the thermal changes to be considered would be that all nine hydrogens in the t-butyl group at higher temperature (155 K) become equivalent through the rapid rotation of the methyl groups in the t-butyl moiety. The observed data are supportive of this

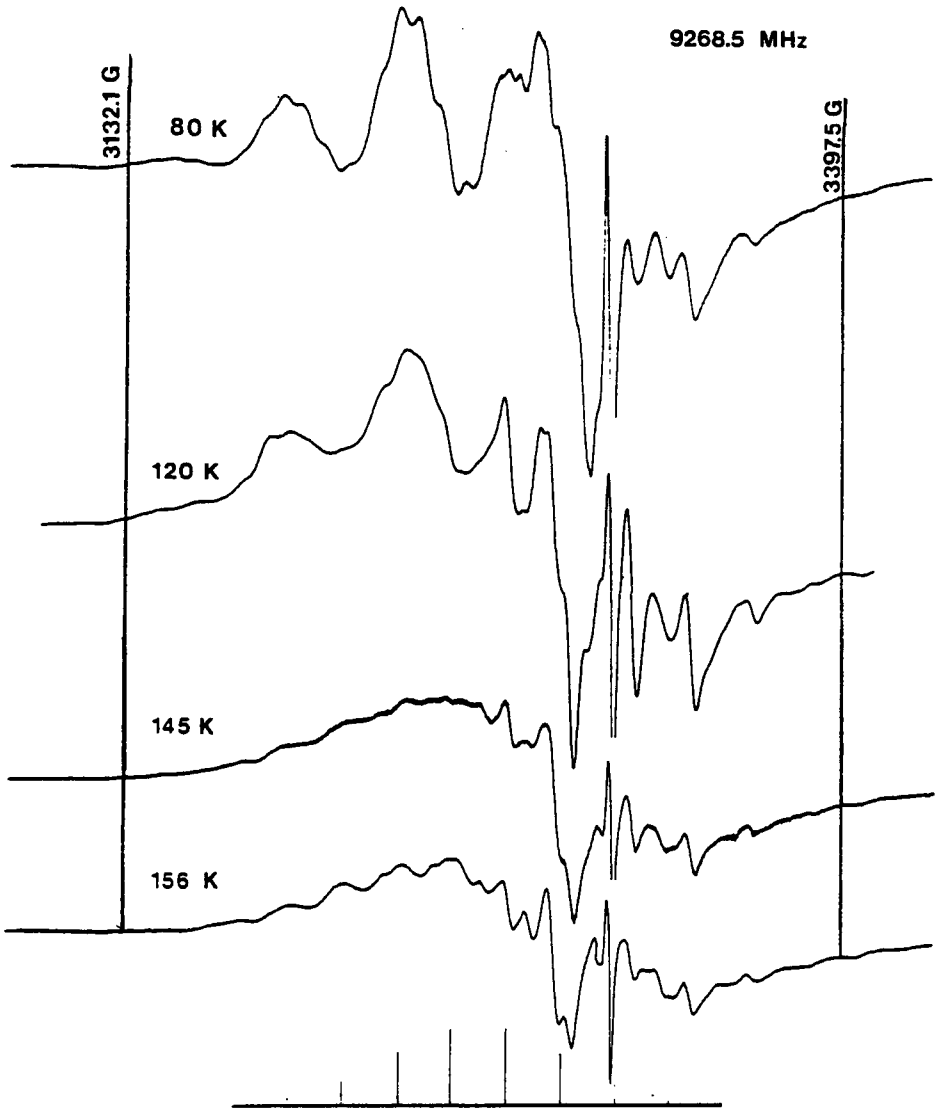

Figure 61. First-derivative ESR spectra of a γ-irradiated sample of t-$BuMe_3Sn$ in $CFCl_3$ between the temperature range of 80 to 156 K.

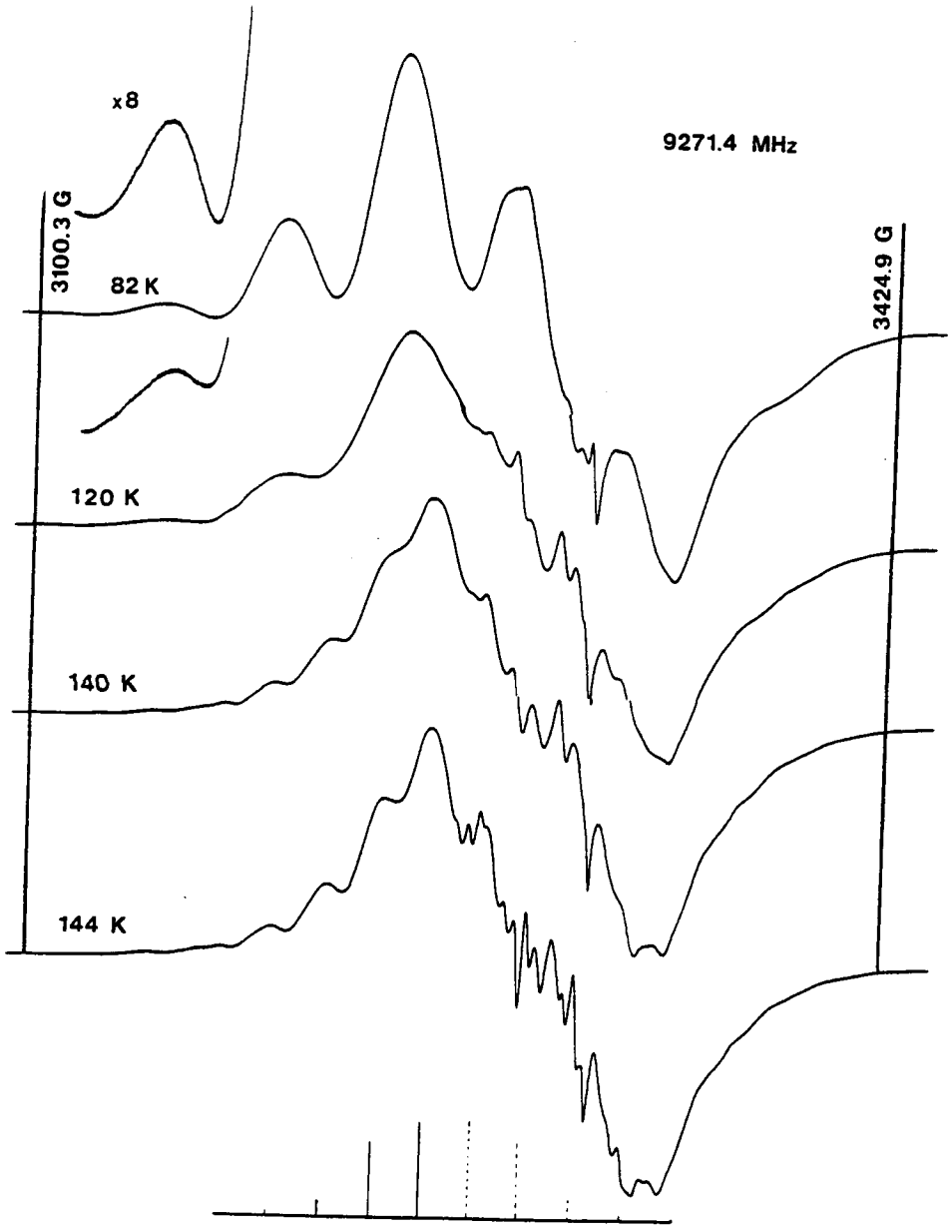

Figure 62. First-derivative ESR spectra of a 1 mole % solid solution of t-$BuMe_3Sn$ at temperatures ranging from 82 to 144 K. The matrix softens at 145 K.

simple interpretation in three ways. First, if the 155 K spectrum, in fact, reflects the limit of fast rotation, then the hyperfine coupling constants should equal the average coupling of the locked conformation. Indeed, the 19.4 G coupling of the 155 K spectrum is almost exactly the average of the locked conformation hyperfine coupling (1/3 (44 + 7.6 + 7.6) of 19.7 G. In connection with this point, in the temperature range between the two limits, that is, between the locked low temperature limit and the freely rotating high temperature limit, the ESR spectrum would be expected to be smeared in the central region of the pattern but the outermost M_I components ($M_I = \pm 9/2$) should be unaffected. These predictions are certainly consistent with the observed data as shown first by the broad unresolved hump in the center two spectra of Figures 61 and 62, pages 231 and 232, and also by the small peak which consistently appears on the low-field side of the broad hump. If the only thermal change is the onset of methyl group rotation, then the g_1 value should be relatively unchanged which once again is supported by the experimental evidence. Taken together, although only five of the expected ten resonances were observed, the others being obscured by the matrix radical, the high temperature ESR spectrum may be confidentally assigned as a decet pattern (A_1(9H) = 19.4 G).

An interesting difference to the above-described reversible thermal changes observed in the Freon-11 and CCl_3CF_3 matrices was observed when the t-$BuMe_3Sn^+$ was generated and annealed in the $CFCl_2CF_2Cl$ matrix. As shown in Figure 63, page 234, the low

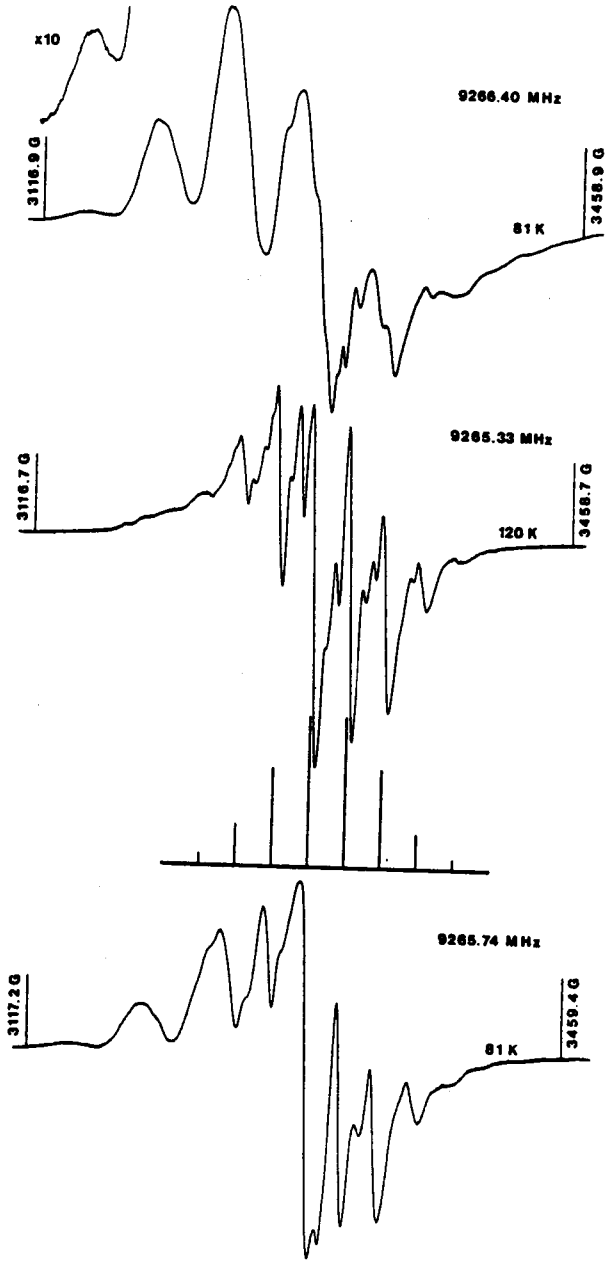

Figure 63. First-derivative ESR spectrum of a γ-irradiated 1 mole % solid solution of t-$BuMe_3Sn$ in $CFCl_2CF_2Cl$.

temperature (81 K) ESR spectrum of a γ-irradiated 1 mole % sample of t-$BuMe_3Sn$ in $CFCl_2CF_2Cl$ at 81 K clearly shows evidence for the t-$BuMe_3Sn^+$. Approximating the thermal changes noted in the Freon-11 matrix, warming the sample to 105 K resulted in a reversible broadening of the quartet of septets into a barely resolvable quartet pattern. However, by warming to 110 K the broadened pattern was replaced by a clearly defined isotropic looking decet pattern (A_{iso}(9H) = 22.7 G and g_{iso} = 2.0024). These resonances were assigned to the t-butyl neutral radical (A_{iso}(9H) = 22.72 G and g_{iso} = 2.0023).[20] The ESR spectrum of the t-butyl neutral radical was further sharpened by warming to 120 K (as shown by the middle scan in Figure 63, page 234), but at this temperature there was a significant amount of decay of the radical. Comparison of the re-cooled 81 K spectrum (lower scan in Figure 63) with the initial 81 K spectrum (upper scan in Figure 63) clearly shows that the significant t-$BuMe_3Sn^+$ decay has been matched by a significant t-butyl neutral radical generation.

For completeness, it should be mentioned that several attempts to photobleach the t-$BuMe_3Sn^+$ with either UV or visible light resulted in relatively imperceptible changes in the ESR spectrum.

In summary, the following conclusions can be reached from the analysis of the ESR spectra of the t-$BuMe_3Sn^+$. First, the positive hole is localized between the tin and the central carbon of the t-butyl ligand. Secondly, the trimethyltin moiety becomes planar or near planar upon ionization. Thirdly, the unique t-butyl ligand at low temperature adopts a locked conformation which allows the β-axial

hydrogens to give rise to a smaller hyperfine coupling. Fourthly, at higher temperature (above 140 K) the methyl groups become unlocked and all the β-hydrogens appear to become equivalent. Finally, the dissociation of the parent radical cation to the t-butyl neutral radical was observed in the $CFCl_2CF_2Cl$ matrix.

The utility and the general applicability of this model to other alkyltrimethyltin derivatives will be checked and discussed in the following sections.

The first radical cation that will be examined in terms of this analysis will be the iso-propyltrimethyltin radical cation (i-$PrMe_3Sn^+$).

If the proposed model for the t-$BuMe_3Sn^+$ is applicable in this case, then the semi-occupied molecular orbital would be expected to be localized between the central carbon of the isopropyl group and the tin nucleus. In this case the latter would be expected to be co-planar with the bonds of the three methyl ligands and should give rise to a significant $g_\perp$ shift and a tin-isotope coupling of about 90 G. A large hyperfine interaction would be expected from the two conformationally locked β-axial protons in the isopropyl group. Also by analogy, the two locked isopropyl methyl groups of i-$PrMe_3Sn^+$ would be expected to become unlocked at higher temperature with the net result being that the triplet pattern would change to a septet pattern where the septet coupling should be roughly equal to one-third of the triplet hyperfine coupling. Since the isopropyl group contains one α-hydrogen and the t-$BuMe_3Sn^+$ does not contain any, an

appropriate prediction may be made by analogy with the $(CH_3)_4Sn^+$ which has three α-hydrogens. Hence, by analogy with $(CH_3)_4Sn^+$, the α-hydrogen hyperfine coupling would be expected to be on the order of 13 G where for this hydrogen the coupling should not change with temperature.

A 1 mole % solid solution of i-propyltrimethyltin in CCl_3CF_3 was γ-irradiated and the ESR spectrum was observed initially at 81 K (shown in upper portion of Figure 64, page 238). The low temperature (81 K) ESR spectra of i-$PrMe_3Sn^+$ are characterized by a triplet of doublets ($A_\perp$(2H) = 48.6 G, $A_\perp$(1H) = 11 G, and $g_\perp$ = 2.0473) where the triplet is assigned to the conformationally locked β-axial hydrogens and the doublet arises from the unique α-hydrogen. On the low-field side of the main perpendicular features, a partial replica of the main pattern was detected at higher gain and was assigned as a satellite pattern originating from an additional hyperfine interaction with tin ($A_\perp(^{117,119}Sn)$ = 89 G). Thus, the low-temperature results for the i-$PrMe_3Sn^+$ nicely fit with the proposed model.

As shown in the lower portion of Figure 64, warming the sample resulted in a significant change in the shape of the observed ESR pattern which was completely reversible by returning to 81 K. The spectrum taken at 142 K (bottom scan in Figure 64) may be straightforwardly analyzed as a septet of doublets ($A_\perp$(6H) = 24 G, $A_\perp$(1H) - 11.0 G, $g_\perp$ = 2.0473). Shown at higher gain on the low-field side of the main pattern are the tin satellite lines which exactly parallel the thermal changes of the main line pattern. Therefore, the model

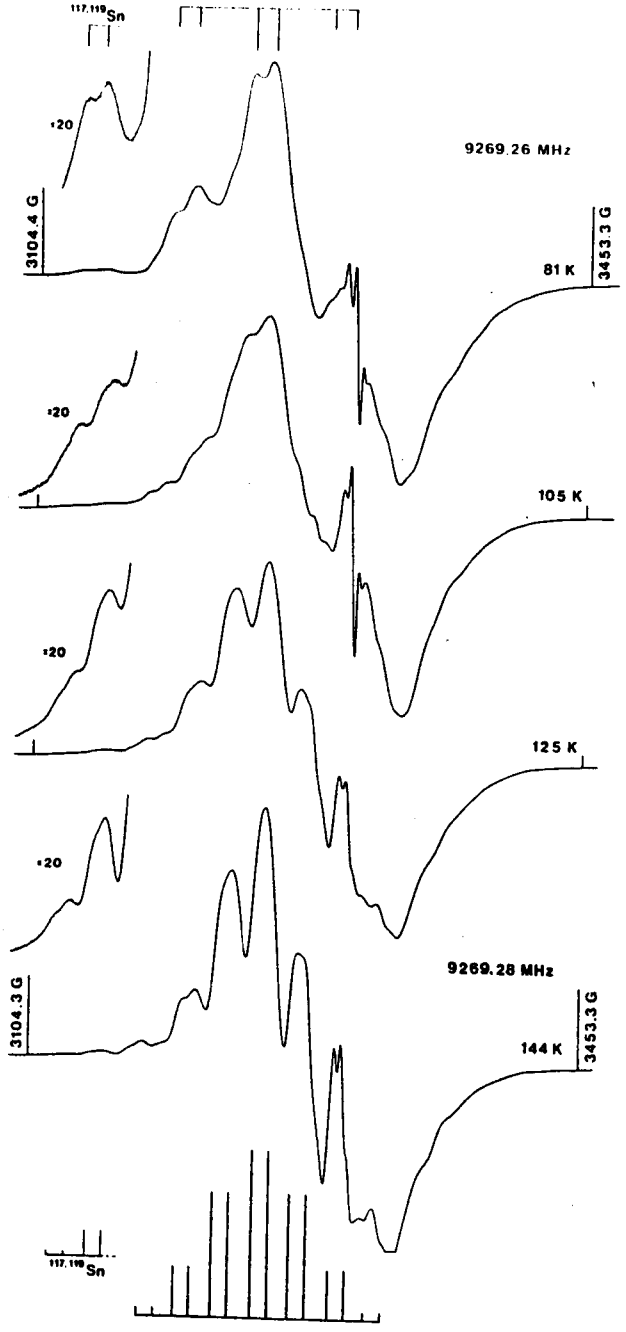

Figure 64. First-derivative ESR spectra of a γ-irradiated 1 mole % solid solution of i-$PrMe_3Sn$ in CCl_3CF_3 at various temperatures ranging from 81 K (upper) to 142 K (lower).

has proved to be appropriate for predicting the changes in the hyperfine pattern of the i-$PrMe_3Sn^+$ with temperature.

Before turning to the next alkyltrimethyltin radical cation, the following points should be mentioned. First, although the t-$BuMe_3Sn^+$ could be generated in CF_3CCl_3, the ESR spectra from an γ-irradiated 5 mole % solid solution of i-propyltrimethyltin in Freon-11 were ill-defined and several of the resonances yielded evidence for the isopropyl radical[199] (Figure 65, page 240). Exposure of the i-$PrMe_3Sn^+$ in CCl_3CF_3 to visible light resulted in virtually no change in the observed ESR spectra.

Turning now to the next test of the model, if the model is appropriate for the ethyltrimethyltin radical cation, then the following predictions may be made. First, the unpaired electron would be expected to be localized between the inner carbon of the ethyl group and the tin nucleus. The central bonds of the trimethyltin moiety would be expected to become planar and the structure should again give rise to a significant g_1 shift together with a small perpendicular tin isotope coupling on the order of 90 G. The unique ethyl ligand would be expected to adopt a locked conformation at low temperature (~ 80 K) but be unlocked at higher temperatures (> 120 K), the net result being that the hyperfine coupling pattern would change from a large doublet coupling from a locked β-axial hydrogen (80 K) to an averaged quartet hyperfine pattern at higher temperature. The two α-hydrogens would be expected to show a hyperfine coupling on the order of 13 G which would be expected to be temperature independent.

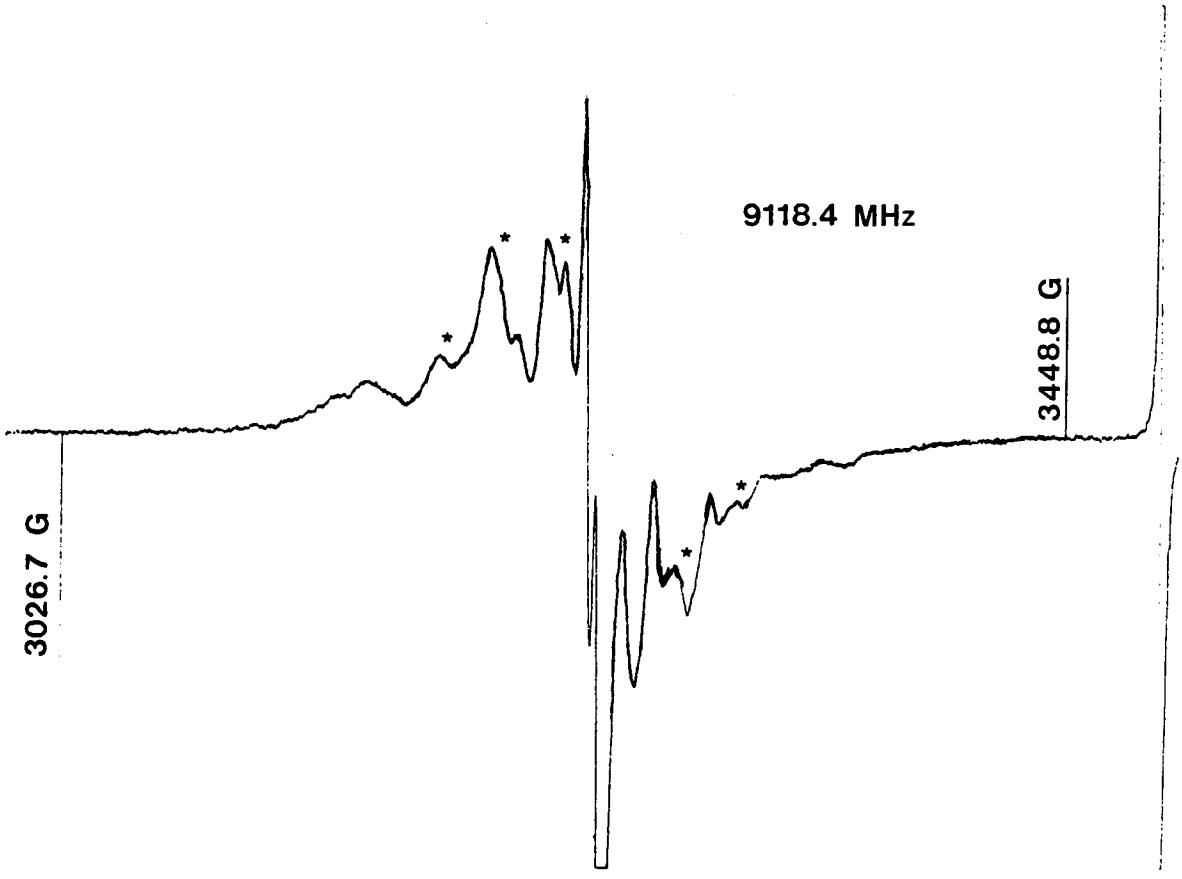

Figure 65. First-derivative ESR spectrum of a γ-irradiated 8 mole % solid solution of i-$PrMe_3Sn$ in $CFCl_3$ at 85 K. This sample was not annealed above 85 K prior to this spectrum. The features marked with asterisks correspond to the i-Pr neutral radical.

The radical cation of ethyltrimethyltin ($EtMe_3Sn^+$) was generated by the action of γ-irradiation on a 1 mole % solid solution of the parent organometal dissolved in CCl_3CF_3. The intense features (as shown in the upper scan of Figure 66, page 242) in the ESR spectrum taken at 90 K were assigned to the perpendicular hyperfine couplings of the ethyltrimethyltin radical cation ($EthMe_3Sn^+$). By warming the sample to 140 K (lower portion of Figure 66), the 90 K pattern was replaced by a pattern which was analyzed as a quartet of triplets ($A_1(3H)$ = 29 G, $A_1(2H)$ = 15.0 G, and g_1 = 2.054).

Due to the unresolved nature of the pattern obtained at 90 K, an unequivocal analysis is difficult. However, the analysis of the high temperature pattern (140 K) provides a clue for a possible low temperature analysis. Given that the g_1 value and the tin isotope and α-hydrogen hyperfine couplings should all be essentially independent of temperature and that the hyperfine interaction at high temperature occurs to three β-hydrogens as well as the two α-hydrogens, a tentative analysis of the low-temperature pattern may be made using the high temperature g_1, $A_1(2H_\alpha)$, and $A_1(^{117,119}Sn)$ values and some trial values such as $A_1(1H_{\beta,axial})$ = 50 G and $A_1(2H_{\beta,non\text{-}axial})$ = 20 G. This analysis is reproduced as a stick diagram in Figure 66, and fits fairly well with the observed peaks. Even if this analysis were to be incorrect, the observed low temperature spectrum still confirms the qualitative predictions of the proposed model because it definitely shows clear evidence for a large doublet splitting of at least 42 G arising from a locked β-hydrogen and definitely shows

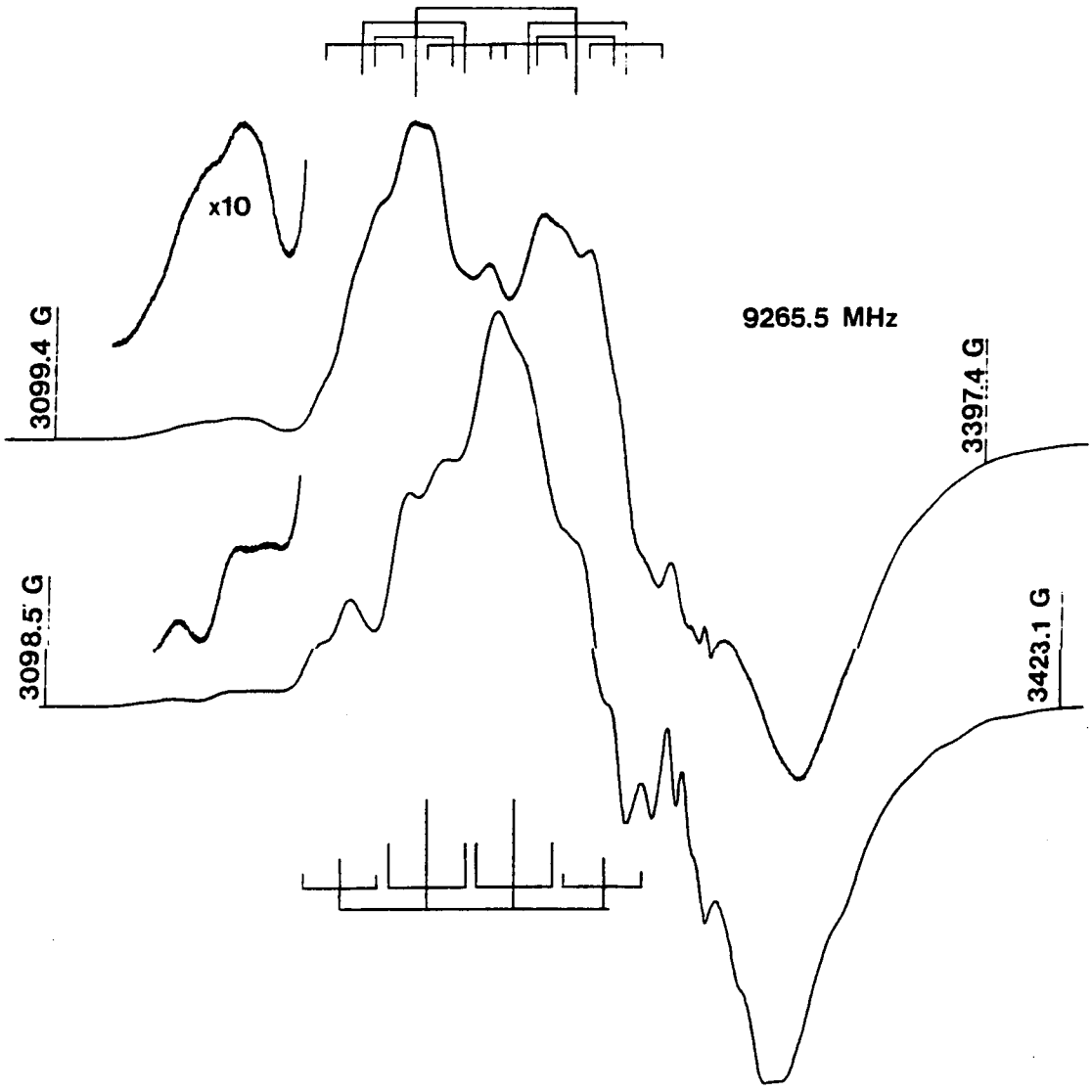

Figure 66. First-derivative ESR spectrum of a γ-irradiated 1 mole % solid solution of $EtMe_3Sn$ in CCl_3CF_3 at 83 K (upper) and 140 K (lower). The stick diagrams suggest a possible interpretation of the spectra.

evidence for a small perpendicular tin isotope hyperfine coupling of 105 G.

Attempts to generate the $EtMe_3Sn^+$ in a Freon-11 matrix were unsuccessful; that is, when a 5 mole % solid solution of ethyltrimethyltin and Freon-11 was γ-irradiated, the most intense resonances in the observed ESR spectrum (Figure 67, page 244) taken at 90 K were assigned to the ethyl radical. This result parallels the findings for $i\text{-}PrMe_3Sn^+$.

The cyclohexyltrimethyltin radical cation ($c\text{-}C_6H_{11}Me_3Sn^+$) allows an unique opportunity to check the proposed model since for this molecule none of the four β-hydrogens can occupy an axial position as long as the cyclohexyl group retains the sterically favored chair conformation shown below.

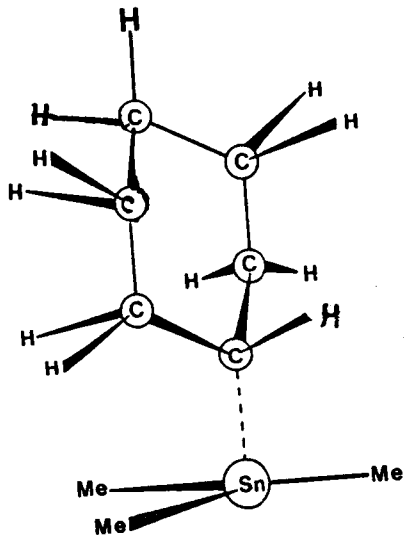

As in previous cases, the model predicts that the positive hole should be localized along the C-Sn bond of the cyclohexyl group.

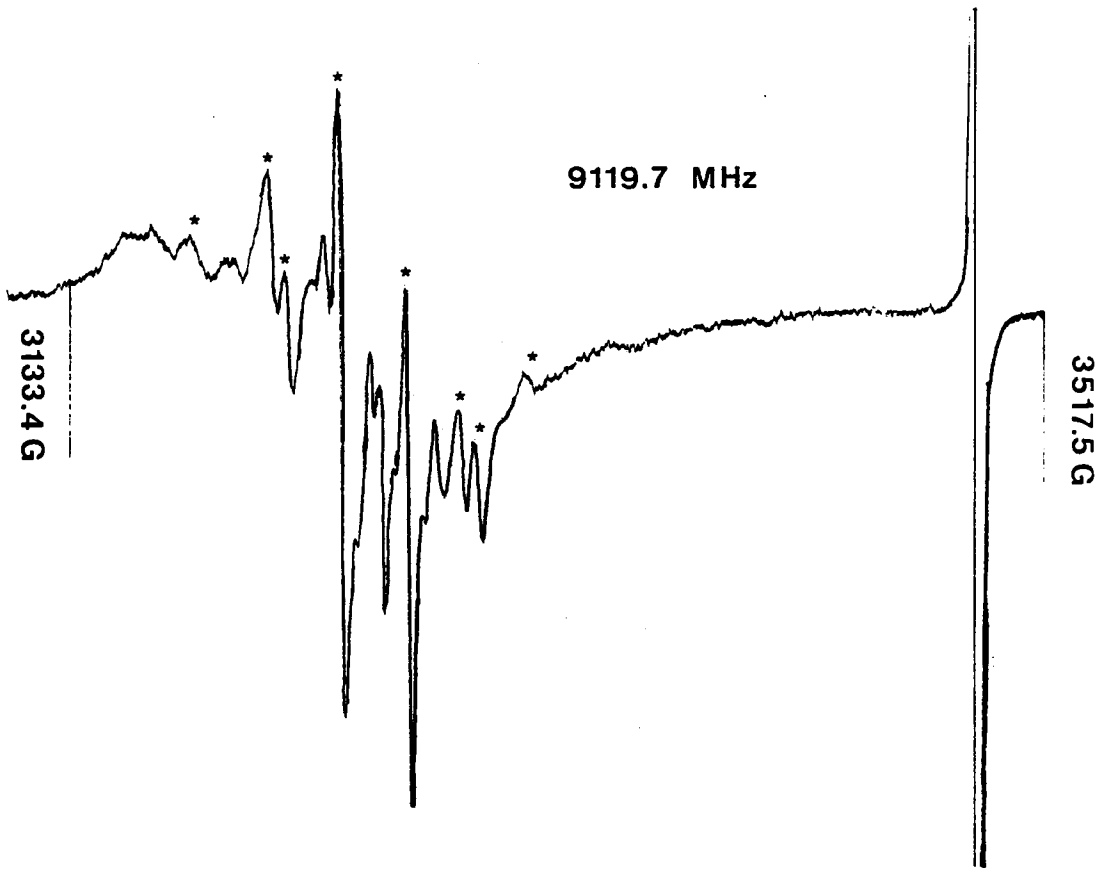

Figure 67. First-derivative ESR spectrum of a γ-irradiated 5 mole % sample of $EtMe_3Sn$ in $CFCl_3$. The resonances marked with asterisks correspond to the ethyl radical.

Again the trimethyltin moiety is predicted to be planar and should give rise to a small tin isotope coupling, while the tin 4d-electrons are expected to induce a significant positive $g_{\perp}$ shift. Turning to the alkyl group, the simple model would predict that in the absence of any β-axial hydrogens in this radical cation, no large hyperfine couplings (~ 40 G) would be expected and that the only significant hyperfine coupling should arise from the α-hydrogen.

The $c\text{-}C_6H_{11}Me_3Sn^+$ was generated by γ-irradiating a 2 mole % solid solution of the parent organometal in a Freon-11 matrix, and it was observed at 85 K (Figure 68, page 246). An unresolved broad resonance (line width ~ 25 G) centered at $g_{\perp}$ = 2.041 was assigned to the $c\text{-}C_6H_{11}Me_3Sn^+$ while the weaker satellite resonance located on the low-field side of the main resonance was assigned to an additional hyperfine interaction with tin ($A_{\perp}(^{117,119}Sn)$ = 112 G). The shape of the large resonance did not significantly change with temperature.

Indeed, the experimental results confirm the qualitative predictions made by the simple model, namely that as a result of no β-axial protons being in the radical cation no large couplings on the order of 40 G were observed. Although the unique α-proton would have been expected to show a resolved hyperfine coupling on the order of 13 G, no such coupling was resolved. Nevertheless, the fact that the width of the perpendicular feature was on the order of 25 G is certainly suggestive of an unresolved hyperfine coupling on the order of 10-15 G with the lack of resolution arising from either small couplings to the non-axial β-protons or to the γ-protons of the cyclohexyl group.

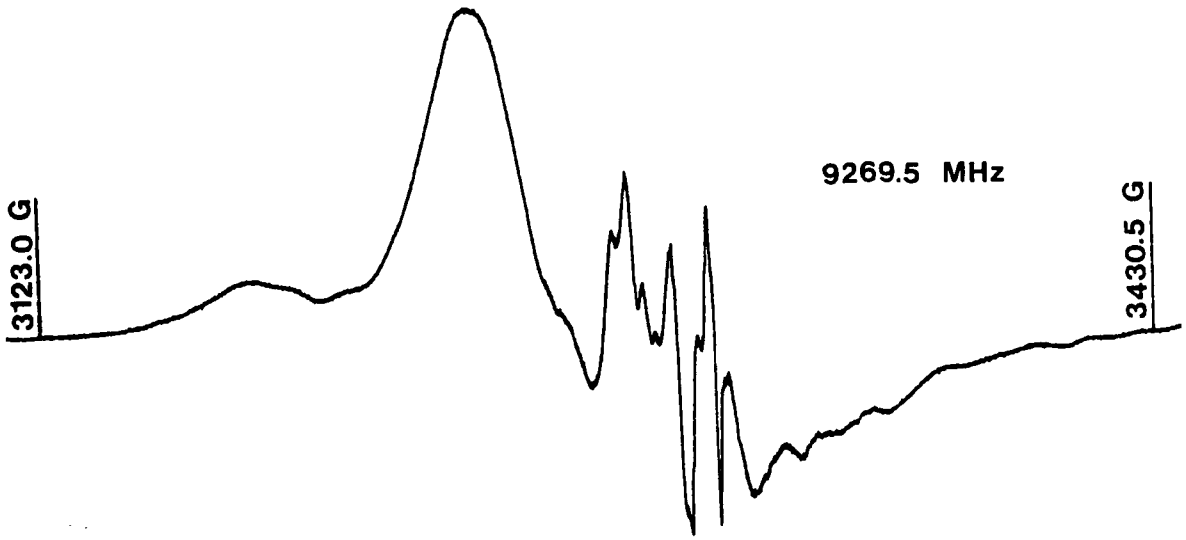

Figure 68. First-derivative ESR spectrum of a γ-irradiated 2 mole % sample of cyclohexyltrimethyltin in $CFCl_3$ at 85 K.

The neo-pentyltrimethyltin radical cation (neo-$PeMe_3Sn^+$) also allows an interesting extension of the proposed model since in this radical cation there are only α and γ alkyl hydrogens and no β-alkyl hydrogens, as shown below.

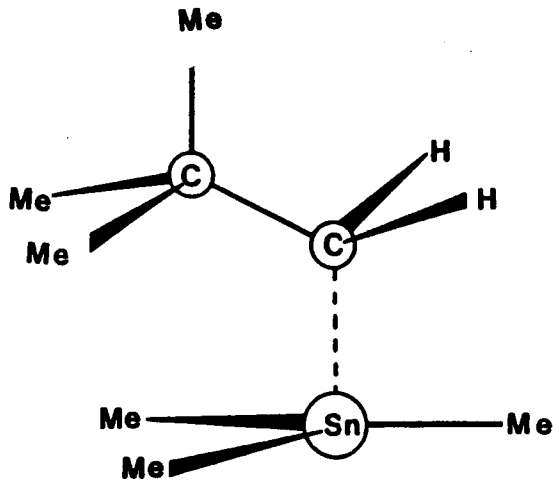

The model would predict that the positive hole will be localized along the C-Sn bond of the neo-pentyl group. As in earlier cases, the Sn-Me bonds of the trimethyltin moiety would be assumed to be co-planar and that the cation would be characterized by a large positive g_1 shift and a perpendicular tin hyperfine coupling on the order of 90 G. In this case, the model would predict for the neopentyl group that the two α hydrogens would show a hyperfine coupling of about 13 G which should be temperature independent.

The ESR spectral features observed at 84 K which were assigned to the neo-$PeMe_3Sn^+$ (Figure 69, page 248) were obtained by γ-irradiating a 3 mole % solid solution of the parent organometal in Freon-11. Although only partially resolved, the intense feature

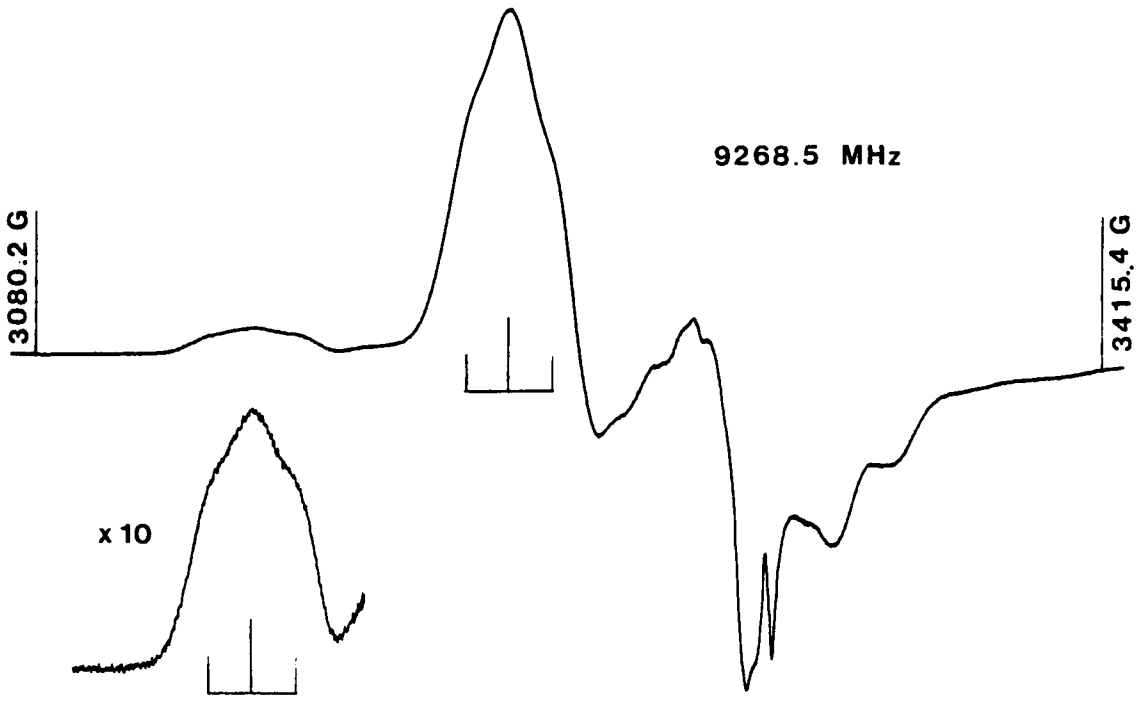

Figure 69. First-derivative ESR spectrum of a γ-irradiated solid solution of $(CH_3)_3CCH_2SnMe_3$ in $CFCl_3$.

centered at $g_\perp$ = 2.0519 may be analyzed as a triplet ($A_\perp$(2H) = 14 G). At higher gain a replica pattern of the main resonance was observed and was assigned to the tin satellite lines ($A_\perp(^{117,119}Sn)$ = 161 G). Warming the sample from 84 K to even 155 K did not change the ESR spectrum. Annealing above 155 K resulted in the rapid and irreversible decay of the radical cation. Exposure of the sample to UV light did not change the spectrum.

Although the ESR results for neo-$PeMe_3Sn^+$ reaffirm the general validity of the model, the fact that no γ hyperfine couplings were resolved may simply have been the result of the fact that the neo-pentyl methyl groups were not locked at 84 K and that it is the average of the γ-hydrogens that is unresolved. This latter consideration will be explored further with the ESR results for the n-propyltrimethyltin radical cation. Incidentally, the slightly larger tin hyperfine coupling in this case may be the result of the neo-pentyl group causing the trimethyltin moiety to be slightly non-planar through a steric effect (as shown below) thereby inducing slightly more tin s-orbital character.

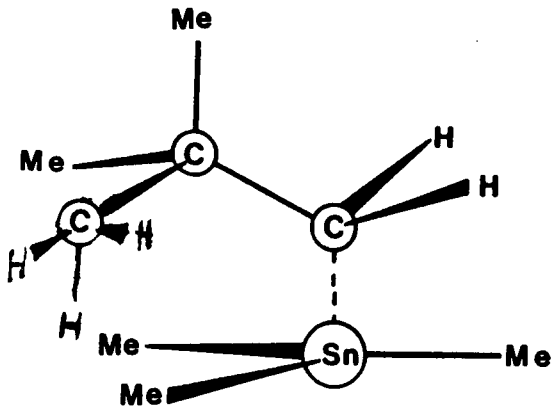

Since the structure and hyperfine pattern of the unique alkyl groups of the alkyltrimethyltin radical cations have roughly paralleled the structures of the corresponding hydrocarbon radical cations, it would be anticipated that the unique alkyl group of the radical cation n-propyltrimethyl tin ($PrMe_3Sn$) would likewise parallel the results found for the propane radical cation.[202] To this end, the hyperfine pattern would be expected to be a doublet where the large doublet would arise from the conformationally locked hydrogen which follows the W-plan as shown below.

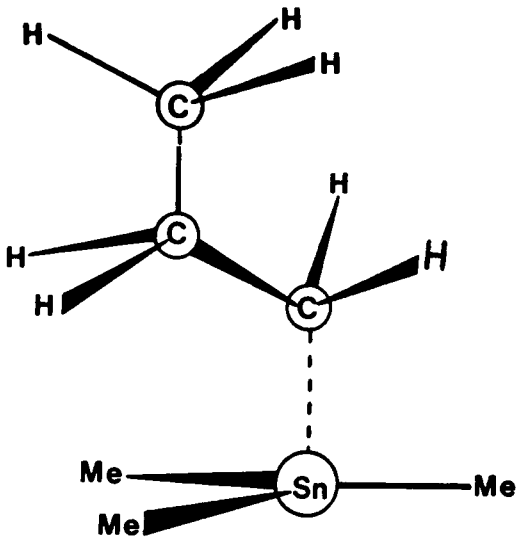

It might be further argued by comparison with the primary alkane radical cations that the doublet coupling in n-$PrMe_3Sn^+$ should be smaller than the doublet coupling in $EtMe_3Sn^+$. The previously described model would predict that the α-hydrogens in each case should give rise to a coupling on the order of 15 G, the main perpendicular feature should be centered at g ~ 2.045, and the tin isotope coupling should be about 80 G in each case.

Features which were assigned to the radical cation of n-$PrMe_3Sn$ were observed from a γ-irradiated 1 mole % sample of the parent organometal in CCl_3CF_3. In this case the observed ESR spectrum at 85 K (Figure 70, page 252) clearly showed evidence of a triplet ($A_\perp(2H)$ = 17.6 G) and to a lesser extent evidence of the anticipated doublet ($A_\perp(1H)$ = 44.7). That the high-field doublet component is more intense than the low-field component may merely be the result of this feature overlapping with some other unresolved resonances in the same region. The $EtMe_3Sn^+$ also showed this effect. Assuming the doublet analysis is correct, the perpendicular pattern centers at $g_\perp$ = 2.0505. This analysis is marked by the stick diagram in Figure 70. At higher gain, a partial replica of the perpendicular feature was observed on the low-field side of the previously described pattern and was assigned to an additional hyperfine interaction with the magnetic isotopes of tin ($A_\perp(^{117,119}Sn)$ = 128 G). Warming the sample to 142 K resulted in only a slight broadening of the hyperfine lines.

Certainly the significant $g_\perp$ shift and the small tin isotope coupling confirm the general appropriateness of the model to this particular radical cation. Thus, following the predictions of the afore described model, the doublet coupling is assigned to the conformationally locked γ-hydrogen while the triplet splitting is assigned to the two α-protons. Although the conformationally locked γ-proton did not change over into a time averaged unlocked situation as did the β-protons in the ethyl isopropyl, and tert-butyl derivatives, this

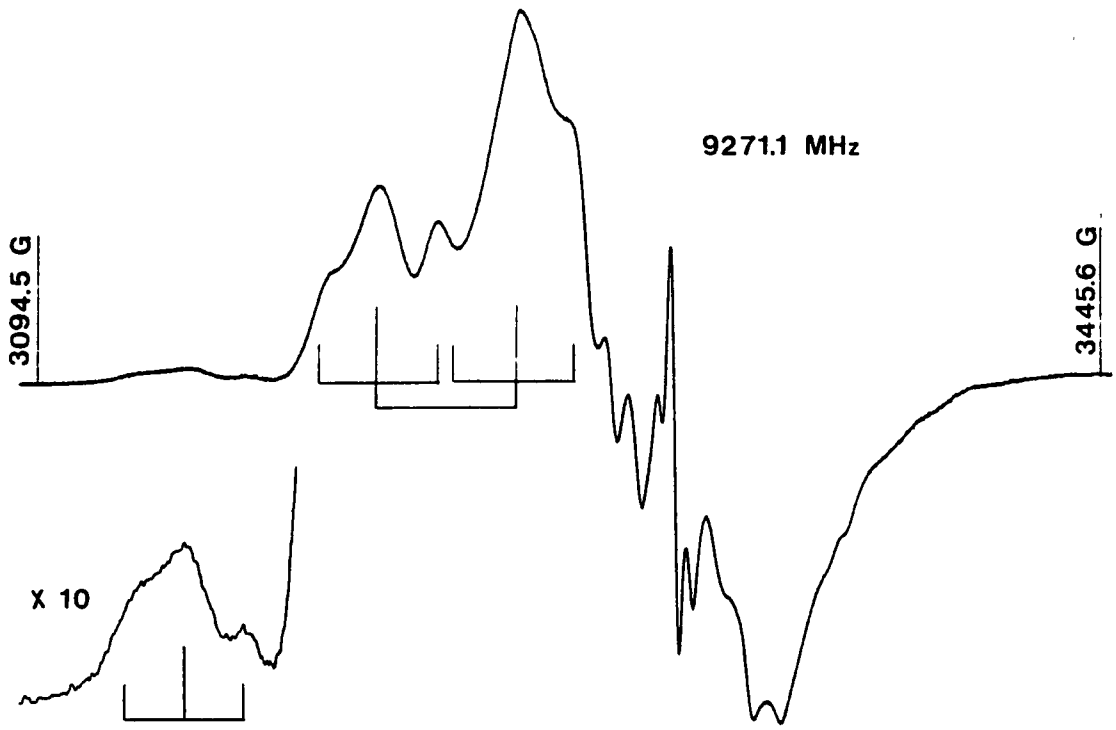

Figure 70. First-derivative ESR spectrum of a γ-irradiated sample of n-$PrMe_3Sn$ in CCl_3CF_3.

lack of unlocking may reflect the strong conformational locking characteristic of the n-alkane radical cations. As a point of reference, n-butane even at 150 K in Freon-11 shows evidence of a locked structure.[203]

That the spectrum did not appreciably change with exposure to visible light parallels the results for the other organometallic radical cations described in this section. Also, a γ-irradiated 1 mole % sample of $PrMe_3Sn$ in Freon-11 did not give clear evidence for the radical cation but instead several resonances were observed about g = free spin indicative of neutral radical generation.

In summary, a unified model for interpreting the perpendicular ESR components of the alkyltrimethyltin radical cations has been proposed and this model has been found to be generally applicable to a relatively diverse group of test cases.

E. Tetramethyllead Radical Cations

An extension of the previously described ESR work on Me_4Si^+, Me_4Ge^+,[186] and Me_4Sn^+[187] to the next member of the Group IVB organometal family, Me_4Pb^+, was natural. While the first two members of this organometallic radical cation series, Me_4Si^+ and Me_4Ge^+, adopt C_{2v} structures, the third member of the series, Me_4Sn^+ approximates a C_{3v} structure. Hence, the identification of the tetramethyllead radical cation was of particular importance since it was of interest to determine if it adopts either a C_{2v} or C_{3v} or yet some other structure.

Figure 71, page 255, presents a typical spectrum obtained from a γ-irradiated 2 mole % solid solution of tetramethyllead in Freon-11 at 81 K. A spectrum very similar to Figure 71 was obtained from samples where the concentration of Me_4Pb was varied from about 0.5 mole % to about 8 mole %. Also, some samples were prepared using a 15% mixture of toluene in Me_4Pb, but except for a slightly increased number of resonances centered about free spin (these extra features presumably arising from the toluene radical cation) the spectra from the blends were indistinguishable from the purer material. The ESR spectra of Me_4Pb^+ were characterized by a well-resolved 1:3:3:1 quartet and were analyzed as the set of perpendicular components resulting from hyperfine coupling to three protons ($A_\perp(3H)$ = 14.7 G and $g_\perp$ = 2.110). Although the magnetic isotope ^{207}Pb occurs in a natural abundance of 22.6%, there was no evidence in the X-band spectra indicating a hyperfine interaction to lead.

A sample containing Me_4Pb was examined using a Q-band spectrometer to confirm the X-band analysis. Figure 72, page 256, presents a Q-band spectrum obtained from a γ-irradiated (3.1 Mrad) 5 mole % solid solution of Me_4Pb in Freon-11 at about 80 K. The fact that the simple quartet pattern which was obtained at X-band is not reproduced in the Q-band spectra is probably because there is a slight inequivalence between g_x and g_y, the net result being that at Q-band these slightly inequivalent g values split apart. In any event, the broad low-field hump corresponds to an average $g_\perp$ of 2.107 and the slight inflections on the broadened feature correspond to a coupling of about 15 G.

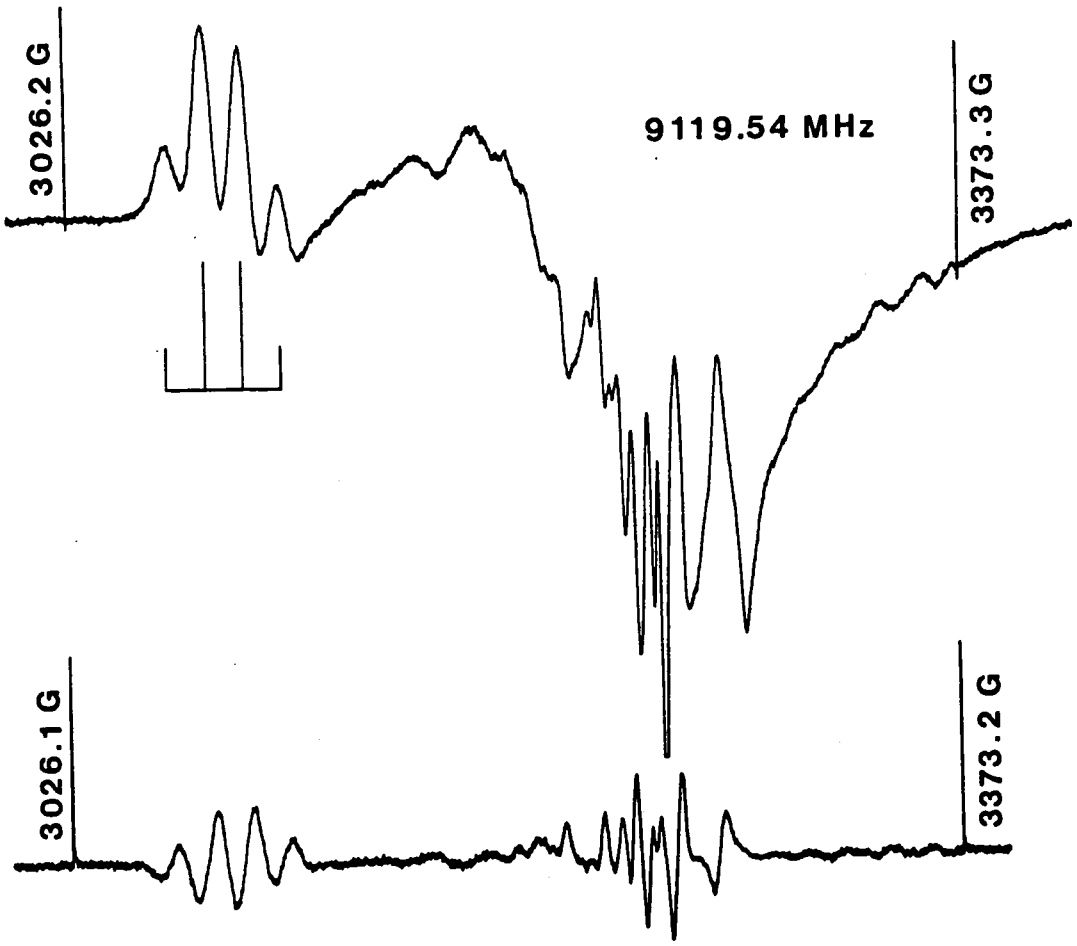

Figure 71. First-derivative (upper) and second-derivative (lower) ESR spectra of a γ-irradiated (dose 1.3 Mrad) solid solution of 2 mole % tetramethyllead in trichlorofluoromethane at 90 K. The quartet stick diagram shows the line components assigned to the perpendicular features of the radical cation.

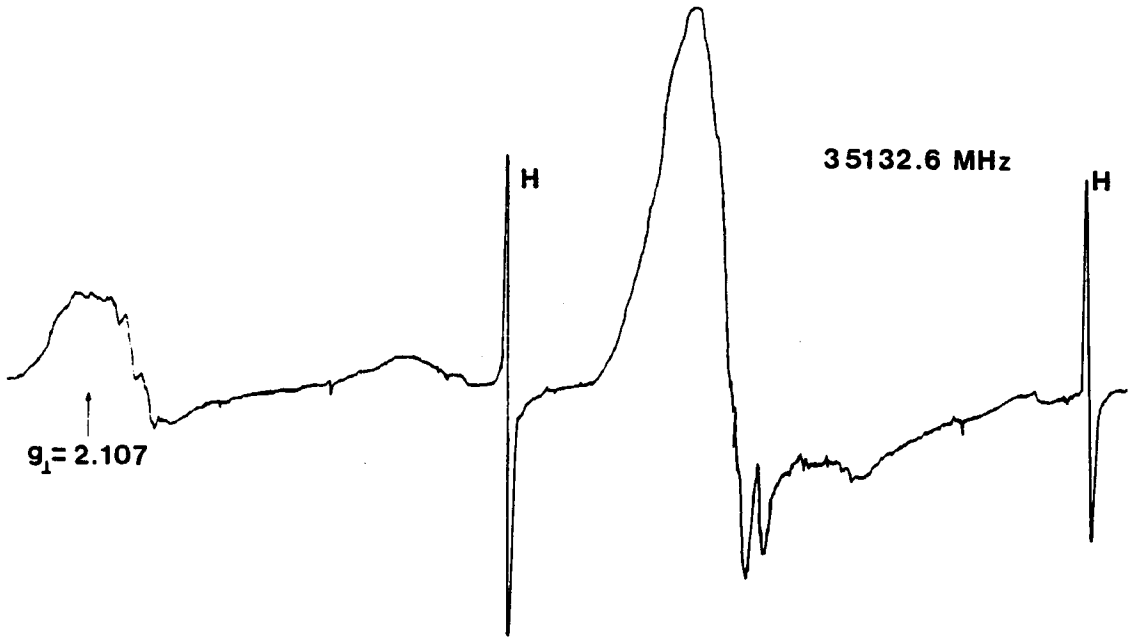

Figure 72. First-derivative ESR spectrum of a γ-irradiated 5 mole % sample of Me_4Pb in $CFCl_3$. The lines marked with H corresponds to the hydrogen atom lines.

Interestingly, after γ-irradiating a sample containing Me_4Pb in Freon-11 a white precipitate was noticed in the bottom of the ESR sample tube. Subsequent γ-irradiations continued to increase the amount of white precipitate which collected at the bottom of the ESR tube. The white precipitate was collected from an ESR sample tube and analyzed using a mass spectrometer. Two high molecular weight peaks which were obtained corresponded to the masses of Me_3PbCl and Me_2PbCl. No peaks were obtained for masses greater than the mass of $Me_3{}^{208}Pb{}^{37}Cl$ (290 AMU). Thus, it seems reasonable that the white powder formed during γ-irradiation is Me_3PbCl. A white powder was also obtained when a sample of Me_4Pb was dissolved in perfluoromethylcyclohexane and γ-irradiated. In this latter case, the results obtained from a mass spectrometer yield evidence of molecules with masses corresponding to Me_3PbF and Me_2PbF, but in this case there were no masses greater than that which corresponds to $Me_3{}^{208}PbF$ (272 AMU). Hence, the white precipitate in this case was probably Me_3PbF. In each case, these salts are possibly formed by an ion-ion reaction between the trimethyllead cation and the corresponding halide ion, as shown below.

$$Me_3Pb^+ + Cl^- \rightarrow Me_3PbCl$$

$$Me_3Pb^+ + F^- \rightarrow Me_3PbF$$

The analysis of the hyperfine pattern in the present case is readily straightforward using the ESR results and interpretations found for the tetramethyltin radical cation. Thus, in light of this prior work, the three equivalent protons are assigned to the unique

methyl ligand of a trigonal pyramidal structure, as illustrated below:

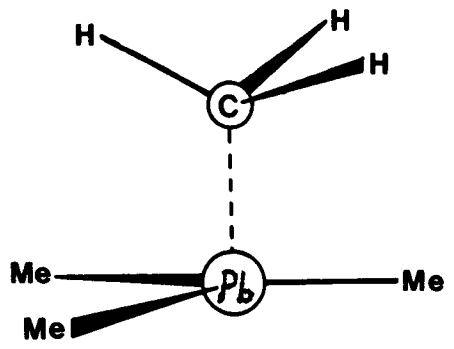

The appropriateness of the comparison to Me_4Sn^+ is further suggested by the significant $g_\perp$ shift.

The fact that the radical exhibits such a significant g-shift provides evidence suggesting that the SOMO probably contains the lead nucleus. This being the case, there should be a non-zero spin density on the Pb nucleus; hence, a ^{207}Pb hyperfine interaction should arise. All attempts at detecting the satellite lines from a ^{207}Pb hyperfine interaction, however, were inconclusive.

It could be argued that the ^{207}Pb hyperfine coupling is within the typical resolution capabilities of solid state ESR, however, such a case would only occur from an extremely fortuitous cancellation of A and B where $A_\perp = A - B$ (see also Equations (30) and (31), page 23). Since the atomic values[52] $A_o = 29{,}100$ G and $B_o = 232$ G are so large, the slightest shift in the spin distribution due to changes in the matrix or temperature might be expected to break this postulated fortuitous cancellation, thereby allowing the detection of the ^{207}Pb satellite lines. However, even these changes did not allow the detection of a ^{207}Pb hyperfine interaction.

It might alternatively be argued that the ^{207}Pb hyperfine coupling is anisotropically broadened and therefore not detected. If the conclusion derived from the Q-band experiment that g_x is not exactly equal to g_y is correct, then the ^{207}Pb hyperfine coupling might be expected to be split into an A_x and A_y. This being the case, the ^{207}Pb anisotropic hyperfine tensor could be smeared to such an extent that it would not be detected.

In any event, the radical giving rise to the quartet pattern is clearly the Me_4Pb^+ which has been interpreted as adopting a trigonal pyramidal structure much like Me_4Sn^+.

F. Dimetallic Radical Cations

Not only have the tetralkyl Group IVB organometals established themselves as an important class of primary electron donors,[173] but the family of hexamethyldimetal Group IVB organometallic compounds are also known as excellent electron donors.[204] These latter organometallic species are in some cases better electron donors than the organometallic species which contain only one metal atom per molecule. This high tendency of these hexamethyldimetal species to donate an electron has prompted several studies into their reactivity.[205-208]

The first hexamethyldimetal radical cation to be discussed will be the radical cation of hexamethyldisilane ($Me_3SiSiMe_3$). This radical cation was first generated in a Freon-11 matrix and was reported in 1980.[169,170] The present effort on this radical cation was two-fold. First, in view of the many types of solvent interactions

which are known, the generation of the $Me_3SiSiMe_3^+$ in a different matrix was attempted since reproducing the same hyperfine pattern in two different matrices will almost certainly establish that a matrix interaction is not significant. To this end, the generation of $Me_3SiSiMe_3$ was attempted in a CCl_3CF_3 matrix. Secondly, since the detection of an additional hyperfine interaction to the magnetic isotope of silicon (^{29}Si, I = 1/2, 4.70% natural abundance) would provide valuable information concerning the geometry about the trimethylsilyl groups, the detection of these resonances was sought.

An ESR spectrum almost exactly like the previously reported spectrum of the $Me_3SiSiMe_3^+$ was observed from a γ-irradiated 0.5 mole % mixture of hexamethyldisilane in CCl_3CF_3. This fact alone confirms the previous analysis. Attempts to observe ^{29}Si isotope resonances in the wings of the spectrum at much higher spectrometer gain were unsuccessful.

Prior to the present work only the homonuclear hexaalkyldimetal radical cations, $Me_3MMMe_3^+$ (M = Si, Ge, Sn),[169,170,190] were known. In each of these examples the positive hole was shown to be localized equivalently between the two metal centers in a σ orbital. In another extension of this project on dimetal radical cations, a few heteroatom dimetallic radical cations were examined. For the heteroatomic dimetallic radical cations, the primary objective of each investigation was to determine if the spin densities at each metal center remained evenly distributed, that is 50% on each metal, or if the spin density shifted to either metal.

Trimethylsilyltrimethylgermane ($Me_3SiGeMe_3$) will be the first hexamethyldimetal radical cation to be discussed.

The second derivative ESR spectra of a γ-irradiated 5 mole % solid solution of the hexamethyldimetal species in Freon-11 are shown in Figure 73, page 262. The observed spacings, however, do not follow a simple Boltzman distribution as would be expected for 18 equivalent hydrogens, instead at least 23 evenly spaced resonances are observed. This result may be rationalized in one of two ways. In one case, the additional hyperfine interactions could be assumed to arise from a large inequivalence of the hydrogen from one moiety over the other moiety. Since the hyperfine spacings are relatively constant and there are at least 23 evenly spaced lines, this analysis must assume that the hyperfine couplings from one moiety must be fortuitously larger than the other moiety by a whole number ratio greater than two. However, silicon and germanium species are generally very similar. For example, the hydrogen hyperfine couplings for the hexamethyldimetal radical cations are 5.55 G ($Me_6Si_2^+$) and 5.18 G ($Me_6Ge_2^+$), likewise the couplings for the trimethylmetal neutral radicals are very similar at 5.34 G ($Me_3Si\cdot$) and 5.24 G ($Me_3Ge\cdot$). Given these similarities, it seems unreasonable that the hyperfine coupling from the one moiety would be a factor of at least three times greater than the hyperfine couplings from the other moiety.

Since it seems reasonable that the sample could be contaminated with a small amount of the homonuclear hexamethyldimetal species,

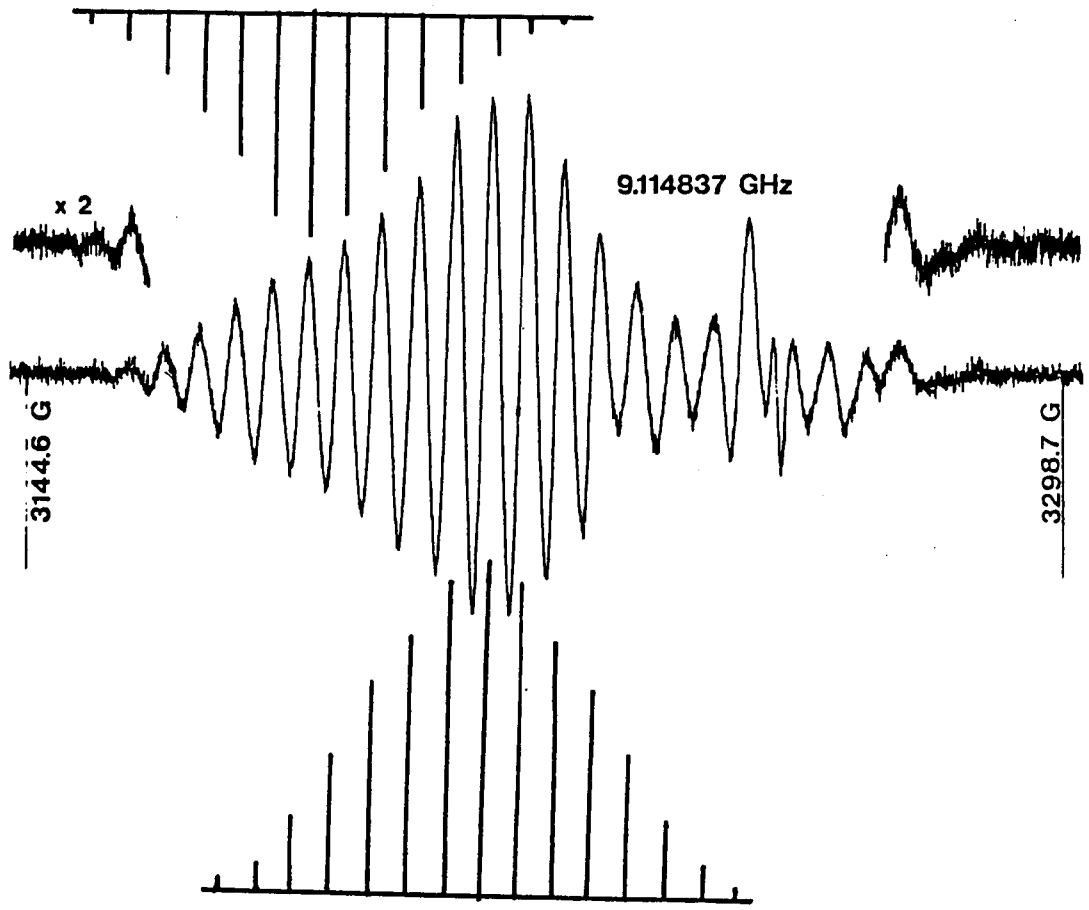

Figure 73. Second-derivative ESR spectrum of a γ-irradiated 5 mole % sample of $Me_3SiGeMe_3$ in $CFCl_3$ at 145 K.

($Me_3SiSiMe_3^+$ and $Me_3GeGeMe_3^+$), an alternative analysis would explain the observed pattern as the composite of all three organometallic radical cations. The reasonableness of this analysis is shown by the stick diagrams in Figure 72, page 256.

The initial attempt at generating the radical cation of $Me_3SiSnMe_3$ in a CCl_3CF_3 matrix was unsuccessful because the organometal solution which was used to prepare the sample was contaminated with tetrahydrofuran (THF). This contamination was discovered when the prominent features in the ESR spectra of the γ-irradiated sample corresponded precisely with the hyperfine parameters of the known THF radical cation.[209] The organometal solution was purified by simply vacuum distilling the THF from the hexamethyldimetal. The ESR spectrum of $Me_3SiSnMe_3^+$ (Figure 74, page 264) was obtained from a γ-irradiated 2 mole % sample of the purified organometal solution in CCl_3CF_3. As shown in Figure 74, page 264, a large g anisotropy was observed for the radical cation of $Me_3SiSnMe_3$. The intense low-field feature was assigned to the perpendicular component of an axially symmetric hyperfine interaction. This low-field feature showed evidence of a small, partially resolved hyperfine interaction to possibly nine equivalent protons ($A_\perp$(9H) = 11.4 G). The weaker feature at low-field which is a replica of the previously described feature (shown at higher gain in Figure 74) is assigned to the low-field perpendicular hyperfine component of the tin satellite ($A_\perp(^{117,119}Sn)$ = 101 G). A search for ^{29}Si satellite lines in natural abundance (^{29}Si = 4.7%) was unsuccessful. It should be noted that the

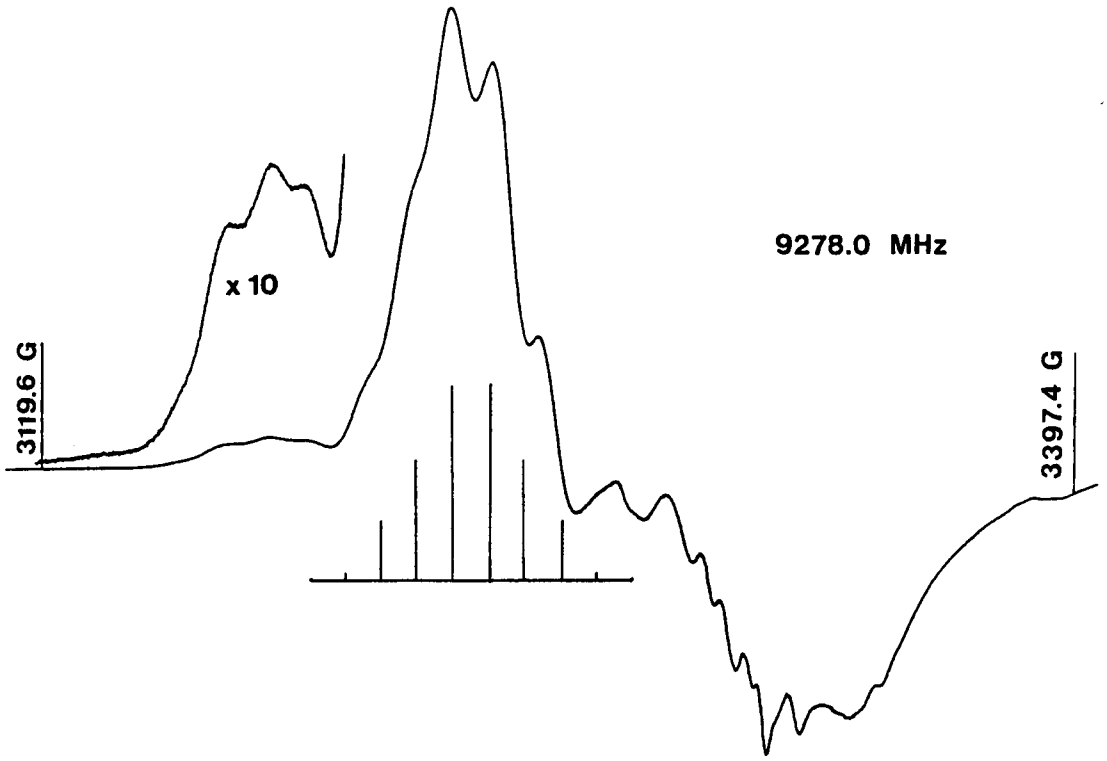

Figure 74. First-derivative ESR spectrum of a γ-irradiated 1 mole % sample of $Me_3SiSnMe_3$ in CCl_3CF_3. The hyperfine pattern is defined by the lower stick diagram.

slight amount of asymmetry of the large feature could be the result of hyperfine interactions from features assigned to $Me_6Si_2^+$. The features assigned to $Me_3SiSnMe_3^+$ irreversibly decayed above 145 K.

A comparison of the hyperfine couplings in the present case to other radical cations with this basic framework is given in Table XVII, page 200. Interestingly, for those hexamethyl heteronuclear radical cations where the metals are adjacent to each other in the Group IVB column ($Me_3SiGeMe_3^+$ and $Me_3GeSnMe_3^+$), the radical cations very closely approximated the average of the respective hexamethyl homonuclear species. For example, the $g_\perp$ value for $Me_3GeSnMe_3$ is reported as 2.077 which is almost exactly the average of the $g_\perp$ values for $Me_3GeGeMe_3^+$[170] and $Me_3SnSnMe_3^+$[190] (1/2 (2.0441 + 2.110) = 2.0775). Likewise, the apparent proton hyperfine coupling constant for $Me_3SiGeMe_3^+$ of 5.4 G approximates the average of the hyperfine couplings for $Me_3SiSiMe_3^+$[169,170] and $Me_3GeGeMe_3^+$[170] (1/2 (5.55 G + 5.18 G) = 5.36 G). In contrast, for those hexamethyl heteronuclear radical cations where the central heteroatoms are not adjacent to each other in the Group IVB column, a greater amount of the spin density in the σ-orbital appears to be shifted to the lighter central atom. For example, the central atom of the Me_3C moiety in $Me_3CSnMe_3^+$, possesses a greater spin density than the central atom of the Me_3Sn moiety, as discussed previously, Chapter IV, Section B). Also, the fact that the ESR spectra were analyzed according to only nine protons instead of 18 as with the other more similar hexamethyldimetal radical cations indicates the inequivalence of the σ-orbital.

In summary, this study has extended the σ-orbital model found for the homonuclear hexamethyldimetal radical cations to the heteronuclear hexamethyldimetal radical cations.

In the following section a different type of hexamethyldimetal radical cation will be considered, namely the radical cations of hexamethyldisiloxane ($(Me_3Si)_2O$) and hexamethyldisilylthiane ($(Me_3Si)_2S$).

The radical cations of $(Me_3Si)_2O$ and $(Me_3Si)_2S$ were generated at 77 K by γ-irradiation of a 5 mole % solid solution of the parent compounds dissolved in Freon-11. At 77 K, the ESR spectrum (Figure 75, page 267) of $(Me_3Si)_2O^+$ is characterized by at least 19 lines. These hyperfine interactions were reversibly lost when the sample was annealed above 140 K. The observed pattern was not changed when exposed to visible light.

The fact that the line intensities of the observed hyperfine pattern at 77 K do not appear to fit the intensity distribution for a binomial set of 19 lines implies that the 18 protons are not equivalent. The hyperfine pattern may be fit by assuming six strongly coupled protons being split by 12 protons. This tentative analysis is shown by the stick diagram in the lower portion of Figure 75. This analysis implies either that the methyl groups are locked with one proton of each methyl group coupling strongly, or that all of the protons in two methyl groups are coupling strongly. A recent photoelectron spectroscopy study has suggested that the highest molecular orbital, and therefore most likely the semi-occupied

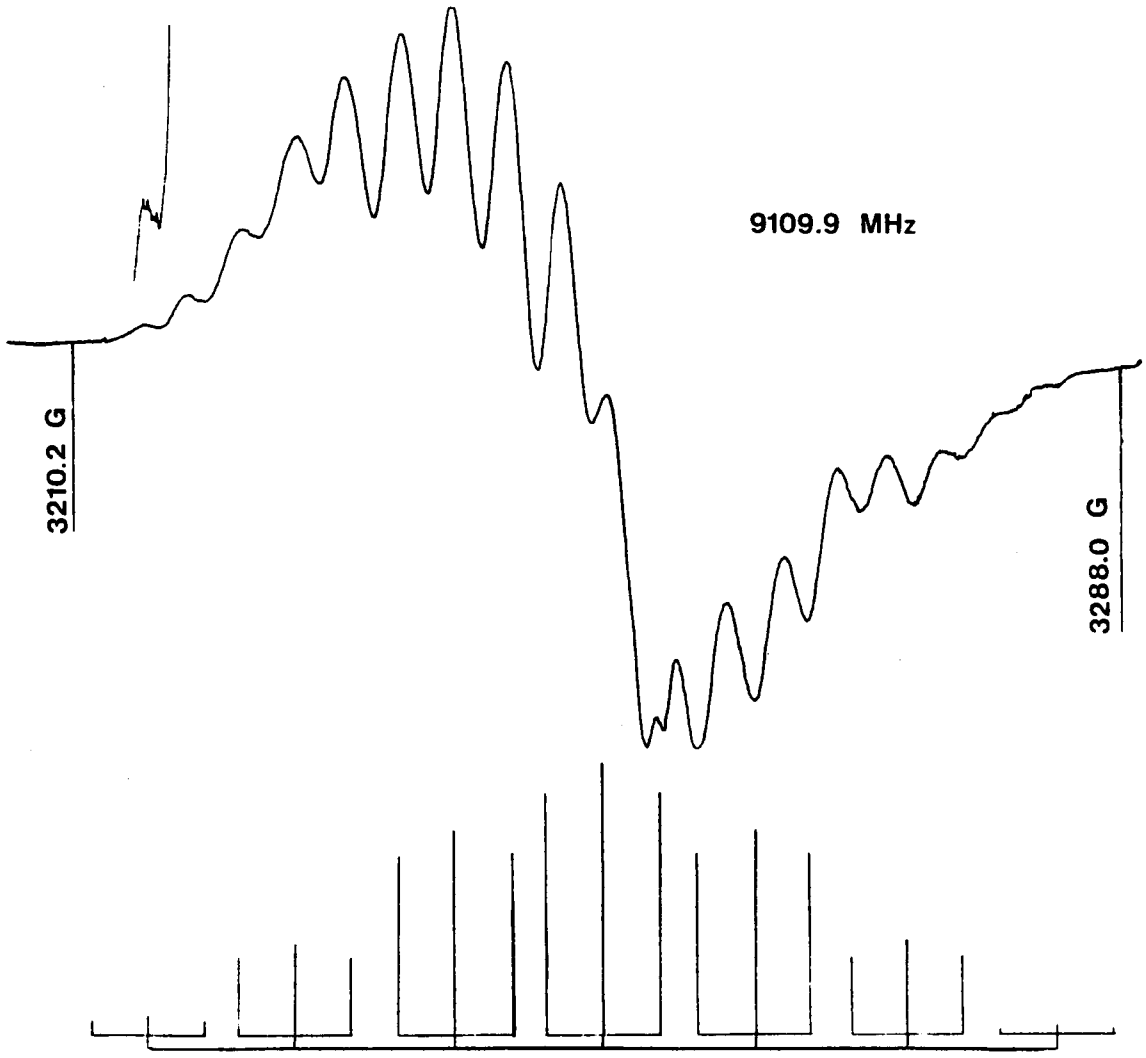

Figure 75. First-derivative ESR spectrum of a 5 mole % solid solution of $(Me_3Si)_2O$ in CF_3Cl_3 at 85 K. The observed ESR pattern of a septet of overlapping 13-line patterns is defined by the lower stick diagram. Only the central three lines of the 13-line pattern are shown.

molecular orbital in the radical cation of $(Me_3Si)_2O$, is a 2p orbital on onxygen. Incidentally, the $SOMO_5$ for Me_3O^+,[211] Me_2S^+,[209] and Me_2Se^{+}[209] are, in each case, thought to occupy a $2p_z$ orbital on the central atom. This being the case the SOMO may be drawn as shown below:

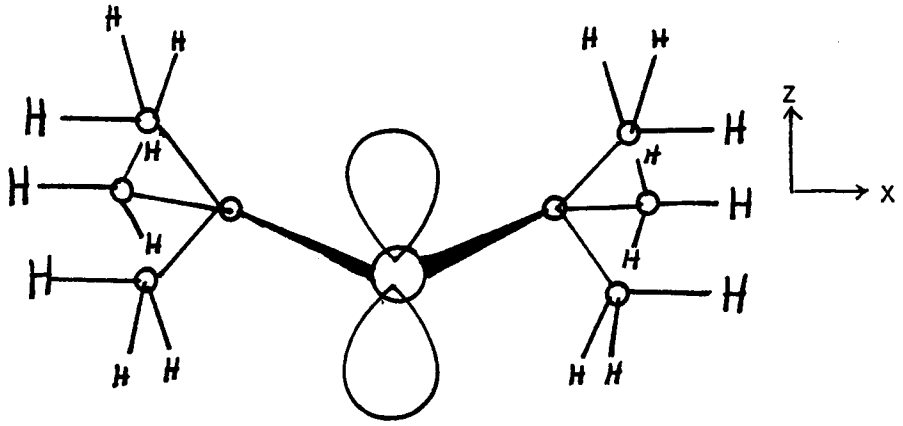

A radical with an essentially very similar structure is the neopentyl radical, as shown below.

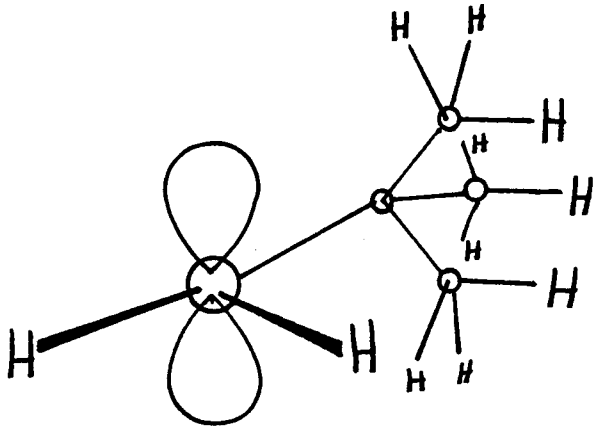

In one particular study where the hyperfine pattern was particularly well-resolved,[210] it was found that the methyl groups were locked and that the three γ-axial protons gave rise to a larger hyperfine interaction than the six γ-non-axial protons. By analogy to the present case, six protons would be expected to strongly couple while the other

12 would have a smaller hyperfine coupling. The analogy between $(Me_3Si)_2O^+$ and $Me_3CCH_2^{\cdot}$ is further strengthened by the observation that in both cases annealing the radicals results in the unlocking of the methyl groups. This unlocking for $(Me_3Si)_2O^+$ due to annealing results in the smearing of the hyperfine pattern. This change with temperature is completely reversible.

The ESR spectra of $(Me_3Si)_2S^+$ reveal a possible splitting of the g tensor into three anisotropic components, g_x, g_y, and g_z, as shown in Figure 76, page 270. Incidentally, the Me_2S^+ also was analyzed according to three g values. The analysis given for $(Me_3Si)_2O^+$ seems applicable in this case also. It should be noted that warming the sample above 145 K resulted in the disappearance of the resolution of the hyperfine pattern on g_z.

In summary, these studies have shown for the $(Me_3Si)_2O^+$ and $(Me_3Si)_2S^+$ that the unpaired electron occupies a π orbital which is in contrast to the σ-orbital characteristic of the hexamethyldimetal radical cations.

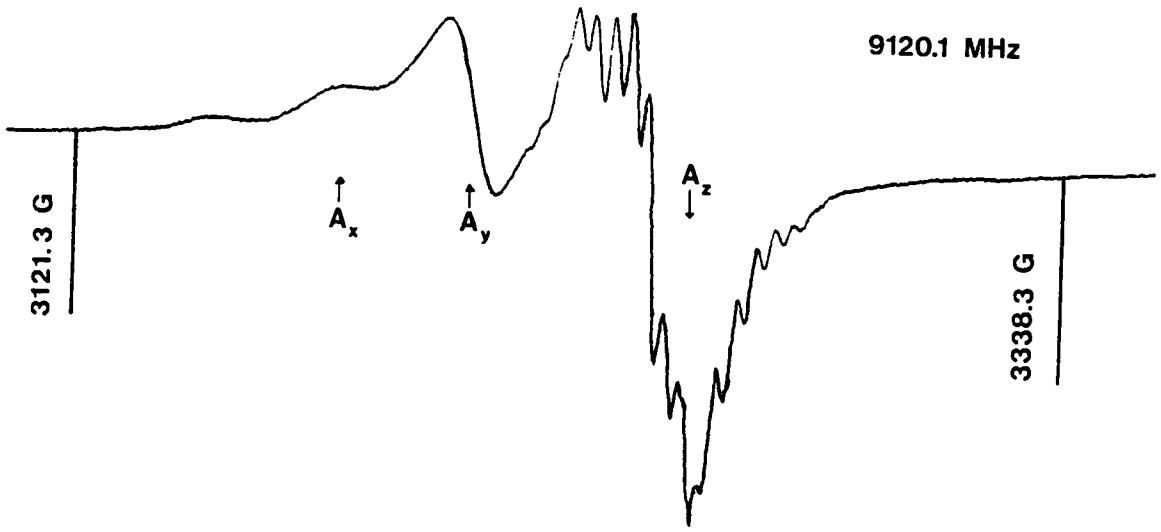

Figure 76. First-derivative ESR spectrum of a γ-irradiated 1 mole % sample of $(Me_3Si)_2S$ in $CFCl_3$. The A_x, A_y, and A_z features are defined by the arrows.

CHAPTER V

NEUTRAL RADICALS

A. Introduction

Probably the largest class of radicals characterized by ESR spectroscopy would be those radicals which possess an unpaired electron but are electronically neutral. Neutral radicals are often formed from diamagnetic molecules by the breaking of a molecular bond or by the addition of a neutral radical to an unsaturated bond. For example, photolysis of molecules having a particularly weak bond, such as peroxides,[212] often leads to the breaking of the weak bond.

$$ROOR' \rightarrow RO\cdot + R'O\cdot$$

Along the same line, x-rays have been used to generate a host of neutral radicals which were detected in liquid xenon.[213]

$$\xrightarrow{\text{x-ray}} CH_3CH_3 \rightarrow 2CH_3\cdot$$

An example of a neutral radical being formed by the addition of a neutral radical to an unsaturated molecule is the ethyl radical. In this case the ethyl radical could be formed by the addition of a hydrogen atom to ethylene.[213]

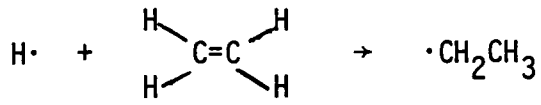

Neutral radicals are also formed by the decomposition of radical ions. For example, the t-butyl neutral radical may be formed by scission of the central C-Sn bond of $Me_3CSnMe_3^+$ (page 231) at 120 K.

$$Me_3CSnMe_3 \xrightarrow{\Delta} Me_3C\cdot + Me_3Sn^+$$

Trifluoromethyl radical formation by the dissociation of a chloride ion in CF_3Cl^- serves as another example of a radical ion decay method.[7]

$$CF_3Cl^- \xrightarrow{\Delta} CF_3\cdot + Cl^-$$

The neutral radicals which will be discussed in this chapter were probably all formed by the decay of a parent radical ion. In the case of the $\cdot CH_2M(CH_3)_3$ radicals, both the parent radical ion and the neutral radical were detected.

B. $Me_3MCH_2\cdot$ Type Radicals

Organometallic alkyl radicals where the spin is either α or β to the metal are distinguished from other simple organic radicals due to the potentially strong proximal interaction of the carbon with the metal center.[214,215] In particular, the relative importance of d-orbital participation has been discussed by several authors.[216-218] The simplest radicals to test the relative significance of d-orbital participation in α-metalloalkyl radicals is the family of $\cdot CH_2M(CH_3)_3$ type radicals where M = C, Si, Ge, Sn, and Pb. Although ESR spectra for each member of this family have been observed, hyperfine couplings have not been detected to ^{29}Si or ^{73}Ge nor have any ^{13}C hyperfine couplings been reported for any members of the series. Consequently, when very well-resolved isotropic hyperfine interactions were observed for $\cdot CH_2SnMe_3$ in a perfluoromethylcyclohexane matrix at 140 K, the utility of this matrix to likewise characterize the remaining members

in the family of $\cdot CH_2MMe_3$ type radicals where M = Si, Ge and Pb was soon realized.

The experimental aspects of this project will now be considered. As stated previously, the matrix used in this investigation was perfluoromethylcyclohexane (PFMCH). In each case, about 1 mole % of the organometal was dissolved in PFMCH and γ-irradiated at 77 K. The two radicals observed at about 80 K immediately following γ-irradiation were the PFMCH radical anion and the parent organometal radical cation; both of these radicals have already been discussed. By warming the samples to about 125 K, the resonances assigned to the PFMCH radical anion and the parent organometal radical cation decayed, but their decay was matched by the growth of a new set of features. The new radical presumably was formed by the loss of a proton from the organometal radical cation. When the solute was $(CH_3)_4Si$, $(CH_3)_4Ge$, $(CH_3)_4Sn$ and $(CH_3)_4Pb$, the pattern was readily analyzed as a triplet as will be discussed later. When the solute was the ^{13}C enriched $(^{13}CH_3)_4Sn$, the main features in the ESR spectrum were assigned as a doublet of triplets, discussed later. In each case, warming the samples from 125 K to about 140 K even further sharpened the ESR spectra. Annealing above 140 K resulted in the irreversible decay of the above described radicals.

For the organosilicon and germanium samples, increasing the spectrometer gain revealed resonances which could be assigned as an additional satellite coupling to the ^{13}C and ^{29}Si nuclei (Figure 77, page 275) in the first sample and to ^{73}Ge (Figure 78, page 275, in

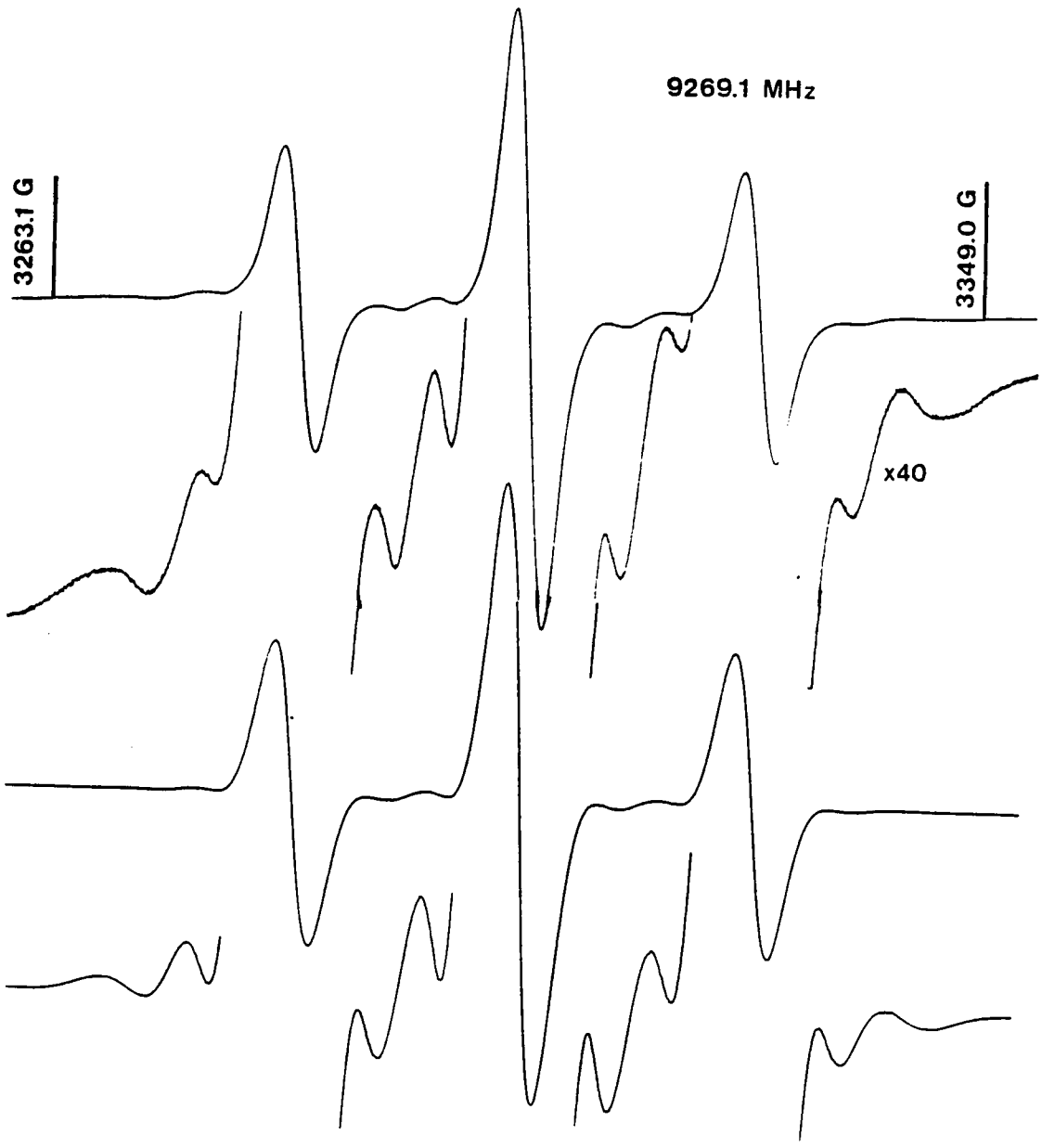

Figure 77. First-derivative ESR spectrum of a γ-irradiated solid solution of Me_4Si in PFMCH at 140 K. There is an excellent fit of the computer simulation to the observed spectrum while using the hyperfine parameters in Table XXI, page 280.

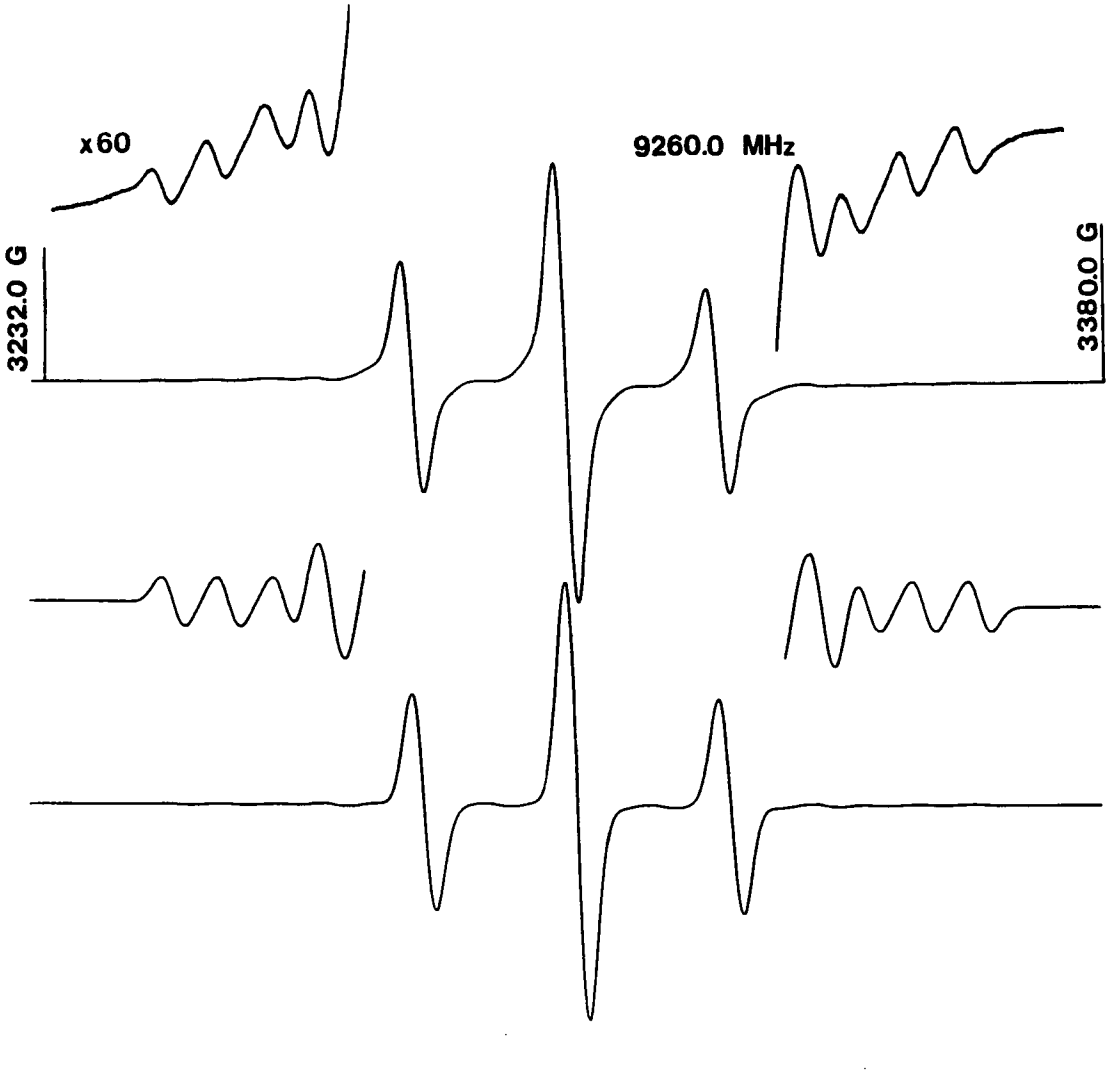

Figure 78. First-derivative ESR spectrum of a γ-irradiated solid solution of Me_4Ge in PFMCH at 140 K. There is an excellent fit of the computer simulation to the observed spectrum while using the hyperfine parameters in Table XXI, page 280.

the latter sample. For the tetramethyltin and lead samples, an increase in the spectrometer gain was not necessary to reveal the resonances arising from an additional hyperfine interaction to the $^{117,119}Sn$ (Figure 79, page 277) and ^{207}Pb (Figure 80, page 278) magnetic nuclei. Using the isotopically enriched $(^{13}CH_3)_4Sn$, the ^{13}C hyperfine interaction of the central carbon was detected, Figure 81, page 279. The coupling constants and spin densities for these radicals are collected in Table XXI, page 280.

The comparison given in Table XXI is particularly useful since in each case the radical was generated in exactly the same matrix; hence, differences in the matrix need not be considered when comparing the hyperfine coupling constants. As noted in Table XXI, page 280, there appears to be no clear trend in either the α-hydrogen hyperfine coupling or in the ^{13}C-hyperfine coupling. Assuming that the atomic values used to estimate the metal s-orbital spin density are correct, the s-orbital spin densities for Si, Ge, and Sn are all the same with the s-orbital spin density for the Pb analog being only slightly lower. Hence, there appears to be no clear trend in the metal ρ_s spin densities. The only trend is shown by the g_{iso}-values where with increasing atomic number there is a decrease in the g_{iso} value from a high for $\cdot CH_2SiMe_3$ of 2.0028 to a low of 1.9967 for $\cdot CH_2PbMe_3$.

By virtue of the fact that there are at most only minor shifts in spin density as judged by the H_α, ^{13}C, and isotopic metal-hyperfine couplings, the changes in g_{iso}-values cannot be explained in terms of spin density transfer into the d orbitals of the metal and must be explained with a constant spin density on the CH_2 group.

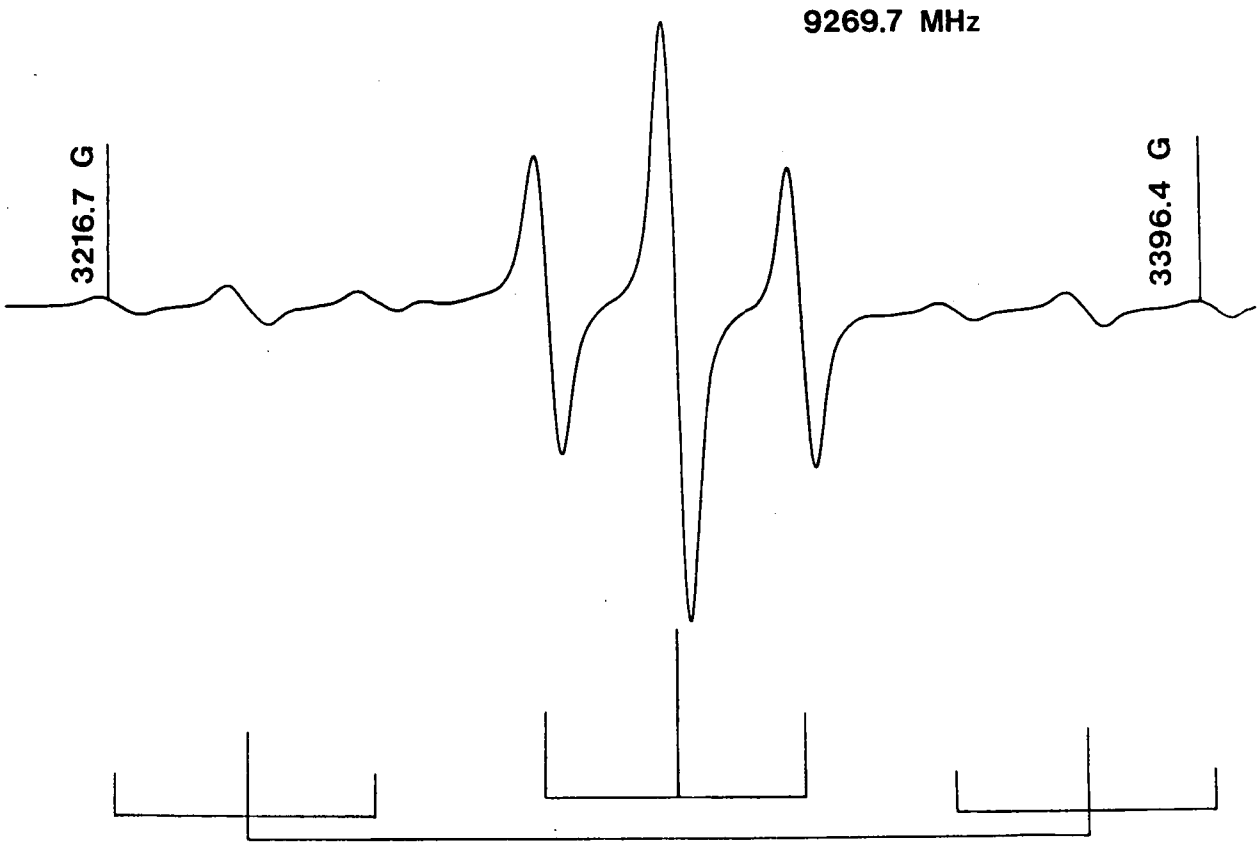

Figure 79. First-derivative ESR spectrum of a γ-irradiated sample of Me_4Sn in PFMCH at 140 K.

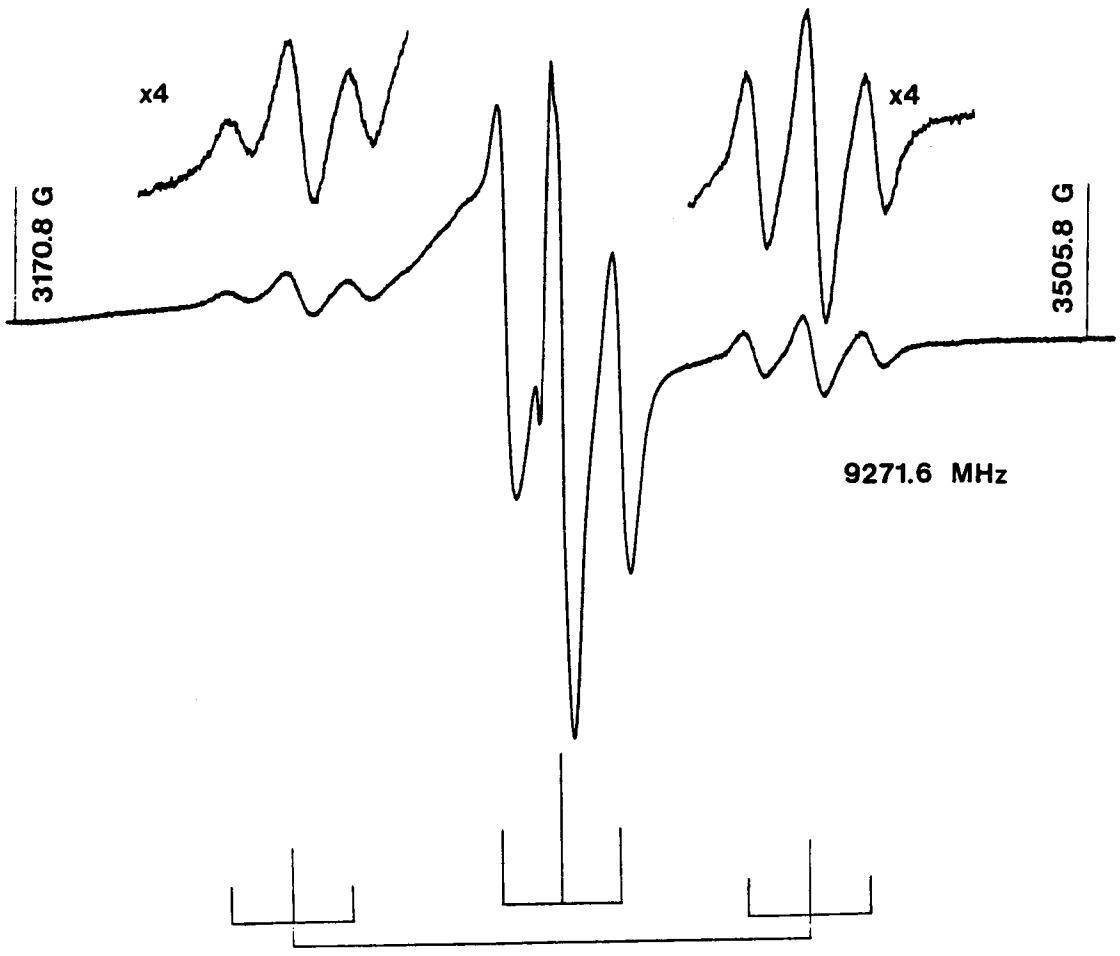

Figure 80. First-derivative ESR spectrum of a γ-irradiated sample of Me_4Pb in PFMCH at 140 K.

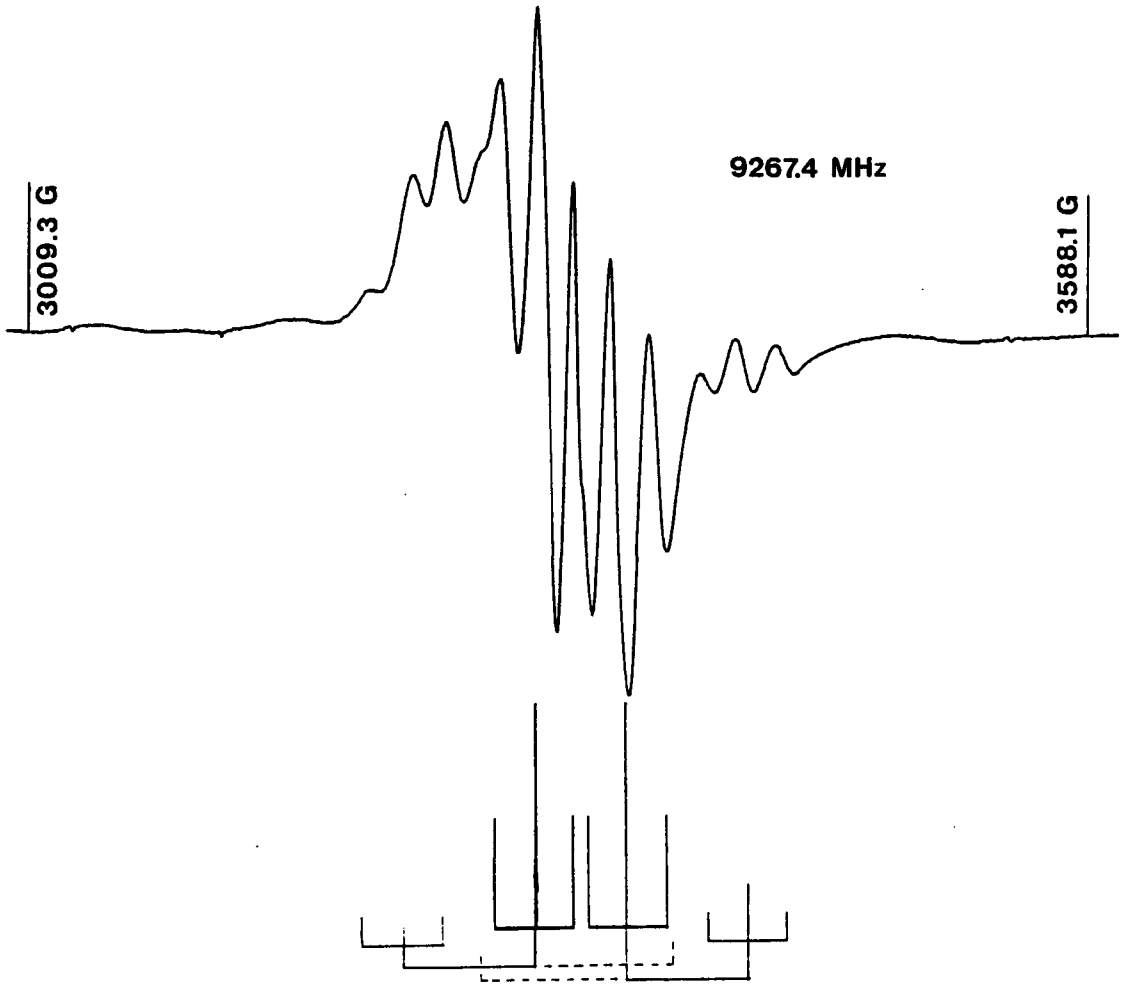

Figure 81. First-derivative ESR spectrum of a γ-irradiated sample of $(^{13}CH_3)_4Sn$ in PFMCH at 140 K.

TABLE XXI

HYPERFINE COUPLING CONSTANTS FOR $Me_3MCH_2\cdot$ NEUTRAL RADICALS IN A PFMCH MATRIX

Compound Me_3MCH_2 where M =	g-Value	Hyperfine Coupling Constants (G) $^2H_\alpha$	^{13}C	Metal Nucleus	Metal s-Spin Density
Si	2.0028	21.16	28.4	14.4	.0088
Ge	2.00194	21.47		7.71	.0091
Sn	2.0004	21.02	28.9	138	.0088
Pb	1.9967	21.3		184	.0063

C. $CF_3CCl_2\cdot$ Neutral Radical

Progressive introduction of α-fluorine substituents is well-known to induce pyramidality at the trigonal carbon in simple alkyl radicals.[220] A similar effect might be expected for α-chlorine substitution. Since there are fewer examples of this latter class of radicals, this effect is not as well tested. In fact, prior to the present work, the only ^{13}C hyperfine data for this class of compounds has been limited to the $CCl_3\cdot$ radical.[221-222] In this project, the detection and the interpretation of the magnitude of the trigonal-^{13}C coupling for the $CF_3CCl_2\cdot$ radical will be discussed. This radical has previously been described, but no ^{13}C-hyperfine interactions were reported.[220]

In Figure 82, page 282, the first derivative ESR spectrum of a γ-irradiated pure sample of CCl_3CF_3 is shown at 167 K. The observed pattern is readily analyzed as a quartet of overlapping septets. The quartet structure sensibly arising from three equivalent fluorines (I = 1/2) and the septet structure arising from two equivalent chlorine nuclei (I = 3/2). The ESR parameters (Table XXII, page 283) are in excellent agreement with those previously reported for a high-resolution spectrum of the $CF_3CCl_2\cdot$ radical in solution.[220]

At much higher spectrometer gain (X 100), a well-defined partial replica of the central pattern was observed in the wings of the spectrum. These weaker features may be sensibly assigned to an

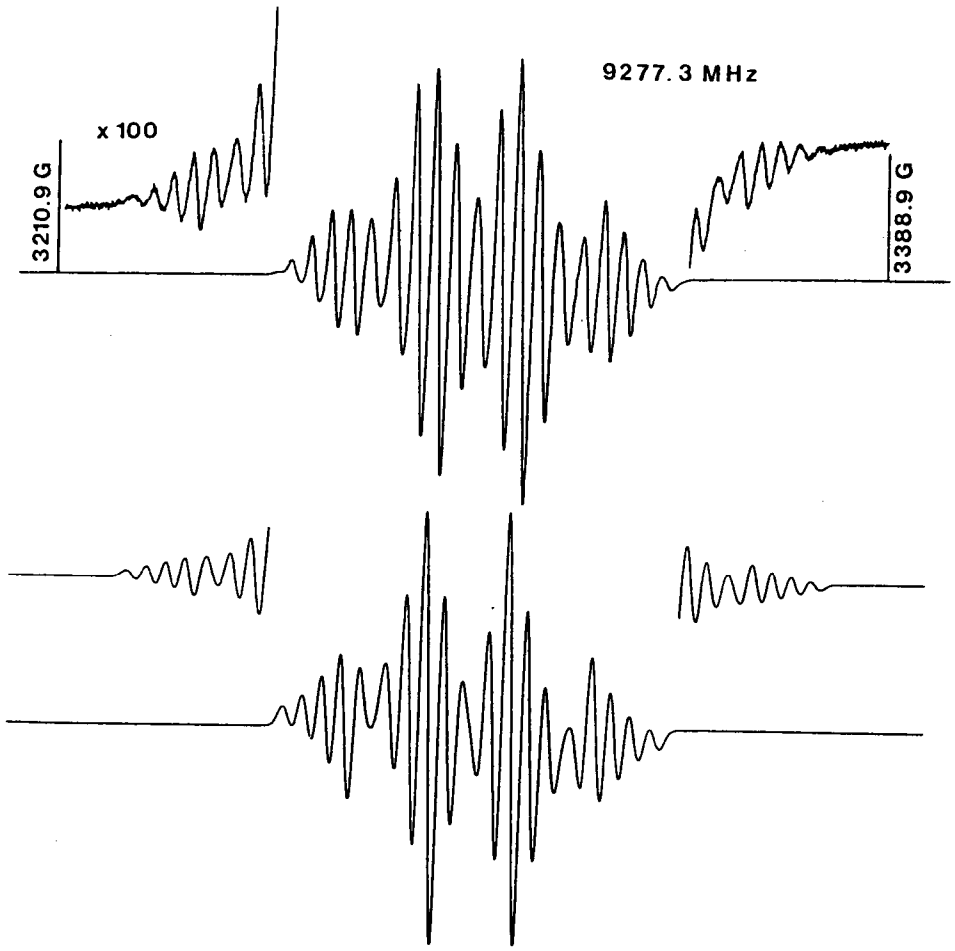

Figure 82. Observed (upper spectrum) and computer-simulated (lower spectrum) first derivative ESR spectra of the CF_3CCl_2 radical. The upper spectrum is of a γ-irradiated sample of pure 1,1,1-trichlorotrifluoroethane observed at 167 K following irradiation at 77 K for a dose of 1 Mrad. The lower spectrum was simulated using the ESR parameters in Table I, page 25, and included the calculated contribution from species containing ^{37}Cl. The gaussian linewidth parameter was 3.2 G.

TABLE XXII

ISOTROPIC ESR PARAMETERS FOR CF_3CCl_2 AND RELATED RADICALS

Radical	Hyperfine Couplings (G) $a(^{13}C)$	$a(^{35}Cl)$	$a(^{19}F)$	g-Values	Reference
CF_3CCl_2		4.14	18.56(β-F)	2.00797	220
CF_3CCl_2	67.3	4.2	18.5 (β-F)	2.0077	This Work
CCl_3	114, 117	6.25, 7.0		2.0093, 2.0115	221[a]
CCl_3	116.7	8.0		2.0138	222, 223[b]
$CFCl_2$		10.5	84.6		c
$CFCl_2$		10.8	83.7		107
$CFCl_2$		10.2	84.7	2.0068	82
CF_2Cl		16.1	109.8		d
CF_2Cl		16.2	109.1	2.0052	82
CF_3	271.6		145.3	2.00287	105
CF_3			144.7	2.0031	82

[a]Parameters are given for two radical sites.

[b]Calculated from Reference 6.

[c]A. Bowles, A. Hudson, and R. A. Jackson, Chem. Phys. Lett., 5, 552 (1970).

[d]J. Cooper, A. Hudson, and R. A. Jackson, Mol. Phys., 23, 209 (1972).

additional hyperfine interaction to ^{13}C in natural abundance. The fact that these features are almost exactly 1/200 the intensity of the central features provides an addition argument that these features are correctly assigned. The excellent fit of the computer simulation with the experimental spectrum also helps confirm this analysis.

Since ^{13}C hyperfine interactions in CF_3 substituents are generally no larger than 20 G,[224] the 67.3 G ^{13}C hyperfine interaction in this case must be associated with the trigonal carbon.

The ^{13}C hyperfine interaction of 67.3 G is much closer to the ^{13}C coupling constant found for the planar methyl radical (38.5 G) than the pyramidal CF_3 radical (271.6 G). A previous investigation found that the barrier to rotation about the C_α-C_β bond to be close to zero,[220] as would be expected for a radical containing a sixfold barrier to rotation. Hence, the finding that the trigonal carbon is close to planar nicely complements these earlier studies.

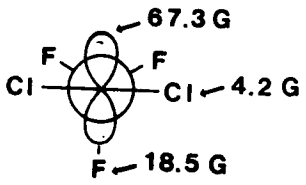

Since the trigonal carbon in $CF_3CCl_2\cdot$ is more planar than the carbon in the $CCl_3\cdot$ radical, the present results strongly support the argument that π-conjugative destabilization[224,225] is more important than electronegativity[226] effects in determining the planarity of alkyl radicals.

LITERATURE CITED

LITERATURE CITED

1. E. Zavoisky, J. Phys. U.S.S.R., 9, 211, 245 (1945).

2. E. Fermi, Z. Physik, 60, 320 (1930).

3. A. D. Walsh, J. Chem. Soc., 2260 (1953) and following papers.

4. G. N. Lewis, D. Lipkin, and T. T. Magel, J. Am. Chem. Soc., 63, 3005 (1941).

5. G. N. Lewis and D. Lipkin, J. Am. Chem. Soc., 64, 2801 (1942).

6. J. E. Wertz and J. R. Bolton, "Electron Spin Resonance: Elementary Theory and Practical Applications." McGraw-Hill, New York, N. Y., 1972, p. 451.

7. A. Hasegawa and F. Williams, Chem. Phys. Lett., 46, 66 (1977).

8. B. W. Walther and F. Williams, J. Chem. Soc., Chem. Commun., 270 (1982).

9. J. Roncin, Molec. Crystallogr., 3, 117 (1967).

10. (a) P. J. Krusic and J. K. Kochi, J. Am. Chem. Soc., 91, 6161 (1969).
(b) A. Hudson and H. A. Hussain, J. Chem. Soc. B., 793 (1969).

11. F. J. Adrian, E. L. Cochran, and V. A. Bowers, "Free Radicals in Inorganic Chemistry." Amer. Chem. Soc., Washington, D. C., 1962, p. 50.

12. R. J. Holman and M. J. Perkins, J. Chem. Soc. (C), 2324 (1971).

13. S. Terabe and R. Konaka, J. Chem. Soc., Perkin Trans. 2, 369 (1973).

14. P. Neta, J. Phys. Chem., 75, 2570 (1971).

15. B. Smaller and M. Matheson, J. Chem. Phys., 28, 1169 (1958).

16. G. N. Lewis and D. Lipkin, J. Am. Chem. Soc., 64, 2801 (1942).

17. G. W. Neilson and M. C. R. Symons, Mol. Phys., 27, 1613 (1974).

18. C. M. L. Kerr, K. Webster, and F. Williams, J. Phys. Chem., 79, 2650 (1975).

19. L. B. Knight and J. Steadman, J. Chem. Phys., 77, 1750 (1982).

20. R. W. Fessenden and R. H. Schuler, J. Chem. Phys., 39, 2147 (1963).

21. B. C. Gilbert in "Electron Spin Resonance," ed. R. O. C. Norman (Specialist Periodical Report). The Chemical Society, London, Vol. 1, 1973.

22. J. Slater and M. C. R. Symons, J. Phys. Chem., 52, 1003 (1970).

23. H. L. Strauss, T. J. Katz, and G. K. Fraenkel, J. Am. Chem. Soc., 85, 2360 (1963).

24. E. G. Janzen and M. Buchheit, J. Phys. Chem., 76, 937 (1972).

25. J. R. Bolton and J. T. Warden, Creat. Detect. Excited State, 2, 63 (1974).

26. C. K. Jen, S. N. Foner, E. L. Cochran, and V. A. Bowers, Phys. Rev., 112, 1169 (1958).

27. T. Cole, H. O. Pritchard, N. B. Davidson, and H. M. McConnell, Mol. Phys., 1, 406 (1958).

28. J. T. Wang and F. Williams, J. Am. Chem. Soc., 103, 6994 (1981).

29. A. G. Harrison, A. Irko, and T. W. Shannon, Can. J. Chem., 44, 1351 (1966).

30. R. L. Heath, "Handbook of Chemistry and Physics," R. C. Weast, ed. CRC Press, Cleveland, Ohio, 1974, p. B-341.

31. R. L. Heath, "Handbook of Chemistry and Physics," R. C. Weast, ed. CRC Press, Cleveland, Ohio, 1974, p. B-260.

32. A. Einstein, Ann. D. Physik., 17, 145 (1905).

33. A. H. Compton and S. K. Allison, "X-Rays in Theory and Experiment," D. Van Nostrand Co., Princeton, N. J., 1935, Chapter 7.

34. (a) A. J. Swallow, "Radiation Chemistry." Halsted Press, New York, N. Y., 1973, p. 25.
(b) "Fundamental Processes in Radiation Chemistry," P. Ausloos, Ed. Wiley, New York, 1968.

35. M. C. R. Symons, Pure and Appl. Chem., 53, 223 (1981).

36. B. H. Mahan and C. E. Young, J. Chem. Phys., 44, 2192 (1966).

37. R. K. Asundi and J. D. Craggs, Proc. Phys. Soc., 83, 611 (1964).

38. See, for example: (a) A. J. Bard and A. Martz, J. Am. Chem. Soc., 101, 2959 (1959).
(b) R. F. C. Claridge and J. E. Willard, J. Am. Chem. Soc., 87, 4992 (1965).

39. W. H. Hamill, "Radical Ions," E. T. Kaiser and L. Kevan, eds. Wiley, New York, 1968, p. 321.

40. J. T. Wang and F. Williams, J. Am. Chem. Soc., 84, 3156 (1980).

41. J. K. Kochi, "Organometallic Mechanisms and Catalysis." Academic Press, New York, N. Y., 1978, p. 292.

42. D. Becker, K. Plante, and M. D. Sevilla, J. Phys. Chem., 87, 1648 (1983).

43. L. D. Snow and F. Williams, Chem. Phys. Lett., 100, 198 (1983).

44. A. Hasegawa and M. C. R. Symons, J. Chem. Soc. Faraday Trans., I, 79, 93 (1983).

45. X.-Z. Qin, B. W. Walther, and F. Williams, J. Chem. Soc., Chem. Commun., accepted for publication.

46. J. E. Wertz and J. R. Bolton, "Electron Spin Resonance: Elementary Theory and Practical Applications." McGraw-Hill, New York, N. Y., 1972, p. 38.

47. A. Carrington and A. D. McLachlan, "Introduction to Magnetic Resonance." Harper and Row, New York, N. Y., 1967, p. 4.

48. P. W. Atkins and M. C. R. Symons, "The Structure of Inorganic Radicals." Elsevier, Amsterdam, 1967, p. 257.

49. R. S. Alger, "Electron Paramagnetic Resonance." Wiley, New York, N. Y., 1968, p. 8.

50. J. E. Wertz and J. R. Bolton, "Electron Spin Resonance: Elementary Theory and Practical Applications." McGraw-Hill, New York, N. Y., 1972, p. 21.

51. J. R. Morton and K. F. Preston, J. Magn. Reson., 30, 577 (1978).

52. J. E. Wertz and J. R. Bolton, "Electron Spin Resonance: Elementary Theory and Practical Applications." McGraw-Hill, New York, N. Y., 1972, p. 112.

53. H. M. McConnell and D. B. Chesnut, J. Chem. Phys., 28, 107 (1958).

54. C. Thomson, "Electron Spin Resonance," R. O. C. Norman, ed. (Specialist Periodical Reports). The Chemical Society, London, 1973, Vol. 1, p. 1.

55. A. Carrington and A. D. McLochlan, "Introduction to Magnetic Resonance." Harper and Row, New York, N. Y., 1967, p. 132.

56. This is discussed in more detail in Chapter IV, Section C, page 202.

57. J. E. Wertz and J. R. Bolton, "Electron Spin Resonance: Elementary Theory and Practical Applications." McGraw-Hill, New York, N. Y., 1972, p. 131.

58. L. F. Williams, M. B. Yim, and D. E. Wood, J. Am. Chem. Soc., 95, 6475 (1973).

59. M. B. Yim and D. E. Wood, J. Am. Chem. Soc., 97, 1004 (1975).

60. R. W. Fessenden and R. H. Schuler, "Advances in Radiation Chemistry," M. Burton and J. L. Magee, eds. J. Wiley, New York, N. Y., 1970, Vol. 2, p. 1.

61. (a) R. W. Fessenden, J. Magn. Reson., 1, 277 (1969).
(b) P. Burkhard and H. Fischer, J. Magn. Reson., 40, 335 (1980).
(c) J. R. Morton and K. F. Preston, J. Magn. Reson., 41, 127 (1980).

62. A. Hasegawa, M. Hayashi, C. M. L. Kerr, and F. Williams. J. Mag. Reson., 48, 192 (1982).

63. M. A. Rashid, J. Phys. A., 10, L135 (1977).

64. H. Fierz and A. von Zelewsky, Inorg. Chem., 10, 1556 (1971).

65. H. A. Kuska, M. T. Rogers, and R. E. Drullinger, J. Phys. Chem., 71, 109 (1967).

66. H. So and R. L. Belford, Inorg. Chem., 9, 2194 (1970).

67. P. H. Daus and R. L. Belford, Inorg. Chem., 10, 1558 (1971).

68. R. I. McNell, F. Williams, and M. B. Yim, Chem. Phys. Lett., 61, 293 (1979).

69. P. H. Kasai, W. Weltner, Jr., and E. B. Whipple, J. Chem. Phys., 42, 1120 (1965).

70. E. L. Cochran, F. J. Adrian, and V. A. Bowers, J. Chem. Phys., 34, 1161 (1961).

71. P. C. Taylor, J. F. Baugher, and H. M. Kriz, Chem. Reviews, 75, 203 (1975).

72. H. J. M. Slangen, J. Phys., E, 3, 775 (1970).

73. R. J. Faber and G. K. Fraenkel, J. Chem. Phys., 47, 2462 (1967).

74. P. W. Atkins and M. C. R. Symons, "The Structure of Inorganic Radicals." Elsevier, Amsterdam, 1967, p. 43.

75. R. L. Hudson, Ph. D. Dissertation, The University of Tennessee, Knoxville, 1978, p. 24.

76. T. Dahlgren, T. Gillbro, G. Nilsson, and A. Lund, J. Phys., E, 4, 61 (1971).

77. R. L. Hudson, Ph. D. Dissertation, The University of Tennessee, Knoxville, 1978, p. 32.

78. J. A. Pople and D. L. Beveridge, "Approximate Molecular Orbital Theory." McGraw-Hill, New York, N. Y., 1970.

79. Castellano and Bothner-By, J. Chem. Phys., 45, 1845 (1966).

80. H. Kubodera, T. Shida, and K. Shimokoshi, J. Phys. Chem., 85, 2583 (1981).

81. E. D. Sprague and F. Williams. J. Chem. Phys., 54, 5425 (1971).

82. A. Hasegawa, M. Shiotani, and F. Williams, Disc. Faraday Soc., 63, 157 (1977).

83. M. Shiotani and F. Williams, J. Am. Chem. Soc., 98, 4006 (1976).

84. B. W. Walther, F. Williams, and D. M. Lemal, J. Am. Chem. Soc., 106, 548 (1984).

85. J. T. Wang and F. Williams, Chem. Phys. Lett., 72, 557 (1980).

86. Chem. and Engr. News, 21, December 19, 1983.

87. T. G. Lee, J. Phys. Chem., 67, 360 (1963).

88. P-O. Samskog, L. D. Kispert, and B. Kalyanaraman, J. Chem. Soc. Faraday Trans., 2, 80, 267 (1984).

89. J. T. Wang and F. Williams, unpublished results.

90. J. R. Morton and K. F. Preston, J. Chem. Phys., 73, 4914 (1980).

91. M. T. Rogers and L. D. Kispert, J. Chem. Phys., 46, 3193 (1967).

92. B. Kalyanaraman and L. D. Kispert, J. Chem. Phys., 68, 5219 (1978).

93. D. Pace, K. Ezell, and L. D. Kispert, J. Chem. Phys., 71, 3971 (1979).

94. H. Muto and L. D. Kispert, J. Chem. Phys., 72, 2300 (1980).

95. J. R. Morton and W. E. Falconer, J. Chem. Phys., 39, 427 (1963).

96. C. Lifshitz, T. O. Tiernan, and B. M. Hughes, J. Chem. Phys., 39, 427 (1963).

97. M. C. R. Symons and D. Griller, J. Magn. Reson., 39, 355 (1980).

98. C. A. Coulson, "Valence," 2nd ed. Oxford University Press, New York, N. Y., 1962, p. 111.

99. The angles are defined as θ = <FCF and ϕ = <FC (C_3 axis). See R. L. Hudson, Ph. D. Dissertation, The University of Tennessee, Knoxville, 1978, p. 21.

100. T. Clark, J. Chem. Soc., Chem. Commun., 93 (1984).

101. D. Griller, K. U. Ingold, P. J. Krusic, B. E. Smart, and E. R. Wonchoba, J. Phys. Chem., 86, 1376 (1982).

102. R. G. Florin, H. W. Brown, and L. A. Wall, J. Phys. Chem., 66, 2672 (1962).

103. R. I. McNeil, M. Shiotani, F. Williams, and M. B. Yim, Chem. Phys. Lett., 51, 433 (1977).

104. J. R. Morton, K. F. Preston, J. T. Wang, and F. Williams, Chem. Phys. Lett., 64, 71 (1979).

105. R. W. Fessenden and R. H. Schuler, J. Chem. Phys., 43, 2704 (1965).

106. L. D. Kispert and F. Myers, J. Chem. Phys., 56, 2623 (1972).

107. H. C. Wang, M. D. Pace, and L. D. Kispert, J. Chem. Phys., 74, 246 (1981).

108. L. N. Shchegoleva, I. I. Bilkis, and P. V. Schastnev, Zh. Struct. Khim., 25, 19 (1984).

109. L. N. Shchegoleva, I. I. Bilkis, and P. V. Schastnev, Chem. Phys. 82, 343 (1983).

110. L. N. Shchegoleva, I. I. Bilkis, and P. V. Shastnev. Chem. Phys. Lett., 104, 348 (1984).

111. The designation of the orbital is dependent upon the convention used. Using the Snyder convention (L. C. Snyder and H. Basch, "Molecular Wave Functions and Properties" (Wiley, New York, 1972), pp. T-378 to T-386), the orbital is labeled 5 b_{1u} while using the Hertzberg convention (G. Hertzberg, Molecular Spectra and Molecular Structure, Vol. 2 (Van Nostrand, Princeton, 1945), pp. 106-108), the orbital would be designated $5b_{2u}$.

112. J. E. Bloor, R. A. Paysen, and R. E. Sherrod, Chem. Phys. Lett., 60, 476 (1979).

113. M. C. R. Symons, J. Chem. Research (5), 286 (1981).

114. S. Merry and C. Thomson, Chem. Phys. Lett., 82, 373 (1981).

115. M. N. Paddon-Row, N. G. Rondan, K. N. Houk, and K. D. Jordan, J. Am. Chem. Soc., 104, 1143 (1982).

116. J. L. Carlos, Jr., R. R. Karl, Jr., and S. H. Bauer, Chem. Phys., 70, 177 (1974).

117. S. P. So, J. Chem. Phys., 67, 2929 (1977).

118. M. A. Benzel, A. M. Maurice, R. L. Belford, and C. E. Dykstra, J. Am. Chem. Soc., 105, 3802 (1983).

119. David M. Lemal, Department of Chemistry, Dartmouth College, Hanover, NH 03755.

120. T. K. Katz, W. H. Reinmuth, and D. E. Smith, J. Am. Chem. Soc., 84, 802 (1962).

121. H. L. Strauss, T. J. Katz, and G. K. Fraenkel, J. Am. Chem. Soc., 85, 2360 (1963).

122. D. M. Lemal, J. M. Buzby, A. C. Barefoot III, M. W. Grayston, and Evan D. Laganis, J. Org. Chem., 45, 3118 (1980).

123. B. B. Laird and R. E. Davis, Acta Cryst., B38, 678 (1982).

124. (a) P. B. Ayscough, R. G. Collins, and F. S. Dainton, Nature (London), 205, 965 (1965).
(b) C. Chachaty, J. Chim. Phys., 64, 614 (1967).

125. D. R. Smith, J. J. Pieroni, Can. J. Chem., 43, 876, 2141 (1965).

126. W. H. Hamill, "Radical Ions," E. T. Kaiser and L. Kevan, Eds. Interscience-Wiley, New York, 1968, pp. 345-351.

127. (a) M. A. Bonin, K. Tsuji, and F. Williams, Nature (London), 218, 946 (1968).
(b) M. A. Bonin, K. Takeda, and F. Williams, J. Chem. Phys., 50, 5423 (1969).

128. See Chapter V, Section B.

129. J. T. Wang and F. Williams, Chem. Phys. Lett., 71, 471 (1980).

130. M. E. Akhmetova, N. M. Bazhin, Yu. V. Pozdnykovich, V. D. Schteingarts, and L. N. Shchegoleva, Teor. Eksp. Khim., 10, 613 (1974).

131. P. V. Schastnev, G. M. Zhidomivov, and N. D. Chuvylkin, Zh. Strukt. Khim., 10, 998 (1969).

132. C. Thomson and W. J. MacCulloch, Mol. Phys., 19, 817 (1970).

133. T. Chen, F. Graf, and Hs. H. Gunthard, Chem. Phys., 75, 165 (1983).

134. J. H. Hammons, M. Bernstein, and R. J. Myers, J. Phys. Chem., 83, 2034 (1979).

135. D. L. Taggart, W. Peppercorn, and L. B. Anderson, J. Phys. Chem., 88, 2875 (1984).

136. C. Chachaty, A. Forchioni, and M. Shiotani, Canad. J. Chem., 48, 435 (1970).

137. (a) J. F. Liebman, J. Fluorine Chem., 3, 27 (1973/74).
(b) C. Lifshitz, T. O. Tiernan, and B. M. Hughes, J. Chem. Phys., 59, 3182 (1973).

138. T. Gillbro, C. M. L. Kerr, and F. Williams, Mol. Phys., 28, 1225 (1974).

139. J. T. Wang and F. Williams, J. Am. Chem. Soc., 102, 2860 (1980).

140. I. Langmuir, J. Am. Chem. Soc., 41, 1543 (1919).

141. C. A. Coulson, "Valence," 2nd Ed. Oxford University Press, New York, N. Y., 1962, p. 111.

142. S. P. Mishra and M. Symons, J. C. S. Chem. Comm., 280 (1974).

143. J. R. Morton and K. F. Preston, Chem. Phys. Lett., 18, 98 (1973).

144. (a) A. R. Boats, A. J. Colussi, J. R. Morton, and K. F. Preston, Chem. Phys. Lett., 37, 135 (1976).
(b) J. R. Morton, K. F. Preston, and S. J. Strach, J. Magn. Reson., 37, 321 (1980).

145. J. R. Morton, Amer. Chem. Soc. Symposium Series, 66, 386 (1978).

146. J. R. Morton, Canad. J. Phys., 41, 706 (1963).

147. R. W. Fessenden and R. H. Schuler, J. Chem. Phys., 45, 1845 (1966).

148. Karl O. Christe, Rocketdyne Division, North American Rockwell Corp., Canoga Park, CA 91304.

149. A. Hasegawa and F. Williams, Chem. Phys. Lett., 45, 275 (1977).

150. K. O. Christe, E. C. Curtis, C. J. Schack, and D. Pilipovich, Inorg. Chem., 11, 1679 (1972).

151. K. O. Christe, C. J. Schack, D. Pilipovich, E. C. Curtis, and W. Sawodny, Inorg. Chem., 12, 620 (1973).

152. J. R. Morton and K. F. Preston, J. Chem. Phys., 58, 3112 (1973).

153. K. Nishikida, F. Williams, G. Mamantov, and N. Smyrl, J. Am. Chem. Soc., 97, 3526 (1975).

154. J. R. Morton and K. F. Preston, Amer. Chem. Soc. Symposium Series, 66, 386 (1978).

155. J. R. Morton, K. F. Preston, and S. J. Strach, J. Phys. Chem., 83, 3418 (1979).

156. J. R. Morton and K. F. Preston, Mol. Phys., 30, 1213 (1975).

157. R. W. Fessenden and R. H. Schuler, J. Chem. Phys., 45, 1845 (1966).

158. A. J. Colussi, J. R. Morton, and K. F. Preston, Chem. Phys. Lett., 30, 317 (1975).

159. A. R. Gregory, S. E. Karavelas, J. R. Morton, and K. F. Preston, J. Am. Chem. Soc., 97, 2206 (1975).

160. A. R. Gregory, J. Chem. Phys., 60, 3713 (1974).

161. S. R. Ungemach and H. F. Schaefer, J. Am. Chem. Soc., 98, 1658 (1977).

162. S. P. So and W. G. Richards, J. Chem. Soc. Faraday Trans., 2, 55 (1979).

163. R. L. Hudson, private communication, Eckerd College, Department of Chemistry, St. Petersburg, Florida.

164. T. Shida and W. H. Hamill, J. Chem. Phys., 44, 2369, 2375, 3472 (1966).

165. A. Grimison and G. A. Simpson, J. Phys. Chem., 72, 1776 (1968).

166. T. Shida and T. Kato, Chem. Phys. Lett., 68, 106 (1979) and references contained therein.

167. (a) M. C. R. Symons and I. G. Smith, J. Chem. Res. (S), 382 (1979).
(b) M. C. R. Symons, Chem. Phys. Lett., 69, 198 (1980).

168. J. T. Wang and F. Williams, J. Phys. Chem., 84, 3156 (1980).

169. T. Shida, H. Kubobera, and Y. Egawa, Chem. Phys. Lett., 79, 179 (1981).

170. J. T. Wang and F. Williams, J. Chem. Soc., Chem. Commun., 666 (1981).

171. T. Shida, E. Haselbach, and T. Bally, Acc. Chem. Res., 17, 180 (1984).

172. M. C. R. Symons, Electron Spin Resonance," R. O. C. Norman, ed. (Specialist Periodical Reports). The Chemical Society, London, 1983, Vol. 8, p. 143.

173. J. K. Kochi, Accounts Chem. Res., 7, 351 (1974).

174. A. E. Jonas, G. K. Schweitzer, F. A. Grimm and T. A. Carlson, J. Electron Spectroscop. Relat. Phenom., 1, 29 (1972).

175. R. J. Klinger and J. K. Kochi, J. Am. Chem. Soc., 102, 4790 (1980).

176. X.-Z. Qin and F. Williams, Chem. Phys. Lett. (1984). Accepted for publication.

177. A. D. Baker, D. Betteridge, N. R. Kemp, and R. E. Kirby, J. Mol. Structure, 8, 75 (1971).

178. J. A. Pople, Int. J. Mass Spectrom. Ion Phys., 17, 1 (1976).

179. M. J. S. Dewar and H. S. Rzepa, J. Am. Chem. Soc., 99, 7432 (1977).

180. F. A. Grimm and J. Godoy, Chem. Phys. Lett., 6, 336 (1970).

181. L. B. Knight, J. Steadman, D. Feller, and E. R. Davidson, J. Am. Chem. Soc., 106, 3700 (1984).

182. D. Feller and E. R. Davidson, J. Chem. Phys., 80, 1006 (1983).

183. M. C. R. Symons, T. Chen, and C. Glidewell, J. Chem. Soc., Chem. Commun., 326 (1983).

184. C. A. Coulson and H. L. Strauss, Proc. Roy. Soc., 269A, 443 (1962).

185. M. Iwasaki, T. Toriyama, and K. Numone, J. Am. Chem. Soc., 103 3591 (1981).

186. B. W. Walther and F. Williams, J. Chem. Soc., Chem. Commun., 270 (1982).

187. B. W. Walther, F. Williams, W. Lau, and J. K. Kochi, Organomet., 2, 688 (1983).

188. M. C. R. Symons, J. Chem. Soc., Chem. Commun., 869 (1982).

189. A. Hasegawa, S. Kaminaka, T. Wakabayashi, M. Hayashi, and M. C. R. Symons, J. Chem. Soc., Chem. Commun., 1199 (1983).

190. M. C. R. Symons, J. Chem. Soc., Chem. Commun., 1281 (1981).

191. D. M. Chipman, J. Chem. Phys., 78, 3112 (1983).

192. M. C. R. Symons, Mol. Phys., 24, 461 (1972).

193. M. A. Bonin, Y. J. Chung, E. B. Sprague, K. Takeda, J. T. Wang, and F. Williams, Nobel Symp., 22, 103 (1972).

194. S. P. Mishra and M. C. R. Symons, J. Chem. Soc., Perkin Trans., 2, 391 (1973).

195. Y. Fujita, T. Katsu, and M. Sato, J. Chem. Phys., 61, 4307

196. N. Shimamoto, Y. Fujita and T. Kwan, Bull. Chem. Soc. Jpn., 43, 580 (1970).

197. J. K. Kochi, "Organometallic Mechanisms and Catalysis." Academic Press, New York, N. Y., 1978, Part III.

198. B. W. Walther, F. Williams, W. Lau, and J. K. Kochi, Organometallics, 3, 948 (1984).

199. R. W. Fessenden and R. H. Schuler, J. Chem. Phys., 39, 2165 (1963).

200. (a) J. R. Holmes and H. D. Kaesz, J. Am. Chem. Soc., 83, 3903 (1961).
(b) L. W. Reeves, M. Suzuki, and J. A. Vanin, Inorg. Chem., 15, 1035 (1976).

201. J. E. Bennett and J. A. Howard, Chem. Phys. Lett., 15, 322 (1972).

202. M. Iwashaki, K. Toriyama, and K. Nunome, J. Am. Chem. Soc., 103, 3591 (1981).

203. J. T. Wang and F. Williams, Chem. Phys. Lett., 82, 177 (1981).

204. J. K. Kochi, "Organometallic Mechanism and Catalysis." Academic Press, New York, N. Y., 1978, p. 12.

205. H. H. Anderson, Inorg. Chem., 2, 108 (1964).

206. S. Kozima, H. Fujita, T. Hetomi, K. Kobayashi, K. Kobayashi, and M. Kawanisi, Bull. Chem. Soc. Jpn., 53, 2953 (1980).

207. H. Gilman, W. H. Atwell, and F. K. Cartledge, Adv. Organomet. Chem., 4, 1 (1966).

208. J. K. Kochi, "Organometallic Mechanism and Catalysis." Academic Press, New York, N. Y., 1978, p. 487.

209. J. T. Wang and F. Williams, J. Chem. Soc., Chem. Commun., 1184 (1981).

210. K. U. Ingold and J. C. Walton, J. Am. Chem. Soc., 104, 617 (1982).

211. J. T. Wang and F. Williams, J. Am. Chem. Soc., 103, 6994 (1981).

212. G. N. Lewis and D. Lipkin, J. Am. Chem. Soc., 64, 2801 (1942).

213. R. W. Fessenden and R. H. Schuler, J. Chem. Phys., 39, 2147 (1963).

214. J. K. Kochi, "Organometallic Mechanism and Catalysis." Academic Press, New York, N. Y., 1978, p.33.

215. G. J. P. Peddle, J. Organomett. Chem., 5, 486 (1966).

216. P. R. Jones and R. West, J. Am. Chem. Soc., 90, 6978 (1968).

217. J. H. Mackey and D. E. Wood, Mol. Phys., 18, 783 (1970).

218. A. R. Lyons, G. W. Neilson and M. C. R. Symons, J. Chem. Soc. Faraday II, 68, 807 (1972).

219. A. Carrington and A. D. McLochlan, "Introduction to Magnetic Resonance." Harper and Row, New York, N. Y., 1967, p. 138.

220. K. S. Chen and J. K. Kochi, J. Am. Chem. Soc., 96, 794 (1974).

221. C. Hesse, N. Leray, and J. Roncin, Mol. Phys., 22, 137 (1971).

222. G. Maass, A. K. Maltsev and J. L. Margrave, J. Inorg. Nucl. Chem., 35, 1945 (1973).

223. S. P. Mishra and M. C. R. Symons, Int. J. Radiat. Phys. Chem., 7, 617 (1975).

224. P. S. Krusic and R. C. Bingham, J. Am. Chem. Soc., 98, 230

225. R. C. Bingham and M. J. S. Dewar, J. Am. Chem. Soc., 95, 7182 (1973).

226. L. Pauling, J. Chem. Phys., 51, 2767 (1969).

VITA

Brian Wayne Walther was born in Glendale, California on July 24, 1957. He attended elementary and high school in the public school system of Hastings, Minnesota. As a high school senior, he was awarded the 3M Creativity Award. He graduated from Hastings High School in June 1975.

In September 1975 he enrolled in Bob Jones University (Greenville, South Carolina). He graduated in June 1979 with a Bachelor of Science in Chemistry degree.

Having accepted a teaching assistantship from The University of Tennessee, Knoxville, he began graduate study in Chemistry in September 1979. He received the ARCO Fellowship for excellence in teaching and research in both 1982 and 1983. He was married to Sandra Brogan on March 14, 1981.

He is a member of Sigma Xi and the American Chemical Society. He received the Ph. D. in Physical Chemistry in December 1984 and is employed at Dow Chemical Company, Louisiana Division.